PhD-FSTC-2018-21
The Faculty of Sciences, Technology and Communication

DISSERTATION

Defence held on 21/03/2018 in Luxembourg

to obtain the degree of

DOCTEUR DE L'UNIVERSITÉ DU LUXEMBOURG

EN SCIENCES DE L'INGÉNIEUR

by

Job DUARTE DA COSTA
Born on 20th December 1988 in Luxembourg (Luxembourg)

STRUCTURAL PROPERTIES OF STEEL – CONCRETE COMPOSITE JOINTS

Dissertation defence committee

Prof. Dr.-Ing. Christoph Odenbreit, dissertation supervisor
Professor, Université du Luxembourg, Faculté des Sciences, de la Technologie et de la Communication

Prof. Dr.-Ing. Stefan Van Baars, chairman
Professor, Université du Luxembourg, Faculté des Sciences, de la Technologie et de la Communication

Dr.-Ing. Mike Tibolt, vice-chairman
Research Engineer, ArcelorMittal Global R&D

Dr.-Ing. Renata Obiala
Head of Construction and Infrastructure Applications Department, ArcelorMittal Global R&D

Prof. Dr.-Ing. Rui António Duarte Simões
Professor, Universidade de Coimbra, Departamento de Engenharia Civil

Preface

The present thesis was realised during my time as a research assistant at the ArcelorMittal Chair of Steel and Façade Engineering at the University of Luxembourg. It was supported by ArcelorMittal Global R&D in the framework of a common research project called "SRCon".

The creation of this thesis was not an individual experience. It is the result of an interesting research involving several persons, whom I would like to thank sincerely.

Firstly, I would like to express my sincere gratitude to my supervisor Prof. Dr.-Ing. Christoph Odenbreit for offering me the opportunity to work in an excellent research environment. His expertise in steel and composite structures and his continuous guidance were primordial for the accomplishment of the present thesis. It was also a great pleasure to discuss different topics around the innumerable cups of coffee. I will keep a great memory of this time.

I would also like to present my special thanks to Dr.-Ing. Renata Obiala for her insightful comments and technical expertise. In particular, her remarkable guidance and her logical and structured analyses have been of great importance throughout my research work. I owe her my eternal gratitude for this. I would like to thank her also for the very pleasant three years of common office and her open ear for personal concerns.

I want to express my sincere thanks to Prof. Dr.-Ing. Stefan Van Baars from the Research Unit in Engineering Sciences, University of Luxembourg, for his participation as chairman of my defence. I especially enjoyed his joyful attitude and the pleasant discussions. My sincere gratitude also to Dr.-Ing. Mike Tibolt, Research Engineer at ArcelorMittal Global R&D, for his advice and suggestions and for his participation as member of the committee of my dissertation defence. I would like to express also my profound gratitude to Prof. Dr.-Ing. Rui António Duarte Simões, from the Civil Engineering Department of the University of Coimbra, for the time invested in travelling a considerable distance for the defence. Many thanks also for the literature and the comments on the thesis.

A special mention to Matthias Braun, Senior researcher at the ArcelorMittal Chair of Steel and Façade Engineering, University of Luxembourg, for his encouragement and technical advice during my research work. I appreciated the many hours spent in countless discussions on my research topic. Many of the theoretical developments presented in this thesis emerged from these inspiring discussions. I can never thank him enough for the permanent motivation in moments of doubt. Vielen Dank Matthias!

Moreover, I would like to express my gratitude to Prof. Dr.-Ing. Olivier Vassart, Executive Director of ArcelorMittal Global R&D Long Carbon and Professor of Steel and Composite Structures at the Catholic University of Louvain in Belgium, for the time invested as member of my dissertation supervisory committee and for his constructive criticism during our annual meetings. I particularly appreciated his very practical approach. Thanks must also go to

Prof. Dr.-Ing. Markus Schäfer, from the Research Unit in Engineering Sciences, University of Luxembourg for his help in technical questions.

During my research, I had the opportunity to exchange my ideas with Prof. Dr.-Ing. Luis da Silva, University of Coimbra and Prof. Dr.-Ing. Jean-Pierre Jaspart, University of Liège. Their help and suggestions are gratefully acknowledged.

I would also like to thank all my colleagues at the University of Luxembourg, who accompanied me during my research work. In particular, special thanks to my colleagues Sebastian Nellinger, Yves Staudt, Maciej Chrzanowski, Andras Kozma and Valentino Vigneri for the pleasant working spirit and their willingness to discuss and help.

I am deeply grateful to the support team of the laboratory of the University of Luxembourg, without whom the experimental part of the thesis would not have been possible. Special thanks to Logan Freitas, Ed Weyer, Marc Seil, Vicente Reis, Ralph Reiter and Claude Collé.

My sincere thanks to Valter de Matos and Aldin Bahovic, students at University of Luxembourg, for their assistance during the experimental investigations.

Last but by no means least, I would like to thank my mother Fatima and my father Salomão for their inexhaustible moral support. They saw the value of a good education and never doubted on my capacities. I have found in their stories of life my biggest motivation. Obrigado!

In the end, I would like to thank God for granting me the necessary strength to raise me up in moments of difficulty and for blessing me with good health all the way.

Luxembourg, in February 2018 *Job Duarte da Costa*

Abstract

The performance of steel and concrete composite frames is influenced by the structural properties of beam-to-column composite joints. The accurate assessment of these properties constitutes therefore an important element for a realistic representation of the structural behaviour at serviceability and ultimate limit state. However, the structural joint properties are not equally covered by current design standards; analytical guidance is provided to assess the resistance and stiffness of composite joints, whereas for the rotation capacity an experimental proof is required. Due to the additional effort required to determine the rotation capacity, the global plastic analysis finds little application in the design of composite frames, resulting in a lack of efficiency and material optimization in the final design.

In the present work, an analytical model to calculate the rotation capacity of composite joints is derived. Based on the knowledge developed in this research, an improvement of the current design rules for the joint stiffness is proposed.

This model is based on an experimental test campaign comprising eight full-scale beam-to-column joints with composite slim-floor beams. Besides, a finite element model was developed with the software Abaqus, which has been validated by the experimental tests. Numerical simulations were performed to investigate in-depth the conducted experiments and to analyse the behaviour of additional composite joints with different reinforcement properties.

This research has resulted in new analytical design rules for the joint stiffness and rotation capacity. The reliability of these new design rules has been demonstrated for different joint typologies using experimental and numerical data. The development of an analytical method for the rotation capacity of composite joints allows composite beams with composite beam-to-column joints to be designed according to the global plastic analysis without need of experimental evidence. Furthermore, the improvement of the current design rules for the stiffness of composite joints induces a more accurate assessment of the action effects at serviceability and ultimate limit state. This thesis provides therefore a complete methodology to design beam-to-column composite joints.

Kurzfassung

Das Tragverhalten von Rahmentragwerken in Verbundbauweise wird wesentlich durch die Eigenschaften von Verbundanschlüssen bestimmt. Somit ist eine genaue Ermittlung dieser Eigenschaften von großer Bedeutung, um das reale Verhalten des Tragwerks sowohl im Grenzzustand der Gebrauchstauglichkeit, als auch im Grenzzustand der Tragfähigkeit abzubilden. Obwohl in den derzeitigen Normen analytische Lösungen für die Tragfähigkeit und Steifigkeit von Träger-Stützenverbindungen angegeben werden, wird zur Bestimmung der Rotationskapazität von Verbundanschlüssen auf eine versuchsgestützte Ermittlung verwiesen. Baupraktisch stellt ein solches Vorgehen einen kaum vertretbaren Aufwand dar, wodurch eine plastische Schnittgrößenermittlung nur sehr begrenzt zum Nachweis von Verbundträgern Anwendung findet, was wiederrum eine wirtschaftliche Bemessung dieser Bauweise stark beeinträchtigt.

In der vorliegenden Arbeit wird ein analytisches Model zur Bestimmung der Rotationskapazität von Verbundanschlüssen angegeben. Basierend auf den hierbei gewonnenen Erkenntnissen, wird ebenfalls eine Verbesserung der derzeitigen Formeln zur Bestimmung der Steifigkeit von Verbundanschlüssen vorgeschlagen.

Das entwickelte Berechnungsmodell stützt sich auf die Auswertung von acht Versuchen an Träger-Stützenanschlüssen in Slim-Floor Bauweise. Es wurde außerdem ein Finite Element Model mit dem Programm Abaqus entwickelt und anhand der Versuchsergebnisse validiert. Mittels des so entwickeltem FE-Models konnten detaillierte Erkenntnisse zum Tragverhalten der Anschlüsse gewonnen werden. Zusätzlich wurden Parameterstudien mit variierenden Bewehrungsgraden und Durchmessern zur Gewinnung weiterer Erkenntnisse durchgeführt.

Das in dieser Arbeit vorgeschlagene Rechenmodell zur Bestimmung der Steifigkeit und der Rotationskapazität wurde anhand von Versuchsergebnissen und FE-Simulationen überprüft und validiert. Mit der hier vorgeschlagenen analytischen Methode kann nun ohne großen Aufwand die Rotationskapaziät von Verbundanschlüssen bestimmt und zum Nachweis des Grenzzustandes der Tragfähigkeit die Schnittgrößen von Verbundträgern plastisch ermittelt werden. Im Grenzzustand der Gebrauchstauglichkeit kann mit diesem neuen Verfahren das Tragverhalten von Rahmentragwerken realistischer abgeschätzt werden. Die hier vorgestellte analytische Methode ermöglicht somit einen vollständigen Nachweis von Träger-Stützenverbindungen in Verbundbauweise.

Résumé

Le comportement des ossatures mixtes acier-béton est influencé par les propritétés structurales des noeuds mixtes poutre-colonne. Par conséquent, il est important de déterminer correctement ces propriétés afin d'évaluer de manière réaliste le comportement structural de l'ossature à l'état limite en service ainsi qu'à l'état limite ultime. Toutefois, les normes actuelles ne prévoient des solutions analytiques que pour évaluer la rigidité et la résistance de noeuds mixtes, tandis que pour la capacité de rotation une vérification expérimentale est requise. L'absence d'une méthode analytique pour calculer la capacité de rotation complique de manière considérable l'analyse globale plastique d'ossatures mixtes, ce qui compromet l'exploitation optimale de ce type de structures.

Dans cette thèse, une méthode est présentée pour calculer la capacité de rotation de noeuds mixtes. De plus, une formule permettant de calculer la rigidité de noeuds mixtes est proposée sur base des connaissances acquises dans le cadre de ce projet de recherche.

Ce modèle de calcul s'appuie sur l'évaluation de huit essais expérimentaux de connections poutre-colonne de type slim-floor. Un modèle d'éléments finis a également été élaboré avec le programme Abaqus. Ce modèle numérique est validé par les essais expérimentaux menés à bien dans ce projet. Il a non seulement permis d'approfondir la recherche sur le comportement de noeuds mixtes mais a aussi permis d'effectuer une étude paramétrique afin d'étudier l'influence de l'armature sur le comportement de noeuds mixtes.

La recherche menée dans le cadre cette thèse a abouti à une nouvelle méthode de calcul pour la rigidité et la capacité de rotation de connections mixtes. La fiabilité de cette méthode a été vérifiée en comparant les résultats obtenus analytiquement à ceux lors d'essais expérimentaux et simulations numériques. Ce nouveau développement facilite le calcul de la capacité de rotation d'un noeud mixte ainsi que l'analyse globale plastique de structures mixtes à l'état limite. À l'état limite en service, cette nouvelle méthode offre la possibilité d'analyser plus précisément le comportement structural d'ossatures mixtes. L'étude décrite dans cette thèse fournit donc une méthodologie complète pour le calcul de noeuds mixtes poutre-colonne.

Contents

Nomenclature

Abbreviations

2D	Two-dimensional
3D	Three-dimensional
acc.	according
Avg.	Average
ca.	circa
CC	Correlation coefficient
CDP	Concrete Damaged Plasticity
cf.	"*confer*" - compare with
const.	constant
CoSFB	Composite slim floor beam
COV	Coefficient of variation
EC	Eurocode
e.g.	"*exempli gratia*" - example given
FEM	Finite Element Method
FEA	Finite Element Analysis
i.e.	"*id est*" - in other words / that is
MC	Model Code
N/A	Not available
No.	Number
RC	Reinforced concrete
Ref.	Reference
Reinf.	Reinforcement
Resp.	Respectively
Std. dev.	Standard deviation
SLS	Serviceability limit state
ULS	Ultimate limit state
vs.	versus

Symbols

Greek letters

α_e	ratio between E_s and E_{cm}
β_1	factor for tension stiffening
β_2	factor for tension stiffening
β_3	factor for tension stiffening
Δ_1	absolute elongation of the upper bolt-row
Δ_2	absolute elongation of the lower bolt-row

Δ_{slab}	absolute elongation of the RC slab on the reinforcement level
$\Delta\sigma_{sr}$	stress increment in reinforcement induced by cracking
ε_c	concrete strain
ε_{c1}	concrete strain at maximal compressive strength
ε_{cu1}	nominal ultimate concrete strain
ε_{ctm}	concrete strain at which cracking occurs
ε_{nom}	nominal strain
ε_s	reinforcement strain
ε_{sm}	modified reinforcement strain with stiffening effect
ε_{sm1}	modified reinforcement strain prior to concrete cracking
ε_{smn}	modified strain in reinforcement after crack formation phase
ε_{smu}	modified strain in reinforcement at ultimate state
ε_{smy}	modified strain in reinforcement at yield stress
ε_{su}	ultimate strain of reinforcement
ε_{sy}	yield strain of reinforcement
ε_{true}	true strain
$\varepsilon_{u,k}$	characteristic ultimate reinforcement strain
κ	cross section curvature
κ_{el}	elastic cross section curvature
κ_{pl}	plastic cross section curvature
μ	average
ν	Poisson's ratio
π	mathematical constant
ρ	longitudinal reinforcement ratio
ρ_{eff}	effective longitudinal reinforcement ratio
σ	stress or standard deviation
σ_c	stress in concrete
σ_{ct}	concrete tensile stress
σ_{nom}	nominal stress
σ_s	reinforcement stress
σ_{sr1}	reinforcement stress at first crack occurrence in concrete
$\sigma_{sr1,kb}$	reinforcement stress at first crack occurrence in concrete including bending effect
σ_{srn}	reinforcement stress after crack formation phase
σ_{true}	true stress
Σ	sum
τ_{bm}	mean bond strength between reinforcement and concrete
Φ_j	joint rotation
Φ_{req}	required joint rotation
Φ_u	rotation capacity of a joint
$\Phi_{u,FEA}$	rotation capacity of a joint obtained from FEA
$\Phi_{u,Test}$	rotation capacity of a joint from test
$\Phi_{u,cal}$	rotation capacity of a joint obtained from analytical calculation

Latin letters

A	percentage elongation after fracture
A_c	total cross-sectional area of concrete
$A_{c,eff}$	effective cross-sectional area of concrete
a_{cr}	distance between two consecutive cracks

A_{gt}	percentage elongation at maximum load
$A_{5.65}$	permanent strain in reinforcement after fracture within a length of 5.65 $\sqrt{A_{rebar}}$ around the fracture
A_{rebar}	cross-sectional area of one reinforcing bar
A_s	cross-sectional area of reinforcement
c_i	translational stiffness of basic joint component "i"
D	total beam depth
d	thickness of concrete flange
E_s	modulus of elasticity of steel
E_{cm}	secant modulus of elasticity of concrete
F_c	load bearing resistance of beam bottom flange in compression
F_{tr}	load bearing resistance of longitudinal reinforcement in tension
$f_{c,cyl}$	concrete compressive strength in cylindrical sample
f_{cd}	design value of concrete compressive strength
f_{ck}	characteristic compressive cylinder strength of concrete
f_{cm}	mean value of concrete cylinder compressive strength
$f_{ctk;0.05}$	5 % fractile of axial tensile strength of concrete
$f_{ctk;0.05}$	95 % fractile of axial tensile strength of concrete
f_{ctm}	mean value of axial tensile strength of concrete
f_{su}	measured tensile strength on reinforcement sample
f_{suk}	characteristic tensile strength of reinforcement
f_{sy}	measured yield strength on reinforcement sample
f_{syk}	characteristic yield strength of reinforcement
f_{syd}	design yield strength of reinforcement
f_u	measured tensile strength on structural steel sample
f_y	measured yield strength on structural steel sample
f_{yd}	design yield strength of structural steel
G_f	fracture energy of concrete
h_c	column depth
$h_{c,ef}$	effective concrete height
h_r	internal lever arm between longitudinal reinforcement and compression point of the joint
K	parameter for CDP model
k_b	factor considering the local bending of the concrete slab
k_i	stiffness coefficient of basic joint component "i"
L	beam length
L_j	effective joint length
L_t	transmission length
S_j	rotational stiffness of a joint
S_{EC}	rotational stiffness of a joint acc. to Eurocode
$S_{j,ini}$	initial rotational stiffness of a joint
$S_{j,Test}$	rotational stiffness of a joint measured in tests
M_{cr}	critical moment resistance of a joint at which the first crack occurs in the concrete slab
M_j	joint moment resistance
$M_{j,Rd}$	design moment resistance of a joint
$M_{pl,cal}$	measured plastic moment resistance of a joint
$M_{u,Test}$	measured maximal moment resistance of a joint
$M_{pl,hogg}$	hogging plastic moment resistance of a composite beam

$M_{pl,sagg}$	sagging plastic moment resistance of a composite beam
$M_{R,sagg}$	sagging moment resistance of a composite beam
n	factor considering the number of main cracks
w	crack width
$z_{i,0}$	vertical distance between the centroids of the uncracked unreinforced concrete flange and the uncracked unreinforced composite section

Terminology

basic component of a joint
Part of a joint that makes a contribution to one or more of its structural properties (EN 1993-1-8, 2005).

boltless joint
A joint configuration without bolts.

composite frame
A framed structure, in which some or all of the elements are composite members and most of the remainder are structural steel members (EN 1994-1-1, 2004).

composite joint
A joint between a composite member and another composite, steel or reinforced concrete member, in which reinforcement is taken into account in the design for the resistance and the stiffness of the joint (EN 1994-1-1, 2004).

composite member
A structural member with components of concrete and of structural or cold-formed steel, interconnected by shear connection so as to limit the longitudinal slip between concrete and steel and the separation of one component from the other (EN 1994-1-1, 2004).

connected member
Any member that is joined to a supporting member or element (EN 1993-1-8, 2005).

connection
Location at which two or more elements meet. For design purposes, it is the assembly of the basic components required to represent the behaviour during the transfer of the relevant forces and moments at the connection (EN 1993-1-8, 2005).

continuous beam
A beam connected to the supporting columns through continuous joints.

global analysis
The determination of a consistent set of internal forces and moments in a structure, which are in equilibrium with a particular set of actions on the structure (EN 1993-1-1, 2005).

joint
Zone where two or more members are interconnected. For design purposes, it is the assembly of all the basic components required to represent the behaviour during the transfer of the relevant forces and moments between the connected members. A beam-to-column joint consists of a web panel and either one connection (single sided joint configuration) or two connections (double sided joint configuration) (EN 1993-1-8, 2005).

joint configuration
Type or layout of the joint or joints in a zone within which the axes of two or more interconnected members intersect (EN 1993-1-8, 2005).

reinforcement ratio
Ratio between the longitudinal reinforcement area and the concrete area.

required joint rotation
The joint rotation required by the structural system to accommodate a plastic bending distribution in the beams.

rotation capacity
In the context of this thesis, it always refers to the available capacity of the joint to rotate at ultimate state.

semi-continuous beam
A beam connected to the supporting columns through semi-continuous joints.

simple beam
A beam connected to the supporting columns through simple joints.

structural properties of a joint
Resistance to internal forces and moments in the connected members, rotational stiffness and rotation capacity (EN 1993-1-8, 2005).

1 Introduction

1.1 Composite construction

The load bearing structure of buildings and bridges consists in most cases of more than one construction material, e.g. steel and concrete, steel and glass or timber and concrete. The most frequently used material combination encountered in construction is, however, that of steel and concrete. The reason for such a recurrent use of both materials lies in their mutual complementarity: steel is efficient in tension and concrete in compression. In reinforced concrete structures, for instance, additional steel reinforcement is provided in areas where tensile stresses are expected. Conversely, for areas of composite members in which steel parts are subjected to compression stresses, the use of concrete ensures a greater buckling resistance. Furthermore, concrete also protects the embedded steel parts against corrosion and thermal insulation at high temperatures.

Steel and concrete composites are conventionally subdivided into two categories: reinforced concrete and composite members (cf. Figure 1.1). This distinction is also anchored in the construction norms, EN 1992-1-1 (2004) providing design rules for reinforced concrete members and EN 1994-1-1 (2004) being the counterpart for composite members. One basic distinction between both types lies in the moment of inertia of the steel part. While in reinforced concrete members, the moment of inertia of the individual steel reinforcement bars is negligible, that of steel sections (commonly I-, H- or hollow sections) in composite members is substantially bigger. It is therefore useful to take advantage of this additional section inertia in design by ensuring a full interaction between both materials. This can be achieved by means of mechanical shear connectors (cf. Figure 1.1). In EN 1994-1-1 (2004), for example, the importance of shear connectors is highlighted in the definition of a composite member:

"*A composite member is a structural member with components of concrete and of structural or cold-formed steel, interconnected by shear connection so as to limit the longitudinal slip between concrete and steel and the separation of one component from the other*".

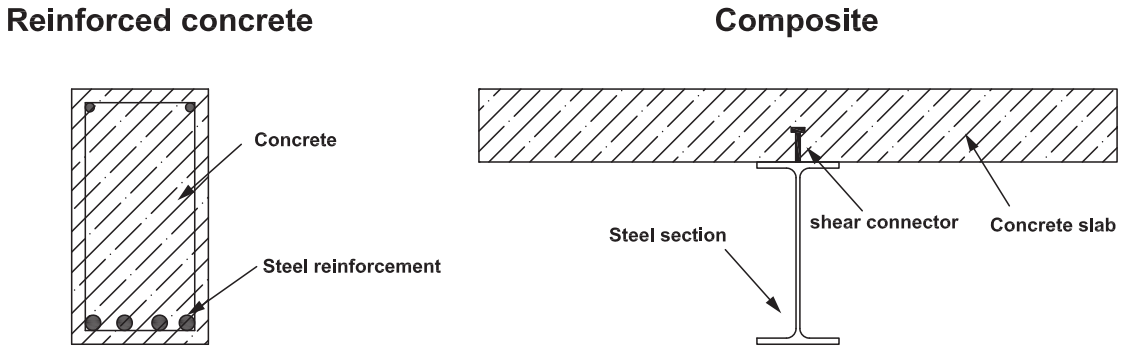

Figure 1.1: Comparison between reinforced concrete and composite member

Historically seen, the origin of composite steel and concrete structures dates back to the 19th century, when steel columns were encased in concrete with the purpose of increasing the fire resistance of steel structures (Couchman, 1994). Although both materials were used in conjunction at that time, the absence of shear connectors did not permit to consider the mixed section as a composite. Thus, steel was designed as the only load bearing component, while concrete was merely used as fire protection of the embedded steel parts.

The need of economical alternatives for reinforced concrete beams and faster construction processes during the erection of structures, boosted the investigation in the domain of composite construction. Hence, since the 1950s, the use of welded headed shear studs as a mechanical connection between steel beams and concrete slabs has become increasingly common (Maquoi and Chabrolin, 1998). The use of shear studs minimises the slip at the steel-concrete interface and assures hereby the composite interaction between steel beam and concrete slab. Due to this composite action, the stiffness and the resistance of composite structures raise significantly. The function of concrete in composite construction is thus extended from the mere fire protective action of steel sections to a load bearing action.

1.2 Composite frames and joints

In a traditional composite beam, the downstanding steel section is mechanically connected to the upper concrete slab (cf. Figure 1.1). Thus, both material components are ideally placed to bear sagging bending moments: the upper concrete flange is efficiently subjected to compression forces, while the steel section is mostly in tension (cf. Figure 1.2). However, when it comes to evaluate the hogging resistance of composite beams, the exploitation of the individual material properties is counter-productive since steel is in compression (local buckling) and concrete is in tension (concrete cracking). In this case, concrete is not bearing any stresses and the reinforcement embedded in the concrete slab is the only load bearing component of the slab (cf. Figure 1.2). Consequently, the hogging bending resistance $M_{pl,hogg}$ of a composite beam is smaller than its sagging resistance $M_{pl,sagg}$.

The position of composite beams within a framed structure is shown in Figure 1.3. In principle, a structural frame consists of three construction elements: slab elements, beams and columns. The composite beams supporting the slab system carry the loads to the columns, which in turn forward these to the foundations. The performance of the overall structure depends not only on the load bearing behaviour of the individual construction elements but also on the interplay between these different element types. The behaviour of the joints, interconnecting the beams to the supporting columns, may therefore substantially influence the design of the overall structure.

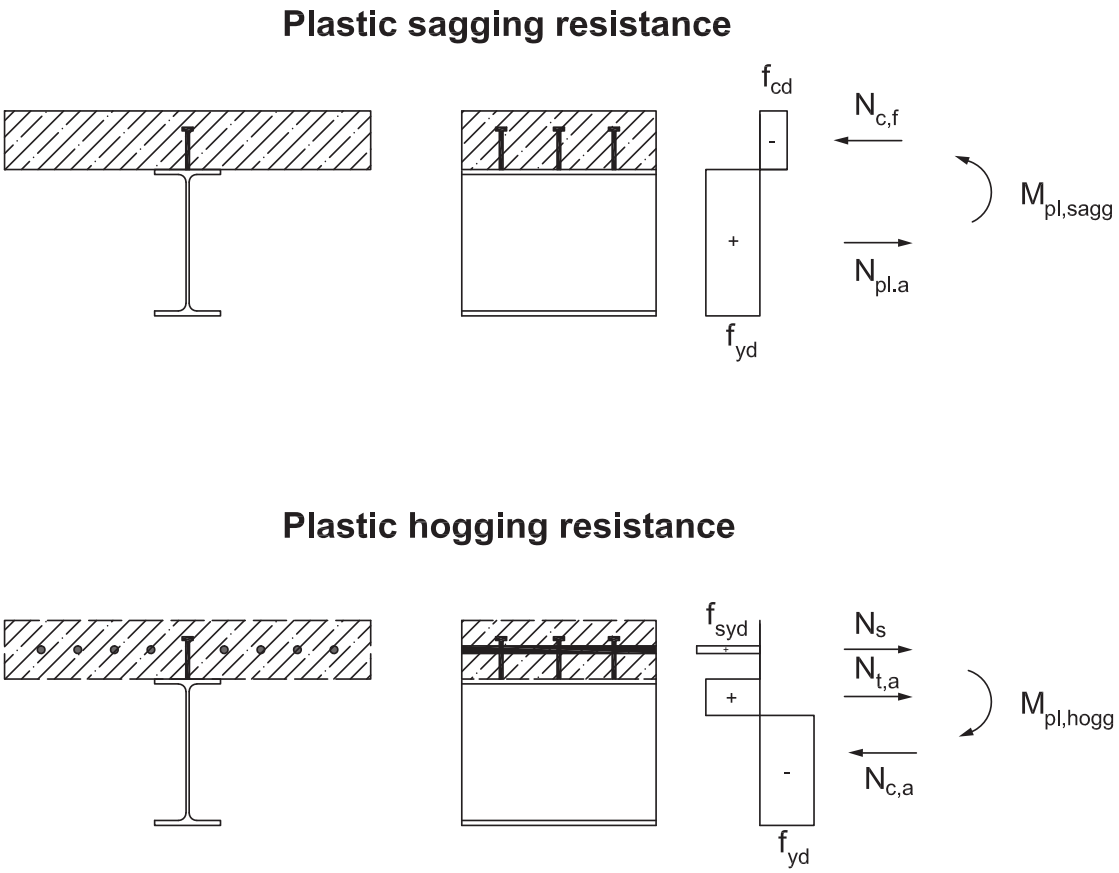

Figure 1.2: Plastic sagging and hogging resistances of composite beams

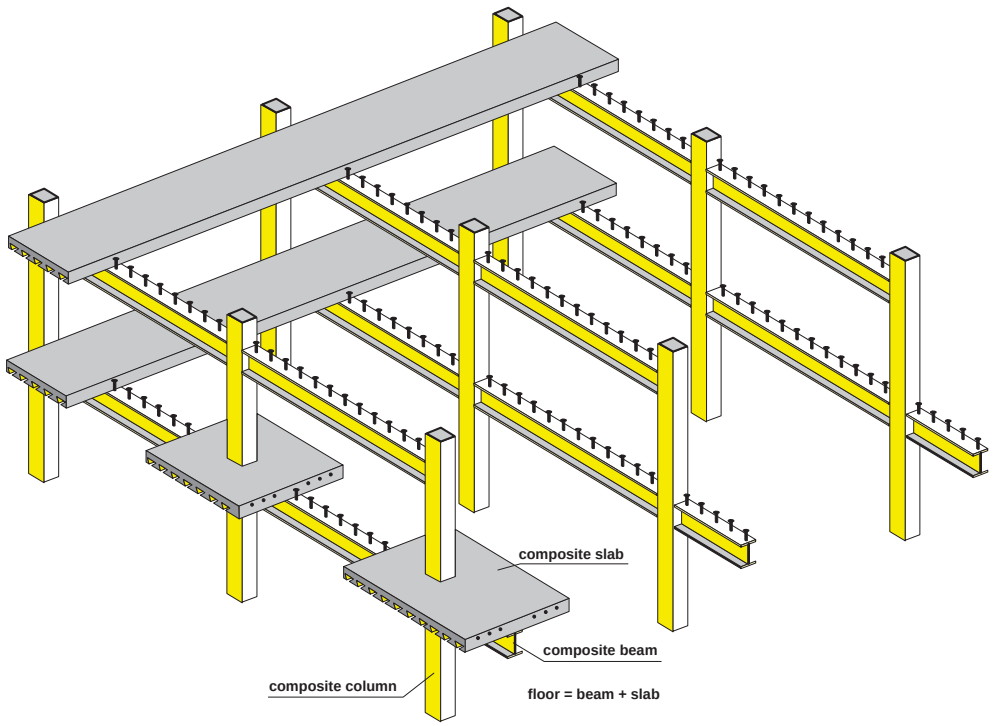

Figure 1.3: Construction elements in a composite structure (Huber, 2000)

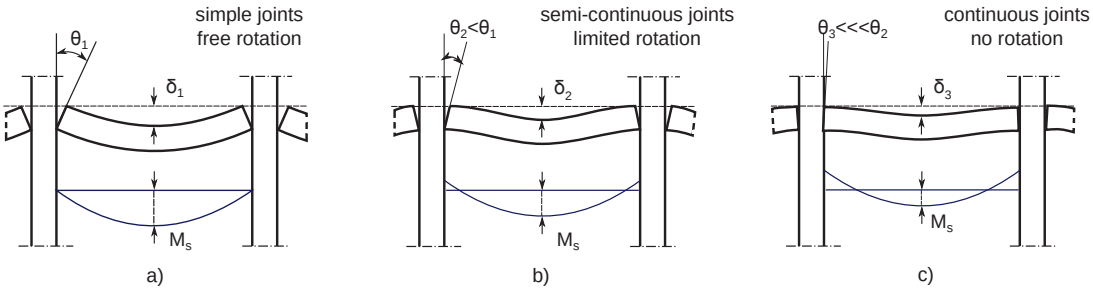

Figure 1.4: Beam-to-column joint modelling

In the design of beam-to-column joints, three types of joint models can be used: simple, semi-continuous or continuous joints (cf. Figure 1.4). EN 1993-1-8 (2005) provides a classification system for joints by stiffness and strength, which allows to categorize each joint in one of the above-mentioned model types (cf. Figure 1.5). Common practice, while designing non-sway composite frames according to EN 1994-1-1 (2004), is to model beam-to-column joints as simple or continuous joints. It is, however, nowadays generally accepted that these ideals represent extreme cases of true joint behaviour since most joints normally regarded as simple possess in reality some rotational stiffness and resistance, while joints which are regarded as continuous often display some flexibility and only a partial strength (Jones et al., 1983). Thus, in most cases, the real joint behaviour is more realistically represented using a semi-continuous modelling strategy, in which the joint stiffness and/or the joint resistance might be smaller than that of the adjacent beam.

Method of global analysis	Classification of joint		
Elastic	Nominally pinned	Rigid	Semi-rigid
Rigid-Plastic	Nominally pinned	Full-strength	Partial-strength
Elastic-Plastic	Nominally pinned	Rigid and full strength	Semi-rigid and partially strength Semi-rigid and full strength Rigid and partial-strength
Type of joint model	Simple	Continuous	**Semi-Continuous**

Figure 1.5: Classification of joints

The design of composite beams is not only affected by the behaviour of joints. The method of global analysis used to determine the action effects on the beams also play an important role. According to EN 1994-1-1 (2004), the action effects can be calculated using elastic or plastic global analysis in ultimate limit state. In an elastic analysis, the distribution of the internal forces is influenced by the stiffness of the joints. Thus, only a joint classification by stiffness is necessary (cf. Figure 1.5). The influence of the joint stiffness on the bending moment acting in a beam is demonstrated in the example illustrated in Figure 1.6.

In this example, a simple supported beam with a uniformly distributed load *q* is considered. Since in an elastic analysis, the only joint characteristic regulating the action effects is the joint stiffness S_j, it is sufficient to model the beam-to-column joint as a rotational spring. Three ranges for the joint stiffness are analysed:

- Simple joint with $S_j = 0$
- Continuous joint with $S_j = \infty$
- Semi-continuous joint with $0 < S_j < \infty$

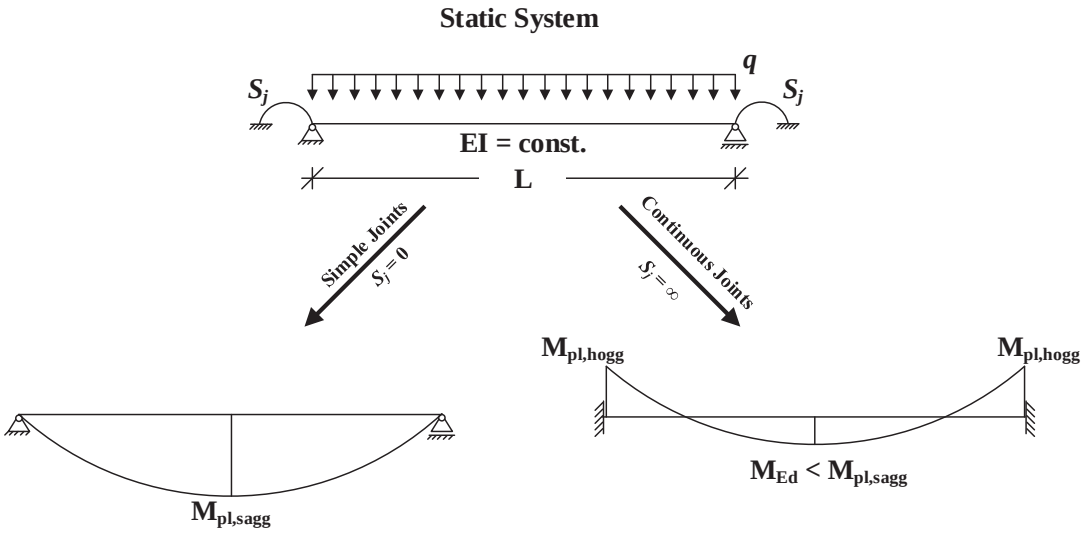

Figure 1.6: Bending moment distribution of simple and continuous beams acc. to elastic global analysis

For simple joints ($S_j = 0$), the load bearing capacity of the beam is reached when the acting bending moment is equal to the sagging bending resistance $M_{pl,sagg}$ in mid-span (cf. Figure 1.6). Assuming a constant bending stiffness EI for the beam over its length L, the elastic load bearing capacity of a simple beam $q_{el,simple}$ may be expressed by:

$$\frac{q_{el,simple} \cdot L^2}{8} = M_{pl,sagg} \Longrightarrow q_{el,simple} = \frac{8}{L^2} \cdot M_{pl,sagg} \tag{1.1}$$

For continuous joints ($S_j = \infty$), the large joint stiffness leads to a support bending moment larger than the sagging moment. In this case, the elastic load bearing capacity of the beam $q_{el,continuous}$ is obtained when the resistance of the beam is reached at the support $M_{pl,hogg}$:

$$\frac{q_{el,continuous} \cdot L^2}{12} = M_{pl,hogg} \Longrightarrow q_{el,continuous} = \frac{12}{L^2} \cdot M_{pl,hogg} \tag{1.2}$$

A comparison of equations (1.1) and (1.2) points out to the conclusion that for beams with homogeneous bending resistances in hogging and sagging regions (i.e. steel beams), the elastic load bearing capacity of continuous beams is larger than that of simple beams ($q_{el,continuous} > q_{el,simple}$).

However, the same conclusion cannot be extrapolated to composite beams. In fact, due to the above-mentioned discrepancy between the hogging and sagging resistance of composite beams ($M_{pl,sagg} > M_{pl,hogg}$), the elastic load bearing capacity of simple beams may, under certain circumstances, exceed that of continuous systems. In this particular example, if the hogging resistance of a composite beam is less than 2/3 of its sagging resistance (cf. equation (1.3)), simple joints represent a more economical modelling approach than continuous joints (in an elastic global analysis).

$$\begin{aligned} q_{el,continuous} &\leq q_{el,simple} \\ \frac{12}{L^2} \cdot M_{pl,hogg} &\leq \frac{8}{L^2} \cdot M_{pl,sagg} \\ M_{pl,hogg} &\leq \frac{2}{3} \cdot M_{pl,sagg} \end{aligned} \tag{1.3}$$

To counter this effect, EN 1994-1-1 § 5.4.4 allows the application of a limited moment redistribution within an elastic analysis. Although this regulation relieves the above-mentioned disadvantage for continuous composite beams, it is not sufficient for an economical design. In this context, semi-continuous composite joints appear as the most efficient solution since it allows for an optimal elastic bending distribution, in which the hogging and sagging resistance are attained simultaneously. Figure 1.7 illustrates the advantages of semi-continuous composite joints on the elastic load bearing capacity of composite beams ($q_{el,semi-rigid} > q_{el,pinned} > q_{el,rigid}$).

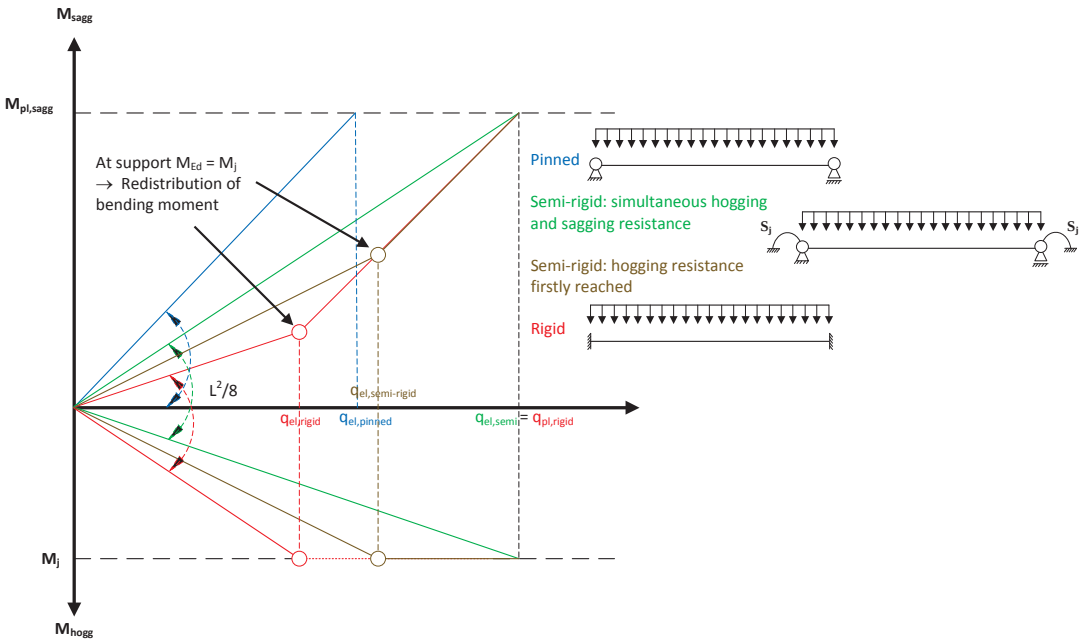

Figure 1.7: Acting bending moment at support M_{hogg} and at midspan M_{sagg} in function of joint stiffness and load

In addition to the already mentioned advantages, semi-continuous joints does not require expensive fabrication. In fact, a certain amount of reinforcement must always be provided in the concrete slab to control the crack occurrence, even for simple supported beams. In this context, clause 7.4.1(4) of EN 1994-1-1 (2004) provides the following condition:

"In cases where beams in buildings are designed as simply supported although the slab is continuous and the control of crack width is of no interest, the longitudinal reinforcement provided within the effective width of the concrete slab according to 6.1.2 should not be less than:

- *0.4 % of the area of the concrete, for propped construction*
- *0.2 % of the area of the concrete, for un-propped construction"*

In other terms, when beam-to-column composite joints are modelled as simple joints, a certain joint stiffness and strength (ensured by the continuous reinforcement) is always available. Thus, by simply adding some longitudinal reinforcement bars, a certain degree of semi-continuity between the beam and the column can be easily ensured, without need of costly and complex detailing.

1.3 Motivation

The case illustrated in Figure 1.7, in which the hogging and sagging resistances are reached simultaneously is theoretically possible. However, the practical relevance of this case is rather limited, since the joint stiffness and resistance are not independent quantities. If, for instance, some rebars are added to increase the joint stiffness, the joint resistance is inevitably also enhanced. Traditionally the stiffness of typical composite joints is such that, the hogging resistance $M_{pl,hogg}$ is reached first. In case of partial strength composite joints ($M_{j,pl} < M_{pl,hogg}$), the hogging resistance is attained even earlier due to the more accentuated discrepancy between hogging $M_{j,pl}$ and sagging resistance $M_{pl,sagg}$ (cf. Figure 1.8). A significant portion of the sagging resistance remains therefore unused.

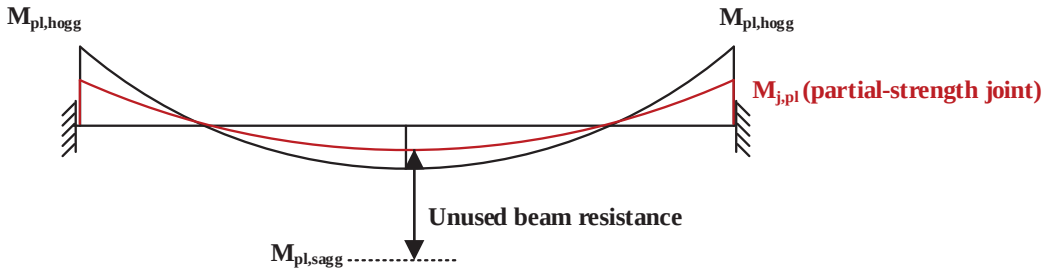

Figure 1.8: Comparison between composite beam with full-strength joints $M_{j,pl} = M_{pl,hogg}$ and partial-strength joints $M_{j,pl} < M_{pl,hogg}$ for an elastic analysis

In order to profit from the sagging resistance of the beam, EN 1994-1-1 (2004) allows under specific conditions to apply the plastic global analysis by accounting for the available rotation capacity of the joint (cf. Figure 1.9). Greater load bearing capacities are consequently achieved . This design approach is particularly interesting for partial-strength composite joints, where per definition, the joint resistance is smaller than that of the adjacent member.

While no restriction is provided for the elastic global analysis, the plastic global analysis is subjugated to certain conditions. The most important one concerns the rotation to which members and joints are subjected, when it comes to moment redistribution within the structural system. For structural members, a useful tool is the cross-section classification, provided by EN 1993-1-1 (2005) and EN 1994-1-1 (2004) to verify the rotation requirements. Regarding the rotation requirements of composite joints, EN 1994-1-1, clause 8.3.4(2) refers to experimental proof. Since no other alternative to experimental evidence is provided by EN 1994-1-1 (2004), the use of semi-continuous composite joints finds nearly no application in practice.

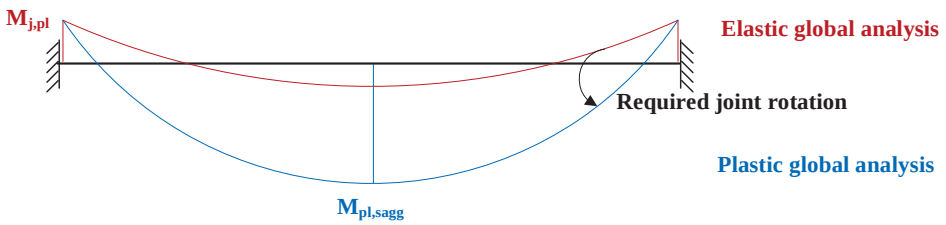

Figure 1.9: Comparison between elastic and plastic global analysis

The only case where the rotation capacity of a beam-to-column joint needs not be expressively determined, are full-strength composite joints with a design resistance of at least 1.2 times that of the adjacent beam (EN 1994-1-1, clause 5.4.5(4)). In this case, the plastic hinge will develop in the beam and not in the joint. The rotation requirements must therefore be supplied by the adjacent beam member itself. A classification of the beam's cross-section in class 1 is sufficient in this case.

In a profitable design strategy, the objective is always to take advantage of the available joint and member capacities in both, hogging and sagging, regions. At ultimate limit state, this is only possible in combination with the plastic global analysis of the structural system. For partial-strength beam-to-column joints, this analysis requires that the joints are able to sustain their plastic resistance moments for a sufficient rotation capacity. Because no analytical assessment method is provided in EN 1994-1-1 (2004) for the rotation capacity of composite joints, practitioners are impeded to efficiently design composite beams, preferring therefore to assume simple beam-to-column joints and to neglect hereby the available joint capacities. This issue represents a shortcoming aspect in the design of composite members. It is the objective of the present research project to overcome this hurdle.

1.4 Research objectives

The purpose of this work is to provide an analytical method, which allows to predict the rotation capacity of composite joints. This method should complete the understanding and knowledge about the behaviour of composite joints. In order to achieve this objective, the hereafter described methodology is applied.

The first step consists in performing an extensive literature review to gather the relevant experiences made by other researchers on the load bearing behaviour of composite joints. Experimental, numerical and theoretical investigations are therefore carefully scrutinised to develop a broad understanding of the joint's behaviour.

Based on the study of the state of the art (cf. Chapter 2), an experimental test program is elaborated to investigate the influence of well-defined parameters on the behaviour of composite joints. These parameters are chosen because they influence the rotation capacity of composite joints and lack in thorough investigations. In fact, as it is shown in Chapter 2, many investigations were conducted on the influence of the longitudinal reinforcement ratio. However, only a few have considered the influence of the rebar diameter independently from that of the reinforcement ratio, since, in most of the experimental investigations, an increase in reinforcement ratio was frequently accompanied by larger rebar diameters. In more recent investigations, however, it was demonstrated that the sole change of rebar diameter can significantly affect the rotation capacity of composite joints. For this reason, the present research work is focussed on the investigation of the following parameters:

- Longitudinal reinforcement ratio ρ and
- Diameter of the longitudinal reinforcement bars $\varnothing$.

In Section 1.3 it was shown that the application of the plastic method of global analysis requires large rotation capacities. Therefore, the test specimens were designed with a significant amount of longitudinal reinforcement ratio and large rebar diameters. Although the primary focus lies in the rotation capacity of composite joints, the influence of these

parameters on the joint's stiffness and resistance is also investigated.

The test campaign carried out within this research project is not limited to the investigation of the aforementioned parameters. The influence of steel endplate connections on the three main structural properties of joints is also studied through an appropriate test program. The objective is to analyse to what extent, the combination of ductile steel connections and large reinforcement ratios influences the stiffness, resistance and rotation capacity of composite joints.

A lot of different test campaigns have been conducted to investigate the rotational behaviour of composite joints with traditional composite beams (cf. Chapter 2). It is to underline that the tests in this research work have been conducted to enlarge the experimental data basis with composite slim-floor beams (CoSFB). The particularity of the CoSFB resides in the fact that the shear connection is achieved by reinforcing dowel bars instead of the traditional shear studs (cf. Figure 1.10). More information about this type of shear connectors is provided by Braun et al. (2014a,b).

A further objective of the present thesis is to develop an advanced finite element (FE) model to simulate the behaviour composite joints. The software (Abaqus 6.14, 2014) is used to elaborate this FE model. The numerical model is validated by the experimental tests performed in the present research work and constitutes therefore an additional analysis tool, which helps to understand more deeply the complex behaviour of joints. In other words, it allows to understand how the different components of a composite joint interact, and to what extent this interplay affects the overall joint's behaviour. The aim of this numerical model is also to perform a parametric study on the influence of the reinforcement component in the joint.

Finally, analytical calculation methods are proposed to determine the three main joint's properties based on the analysis of the experimental and numerical results. These methods are used to predict the results of former experimental investigations on composite joints. An application range for these new calculation methods is also defined.

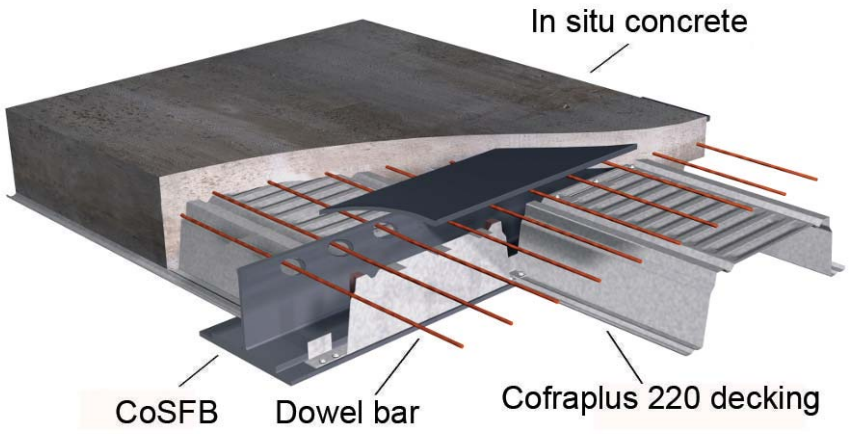

Figure 1.10: Composite slim-floor beam CoSFB (Braun et al., 2014b)

1.5 Structure of the thesis

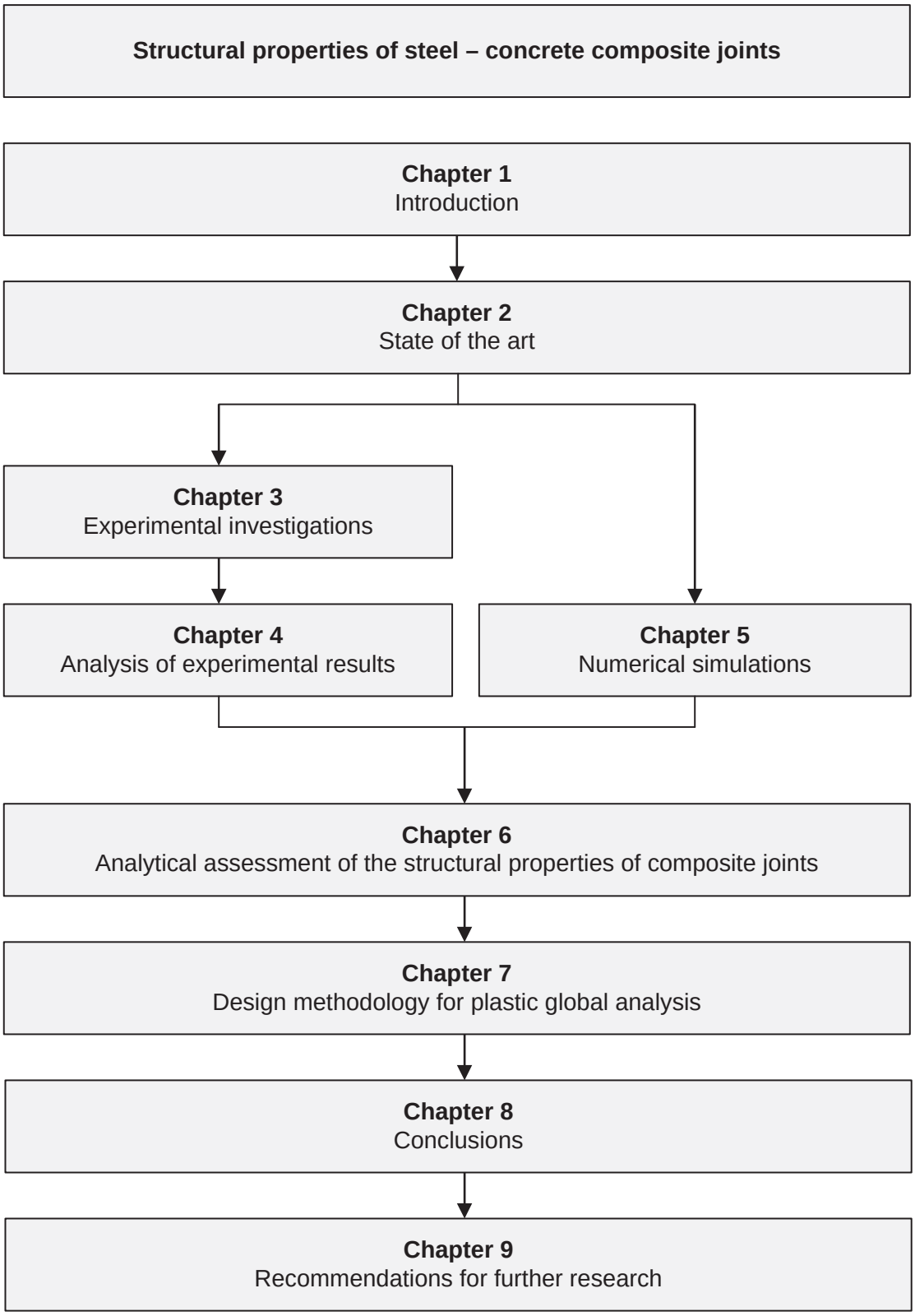

Figure 1.11: Structure of the thesis

The structure of the thesis is shown in Figure 1.11. To begin with, a short **introduction** is presented in Chapter 1, in which the motivation and the purpose of the present research are exposed.

In Chapter 2, the **state of the art** in the field of composite joints is given. This Chapter focuses on the experimental, analytical and numerical investigations conducted on the load bearing behaviour of composite joints.

In Chapter 3, the **experimental investigations** carried out in the framework of the present research are described. The test program and the investigated parameters are presented. Details about the instrumentation, testing procedure and the material properties are furthermore provided.

Chapter 4 introduces the **experimental results** of the test campaign described in the previous Chapter. The results are analysed emphasising on the characteristic properties of composite joints; stiffness, resistance and rotation capacity.

In Chapter 5, the **finite element model** aiming to study the behaviour of composite joints is described. More results on the behaviour composite joints with different reinforcement properties are presented in a parametric study conducted on behalf of the validated FE model.

In Chapter 6, the **analytical approach** to assess the characteristic properties of composite joints is described. A new analytical model for the rotation capacity is derived and an adaptation of the current standard for the joint stiffness is suggested on experimental basis.

In Chapter 7, a **design methodology** allowing for the plastic global analysis of semi-continuous composite beams is proposed. A simplified procedure is provided to calculate the required joint rotation. Furthermore, design charts are given to facilitate the determination of the available rotation capacity. On this basis, a ductility class for composite joints is defined which allows the direct application of the plastic analysis without explicit verification of the joint rotation.

In Chapter 8 the main **findings** of the present research are emphasized.

Finally, in Chapter 9, an **outlook** on further research work is given.

2 State of the art

2.1 Introduction

Research investigations on the load bearing behaviour of composite joints date back to the 1960s. Since then, innumerable researchers performed experimental, numerical and analytical investigations to develop a broad understanding of the characteristic behaviour of composite joints. These investigations are reported in diverse literature types as doctoral theses, research articles or books. The analysis of the existing literature is therefore of great importance to acquire a good overview on this particular topic. This analysis allows to distinguish between what has been accomplished and what still needs to be completed.

In the present Chapter, all the relevant investigations carried out in the field of composite joints are compiled in three Sections. In the first Section, a broad collection of experimental, analytical and numerical research works is presented. All the research programs are described in a chronological structure with information about the author, objectives and results of each study. Since the focus of the present research work lies in the assessment of the key properties of composite joints under static conditions, the investigations involving cycling loading of composite joints are omitted.

The second Section addresses the investigation performed on the required joint rotation allowing for a global plastic analysis. In order to design a composite beam with composite joints using the plastic analysis, it must be verified that the required joint rotation Φ_{req} is less than the joint's rotation capacity Φ_u (cf. Figure 2.1). The objective of this section is therefore to expose the factors influencing the required joint rotation Φ_{req} as well as the available solutions to calculate its value. While the first section occupies mainly with the structural properties of joints (right-hand side of Figure 2.1), the second section deals with the required joint rotation, which depends also on the structural system and properties of the beam (left-hand side of Figure 2.1).

In the last Section, the most relevant conclusions emanating from this literature review are summarised.

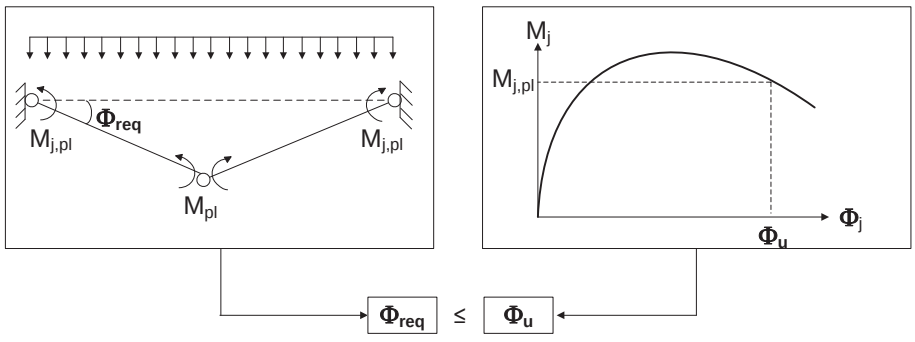

Figure 2.1: Definition of required joint rotation Φ_{req} and rotation capacity of joint Φ_u

2.2 Investigations on the properties of composite joints

The idea of semi-continuity of composite joints was first suggested in 1970 as an alternative modelling approach to continuous composite joints (Barnard, 1970). This idea emanated from investigations performed at the end of the 1960s on the behaviour of continuous composite beams (Johnson et al., 1966; Climenhaga and Johnson, 1972). From these investigations, severe limitations resulted for the slenderness of the beam's web and compression flange to ensure sufficient rotation capacity to composite beams. Barnard proposed controlling the buckling effect through a limited amount of steel reinforcement. Thus, the full continuity of composite joints was not guaranteed, leading to joints with semi-rigid and partial-strength behaviour.

Following these theoretical considerations, Johnson and Hope-Gill (1972) conducted the first experimental studies on the behaviour of semi-continuous composite joints (cf. Figure 2.2). They concluded that semi-rigid composite joints provide a resistance exceeding that of the steel joints and a well-defined stiffness, of which advantage can be taken in the design of beams. Besides, they observed that the rotation capacity of composite beams with semi-rigid composite joints is influenced by the failure of the reinforcement bars instead of the typical flange buckling occurring in rigid jointed beams. A force ratio $A_t f_r / A_g f_y$ was defined, where $A_t f_r$ is the axial resistance of the reinforcement and $A_g f_y$ that of the steel beam section. In Climenhaga and Johnson (1972) it was concluded that for rigid jointed beams, the higher this force ratio, the more critical is web buckling of the column.

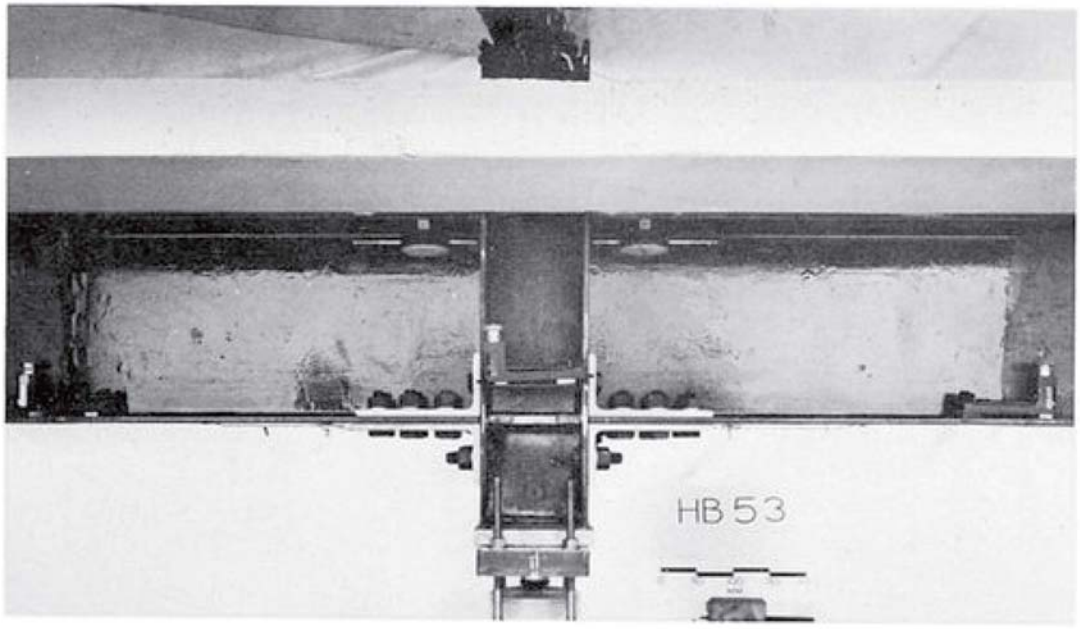

Figure 2.2: First tests on composite joints by Johnson and Hope-Gill (1972)

After these pioneering experimental investigations, many other research projects were initiated to investigate composite joints in-depth. In the literary review published by Zandonini (1989), the main experimental research programs performed before 1989 on the behaviour of composite joints are extensively presented. The investigations conducted by Echeta (1982), Van Dalen and Godoy (1982), Law (1983), Benussi et al. (1986) and Leon and Lin (1986) are only some of the investigations addressed. An equally extensive collection of available experimental data on composite joints was collated by Najafi (1992). Given that the investigations

of the above-mentioned authors are presented in great detail by Zandonini and Najafi, the focus of the present state of the art is put onto more recent investigations. Nevertheless, for the sake of completeness, the most pertinent outcomes of these investigations are included in the concluding summary of the present Chapter.

In 1990, the first tests on composite joints with steel decking were conducted by Davison et al. (1990). A total of 12 tests were performed on composite joints and seven tests on bare steel joints to compare the behaviour of steel connections with that of composite connections. The flexible steel connection comprised a bolted seat cleat with a single-sided web cleat (cf. Figure 2.3). The aim of this study was furthermore to investigate the effect of deck direction, column orientation, internal or external column position and slab reinforcement. The results demonstrated that composite joints present greater stiffness and strength than steel joints. Negative moment capacities approaching that of bare steel beams were attained for the composite joints with more than only mesh reinforcement. Due to the limited ductility of welded fabric mesh, composite joints with only light anticrack mesh reinforcement presented a brittle behaviour. Owing to this fact, it was considered unwise to rely solely on mesh to provide tensile reinforcement.

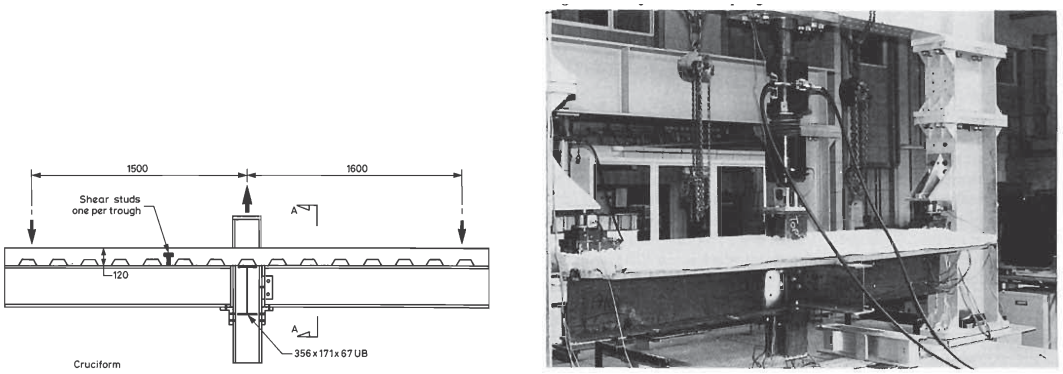

Figure 2.3: Experimental investigations by Davison et al. (1990)

At the same time, a project known as COST C1 program and supported by the European Cooperation in the Field of Scientific and Technical Research, was set up to coordinate the research in this area and to develop general rules and guidelines for the design of composite joints (Cost C1, 1996). Notorious members of this group are among others, D. Anderson, H. Bode, J.-P. Jaspart, A. Colson, G. Huber, F. Tschemmernegg, J.-M. Aribert, F. Benussi, K. Weynand and Y. Xiao. This project assembled the results of different broad test programs. It was for example, in the framework of this program, that Tschemmernegg developed the well-known component model, in which the composite joint is subdivided into 16 components, each of them being represented by a spring (cf. Figure 2.4). With the help of this component method, nowadays incorporated in Eurocode 3 and Eurocode 4, a method to predict the design resistance and the elastic stiffness of composite joints was developed. Huber (2000) gives a detailed description of this component approach in his doctoral thesis and summarises concisely the outcome of the investigations performed within the COST C1 program.

Altmann et al. (1991) studied the behaviour of 38 interior composite joints at the University of Liège. Two types of cleat connections were tested, which differed only by the presence or absence of cleats connecting the upper flange of the beam to the column flange (cf. Figure 2.5). The composite action of the joints was ensured by two layers of 6 rebars. The main parameters investigated were the number of cleat connections (2 or 3 cleats), the thickness

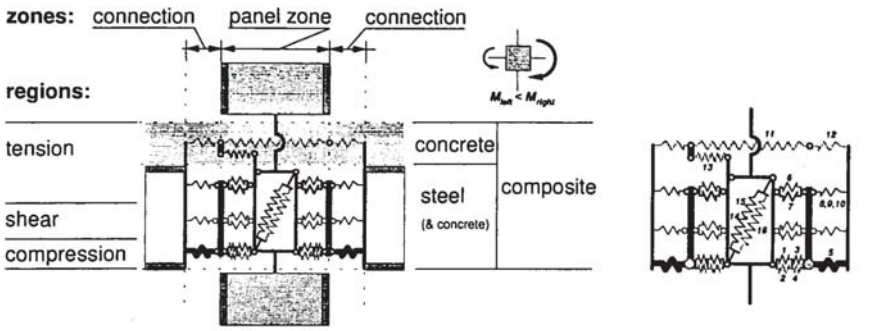

No.	component	zone	region	group
1	interior steel web panel	panel zone	compression	3
2	**concrete encasement**	panel zone	compression	3
3	exterior steel web panel (column flange+local effects)	panel zone	compression	3
4	**effect of concrete encasement on exterior spring**	panel zone	compression	3
5	beam flange (local effects), contact plate, end plate	***connection***	compression	6
6	steel web panel incl. part of flange, fillet radius	panel zone	***tension***	1
7	stiffener in tension	panel zone	***tension***	1
8	column flange in bending (stiffened)	***connection***	***tension***	4
9	end plate in bending , beam web in tension	***connection***	***tension***	4
10	bolts in tension	***connection***	***tension***	4
11	**reinforcement (within panel) in tension**	*panel / conn.*	***tension***	1 / 4
12	**slip of composite beam (due to incomplete interaction)**	*panel / conn.*	***tension***	1 / 4
13	**redirection of unbalanced forces**	*panel / conn.*	***tension***	1 / 4
14	steel web panel in shear	panel zone	*shear*	2
15	steel web panel in bending	panel zone	*shear*	2
16	**concrete encasement in shear**	panel zone	*shear*	2

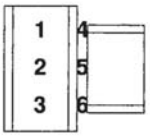

Figure 2.4: Component model (Cost C1, 1996)

of the cleats (10 mm or 13 mm) and the reinforcement ratio of the concrete slab (0.67 %, 1.3 % and 2.1 %). Different rebar diameters (10 mm, 14 mm and 18 mm) were used to obtain different reinforcement ratios. This has to be borne in mind when comparing the tests with different percentage of reinforcement since the influence of the rebar diameter is inevitably enclosed in the results. The test results witnessed a beneficial influence of the reinforcement ratio on the rigidity and resistance of the connection (cf. Figure 2.5). Furthermore, it was observed that a substantial rotation capacity could be achieved if the collapse of the specimen is linked to excessive yielding of the reinforcement. For large reinforcement ratios, the failure of the specimen was governed by buckling of the column web, limiting therefore the rotation capacity of the corresponding composite joints. Conversely, small reinforcement ratios enabled the plastic activation of the reinforcement allowing for larger rotation capacities.

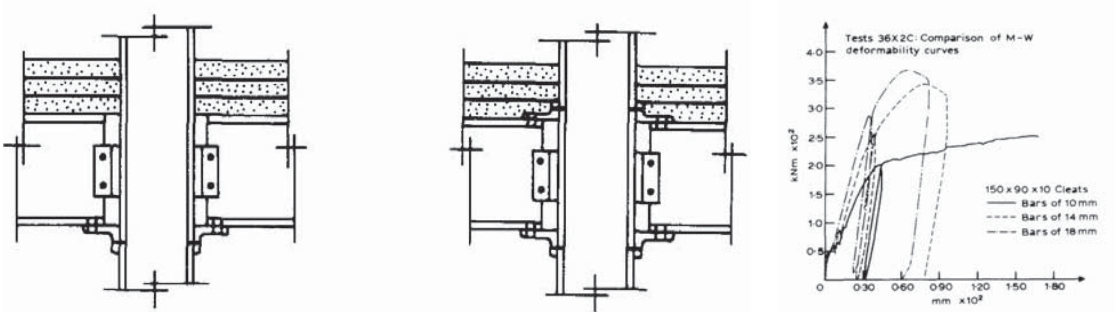

Figure 2.5: Experimental investigations by Altmann et al. (1991)

One year later, Najafi (1992) conducted nine tests on composite and two tests on bare steel joints at the University of Warwick (cf. Figure 2.6). Major and minor axis connections with

profile steel sheeting were investigated. The steel connections consisted of flush endplate connections, except for one test with extended configuration of the endplate. The parameters investigated were the reinforcement ratio, degree of shear connection and the magnitude of unbalanced bending transmitted to the column. Najafi concluded that the ductility of the rebars has a significant influence on the rotation capacity of composite joints and that the bending resistance of composite joints increases with larger amount of reinforcement. It was furthermore observed that increasing the depth of the steel beam induces a larger joint stiffness with consequently lower rotation capacity. Moreover, minor axis connections were stiffer but less ductile than major axis connections. In his thesis, Najafi proposed an analytical method to predict the moment resistance and stiffness of composite joints. In addition, an empirical method was proposed to determine the rotation capacity required for end connections in order to develop a full plastic mechanism. He concluded that the requirements for the joint rotation increase with bigger span but decrease for bigger steel sections. He also stated that the required joint rotations depend only on the resistance distribution at ultimate state and not on the joint stiffness.

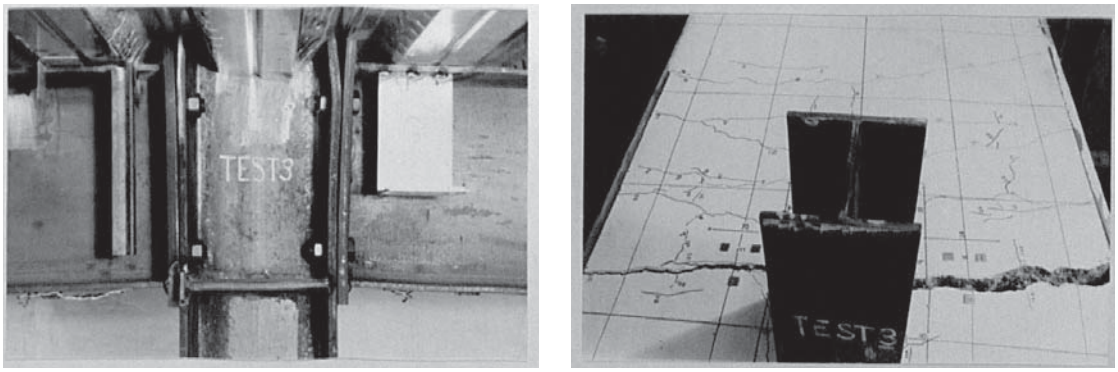

Figure 2.6: Experimental investigations by Najafi (1992)

In Rennes, Aribert and Lachal (1992) performed two tests on major axis steel connections and eight on composite connections with symmetrical cruciform arrangement. The aim was to investigate the influence of slip and type of bolted endplate connection (flush or extended) on the behaviour of composite joints. He concluded that the more rigid and resistant a steel connection, the less the influence of the reinforcement component in the concrete slab. Furthermore, the tests showed that the larger the reinforcement ratio, the larger must also the ductility of the steel connection be to allow for the plastic activation of the reinforcement. An attempt to evaluate the rotational stiffness is presented in which the effect of slip due to partial shear connection is taken into account. In (Aribert, 1995), a design approach for the rotation capacity is also proposed, which considered the elongation of the reinforcement bars over half the column height as well as slip at ultimate state.

Kathage (1994) studied the structural behaviour of semi-continuous and continuous composite joints . A test program involving 16 tests, categorised in 3 series was carried out (cf. Figure 2.7). The first series comprised seven internal beam-to-column composite joints without steel connection. The second series consisted of 6 beam-to-beam composite joints with additional bolted finplate connection. In the third series, continuous composite joints were tested aiming to deduce the influence of the compressive stresses in the column profile. The parameters of this study were: reinforcement ratio, dimension of the contact plate for the transmission of the compression force in the bottom of the beam and the influence of the shear force on the

behaviour of the joint. Several conclusions emerged from this study. It was again observed that mesh reinforcement limits the ductility of a composite joint in comparison to a joint with equal reinforcement ratio and reinforcing bars. The joints with additional finplate presented a slightly higher bending resistance. Moreover, local buckling of the beam flange occurred for tests with large reinforcement ratios, despite the class 1 classification of the beam flange. The shear force did not affect the bending resistance of the joints.

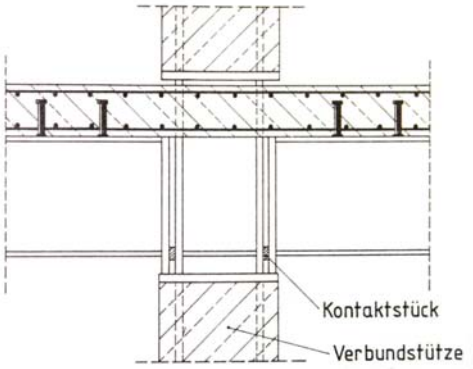

Vers. Nr.	Bew. Φ [mm]	Bewehrungsgrad μ [%]	Kontaktstück cb [mm]	Drucklasche cb [mm]	Zentrierleiste cb [mm]	l_k [m]	P_1 [kN]
VT 1.1	12	1,06	15 × 40 × 180	—	—	2,290	—
VT 1.2	14	1,44	15 × 40 × 60	—	—	2,185	—
VT 1.3	12	1,06	15 × 40 × 60	—	—	2,185	—
VT 2.1	10	0,74	15 × 40 × 180	—	—	2,185	—
VT 2.2	Matte R589	0,74	15 × 40 × 180	—	—	2,185	—
VT 2.3	14	1,44	15 × 40 × 180	—	—	2,185	—
VT 2.4	12	1,41	15 × 40 × 180	—	—	1,250	—
VT 3.1	12	1,06	—	13^5 × 210 × 607	—	2,185	—
VT 3.2	10	0,74	—	13^5 × 210 × 607	—	2,185	—
VT 3.3	14	1,44	—	13^5 × 210 × 607	—	2,185	—
VT 4.1	12	1,06	—	13^5 × 210 × 607	—	1,250	—
VT 4.2	10	0,74	—	13^5 × 210 × 607	—	1,250	—
VT 4.3	14	1,44	—	13^5 × 210 × 607	—	1,250	—
VT 5.1	10	0,65	—	—	25 × 40 × 90	2,000	650
VT 5.2	10	0,65	—	—	25 × 40 × 90	2,000	—
VT 5.3	10	0,65	—	—	25 × 40 × 160	2,000	1200

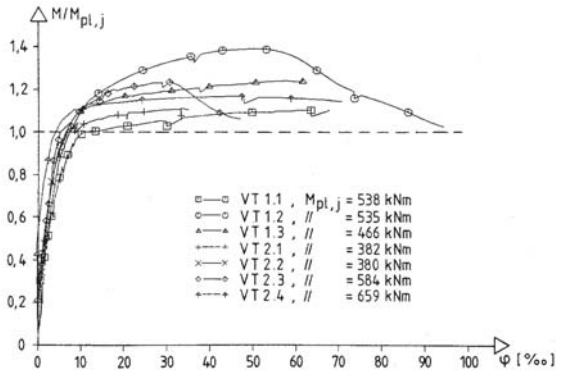

Figure 2.7: Experimental investigations by Kathage (1994)

At the same time, Xiao et al. (1994) initiated an experimental campaign built up on the pilot study of Davison on composite joints with metal decking. 20 composite joints were designed with four different types of steel connections: seating cleat with double web cleats, flush endplates, partial depth endplates and finplates (cf. Figure 2.8). Another parameter investigated in this study was the reinforcement ratio. It could be again concluded on the beneficial effect of larger ratios on stiffness and resistance. The test results showed that a web stiffnener in the compression zone of the column increases the moment resistance of composite joints, without influencing the rotation capacity (cf. Figure 2.8). Alternatively to column web stiffeners, framed-in beams connected to the minor axis of the column proved to be effective in the prevention of web buckling. Excessive deformation of the column flange was, however, observed and could only be avoided by the introduction of backing plates on the column flange. The ideal position of partial depth endplate connections for composite purposes was also studied as well as the behaviour of external beam-to-column composite joints. It was found that a lower placed partial endplate connection presents a better performance and it was suggested to design a simple zero moment capacity joint for the edge and corner joints in order to avoid complicated anchorage reinforcement detailing around the column.

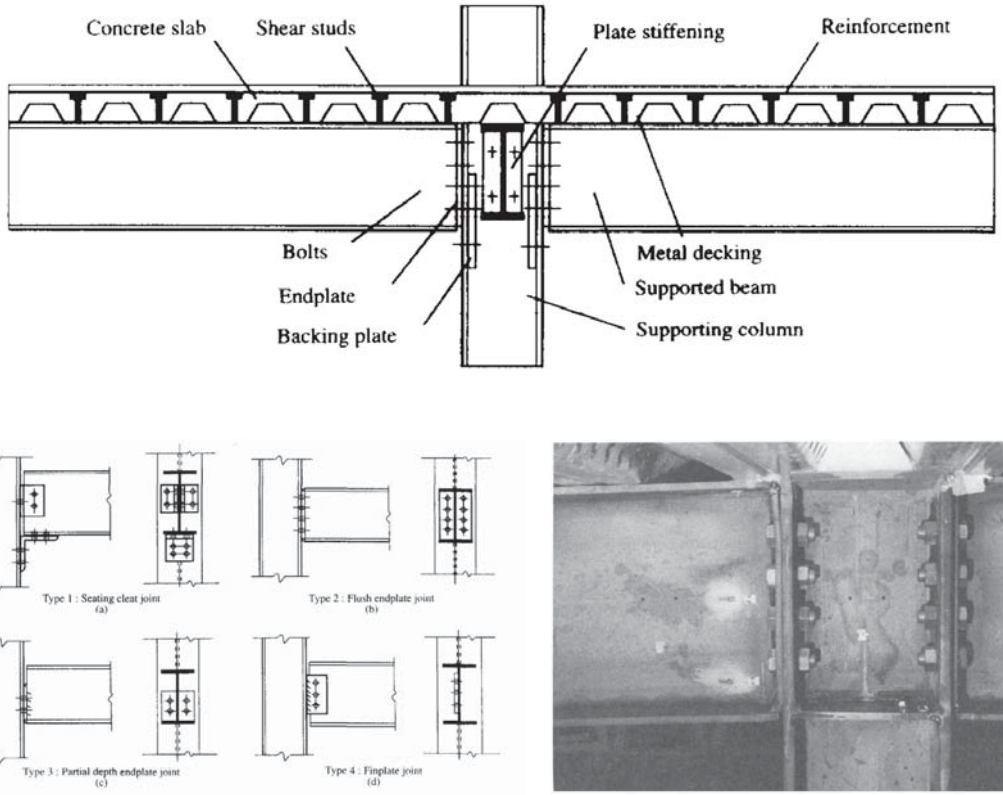

Figure 2.8: Experimental investigations by Xiao et al. (1994)

In Lausanne, Ren (1995) carried out 11 laboratory tests on bare steel joints and three on composite joints. Two types of steel connections were tested; one with bolted web cleats (pinned connection) and one with more rigid flush endplate connections. The concrete slab was reinforced with light mesh. The influence of four additional $\varnothing 12$ rebars was investigated. The results showed a better performance in terms of resistance, stiffness and rotation capacity with these additional rebars. Non-ductile behaviour of joints with only mesh reinforcement was again confirmed. In comparison to bare steel joints, the composite joints tested by Ren provided larger bending resistance but lower rotation capacity (cf. Figure 2.9). Ren developed a non-linear numerical model program called COJOINT to assess the moment-rotation characteristics of composite joints. This program provided good agreement with 14 tests of composite joints. A parametric study was performed with this model to analyse the influence of some parameters on the behaviour of composite joints. A simplified analytical method was proposed for the moment resistance and stiffness of composite joints.

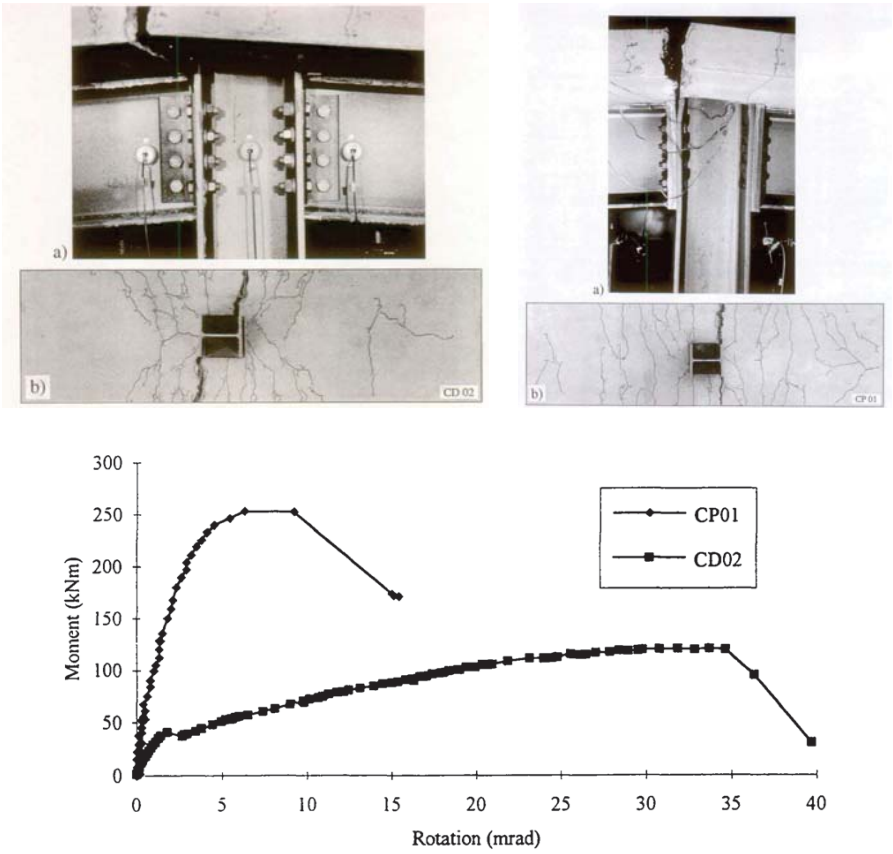

Figure 2.9: Experimental investigations by Ren (1995)

Later, in 1996, the effect of high shear-to-moment ratios and unbalanced moments was analysed in the research work conducted by Li et al. (1996). One test on pure steel joint and six tests on flush composite connections were conducted (cf. Figure 2.10). All tests were stopped due to the stroke limit of the loading equipment so that no specimen failure could be identified. It was found that variations in shear force have little effect on the moment capacities of flush endplate composite connections. An influence was only observed when the shear force was relatively high in comparison to the shear capacity of the steel beam (Li et al., 1996). Concerning the effect of non-symmetrical moments in the nodal region of the column, a notable influence was only observed when the unbalanced rebar force was higher than the shear resistance of the column web.

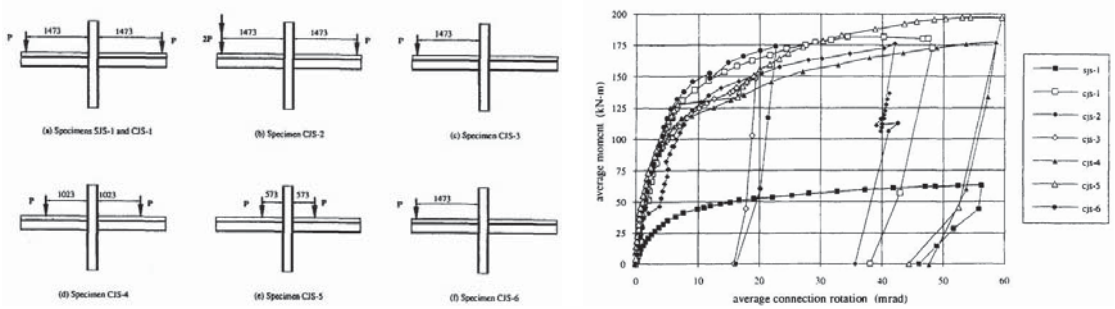

Figure 2.10: Experimental investigations by Li et al. (1996)

In Kaiserslautern, Bode and Kronenberger (1996) presented the results obtained by the research group established in 1991 by the German Research Foundation (DFG) . Symmetrically loaded cruciform tests representing composite joints were performed with the aim of investigating the influence of distribution and degree of shear connection, as well as amount of reinforcement on the behaviour of composite joints. The results showed that partial shear connection and unpropped construction allow for larger rotation capacities. Besides, it was concluded that the rotation capacity of composite joints depends on the position of the first shear stud. The greater the distance of the latter to the column flange, the longer is the tensile band activated in the reinforced concrete slab and the larger is the rotation capacity (cf. Figure 2.11).

Two years later, the same authors published the results of additional tests performed by Elz (2000) on the influence of the reinforced slab component (Bode and Kronenberger, 1998). The beneficial influence of the reinforcement ratio on the stiffness, resistance and rotation capacity of finplate composite joints was again observed (cf. Figure 2.11). In the same period, Michaeli performed 15 more tests on internal composite joints with finplate and flush endplate connections (Bode et al., 1997). Once more, this study showed the brittle behaviour of composite joints with mesh reinforcement. It could also be noted that the stiffness of the joint increases if the column web is stiffened .

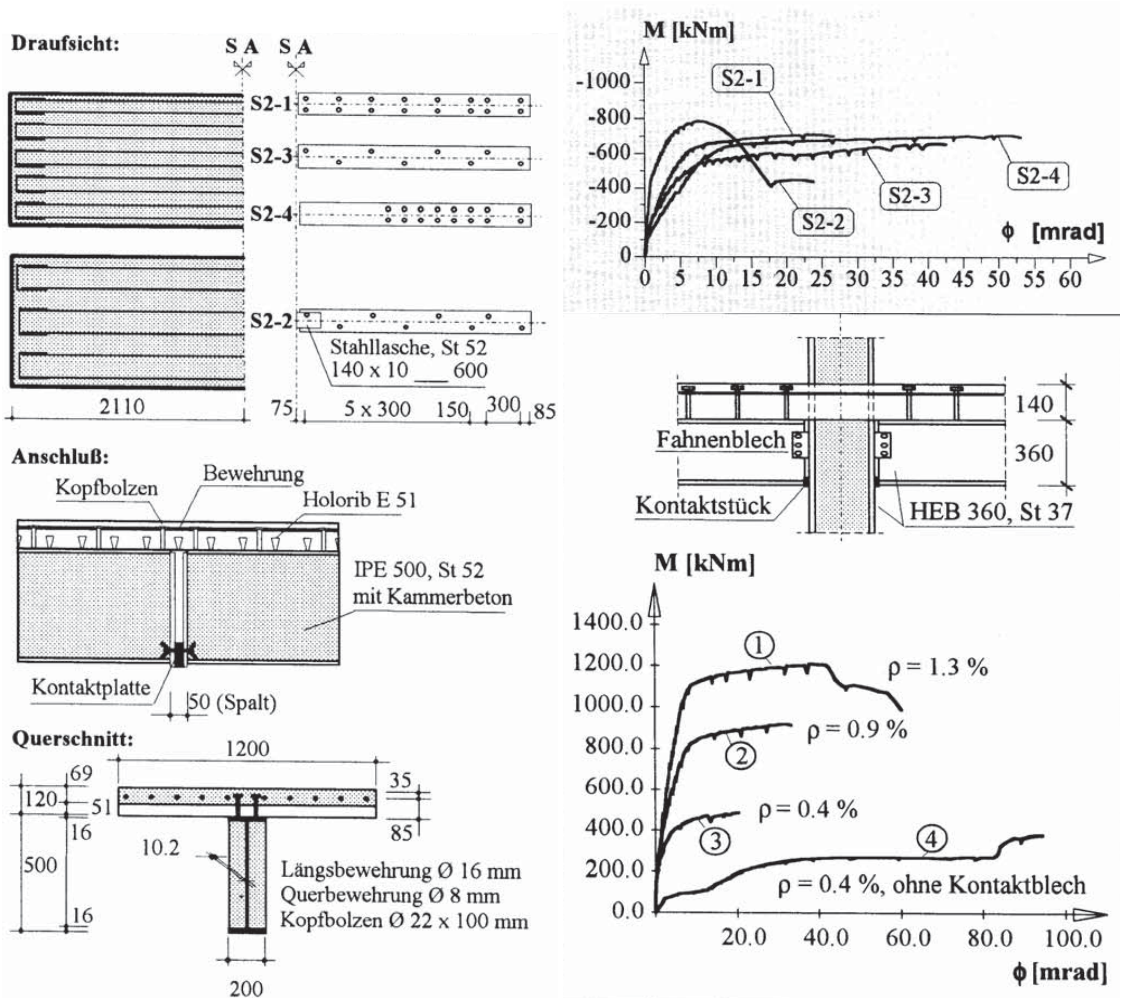

Figure 2.11: Experimental investigations by Bode and Kronenberger (1996, 1998)

In 1996, an analytical model to predict the moment capacity of endplate types of composite connections was proposed (Xiao et al., 1996). This approach is based on the concept of stress blocks, which is also used to calculate the resistance of cross-sections. Close agreement was obtained with 45 test specimens including flush endplate and partial depth endplate connections. On behalf of this calculation approach, a parametric study indicated that the connection moment capacity can reach that of a composite beam in hogging for composite flush endplate connection with sufficiently large reinforcement ratios. However, the same conclusion cannot be extrapolated to more flexible types of steel connections.

The American Institute of Steel Construction (1996) published a design guide for partially restrained composite connection. The design approach is based on empirical and best fitting results. Tabular design aids are provided to ease the design of partially restrained composite frames.

Anderson et al. (1998) revised the design approach for the rotation capacity of composite joints given previously in (Aribert, 1995) and (Anderson and Najafi, 1994). This revision consisted in a re-assessment of the elongation length of the reinforcement. The authors recognised that this length is correlated to the crack pattern of the reinforced concrete slab and provided a formula which accounts for this effect. Experimental observations allowed to conclude that for low reinforcement ratios, one main crack developed at the column flange. This outcome justifies the smaller elongation length for smaller reinforcement ratios. In (Bode and Kronenberger, 1998), it was shown that the design procedure for the joint stiffness according to Eurocode 4 is not suitable since no account is taken for the tension stiffening effect and the larger elongation length observed in experimental tests. A modified formula for the stiffness coefficient of the reinforced concrete slab was proposed.

The Steel Construction Institute (1998) published a design guide for semi-continuous composite connections. This publication aimed to provide ready-to-use tables allowing for the plastic design of semi-continuous composite frames without having to explicitly calculate the stiffness, resistance and rotation capacity of composite joints. Severe limitations were implemented to ensure that the required joint rotations are not exceeding the rotation capacity of the joints. The tables assume, for instance, that only 85 % of the sagging moment capacity is exploited in order to limit the non-linear effects induced by the plastification of the beam. Moreover, the joint resistance must be larger than 30 % of the sagging moment capacity and the span length to total depth ratio must be lower than 20. It was recommended to ignore the contribution of mesh reinforcement to the connection moment capacity and to use ⌀16 or ⌀20 reinforcing bars.

One year later, ECCS document number 109 condensed the findings from the COST C1 project in a design guide for composite joints for buildings (European Convention for Constructional Steelwork, 1999). Analytical prediction methods were provided for the resistance, stiffness and rotation capacity of composite joints based on former research conclusions. The proposition of reducing the sagging moment capacity of composite joints was kept in order to control the required joint rotations.

In Germany, Odenbreit (2000) performed five tests on composite beam-to-column joints, from which two were carried out without any steel connection and 3 with finplate connection. The influence of beam/column encasement and partial shear connection was analysed (cf. Figure 2.12). Furthermore, the effect of column stiffeners in the compression zone was

investigated. No reduction of the joint stiffness was observed for the test with missing column stiffener. Due to the slip between the bolt and the holes, the composite joint with finplate presented a similar stiffness as the one without finplate. An increase in ductility could be observed for the joint with concrete encasement. In the test with partial shear connection, bigger rotation capacities but smaller joint stiffness were achieved. In addition, Odenbreit performed two full-scale beam tests with composite joints. In his thesis, Odenbreit proposed a semi-empirical method to calculate the stiffness and rotation capacity of composite joints on behalf of 56 laboratory tests. A simplified design method for composite beams with bi-linear moment-rotation characteristic of the composite joints was proposed (cf. Figure 2.12). This method was compared to non-linear numerical calculations, which he validated on the basis of the two full-scale beam tests. He concluded that this simplified method provides similar requirements on the joint rotation as the non-linear calculation if the sagging bending capacity is reduced to 90 % of its full plastic resistance.

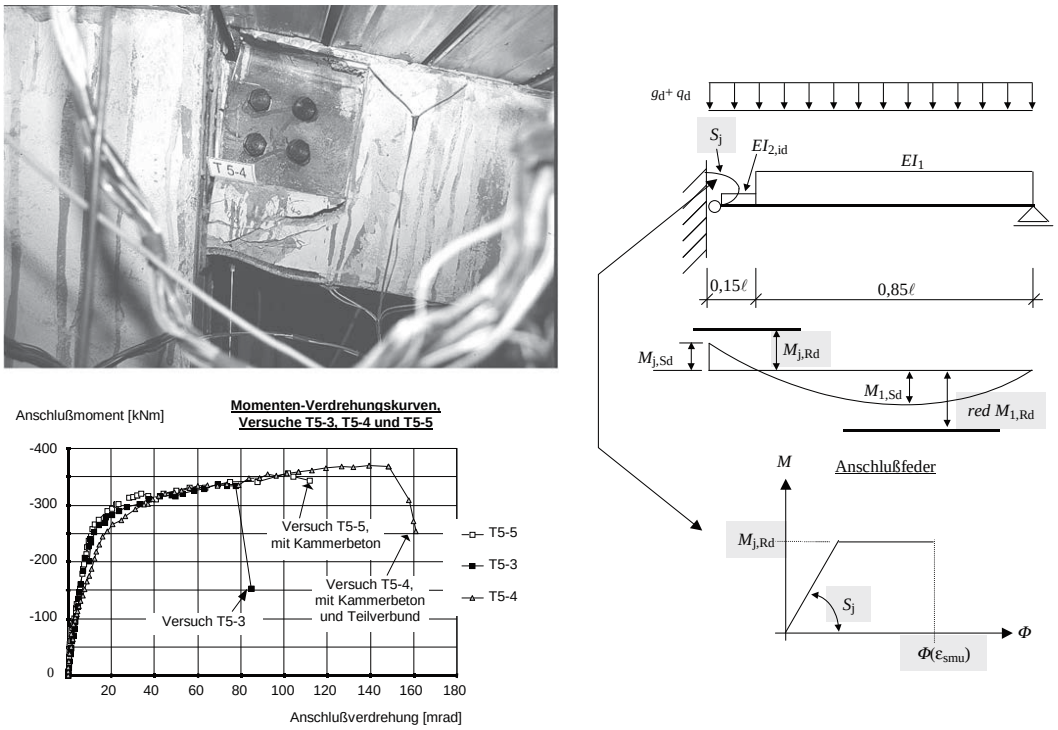

Figure 2.12: Experimental investigations by Odenbreit (2000)

In Finland, the first experimental investigations on semi-continuous composite joints connecting composite slim floor beams to tubular steel column sections filled with concrete were carried out. Malaska (2000) performed two tests on bare steel connections and four tests on composite joints. The composite action was assured ⌀16 mm transverse reinforcement bars, welded on the top flange of the steel beam, which provided relatively stiff full shear connection without development of notable slip (cf. Figure 2.13). The steel connection in all the tests (steel and composite) consisted of a shear flat slotted through the wall of the hollow column section and bolted to the steel beam. Reinforcement ratio, shear-to-moment ratio and concrete strength were the parameters investigated. No failure occurred for the tested specimens and remarkable rotation capacities reaching 80 mrad were attained. The significant elongation capacity was demonstrated for joints with reinforced concrete slabs presenting high reinforcement ratios (0.92 % - 1.43 %) and large rebar diameters (16 mm and 20 mm) as shown in Figure 2.13. The results showed that a larger amount of reinforcement

also induces a stiffer joint connection and that the shear-to-moment ratio and the concrete strength have little influence on the moment-rotation curves of composite joints. Malaska evaluated his results with the analytical prediction method given in ECCS and concluded that the initial rotational stiffness is overestimated with this model. Moreover, the method provided by ECCS significantly underestimated the rotation capacity of composite joints. Despite these differences, Malaska stated that the general design principles are applicable also for composite connections involving slim floor beams.

Specimen	Connection type	Load position *	Reinforcement / ρ [%]	Concrete
SC1	Bare steel	1650 mm	-	-
SC2	Bare steel	1150 mm	-	-
CC1	Composite	1650 mm	10 ϕ 16 mm / 0.92	C35/45
CC2	Composite	1650 mm	10 ϕ 16 mm / 0.92	C25/30
CC3	Composite	1650 mm	10 ϕ 20 mm / 1.43	C25/30
CC4	Composite	1150 mm	10 ϕ 16 mm / 0.92	C25/30

* Distance from the column flange

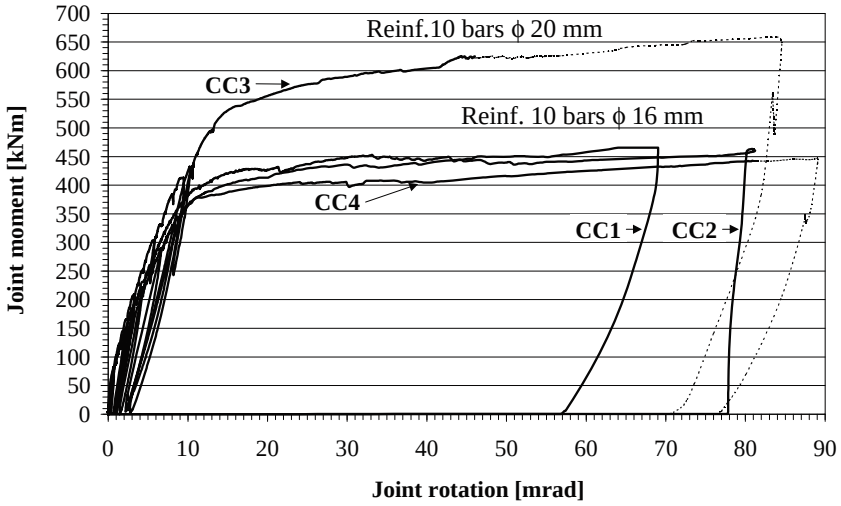

Figure 2.13: Experimental investigations by Malaska (2000)

In Coimbra, Simões (2000) investigated the behaviour of bolted flush endplate joints with four tests on internal and four on external beam-to-column composite joints (cf. Figure 2.14). The test program was designed in order to investigate the effect of concrete confinement in the steel column and to derive the influence of anti-symmetric and cyclic loading on the moment-rotation response of composite joints. It was concluded that the concrete confinement behaves similarly to a stiffener for the column section and increases the stiffness and strength of the corresponding joint. For the internal tests with anti-symmetric loading, the failure was due to horizontal shear of the column web, even for the tests with concrete confined in the steel column. However, an increase in stiffness and strength was observed for the joints with composite column without significant loss in ductility. Moreover, it was observed that for external composite joints (unbalanced bending moment), the column confinement prevented the shear failure of the column web panel.

Ensaio	Ligações	Secção do Pilar	Tipo de Carregamento (Momento à esquerda / Momento à direita)
E1	Nó Interno	Metálica	Estático (M- / M-)
E2	Nó Interno	Metálica	Estático (M+ / M-)
E3	Nó Externo	Metálica	Estático (M-)
E4	Nó Externo	Metálica	Estático (M+)
E5	Nó Externo	Mista	Estático (M-)
E6	Nó Externo	Mista	Estático (M+)
E7	Nó Interno	Mista	Estático (M- / M-)
E8	Nó Interno	Mista	Estático (M+ / M-)
E9	Nó Externo	Metálica	Cíclico
E10	Nó Externo	Mista	Cíclico
E11	Nó Interno	Metálica	Cíclico
E12	Nó Interno	Mista	Cíclico

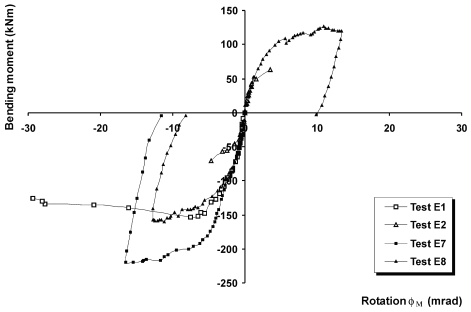

Figure 2.14: Experimental investigations by Simões (2000) and Da Silva et al. (2001)

At nearly the same time, Brown and Anderson (2001) performed similar tests to those conducted by Najafi (1992). Since the same column section and steel beam depth were used as in test S8FD from Najafi it was possible to compare test results with similar reinforcement ratio in order to deduce the influence of the longitudinal rebar diameter (16 mm for Brown and 12 mm for Najafi). This comparison demonstrated that the ductility of the composite joint tested by Brown was three times that of Najafi demonstrating therefore that the use of bigger rebar diameter is beneficial for the rotation capacity. From the other tests of Brown, it was found that the joint resistance of a deeper steel beam is greater at the expense of the rotation capacity of the joint (cf. Figure 2.15).

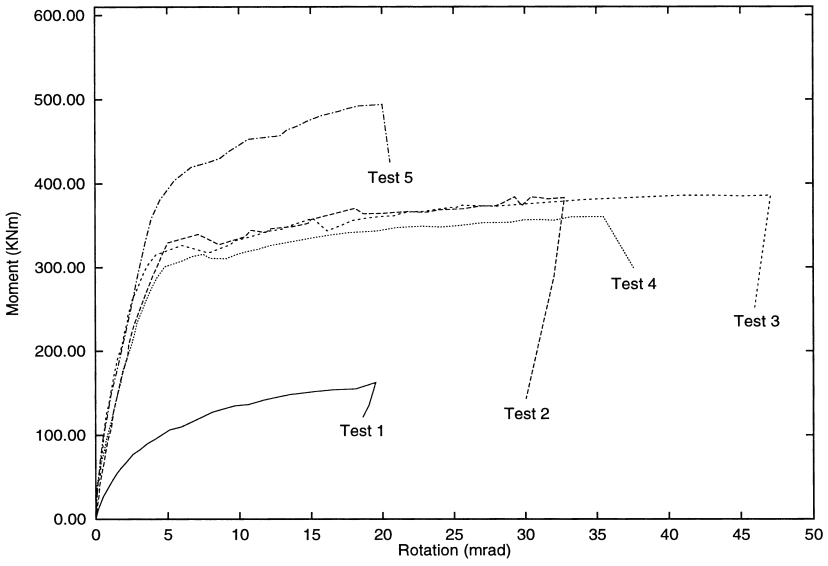

Figure 2.15: Experimental investigations by Brown and Anderson (2001)

In Stuttgart, Schäfer and Kuhlmann conducted nine laboratory tests on composite joints to investigate the influence of a larger tension zone in the reinforced concrete slab (Schäfer, 2005). The reinforcement ratio, the type of loading, the degree of shear connection and the effective concrete width were also investigated. It was observed that increasing the distance between the column flange and the first shear stud activates a larger tension band in the reinforced concrete component. In comparison to composite joints with conventional distribution of shear studs (cf. Figure 2.16), a duplication of the rotation capacity is achieved. These results confirm the conclusions made previously by Bode and Kronenberger (1998). Furthermore, Schäfer showed that the required rotation capacity is underestimated when the non-linear material effects are not considered and proposed a method, known as Beam-Line method, to approximate the required support rotations. A design approach based on joint classes was proposed, conjointly with three design procedures for the required rotation of composite joints.

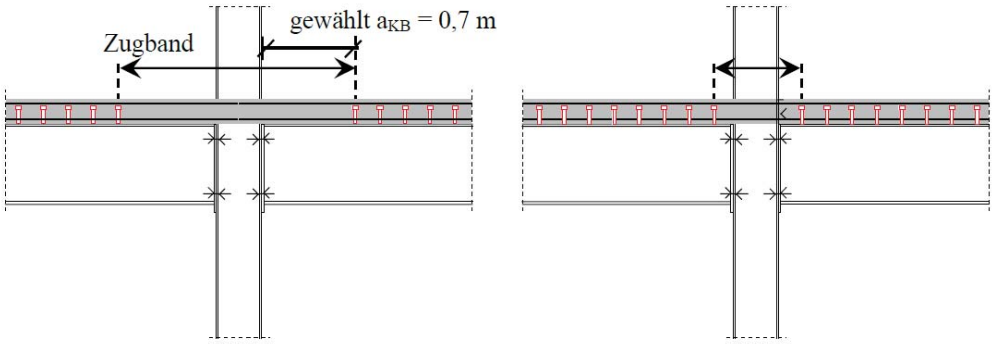

Figure 2.16: Tension band effect Schäfer (2005)

One year later, Loh et al. (2006a) published the results of an experimental study on five composite beam-to-column joints and one bare steel joint. The particularity of these tests consisted in the use of a special type of blind bolting technique with so-called Hollo-bolts (cf. Figure 2.17). These bolts ease the connection between steel beams and concrete filled column square hollow sections. Test failure was induced by flange buckling, slab spalling or excessive deformation in the steel connection. It was once more confirmed that the rotation capacity of composite joints increases with bigger reinforcement ratio and partial shear connection between the steel beam and the concrete slab (cf. Figure 2.17). In a companion paper (Loh et al., 2006b), the available methods to calculate the joint properties are applied to experimental results.

For most of the composite joints specimens tested in laboratory, the concrete slabs were cast on steel decking. The pioneering idea of performing tests with precast hollow-core slabs was developed by Fu and Lam (2006). Eight full-scale tests with variable stud spacing, degree of shear connections, reinforcement ratio and slab thickness were conducted (cf. Figure 2.18). Despite the relatively small amount of reinforcement (2 or 4 rebars of ⌀16 or ⌀20 mm), the behaviour of composite joints was relatively ductile. The beneficial effect of reinforcement ratio on resistance and ductility was once more observed.

In Pamplona, Gil and Bayo (2008a) investigated the issues related to the reinforcement anchorage in external joints. Three tests on composite joints (one on internal and two on external) were performed with the aim of studying the performance of a novel type of reinforcement anchorage for external joints. A detailed description of the tests can be found in (Gil and Bayo, 2008a).

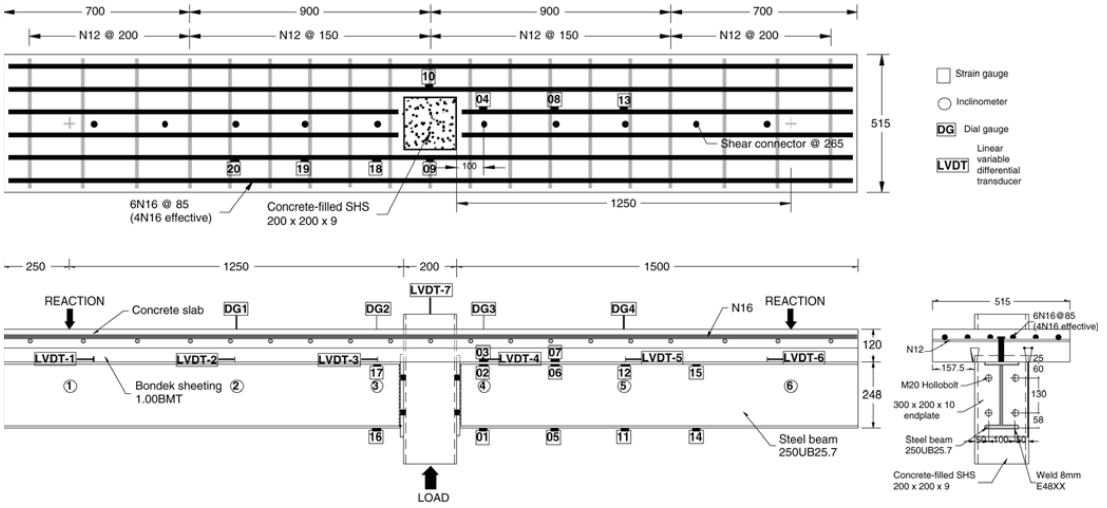

Specimen	Degree of shear connection (%)	Reinforcing bars (Reinforcement ratio, %)	Number of shear connectors in shear span
CJ1	110	4N16 (1.29)	5
CJ2	66	4N16 (1.29)	3
CJ3	44	4N16 (1.29)	2
CJ4	133	2N16 (0.65)	3
CJ5	118	6N16 (1.94)	8
SJ6	Bare steel joint, with concrete-filled column		

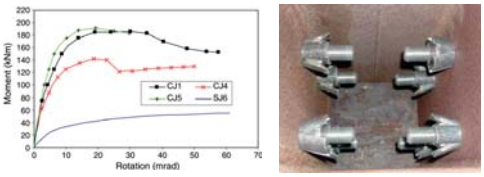

Figure 2.17: Experimental investigations by Loh et al. (2006a)

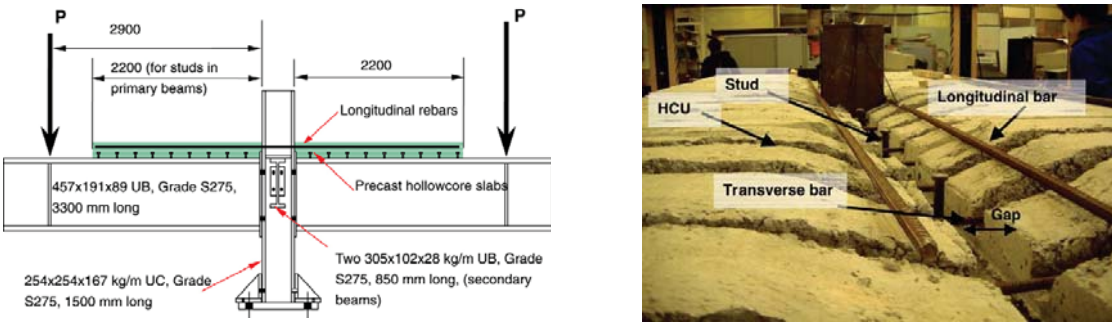

Figure 2.18: Experimental investigations by Fu and Lam (2006)

In Luxembourg, Hahn (2009) focussed on the influence of the rebar diameter on the rotation capacity of composite joints. Five tests on boltless beam-to-column composite joints comparable to those performed by Kathage were carried out. The test outcome confirmed the results obtained by Brown: the rotation capacity increases with larger rebar diameter (cf. Figure 2.19). Some of these tests involving mesh reinforcement presented a brittle behaviour.

Barcewicz (2010) explored the influence of reinforcement ratio and type/thickness of endplate connection (flush or extended) on the behaviour of composite joints. Due to laboratory limitations, the tests were performed under force control, such that only the stiffness and resistance of the composite joints could be evaluated. Independently of the type of endplate connections, the joint stiffness and resistance increased with larger reinforcement ratio. The results are presented in Figure 2.20.

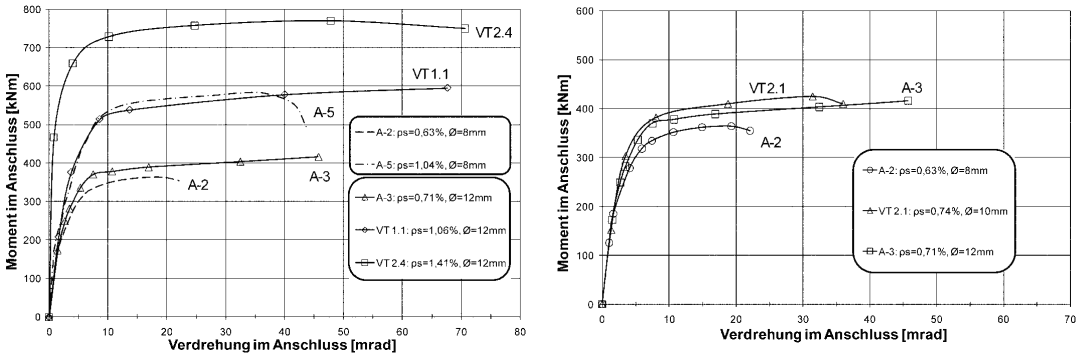

Figure 2.19: Experimental investigations by Hahn (Odenbreit et al., 2009)

Symbol of the tested group (reinforcement ratio)		Symbol of specimen	Type and thickness of the end-plate	Initial stiffness $S_{j,ini,test}$ [kNm/mrad]	Moment resistance	
					$M_{j,R,test}$ [kNm]	$M_{j,R,test*}$ [kNm]
Composite joints	Group I (ρ = 0,60%)	EZ1	Flush, 10 mm	46,91	119,35	124,89
		EZ2	Extended, 10 mm	66,89	147,61	158,89
		EZ3	Extended, 8 mm	53,38	135,44	141,60
		EZ4	Flush, 12 mm	48,28	129,13	137,91
	Group II (ρ = 1,35%)	EZ5	Flush, 10 mm	56,29	166,32	178,79
		EZ6	Extended, 10 mm	78,19	178,56	201,18
		EZ7	Extended, 8 mm	64,71	168,63	183,95
		EZ8	Flush, 12 mm	60,51	166,86	187,88

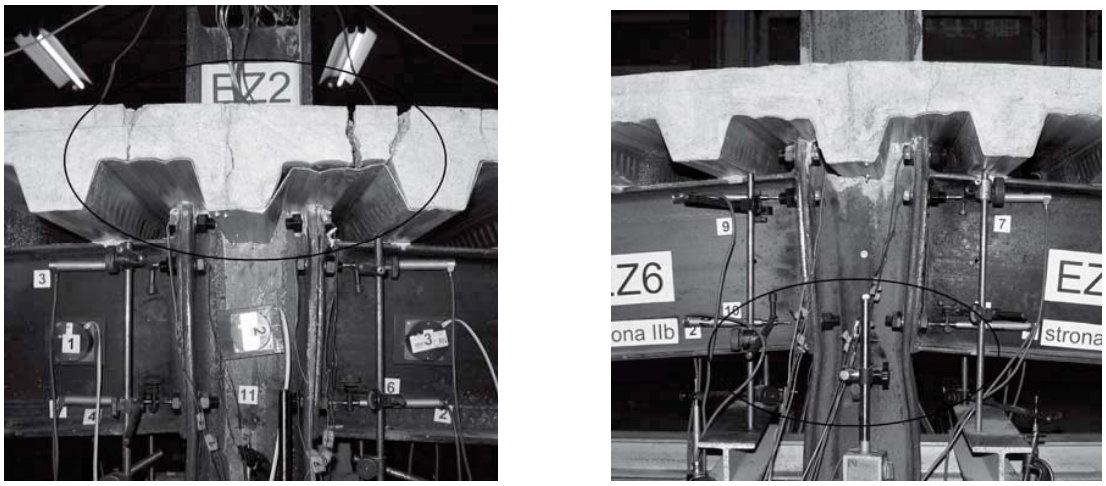

Figure 2.20: Experimental investigations by Barcewicz and Gizejowski (2011)

More recently, the first experimental investigations on composite joints with high strength steel S690 were carried (Ataei et al., 2016). Four internal beam-to-column flush endplate composite joints with post-installed friction-grip bolted shear connectors were tested (cf. Figure 2.21). The failure of the tests was caused by the rupture of the longitudinal reinforcement bars of ⌀10 mm. Despite the small reinforcement ratios, the specimen experienced rotation capacities over 40 mrad mainly due to the yielding of the reinforcement bars over a length of 400 mm away from the column flange. It was concluded that the considerable slip caused by the oversized holes in the precast slab contributed also to large rotation capacities.

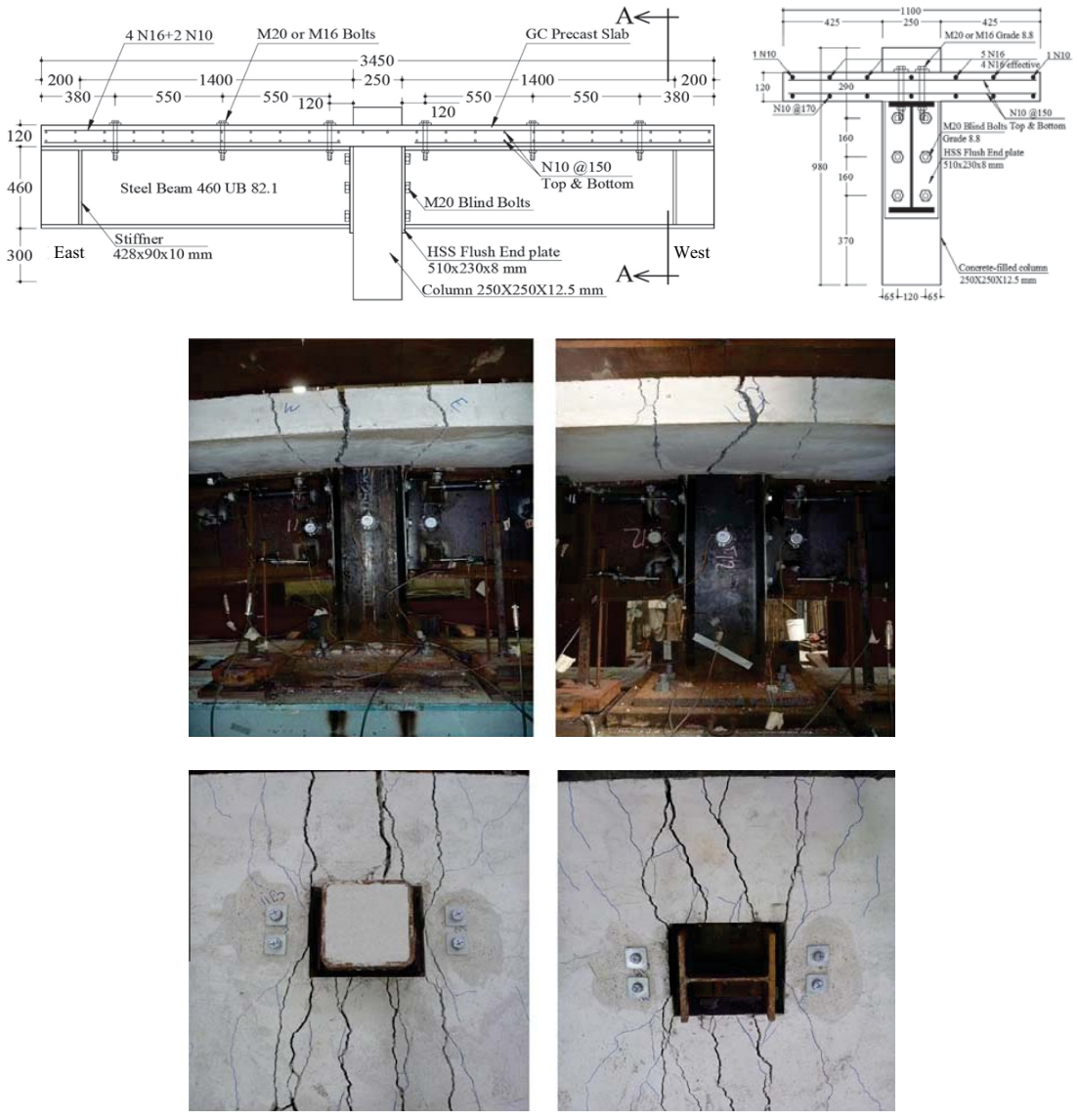

Figure 2.21: Experimental investigations by Ataei et al. (2016)

As it can be seen from the present state of the art, most of the experimental works on composite joints were conducted at the late 1990s and beginning of 2000. In the last ten years, only a few researchers focussed on the experimental investigation of composite joints. Instead, researchers mostly focussed on the 3D finite element modelling of composite joints. Henriques (2013), Dabaon et al. (2009), Fu et al. (2008), Gil and Bayo (2008b), Vasdravellis et al. (2009) and Piluso et al. (2012) are some of the researchers that used numerical simulations to predict the moment-rotation response of composite joints.

2.3 Investigations on the required joint rotation for plastic analysis

Several research works concentrated on the plastic analysis of composite beams with composite joints. One basic issue addressed in all these works is the required joint rotation Φ_{req} allowing for the moment redistribution in a plastic global analysis. Due to the non-linear material effects occurring in the plastic zones, it is unsafe to determine the required joint rotations using linear elastic method of analysis. Moreover, it has been demonstrated, that the required joint rotation does not depend on the elastic joint stiffness (Li et al., 1995a). It is a quantity, which is primarily dependent on the extension of the plastic zones and is therefore related to the hogging and sagging resistance capacities of the system. The research works presented in this section studied the influence of various parameters on the required joint rotation, such as beam depth, steel yielding strength and bending resistance capacity.

Huber and Tschemmernegg proposed a classification system for composite joints according to their rotation capacity. This classification system is based on a very simplified approach for the required joint rotation, in which the non-linear influence of plastic zones is roughly estimated by a factor "2". The formula for the required joint rotation is given below:

$$\Phi_{req} = 2 \cdot \frac{L}{3 \cdot EI} \cdot (M_{pl,sagg} - 0.5 \cdot M_{pl,hogg}) \tag{2.1}$$

An alternative perspective on the required joint rotation is provided by Odenbreit (2000). He defined an upper limit for the required rotation over a simple border-line case. Since the maximum ULS-deflection at midspan can be assumed to L/50 for a simple supported beam according to experimental observations made in (Bakker and Voorn, 1974), (Odenbreit, 2000) and (Huber, 2000), the support rotation Φ can be deducted from simple geometric considerations assuming a parabolic deflection shape of the beam (cf. Figure 2.22):

$$\Phi \approxeq \tan \Phi = \frac{2 \cdot L/50}{L/2} = 80 \text{ mrad} \tag{2.2}$$

According to this, the rotation requirements at support are unlikely to exceed the 80 mrad upper bound. A similar deduction was also drawn by Huber (2000).

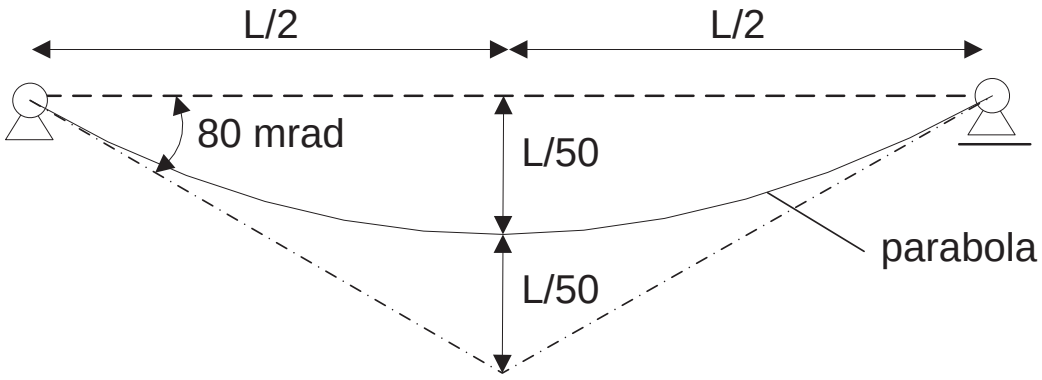

Figure 2.22: Maximal required joint rotation

Since this upper limit of the required joint rotation constitutes a conservative estimation, other research investigations examined this element in greater detail. In 1995, Li and Nethercot provided, for instance, a method to calculate the required joint rotations for three different

loading cases: uniformly distributed load, two-point load and one-point load (Li et al., 1995a). This method relies however on empirical basis since the beam curvature at ultimate limit state was obtained from experimental analysis (cf. Figure 2.23). The proposed calculation procedure for the required rotations was validated against the results of 29 tests (cf. Figure 2.24). The same publication presents a proof that the rotation required from the connections is independent of the joint stiffness. This proof has been accomplished with internal work considerations and Castigliano's first theorem.

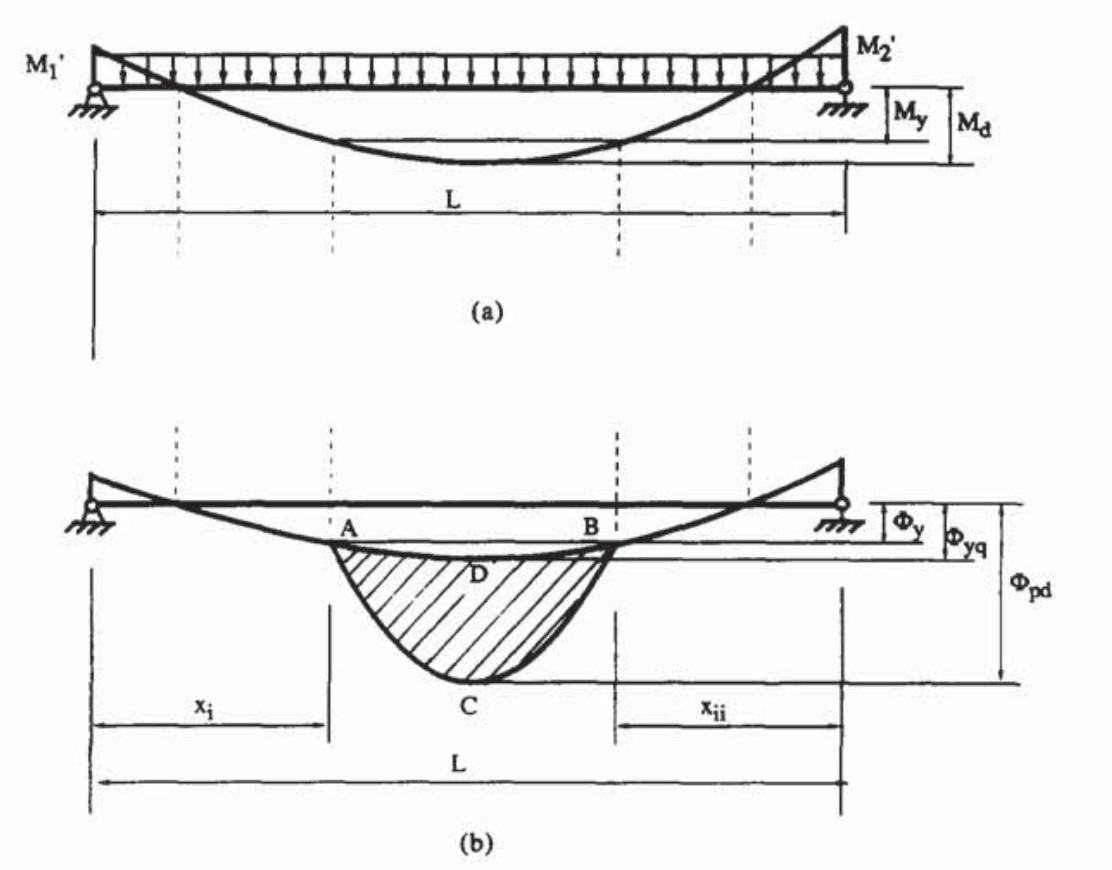

Figure 2.23: Empirical curvature distribution (Li et al., 1995b)

Using the theoretical method in (Li et al., 1995a), Nethercot (1995) derived empirical equations for the required rotations in the support regions of composite frames. These empirical equations are calibrated on a large set of numerical results with 1360 variable combinations of parameters influencing the rotation requirements. All these numerical results assume Grade 43 ($f_y = 275\ N/mm^2$) for the steel beam and high yield bars for the reinforcement ($f_{sy} = 460\ N/mm^2$). Different loading conditions and reinforcement ratios (up to 1.5 %) were also investigated. From this analysis, it was concluded that the main factors affecting the required rotations are the support-to-span moment ratio and the span yield moment-to-design moment ratio. It was furthermore concluded that if the support and span moment capacities are fully utilised, then the required rotation capacities for internal support of commonly used continuous composite beams range from 36 mrad up to 50 mrad (twice the value represented in Figure 2.25). Moreover, it was observed that if the rotation capacity of composite joints is bigger than 20 mrad, the available degree of moment redistribution of semi-continuous composite frames may reach 30 %. The empirical equations are shown in Figure 2.26.

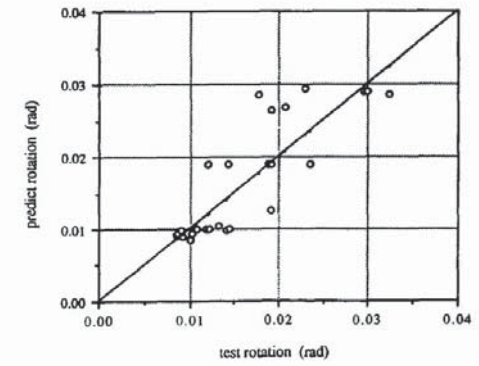

Figure 2.24: Results by Li et al. (1995b)

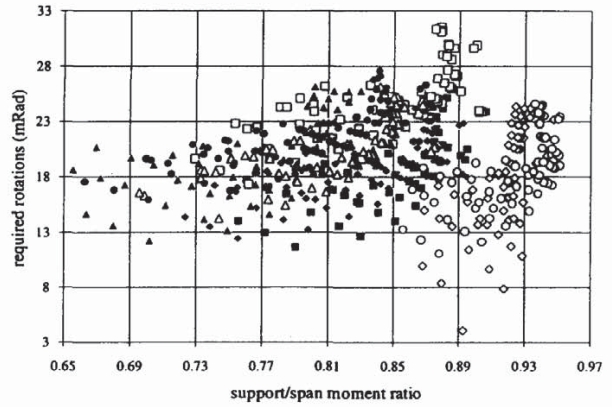

Figure 2.25: Numerical study on the required joint rotations by Nethercot et al. (1995)

Load and support conditions	*Equations for the required rotation of the support with a moment M' ($R' = M'/M_d$)*
Eqn (i) uniformly distributed load with $M' = M''$ $\gamma = 0{\cdot}991$	$\theta_r = \left(0{\cdot}344 - 0{\cdot}212R' + 0{\cdot}561\left(\frac{M_d - M_y}{M_p - M_y}\right)^2 \frac{1}{\sqrt{1+R'}}\right)\frac{M_d L}{EI}$
Eqn (ii) uniformly distributed load with $M'' = 0$ $\gamma = 0{\cdot}990$	$\theta_r = \left(0{\cdot}344 - 0{\cdot}225R' + 0{\cdot}556\left(\frac{M_d - M_y}{M_p - M_y}\right)^2 \frac{1}{\sqrt{1+R'}}\right)\frac{M_d L}{EI}$
Eqn (iii) two-point load with $M' = M''$ $\gamma = 0{\cdot}985$	$\theta_r = \left(0{\cdot}344 - 0{\cdot}211R' + 1{\cdot}144\left(\frac{M_d - M_y}{M_p - M_y}\right)^2 \frac{M_y}{M_p}\right)\frac{M_d L}{EI}$
Eqn (iv) two-point load with $M'' = 0$ $\gamma = 0{\cdot}992$	$\theta_r = \left(0{\cdot}344 - 0{\cdot}270R' + 1{\cdot}091\left(\frac{M_d - M_y}{M_p - M_y}\right)^2 \frac{M_y}{M_p}\frac{1}{(1+R')^2}\right)\frac{M_d L}{EI}$
Eqn (v) one-point load with $M' = M''$ $\gamma = 0{\cdot}987$	$\theta_r = \left(0{\cdot}255 - 0{\cdot}300R' + 0{\cdot}722\left(\frac{M_d - M_y}{M_p - M_y}\right)^2 \left(\frac{1 - M_y/M_d}{1+R'}\right)\right)\frac{M_d L}{EI}$
Eqn (vi) one-point load with $M'' = 0$ $\gamma = 0{\cdot}978$	$\theta_r = \left(0{\cdot}255 - 0{\cdot}252R' + 0{\cdot}610\left(\frac{M_d - M_y}{M_p - M_y}\right)^2 \left(1 - \frac{M_y}{M_d}\right)\right)\frac{M_d L}{EI}$

Figure 2.26: Empirical equation for the required joint rotations (Nethercot et al., 1995)

Li et al. (2000) used the empirical equations defined in (Nethercot et al., 1995) (cf. Figure 2.26), to predict the required rotation of composite joints for different parameters such as connection-to-span moment ratio, span-to-beam depth ratio, steel grade and loading conditions. An almost linear relationship between the required rotations and the connection-to-span moment capacity was deducted. This outcome showed that the larger the connection-to-span resistance ratios, the smaller the rotations required by the structural systems (cf. Figure 2.27). It was also concluded that higher steel grades require larger beam end rotations. Concerning the loading condition, the authors observed that for beams with equal support moments, the two-point load case requires the biggest rotation capacity, while the case with one-point load requires the smallest. The uniformly distributed case lies between both extremes. In the same article, it was suggested to reduce the sagging bending resistance to 90 % of the plastic resistance to limit the required joint rotations.

Maximum span depth ratio of composite beams controlled by connection rotation capacity[a]

Steel grade	M″	M′/M_d	Connection rotation capacity (mRad) UDL 20	UDL 25	UDL 30	2PL 20	2PL 25	2PL 30	1PL 20	1PL 25	1PL 30
235	M′	0.00	19.9	25.5	31.4	15.3	19.6	24.0	30.9	40.0	49.4
		0.25	23.0	29.6	36.4	16.8	21.6	26.5	42.9	55.5	68.4
		0.50	27.1	34.9	43.0	18.7	24.0	29.5	66.6	85.8	105.4
		0.75	32.7	42.2	51.9	21.0	27.0	33.1	130.4	166.3	302.8
		1.00	40.9	52.6	64.6	24.0	30.7	37.7	674.9	866.9	1066.6
	0.00	0.00	19.9	25.5	31.4	15.3	19.6	24.0	30.9	40.0	49.4
		0.25	23.5	30.3	37.3	28.0	36.1	44.4	39.2	50.7	62.7
		0.50	28.3	36.5	44.9	40.0	51.5	63.1	53.2	68.8	84.7
		0.75	34.9	44.9	55.3	58.2	74.6	91.2	80.3	103.2	126.6
		1.00	44.5	57.2	70.1	96.5	122.3	148.4	148.6	189.5	231.1
275	M′	0.00	17.4	22.0	26.9	14.3	17.1	20.8	26.6	34.1	42.0
		0.25	20.0	25.4	31.1	15.0	18.7	22.8	36.5	47.1	57.9
		0.50	23.4	29.9	36.6	16.3	20.7	25.3	56.6	72.7	89.2
		0.75	28.1	36.0	44.1	18.3	23.2	28.4	111.0	141.4	172.2
		1.00	35.1	44.9	54.9	20.8	26.4	32.3	571.8	731.0	896.7
	0.00	0.00	17.4	22.0	26.9	14.3	17.1	20.8	26.6	34.1	42.0
		0.25	20.4	26.0	31.8	24.1	30.8	37.8	33.5	43.1	53.1
		0.50	24.4	31.2	38.2	34.1	43.7	53.5	45.3	58.3	71.7
		0.75	29.9	38.3	47.0	49.5	63.3	77.4	68.3	87.6	107.3
		1.00	38.1	48.8	59.6	82.4	104.3	126.5	126.9	161.4	196.5
355	M′	0.00	16.8	18.9	21.7	14.9	16.6	18.3	21.7	27.2	33.0
		0.25	18.0	20.3	24.8	15.6	17.4	19.2	29.1	36.8	44.9
		0.50	19.5	24.0	29.0	16.4	18.3	20.2	44.3	56.4	68.8
		0.75	22.8	28.6	34.7	17.4	19.4	22.8	86.7	109.7	133.1
		1.00	28.1	35.4	43.0	18.5	21.5	25.8	443.3	561.0	683.4
	0.00	0.00	16.8	18.9	21.7	14.9	16.6	18.3	21.7	27.2	33.0
		0.25	18.2	20.6	25.4	19.8	24.6	29.7	26.9	33.9	41.3
		0.00	0.50	20.0	25.0	30.2	26.9	34.0	41.4	45.6	55.6
		0.75	24.2	30.4	36.8	38.8	49.3	59.9	53.7	68.3	83.1
		1.00	30.5	38.4	46.6	64.6	81.3	98.2	99.9	126.1	152.7

[a] M_d/M_p=0.9; M_d—span design moment; M_p—span section ultimate moment capacity; M′—connection moment capacity; M″—other end connection moment capacity.

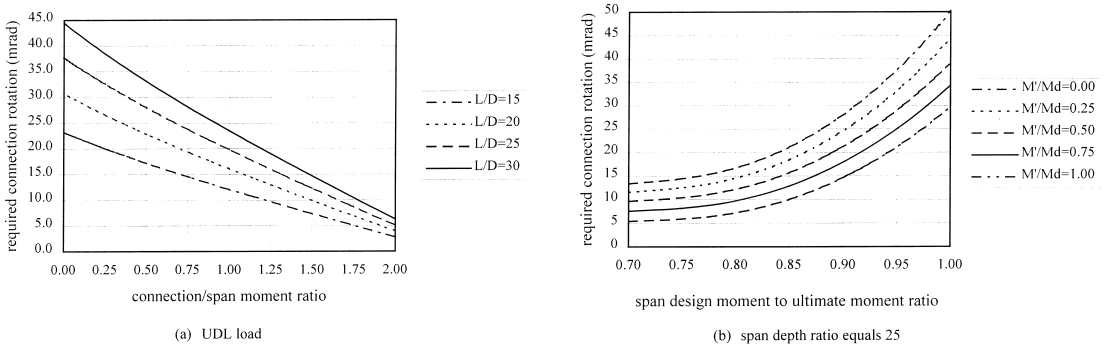

Figure 2.27: Parametric study on the support rotation requirements by Li et al. (2000)

In Lausanne, Kattner (1999) developed a numerical model to simulate the behaviour of composite joints. This model consisted of beam elements representing the steel beam, the reinforced concrete slab and the steel column. The different joint components were modelled with translational springs. This model was validated against experimental results on composite joints and composite beams. Besides, Kattner proposed an analytical method to calculate the required joint rotations. In contrast to Li and Nethercot, this method relies on analytical moment-curvature relationship. This analytical procedure can be subdivided into the following steps:

1. Determination of the moment-curvature relationship $M - \kappa$ of composite beams using the section analysis method (cf. Figure 2.28).
2. Determination of the bending moment distribution M(x) in the composite beam.
3. Identification of the beam area where plastic deformations occur, i.e. where the acting bending moment exceeds the elastic bending resistance of the beam M_{el}.
4. Calculation of the required joint rotation with the principle of virtual forces (cf. Figure 2.29). A virtual support moment is therefore applied on a statically determinate system. The support rotation is then obtained with the integration of the elastic and plastic curvatures over the beam length L:

$$\Phi_{req} = \int_0^L \bar{M} \cdot \kappa \cdot dx \tag{2.3}$$

5. In order to solve equation (2.3), the following analytical function is provided for the non-linear area of the $M - \kappa$ relation of the composite section:

$$\kappa_{pl}(M) = A \cdot \frac{M - M_{el}}{B \cdot M_{pl} - M} + \kappa_{el} \tag{2.4}$$

   The parameters A and B are determined such that the curve obtained in equation (2.4) is identical to that obtained in the first point of the present procedure ($M - \kappa$ relation of the composite section).

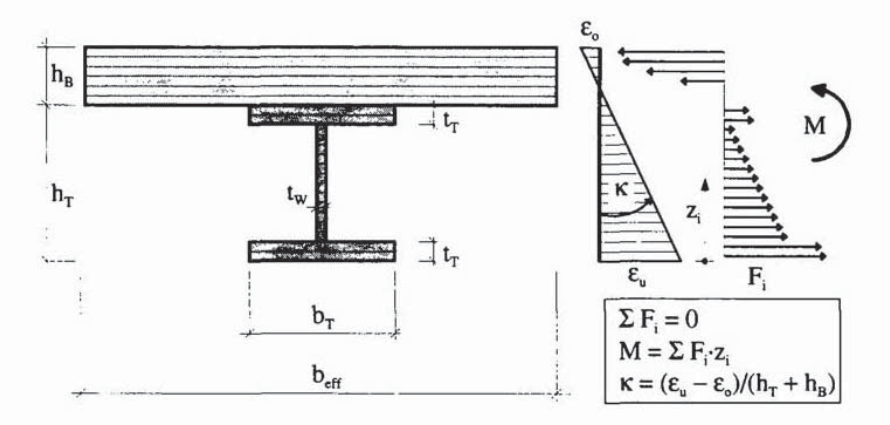

Figure 2.28: Section analysis method for $M - \kappa$ curve of composite beams (Kattner, 1999)

The accuracy of the numerical model is validated by this analytical procedure. On the basis of the non-linear numerical model, Kattner performed an exhaustive parametric study in order to identify the influencing factors on the joint rotations required for the usage of the plastic capacities. Depth and length of the beam, steel and concrete grades as well, degree of shear connection and ratio between joint and sagging resistance were some of the factors varied. The most pertinent conclusions of this study are summarised hereafter:

- The required joint rotations are smaller for larger ratios of joint-to-span resistances (cf. Figure 2.30). In other terms, for a given sagging resistance $M_{pl,sagg}$, the required joint rotation can be reduced by increasing the joint resistance $M_{j,pl}$. This phenomenon is due to the reduction of the plastic zone as depicted in Figure 2.30.
- The required joint rotation increases with smaller beam heights h and greater beam spans L.
- A partial shear connection increases the beam's deflection and therefore also the required joint rotation. At the same time, it also induces a smaller plastic bending resistance with a smaller plastification degree. This compensates the increase in joint rotation such that the rotation requirements may be lesser or greater than for a composite beam with full shear connection.
- The stiffness of the shear connectors may influence the required joint rotations. It was found that stiffer connectors diminish the required joint rotations.
- The required joint rotations increase with greater steel and concrete grades.

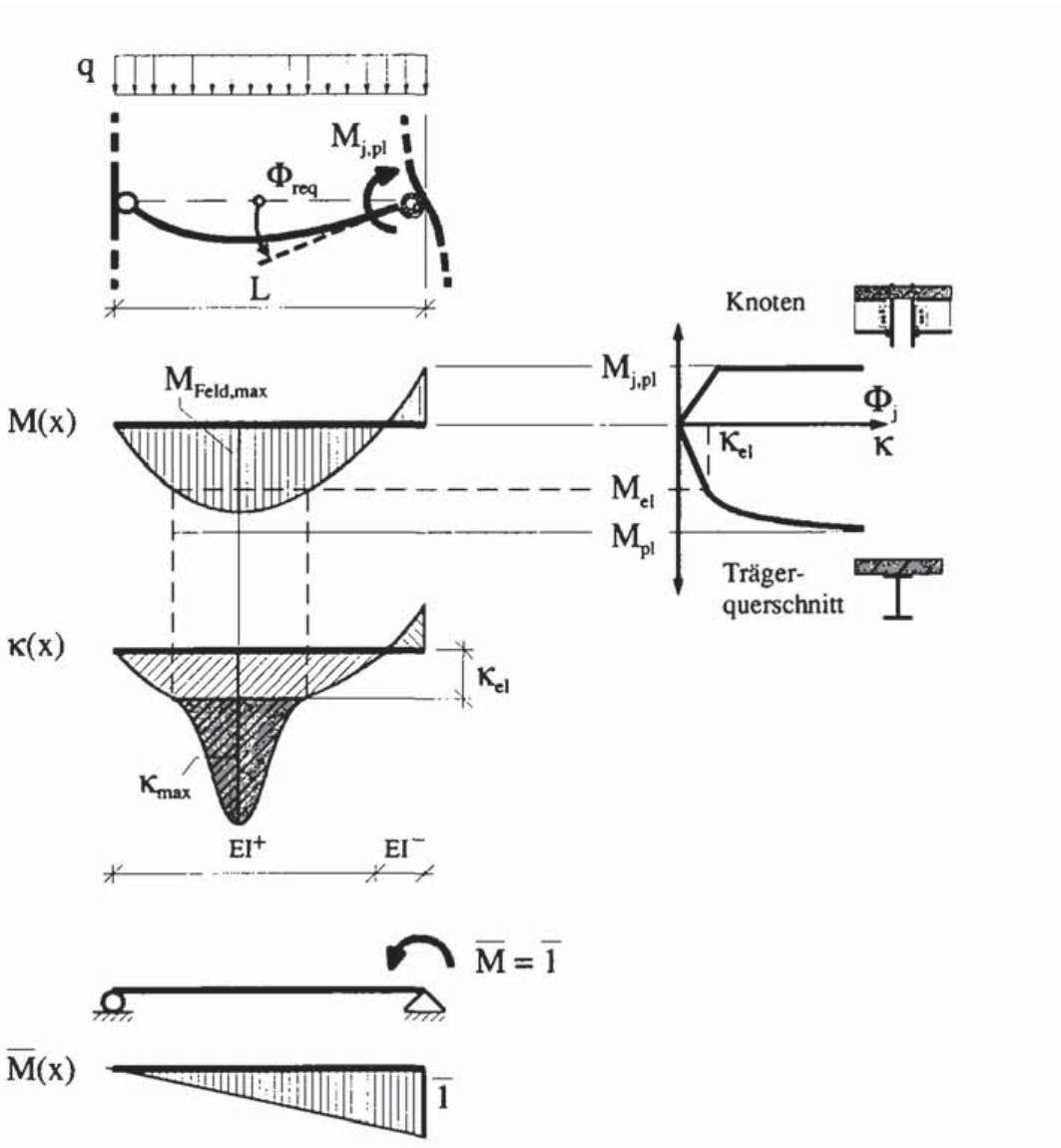

Figure 2.29: Analytical procedure for the required joint rotation (Kattner, 1999)

The numerical investigations undertaken by Kattner on the required joint rotations include parameters that were not taken into account in the investigations of Nethercot. While the latter developed empirical equations assuming rigid shear connection between concrete and steel, Kattner studied the variation of shear connection degrees and rigidity of the individual shear connectors on the required rotations.

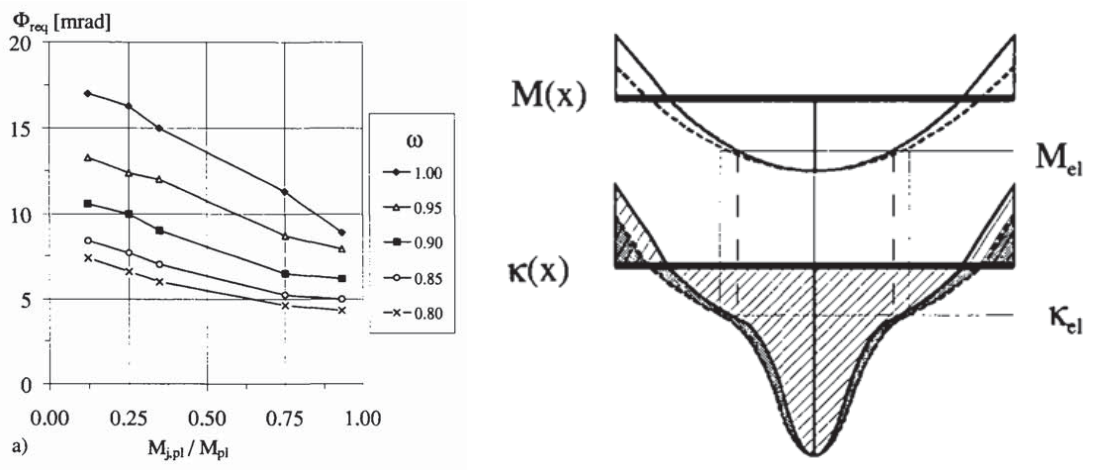

Figure 2.30: Influence of joint-to-sagging resistance on required joint rotations (Kattner, 1999)

One additional issue addressed by all the authors is the incompatibility assuming the plastic moment capacity of composite beams M_{pl} with the stress-block method. Li and Nethercot assumed, for instance, the sagging design moment to 95 % of its plastic moment M_{pl}, justifying this choice by the slight over-strength in the steel at higher strain levels (Li et al., 2000).

For Kattner, the sagging design moment was extracted from the beam's moment-curvature relationship $M - \kappa$ at a specific plastic curvature $\kappa_{pl} = 5.7 \cdot (h_a/h_c)^{0.2} \cdot \kappa_{el}$.

In this context, a strain-based sagging capacity would be the most realistic and appropriate approach. The limits of plastic bending resistance of composite beams are exposed in greater detail by Schäfer (2017). It is shown that the plastic moment resistance of a composite beam may overestimate the real bearing capacity in case of large compression zones. In fact, the plastic resistance based on the stress block method assumes that plastification takes place in each cross-sectional fibre without any strain limitation. According to (Schäfer, 2017), this method may lead to an overestimation of the plastic design moment (cf. Figure 2.31). For the plastic neutral axis close to the bottom flange of the steel section, a concrete failure in the compression zone is more likely to occur before the plastic moment resistance is reached. In this case, the strains in the steel section are limited, such that a strain limited bending resistance is more appropriate. According to (Schäfer, 2017), this strain limiting design concerns especially composite beams with massive concrete chords, partially encased sections and composite slim-floor sections.

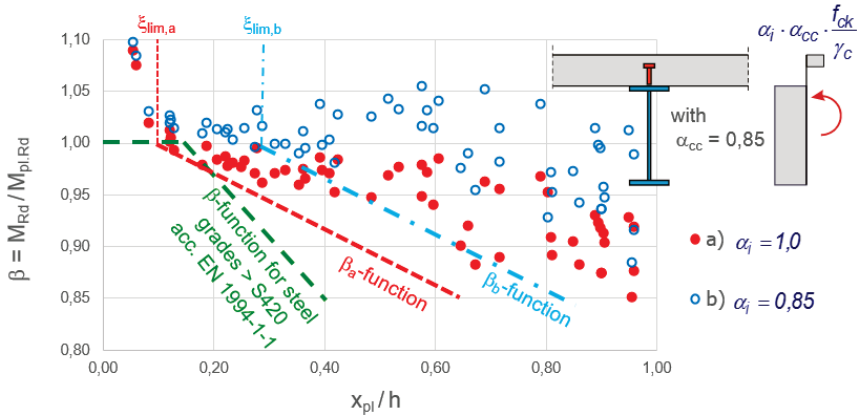

Figure 2.31: Comparison between plastic bending resistance $M_{pl,Rd}$ and strain limited resistance M_{Rd} for different neutral axis positions (Schäfer, 2017)

Discussion

As referred previously, many researchers attempted to provide an analytical expression for the required joint rotations. However, due to the complicated mechanisms taking place during the plastification of the members, an analytical formulation was only obtained with the help of empirical and best fitting results. Although useful, the equations provided by Nethercot in Figure 2.26 are only valid within a certain range (e.g. S275 grade). An extrapolation to different steel grades is therefore not suitable.

Although a more general method was given by Kattner, it requires the determination of moment-curvature shapes of composite beams, which from a practical point of view remains rather inappropriate. The numerical investigations performed by Kattner allow, however, to qualitatively determine the influence of parameters, which are not included in the empirical equations derived by Nethercot.

The conjunction of both research works enables the required joint rotations to be roughly estimated. Moreover, non-linear calculations are nowadays relatively user-friendly with the facilities provided by FE softwares. Numerical simulations constitute therefore an alternative tool to determine the required joint rotations.

Another option for the verification of the joint rotation would consist in the application of the conservative limit of 80 mrad. In other terms, whenever a composite joint provides a rotation capacity over 80 mrad, allowance can be made for the use of the plastic global analysis method to design non-sway composite frames.

2.4 Summary

The analysis of available literature allows the following conclusions to be made:

- Increasing the diameter $\varnothing$ of the longitudinal reinforcement bars enhances the rotation capacity of composite joints (Brown and Anderson, 2001) and (Hahn, 2009).
- The rotation capacity of composite joints increases with larger reinforcement ratio ρ (Elz, 2000), (Loh et al., 2006b) and (Hahn, 2009).
- The larger the reinforcement ratio ρ, the larger is also the stiffness and the resistance of the corresponding composite joint (Altmann et al., 1991), (Najafi, 1992), (Xiao et al., 1994), (Malaska, 2000), (Barcewicz, 2010) and (Hahn, 2009).
- The greater the distance between the column flange and the first stud, the longer is the tensile band activated in the reinforced concrete slab and the more significant is the ductility of the composite joint (Law, 1983), (Bode and Kronenberger, 1996), (Bode et al., 1997) and (Schäfer, 2005).
- Composite joints, reinforced with only welded fabric mesh reinforcement, present a brittle behaviour due to the limited ductility of the mesh reinforcement (Davison et al., 1990), (Kathage, 1994), (Xiao et al., 1994), (Ren, 1995), (Bode et al., 1997) and (Hahn, 2009).
- Substantial rotation capacity is provided when the governing joint component is the reinforced concrete slab (Altmann et al., 1991).
- Increasing the depth of steel beam section increases the internal lever arm. Thus, the joint stiffness increases at the expense of the rotation capacity (Najafi, 1992) and (Brown and Anderson, 2001).
- The presence of beam and column encasement provides a larger rotation capacity due to the more effective stress dispersion in the vicinity of the column flange (Odenbreit, 2000).
- Composite column sections provide greater stiffness and strength to composite joints (Law, 1983) and (Simões, 2000).
- To avoid complicated anchorage or reinforcement detailing around the column, it is suggested to design external beam-to-column joint as simple joints (Davison et al., 1990) and (Xiao et al., 1994).
- Composite joints with partial shear connection allow for larger rotation capacities (Law, 1983), (Bode and Kronenberger, 1996), (Odenbreit, 2000), (Loh et al., 2006b) and (Fu and Lam, 2006).
- High shear-to-moment ratios have insignificant influence on the moment-rotation response of composite joints (Echeta, 1982), (Kathage, 1994) and (Malaska, 2000). Xiao and Li stated however that if the shear force approaches the capacity of the steel beam, the resistance can decrease (Xiao et al., 1994) and (Li et al., 1996).
- The required joint rotation allowing for plastic analysis of semi-continuous composite frames increases for larger span lengths, degree of shear connection and material strength (Najafi, 1992), (Li et al., 2000) and (Kattner, 1999).
- Conversely, the larger the depth of the steel section or the joint-to-span resistance, the lower the requirement on the joint rotation allowing for the full plastic redistribution of bending moments in the beam (Najafi, 1992), (Li et al., 2000) and (Kattner, 1999).

3 Experimental Investigations

3.1 Test set-up

The experimental tests carried out in the present project were designed to represent internal beam-to-column joints. The aim of these tests was to investigate and understand the behaviour of composite joints under hogging bending moments. Accordingly, the configuration of the test set-up was chosen to reflect the real loading condition of internal joints within a structural frame (cf. Figure 3.1). For this purpose, a symmetrical set-up was adopted. The load was introduced by an hydraulic jack pulling on the column, while at both ends of the specimen, a support was provided to restrain the vertical displacement as represented in Figure 3.2.

The dimension of the test set-up was selected in accordance to EN 1994-1-1 (2004). In the latter, the hogging region of a composite beam can be approximated to 15 % of its span for the specific case of an internal beam in a building. For a 16 m long span, the hogging length can thus be estimated to 2.4 m. Accordingly, the cantilever length, which is calculated from the support to the exterior surface of the column flange, was equal to 2.38 m in the present tests.

The column consisted of an HEB 300 profile made of S355 structural steel. For the beams, a slim floor type of composite beams (CoSFB) was chosen. The latter was composed of an HEA 320 profile and a steel plate 500 mm x 25 mm welded to the bottom flange of the HEA 320 profile (cf. Figure 3.3). The particularity of this type of beams resides in the fact that they are integrated in concrete or composite slab systems. Composite slabs, as for instance Cofraplus 220, are typically used in combination with CoSFB. Since the focus of these tests was, however, the longitudinal behaviour of the beam/joint system, the transverse steel decking was omitted in the test specimens. The partial encasement of the steel beam was nevertheless considered in the fabrication of the specimens so as to realistically reproduce the longitudinal behaviour of a CoSFB (cf. Figure 3.3).

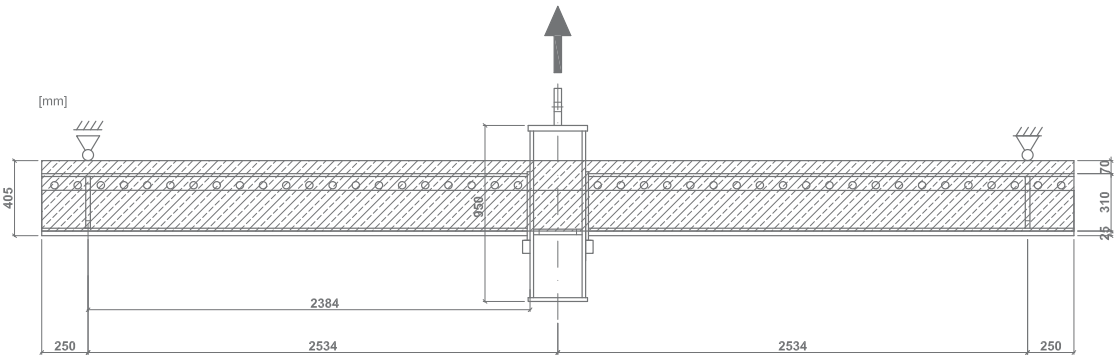

Figure 3.1: Test set-up

In these tests, the composite action between the encased steel section and concrete was assured by a new type of shear connectors, the so-called "CoSFB-Betondübel". As it can be seen in Figure 3.4, it consists of a deep-embedded reinforcing dowel bar of 12 mm diameter placed in the openings drilled in the web of the steel profile. More information about this novel type of shear connectors can be found in (Braun et al., 2014a,b). The German Technical Approval for this type of shear connectors defines its application in sagging regions (DIBt - Deutsche Institut für Bautechnik, 2014). The presented tests and results are the first to involve CoSFB-Betondübel in hogging regions.

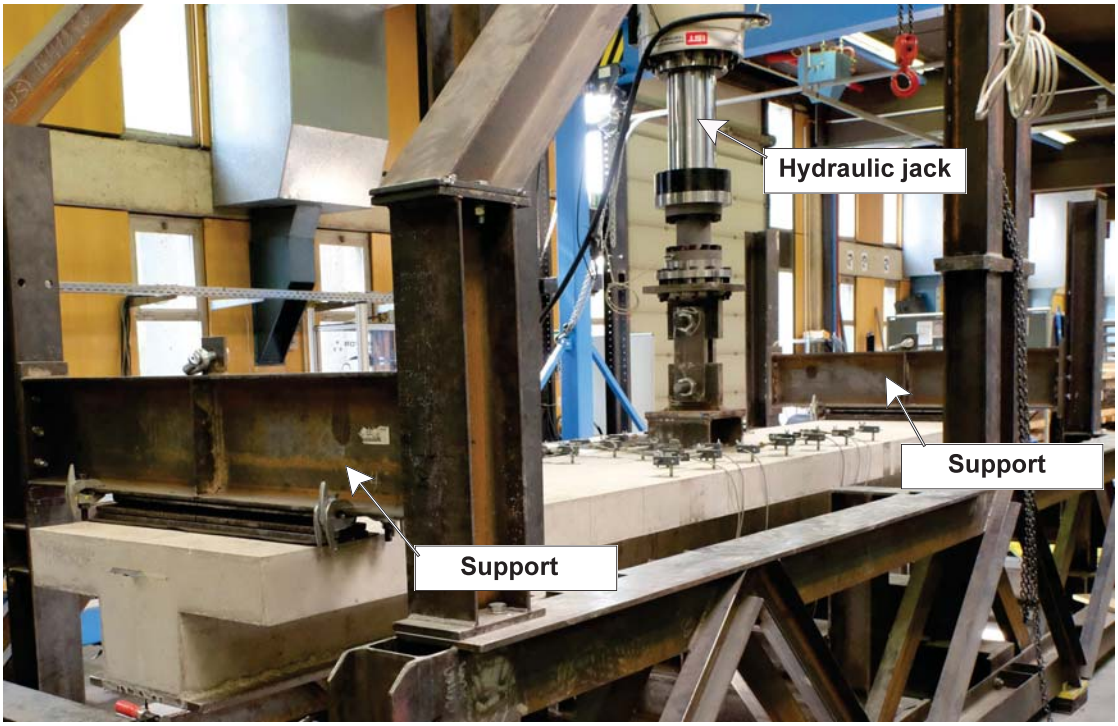

Figure 3.2: Test set-up and testing frame

According to EN 1994-1-1 (2004), the effective concrete width of an internal composite beam of 16 m is about two meters. Due to the dimensions of the testing frame, an effective width of one meter was chosen for the concrete slab, which constitutes a safe-sided choice.

Various reinforcement was embedded in the concrete slab. The reinforcement layout of the concrete slab is shown in Figure 3.6. Longitudinal reinforcement bars of diameter 12 mm, 16 mm and 20 mm were disposed in the upper part of the concrete slab with a clear concrete cover of about 30 mm. Overlapping bars were placed on each side of the column to assure the continuous flux of forces of the central rebars, whose continuity was obstructed by the column. Transverse reinforcement bars of diameter 8 mm were placed in line with the CoSFB dowel bars to provide resistance to transverse bending and prevent the shear failure of the concrete slab.

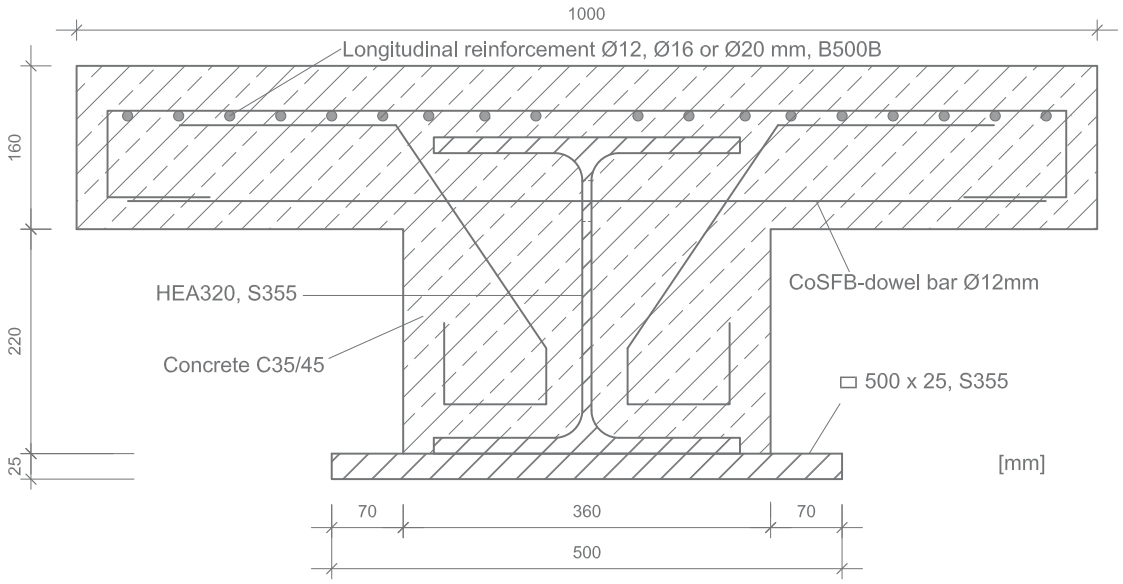

Figure 3.3: Cross-section of the specimen

Figure 3.4: Dowel bars

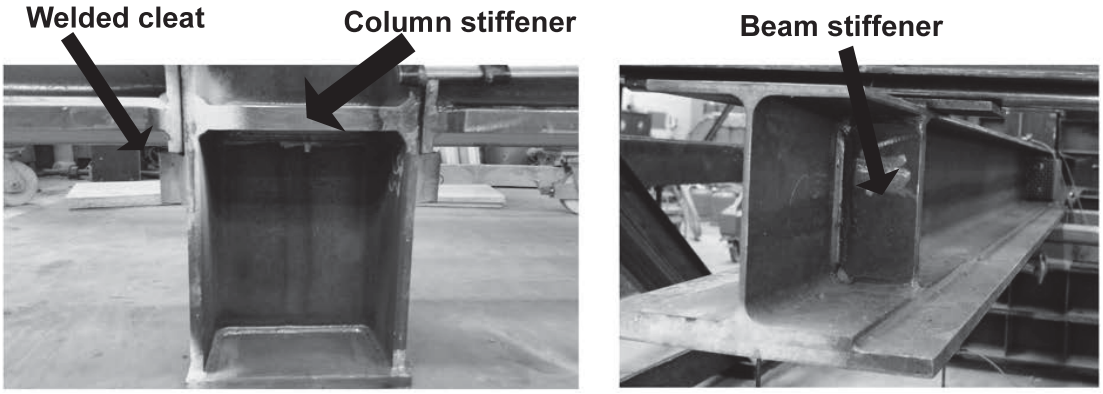

Figure 3.5: Stiffeners in the specimen and welded cleat

Figure 3.6: Reinforcement layout

In former experimental research investigations, no consensus was found concerning the position of the longitudinal rebars. Some researchers opted to place the longitudinal bars upon the transverse reinforcement, while others inverted this arrangement. In the light of this, the transverse bars were placed below the longitudinal rebars in the first two tests B21 and B22 (cf. Figure 3.7). Due to an unexpected failure occurred in test B21 and explained in Chapter 4, the other specimens were fabricated with the longitudinal reinforcing bars being confined under the transverse reinforcement (cf. Figure 3.8). In all tests additional stirrups of diameter 8 mm were inserted in the concrete chamber to avoid the longitudinal shear failure between the chamber and the concrete slab and to guarantee the integrity of the cross-section.

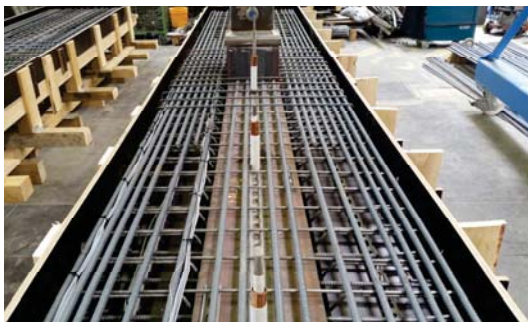

Figure 3.7: Position of longitudinal reinforcement above transverse reinforcement: B21 and B22

Figure 3.8: Position of longitudinal reinforcement under transverse reinforcement: B31 to E32

The experimental campaign involved three different joint configurations. The first was a composite joint without steel connection between the beam and the column (cf. Figure 3.9). The second consisted of a bare steel joint (cf. Figure 3.10), whereas the third configuration concerned a composite joint with an additional steel connection (cf. Figure 3.11). In all the three joint types, an endplate of 15 mm thickness was provided at the end of the beam. For the joints with steel connection (cf. Figure 3.10 and 3.11), a flush endplate connection with 4 M24 bolts in 10.9 grade was provided. A clearance of 2 mm was adopted between the bolts and their holes to facilitate the assembly.

Although the concrete encasement of the column panel region should be sufficient to prevent the web buckling of the column, an additional web stiffener was welded to the column to ensure the same compression points in all the tests (cf. Figures 3.5). At the supports, stiffeners were also provided in the web of the beam to eliminate the influence of local web buckling. These stiffeners allow in addition to prevent the possible occurrence of significant slip between the steel beam and the concrete, which would induce larger joint rotation capacities.

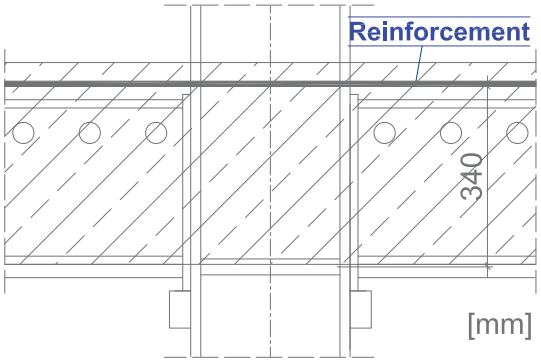

Figure 3.9: Test Series B

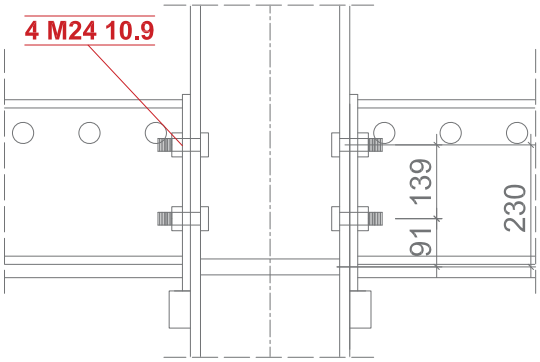

Figure 3.10: Test Series C

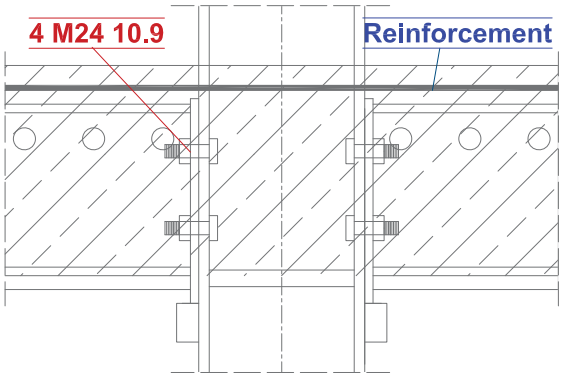

Figure 3.11: Test Series E

The fabrication of the specimens was done in three steps. Firstly, the steel beam was bolted to the steel column using a torque wrench. All the bolts were therefore tightened to 1/3 of the standard tightening torque to ensure the same initial conditions in all the tests. This measure allows neglecting the influence of different bolt preloads on the behaviour of composite joints. Secondly, the reinforcement cage was assembled and fixed in the correct position according to the reinforcement plans (cf. Annex A.2). In parallel, a timber formwork (cf. Figure 3.12) was build up for concrete casting and some curing oil was brushed on the formwork surface for easy demoulding. Finally, concrete was cast in the formwork. Casting of cylinders was carried out at the same time. After a few days, the formwork was removed from the specimen and after the necessary curing time of 28 days, the specimens were transported into the test rig (cf. Figure 3.13). The measurement equipment was then installed on the specimens. Detailed specimen drawings for the steel parts and reinforcement are provided in Appendix A.

Figure 3.12: Formwork structure

Figure 3.13: Curing of concrete and transportation of the specimen

3.2 Test program and investigated parameters

The test program was planned to investigate three fundamental factors influencing the behaviour of composite joints:

1. the reinforcement ratio ρ
2. the diameter $\varnothing$ of the longitudinal reinforcement bars
3. the steel connection

Since these parameters have not been analysed concisely in research (cf. Chapter 2), the present experimental campaign was projected so as to focus on the individual investigation of each of the above mentioned parameters.

The experimental program was subdivided into three test series, each of them defined in such a way to isolate the influence of the identified parameters on the joints' behaviour (cf. Figure 3.14). In the first test **series B**, the focus is put on the reinforced concrete slab component. Longitudinal reinforcement ratio and rebar diameter are the two parameters investigated individually in this series. No steelwork connection between the column and the beam is therefore provided. Hence, the bending resistance of the joint arises from the couple of forces associated to:

1. the tensile bearing resistance of the continuous longitudinal reinforcement bars and
2. the compression resistance of the bottom flange of the beam

The shear force in the beam is transferred to the column over the massive cleat, which is welded to the column flange (cf. Figure 3.5). Since in most of the previous experimental campaigns, an increase in reinforcement ratio was frequently accompanied by larger rebar diameters, the present program presents the particularity of investigating separately the reinforcement ratio ρ and the rebar diameter $\varnothing$. To enable the assessment of the isolated influence of these two parameters ρ and $\varnothing$, 4 tests were performed with variable reinforcement ratio and bar diameter. The influence of the rebar diameter $\varnothing$ on the joint's response stems from the comparison between tests with equal reinforcement ratio (ρ = 1.3 % for tests B21-B31 and ρ = 2.0 % for tests B22-B32), whereas the influence of a variable reinforcement ratio is inferred from the comparison between test B22 and test B31 presenting equal rebar diameters.
Another differentiating factor in the present test program is the substantial reinforcement ratio. Former research projects were, in fact, mostly focussed on rather humble degrees of reinforcement (ρ < 1.0 %) because it avoids large compression forces in the bottom flange. This allowed to avoid that the failure of the specimen is linked to the buckling of the bottom flange. In the present tests, on the contrary, the reinforcement ratios used are rather significant (ρ = 1.3 % and ρ = 2.0 %).

In the second test **series C**, all the concrete components (slab and encasement) were omitted to isolate the steel connection. This enables to solely analyse the behaviour of the bolted connection. One single prototype consisting of a flush endplate connection, with 4 M24 grade 10.9 bolts disposed over two rows, was tested (cf. Figure 3.16). Since the shear force in the beams is transferred over cleats, the bolts are mainly subjected to tensile forces, ensuring a certain bending resistance. Each bolt-row was designed such that its resistance is governed by a ductile mode of failure, which is typically associated with bending failure of the endplate or the failure of the endplate-bolt assembly. With this ductility condition a plastic distribution of internal forces in the joints is enabled to ensures a ductile joint response.

Table 3.1: Test program

Test designation	Reinf.	Concrete slab [cm]	Concrete class	Steel grade	Reinf. grade	Steelwork connection	Comparison (Influence of)
B21	18 ⌀ 12	100 x 16	C35/45	S355	B500 B	-	B31 (rebar diameter)
B22	16 ⌀ 16	100 x 16	C35/45	S355	B500 B	-	B32 (rebar diameter) + B31 (reinforcement ratio)
B31	10 ⌀ 16	100 x 16	C35/45	S355	B500 B	-	B21 (rebar diameter) + B22 (reinforcement ratio)
B32	10 ⌀ 20	100 x 16	C35/45	S355	B500 B	-	B22 (rebar diameter)
E21	18 ⌀ 12	100 x 16	C35/45	S355	B500 B	4 M24 10.9	E21 (steelwork connection)
E22	16 ⌀ 16	100 x 16	C35/45	S355	B500 B	4 M24 10.9	E22 (steelwork connection)
E32	10 ⌀ 20	100 x 16	C35/45	S355	B500 B	4 M24 10.9	E32 (steelwork connection)
C14	-	-	-	S355	B500 B	4 M24 10.9	behaviour steelwork connection

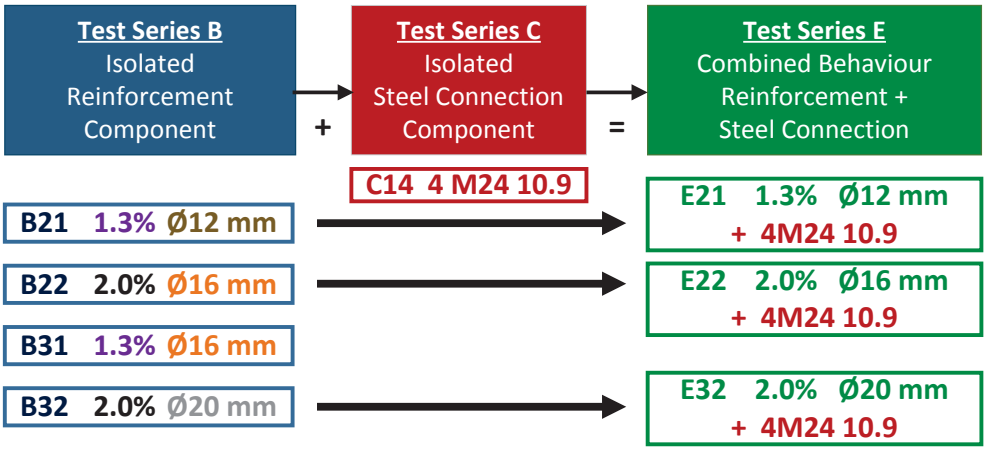

Figure 3.14: Test program

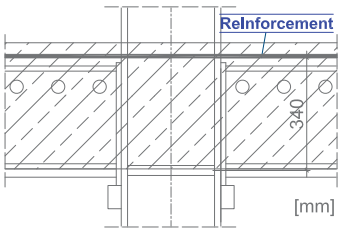

Figure 3.15: Test Series B

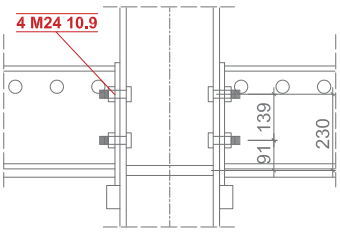

Figure 3.16: Test Series C

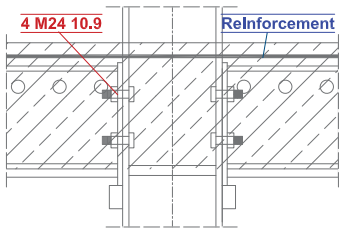

Figure 3.17: Test Series E

Finally, in the third test **series E** the two components, investigated in the two first test series in isolation, were combined (cf. Figure 3.17). Three tests, presenting the same reinforcement layout as in series B, and the same steel connection as in series C, were tested. This series aims to investigate the influence of these additional bolt-rows on the resistance, stiffness and rotation capacity of composite joints. To the author's knowledge, it is the first time that a direct comparison between a boltless and a bolted flush endplate composite connection is performed experimentally, without any other variation of parameters than the presence or absence of the steel connection. A similar comparison was completed in the research conducted by Odenbreit (2000), which was however focussed on bolted finplate connections.

For the correct interpretation of the test results, it was important to only allow for the deformation of the investigated components and to prevent other sources of deformation, which could influence the results. It was demonstrated in (Aribert, 1995) that slip in the steel-concrete interface significantly enhances the rotation capacity of composite joints. To neglect its

influence, a massive web stiffener was welded in the beams on the level of the end supports. This stiffener eliminates also the possibility of web buckling under the load application point provided by the supports. It is also well-known that the deformation in the compression region of a composite joint improves its rotation capacity by increasing, at the same time, the risk of local web buckling in the column. In order to restrict the deformation in the compression region, a stiffener was welded between the column flanges. The introduction of this stiffener in combination with the strong bottom flange of the steel beam leads to a stronger compression component of the joint, which assigns, as desired, the weak joint component to its tension region.

3.3 Instrumentation

The continuous recording of relevant data constitutes an important aspect in the performance of tests. Thus, special attention was paid to the instrumentation of the specimens to extract the informations needed for the deep understanding of the joint's behaviour.

Since, the moment-rotation relationship of a joint allows to compare the performance of different joint configurations, it was essential to measure the bending moment acting in the joint and its corresponding rotation during the test. The bending moment was deduced from the load cell recording the force in the jack. Due to slab deformation and the cracking of the slab, the rotation was more difficult to measure. Owing to the importance of the joint rotation, three independent recording techniques were implemented to verify the accuracy of the results. The first technique consisted in the direct measurement of the rotation using three inclinometers (cf. inclinometers 28-30 in Figures 3.18 and 3.19). One inclinometer was placed in the centre line of the column to verify the symmetry of the system, while the two others were placed on each side of the column at a distance of 182 mm from the column flange on the level of the beam web. In the second method, the joint rotation was evaluated by subtracting the readings between two parallel transducers (1-4). In the third method, the joint rotation was deduced from the deflection of the beam measured by the displacement captors (5-7 in Figure 3.18). In principle, this method is less accurate because both beam deformation components (rigid body deformation and bending deformation) are included in the calculation of the joint rotation. However, due to the significant bending stiffness of encased slim floor beams, the error made can be neglected as it is described in the next Chapter.

The global measurements described above are not sufficient for the deep understanding of the behaviour of the various components of the joints (bolts, reinforcement, concrete slab). It was therefore imperative to incorporate strain gauges in these components to evaluate the stress distribution at the different loading stages. Since test series B focussed on the reinforcement component, eight strain gauges were glued on the longitudinal rebars (cf. Figure 3.20). In test series C and E, strain gauges were applied in 4 bolts for each specimen, two being in upper and two in bottom bolts (cf. Figure 3.21 and 3.23). Each instrumented bolt was supplied with three strain gauges to enable an accurate assessment of the bolt forces. A plan of the instrumented bolt is presented in Appendix (cf. Figure A.15). In test series E, no strain gauges were applied to the reinforcement bars.

Horizontal displacement captors (16-25 and 31-32) were positioned in 300 mm intervals on the slab to measure the elongation of the concrete slab during the test performance (cf. Figure 3.18 and 3.22). Several displacement captors (10-15) were also provided to measure the occurrence of slip between the concrete and the steel section. Finally, the displacement

captors 26 and 27 measured the bending deformation of the endplate connection on each side of the column.

Another important element in the analysis of a composite structure is the development of cracks in the concrete slab. Therefore, the specimens were carefully inspected to mark the occurrence of new cracks or the development of existing ones during the realisation of the tests. This allowed to follow the crack development in the concrete slab and to reconstitute the crack pattern.

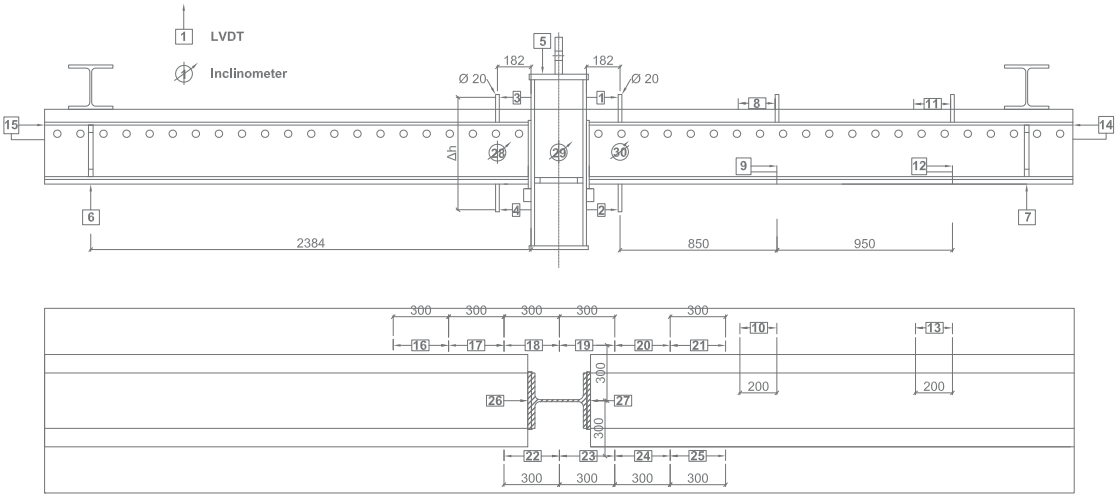

Figure 3.18: Instrumentation of the first tests

Figure 3.19: Inclinometers

Figure 3.20: Strain gauge on rebar

Figure 3.21: Strain gauge on bolt

Figure 3.22: Captors on concrete surface

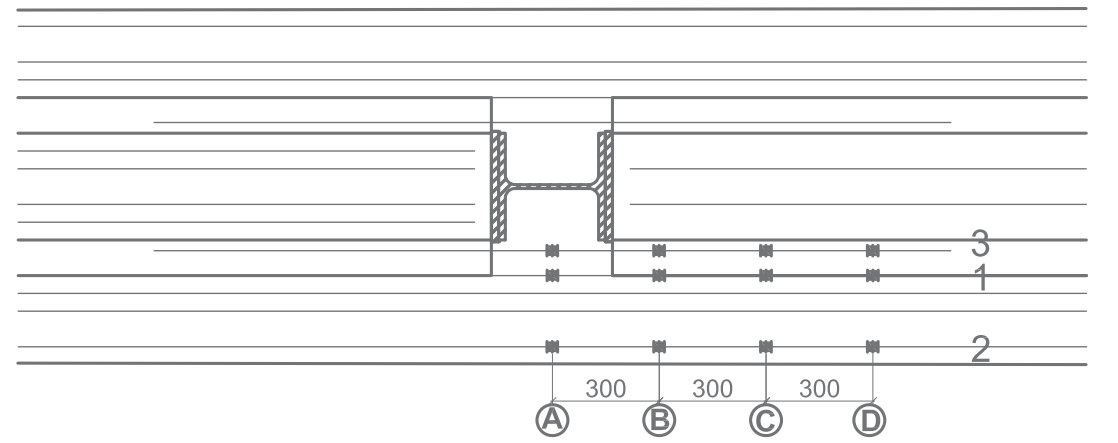

Figure 3.23: Arrangement of strain gauges in reinforcement

The results obtained in the first two tests confirmed the absence of any significant slip (below 0.5 mm). For this reason, the captors 10-13 were deleted and replaced by additional horizontal displacement captors on the top of the concrete (31-32) as well as vertical captors (33-34) measuring the deflection of the beams. As it is shown in the next Chapter, the inclinometers provide reliable results. The horizontal captors 1-4 were therefore omitted in the remaining tests. In tests B31 and B32, four additional strain gauges were glued on the overlapping reinforcement bars to verify the activation of these bars. The alternative instrumentation of the tests B31, B32, E21, E22 and E32 is detailed in Figure 3.24.

For the test on the bare steel joint, all the captors associated to concrete elongation (14-25 and 31-32) have been removed. More detailed information about the instrumentation is provided in Appendix A.

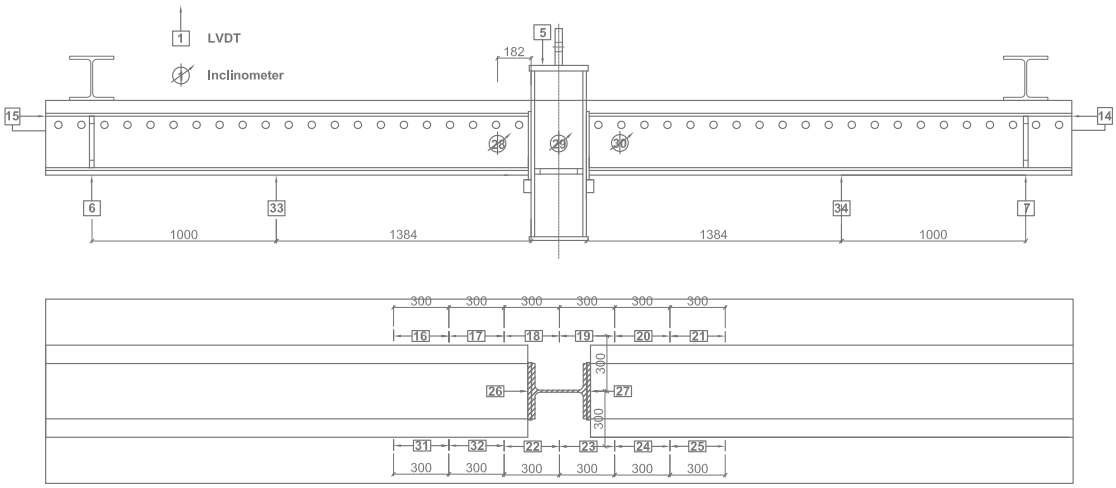

Figure 3.24: Alternative instrumentation of the tests

3.4 Test procedure

All the experiments followed the same test procedure. The load was applied monotonically by a displacement controlled hydraulic jack at a rate of 1 mm/minute. At each load increment of 50-100 kN, the jack was held at the same position for approximately 10 minutes. During this time, a small drop of load was registered, which is the result of the relaxation of the specimen. In the final evaluation of the results, these dynamic effects can be eliminated by considering only the lower static load values. During these time intervals, the specimens were inspected and the occurrence of new cracks was marked. The tests were performed following the testing procedure proposed in EN 1994-1-1 Annex B.2.4. Accordingly, the load was first applied in increments up to 40 % of the expected load and then cycled 25 times between 5 % and 40 % of the expected load failure. Once the first signs of non-linear joint behaviour were identified, the displacement rate was increased to 2 mm/min. The test was stopped due to the clear failure of the specimen (load drop) or to excessive deformations, which made it necessary to interrupt the test for safety reasons.

3.5 Material properties

During the concreting work on the test specimens, three cylindrical concrete samples (cf. Figure 3.26) were cast at the same time for each specimen and cured in a water tank. On days of tests, three samples were tested in compression. The average compressive strengths for all specimens are summarised in Table 3.2.

All the steel parts were delivered in grade S355. The real mechanical properties were deduced from tensile test coupons (cf. Figure 3.27), whose results are given for each steel part in Table 3.3.

Reinforcement bars of class B500B were used. Since the real strength and ductility of the bars are essential for the later evaluation of the test results, tensile tests for the different bar diameters (cf. Figure 3.28) were performed with two different testing machines. Similar results were obtained, which confirms the reliability of the values given in Table 3.4. This table includes two different strain measures; A_{gt} is the percentage elongation at maximum

load while $A_{5.65}$ represents the permanent strain after fracture in a region of $5.65 \cdot \sqrt{A_{rebar}}$ around the fracture point (cf. Figure 3.25).

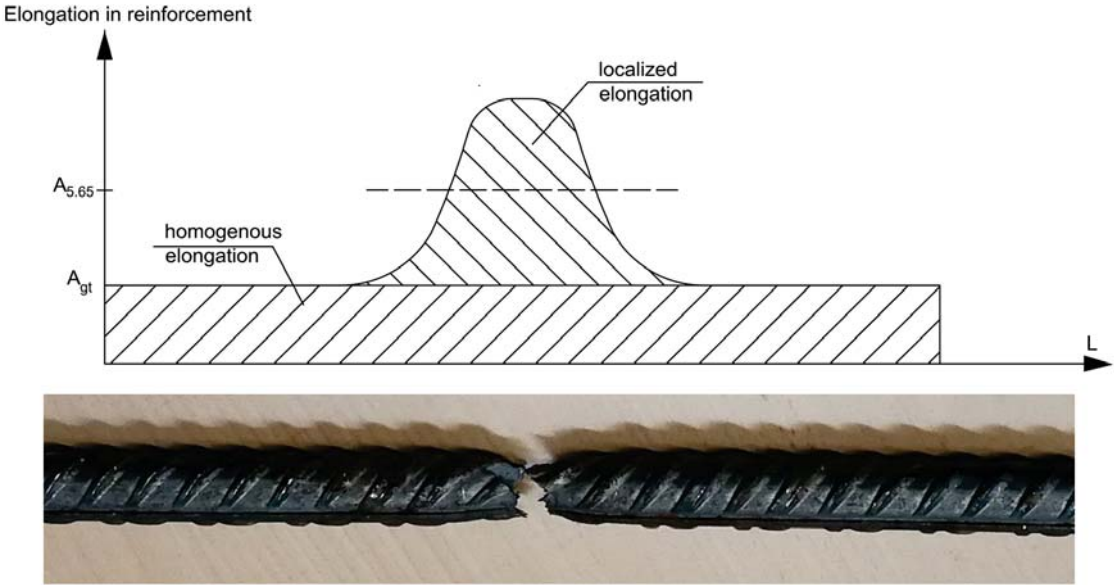

Figure 3.25: Strain distribution along rebar axis during material tests

Table 3.2: Mean strength values of concrete cylinders on the day of testing

Specimen	Compressive strength $f_{c,cyl}$ $[N/mm^2]$
B21	59
B22	57
B31	45
B32	45
E21	60
E22	61
E32	47

Table 3.3: Mean tensile strength of the steel members

Steel member	Yield strength f_y $[N/mm^2]$	Tensile strength f_u $[N/mm^2]$
Beam HEA	499	554
Bottom plate 500x25	412	534
Endplate	425	549
Column HEB	429	526

Table 3.4: Material properties of reinforcement bars

Reinforcement	Yield strength f_{sy} $[N/mm^2]$	Tensile strength f_{su} $[N/mm^2]$	A_{gt} [‰]	$A_{5.65}$ [‰]
∅12 mm	534	655	102	236
∅16 mm	547	671	99	204
∅20 mm	578	674	97	225

Figure 3.26: Cylindrical concrete samples

Figure 3.27: Tensile test coupons of endplate

Figure 3.28: Tensile tests on reinforcement bars of different diameter

4 Analysis of Experimental Results

4.1 Introduction

The moment-rotation relationship $M_j - \Phi_j$ of a composite joint is a characteristic defining its behaviour. The exact definition for the bending resistance M_j and the joint rotation Φ_j is therefore essential for a research dedicated to the analysis of results and comparison of different joint configurations. The need for a unique definition was already pointed out by Zandonini (1989). To provide a common ground for a consistent comparison of different experimental results, Zandonini suggested the following definitions: The bending moment M_j is evaluated in the contact section between the column flange and the beam plate, while the joint rotation Φ_j corresponds to the variation of the angle between the tangent to the beam axis and the tangent to the column axis (cf. Figure 4.1). All moment-rotation curves, provided in this work, are given in accordance with this standard definition.

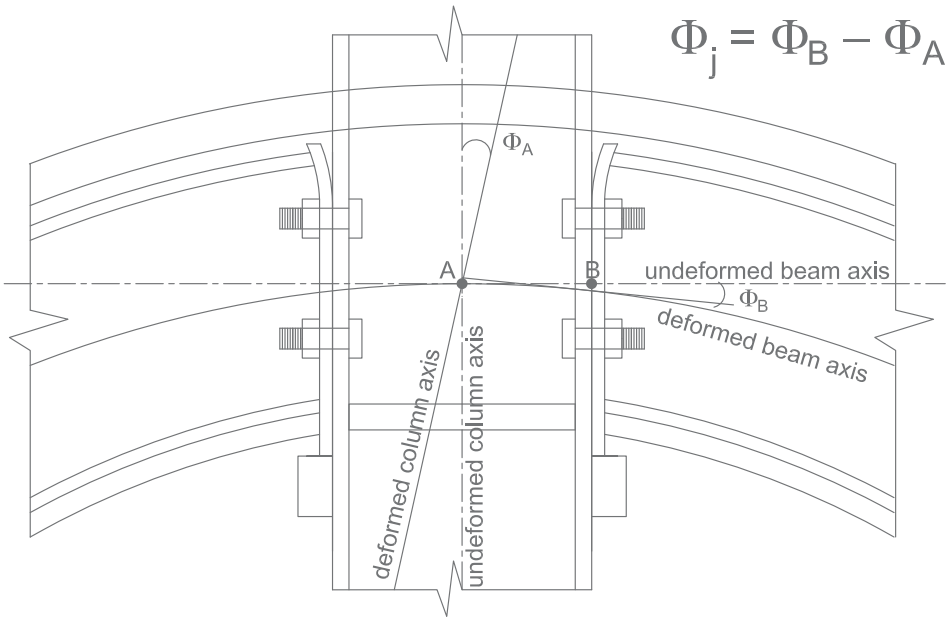

Figure 4.1: Definition of the joint rotation

Figure 4.2 compares the typical moment-rotation curve obtained from testing with the idealised curve suggested by EN 1994-1-1 (2004). From this curve, the three structural properties characterising the global behaviour of joints can be retrieved; namely the stiffness, the bending resistance and the rotation capacity. These values are derived from the test curve according to the following procedure:

- *Joint stiffness* $S_{j,Test}$

  The joint stiffness $S_{j,Test}$ is defined at 2/3 of the expected plastic bending resistance of the joint $M_{pl,cal}$, which is calculated using the measured yield strength of materials. This definition allows to compare the stiffness values obtained from the tests $S_{j,Test}$ with the analytical values $S_{j,ini}$ according to EN 1994-1-1 (2004).

- *Ultimate bending resistance* $M_{u,Test}$

  The ultimate bending resistance of a joint $M_{u,Test}$ corresponds to the maximum resistance reached in the moment-rotation relationship. The values obtained for the different tests are compared to the analytical values, which are calculated using the measured ultimate strength of materials.

- *Rotation capacity* Φ_u

  The rotation capacity of a joint is defined as the rotation at which the rupture of a reinforcement bar occurs or at which the test is stopped owing to the excessive deformation of the specimen. In the second case, the rotation capacity of the correspondent composite joint is in reality bigger. This must be borne in mind when assessing the rotation capacity of joints.

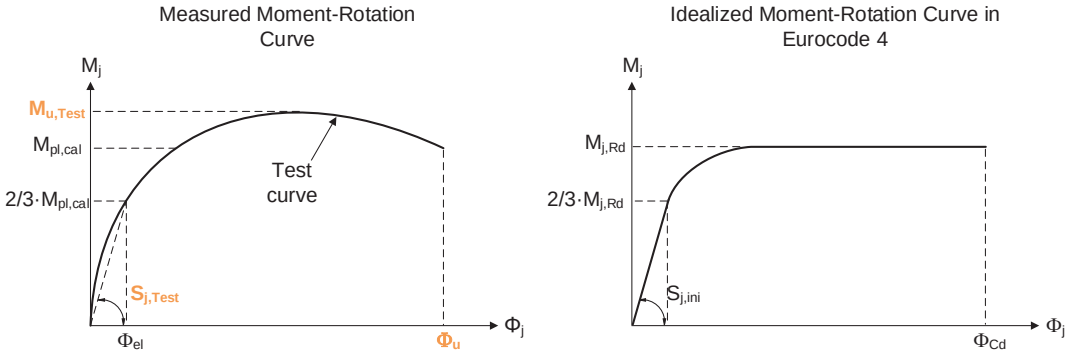

Figure 4.2: Determination of the joint's structural properties from the test and comparison to Eurocode 4

As explained in Section 3.3, three independent techniques to record the joint rotation were employed. Figure 4.3 compares the moment-rotation curves obtained with each measurement method for test B21. The inclinometers and the horizontal transducers provide similar rotation values, while the third method slightly overestimates the joint rotation. This discrepancy is explained by the fact that for the third method, the joint rotation is calculated from the vertical deflection of the beam, which inevitably includes the bending deformation over the whole beam length. Due to the fact that the two first methods provide similar and reliable results for the joint rotation, the moment-rotation curves presented in the next sections emanate from the inclinometers. Although no significant asymmetry was recorded by the central inclinometer, an averaged moment-rotation curve between the left and the right inclinometers is provided to compensate the little asymmetry.

As referred in the test procedure (cf. Section 3.4), load drops at all test pauses could be observed due to the relaxation of the specimen. For this reason, the moment-rotation curves obtained from the measurement devices include small load drops (cf. Figure 4.4). Thus, for the final static moment-rotation curve only the lower resistance values were considered.
For clarity of the presented results, the load cycles (cf. Section 3.4) are also omitted in the further representation of the moment-rotation curves. The graphs represent therefore the measurements recorded after the initial 25 cycles performed at 40 % of the expected load bearing capacity.

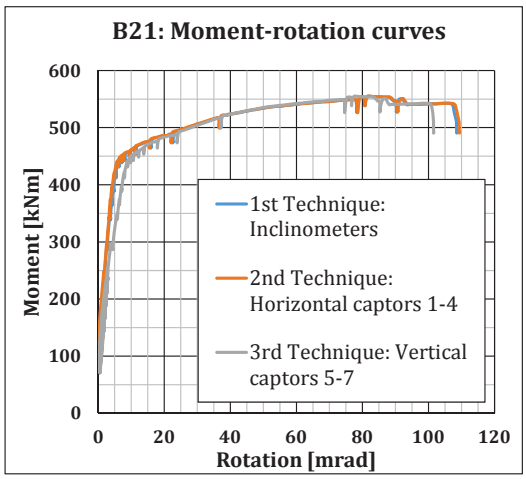

Figure 4.3: Comparison of the ultimate joint rotation using different measurement techniques

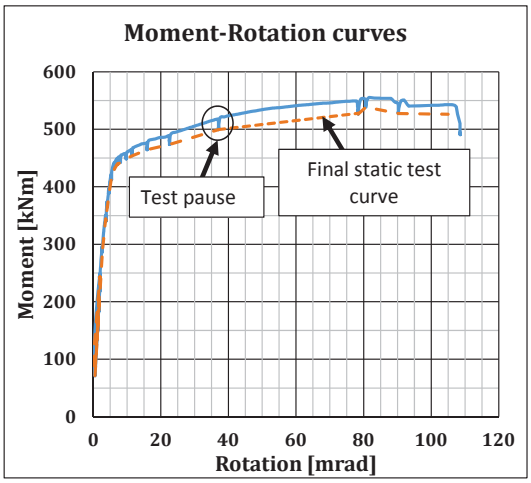

Figure 4.4: Comparison between measured and static moment-rotation curves

4.2 Test series B

4.2.1 Moment-rotation curves and observations

The moment-rotation curves of the composite joints tested in series B are detailed in Figure 4.5. From the four specimens tested in this series, only those with lower reinforcement ratio B21 and B31 failed due to the rupture of a longitudinal reinforcement bar (cf. Figure 4.6). For the other two specimens, the tests were terminated at large rotations due to the excessive deformation of the joint. The comparison of tests B21 and B31 shows that the rotation capacity is slightly larger in test B21, using smaller rebar diameter ⌀. However, this outcome should be used with caution. As explained in Section 3.1, in the two tests B21 and B22, which were first performed, the reinforcement layout was different than in the other tests. The longitudinal reinforcement bars were placed above the transverse reinforcement, while in the other tests these longitudinal rebars were placed below the transverse reinforcement.

In test B22, two consecutive drops in resistance could be observed due this different reinforcement layout (cf. Figure 3.15). This load drops occurred in the plastic branch of the moment-rotation curve at about 25 mrad and 42 mrad. Simultaneously, a long longitudinal crack on each side of the concrete slab (cf. Figure 4.7) was detected. This observation explains the loss of resistance recorded by the measurement devices: the shear failure of the slab led to an anchorage failure of two outer longitudinal reinforcement bars, which originated the decrease in joint resistance.

Such a failure was not observed in test B21. The reason for this resides in the fact that the amount of reinforcement in test B21 is smaller than that of test B22. Consequently, lower splitting forces developed in the concrete slab. Although this difference in reinforcement layout did not visibly affect the moment-rotation curve of test B21, the lack of transverse reinforcement above the longitudinal rebars allowed for a larger effective length of reinforcement. This could possibly be the reason for the larger rotation capacity developed in test B21 in comparison to test B31.

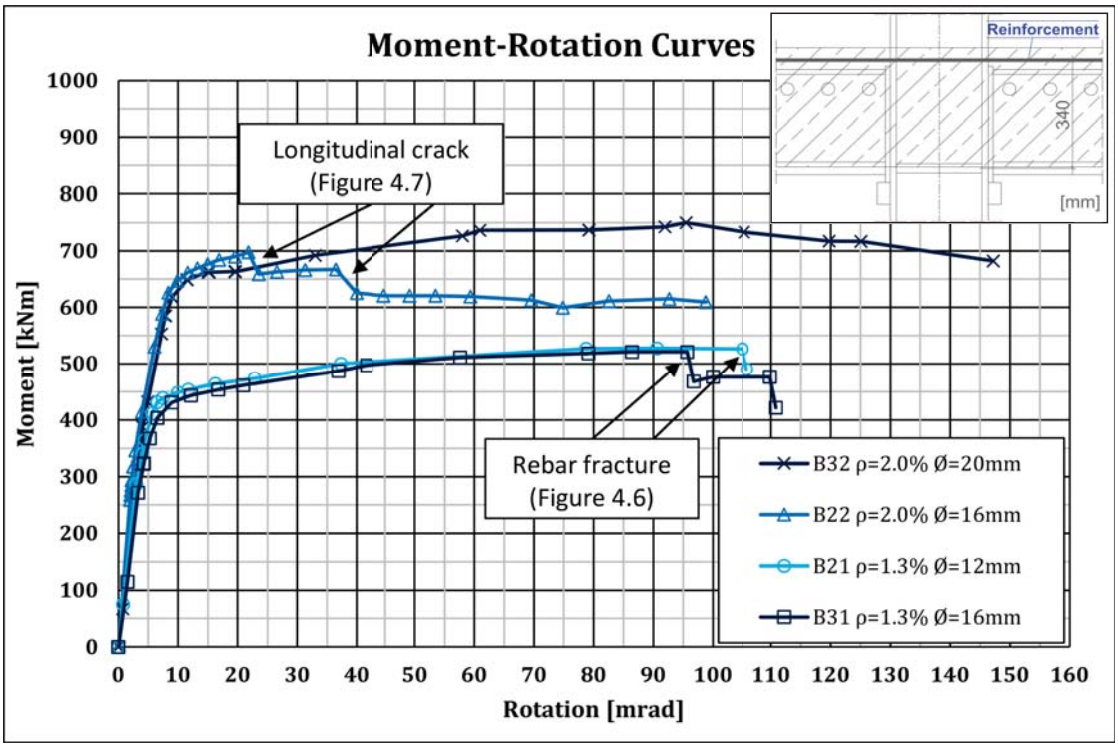

Figure 4.5: Test series B: Moment-rotation curves

Figure 4.6: Rupture of reinforcement in test B21

Figure 4.7: Test B22: Longitudinal crack of the slab

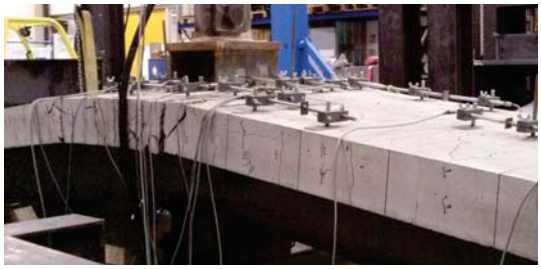

(a) Test B21

(b) Test B22

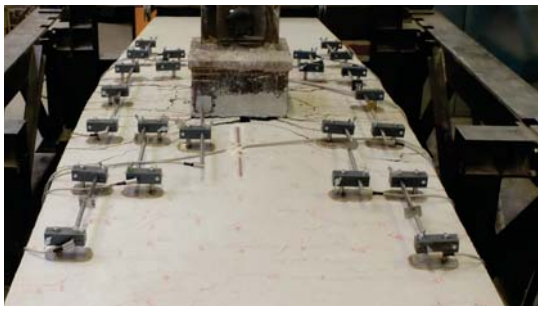

(c) Test B31

(d) Test B32

Figure 4.8: Deformed shape of specimen at around 100 mrad

During the tests, a substantial transverse bending of the test specimen was observed at large rotation (cf. Figure 4.8). This phenomenon was more pronounced for the specimen B32, whereas for the other specimens of this series, transverse bending remained more moderate. To explain this phenomenon, the two specimens B22 and B32 are compared. Both specimens present the same reinforcement ratio. The only difference is related to the diameter $\varnothing$ of the longitudinal rebars. At large joint rotations, the longitudinal reinforcement is subjected to significant bending in longitudinal direction as depicted in Figure 4.9. Due to this longitudinal bending, large deviation forces are developed in the specimens. The deviation forces u_{16} and u_{20}, corresponding to the deformation of a rebar diameter 16 mm (test B22) and 20 mm (test B32) respectively, are directly related to the tensile forces in each rebar. Since the reinforcement ratio is the same in both specimens, the sum of the individual deviation forces is identical ($\sum u_{20} = \sum u_{16}$). However, due to the larger section of the diameter 20 mm rebar, the deviation force u_{20} developed in one single bar is bigger for test B32. Figure 4.10 shows the transverse deflection of the cross-section of the specimen and the distribution of the forces. In order to determine the influence of these deviation forces in transverse direction, a cantilever on which these forces act as point loads is modelled. B31

presents a homogeneous distribution of the forces on the cantilever while in test B32 the larger deviation forces u_{20} act punctually on the slab causing a greater vertical deflection in transverse direction. It can be therefore concluded that it was the conjunction of both parameters - large reinforcement ratio ρ with large rebar diameter $\varnothing$ - which induced a larger transverse deflection of the specimen B32.

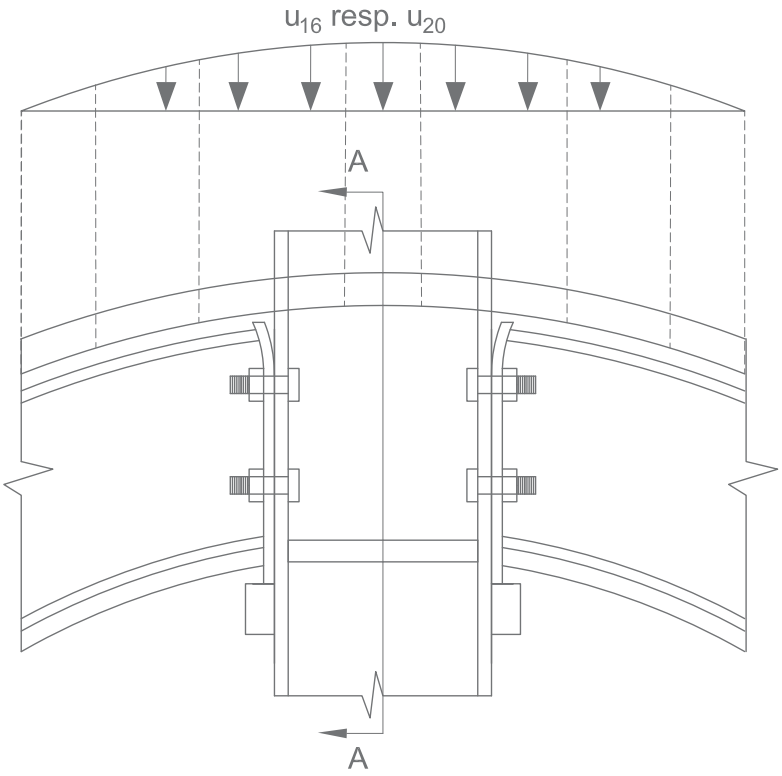

Figure 4.9: Deviation forces acting on specimen due to longitudinal bending

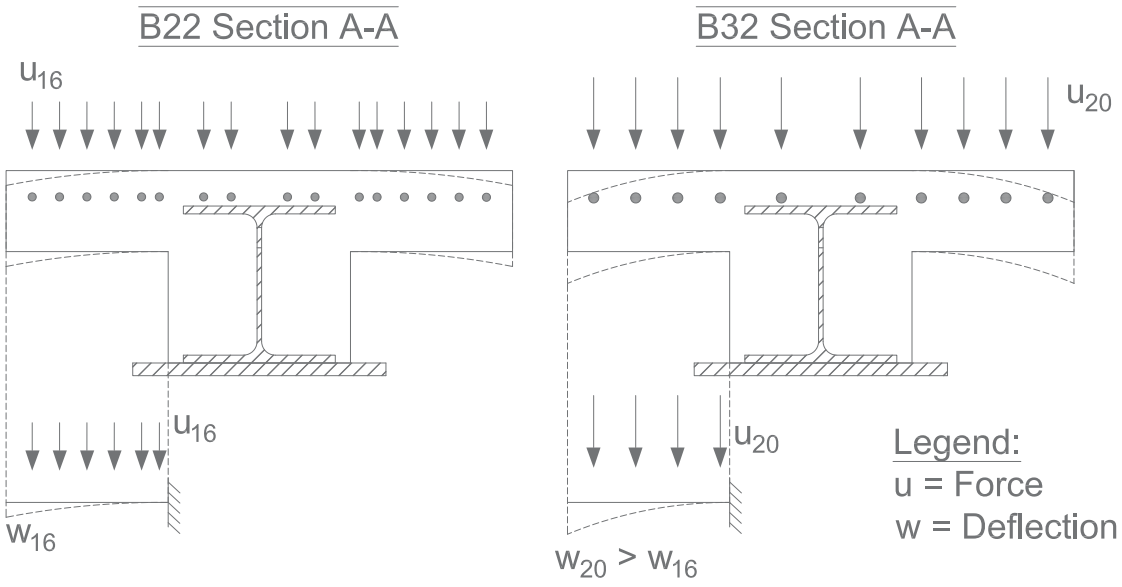

Figure 4.10: Transverse bending of concrete slab due to deviation forces

4.2.2 Stiffness

The joint stiffness $S_{j,Test}$ obtained from the moment-rotation curves of the joints in series B is derived according to the procedure described in Section 4.1. Comparison of the different joint stiffnesses in series B is presented in Figure 4.11. The following conclusions are drawn:

- Influence of bar diameter (test B21 vs. test B31):
  Both specimens have the same reinforcement ratio (1.3 %) but different rebar diameter. The joint stiffness of specimen B31 (⌀ 16) is 0.7 times smaller than that of specimen B21 (⌀ 12). Hence, a larger rebar diameter engenders a lower joint stiffness leading to an inversely proportional relationship between these two quantities.
- Influence of bar diameter (test B22 vs. test B32):
  The conclusion made above is confirmed by the comparison between B22 and B32. Both specimens present larger reinforcement ratios (2.0 %) than above. It can be observed that the stiffness of joint B32 (⌀ 20) is 0.8 times lower than that of joint B22 (⌀ 16). It is noteworthy that the differences in joint stiffness correspond to the ratio between the rebar dimensions.
- Influence of reinforcement ratio (test B22 vs. test B31):
  The same rebar diameter (16 mm) was used in both specimens B22 and B31. The only difference between both tests is the amount of reinforcing bars. In this context, it is noted that the joint stiffness increases with larger reinforcement ratio; the joint stiffness of B22 (ρ = 2.0 %) is about 1.5 times greater than that of B31 (ρ = 1.3 %).

4.2.3 Resistance

The ultimate bending resistance $M_{u,Test}$ of the specimens tested in series B are compared in Figure 4.12.

- Influence of bar diameter (test B21 vs. test B31):
  The ultimate resistance of both specimens is identical, indicating no apparent influence of the rebar diameter.
- Influence of bar diameter (test B22 vs. test B32):
  As above, the differences in ultimate bending resistance are insignificant. The slight differences result from the higher tensile strength of the diameter 20 rebars (cf. Table 3.4).
- Influence of reinforcement ratio (test B22 vs. test B31):
  The ultimate bending resistance of specimen B22 (ρ = 2.0 %) is 1.35 times bigger than that of specimen B31 (ρ = 1.3 %) . The same rebar diameter (⌀ 16) was employed in both tests such that this difference can only emanate from a different amount of reinforcement in the concrete slab. This comparison allows to conclude that the bigger the reinforcement ratio, the bigger is also the ultimate bending resistance. This outcome is not new since many researchers have already identified the same correlation in the past (cf. Section 2).

4.2.4 Rotation capacity

The rotation capacities measured in series B are compared in Figure 4.13. These values were determined according to the definition given in Section 4.1. Specimen failure in the form of rebar rupture occurred only in the tests B21 and B31 with lower reinforcement ratio (ρ = 1.3 %). In test B21, for instance, the rotation capacity reached 105 mrad, while in test B31,

the failure occurred already at about 95 mrad. In the moment-rotation curve of the later, it can be recognised that despite the rupture of one rebar, the test was continued until the fracture of a second rebar at about 110 mrad.
In the specimens with large reinforcement ratio (ρ = 2.0 %), no failure or rebars was observed. The rotation capacities, given in Figure 4.13, represent only a lower threshold for the real rotation capacities of these joints.

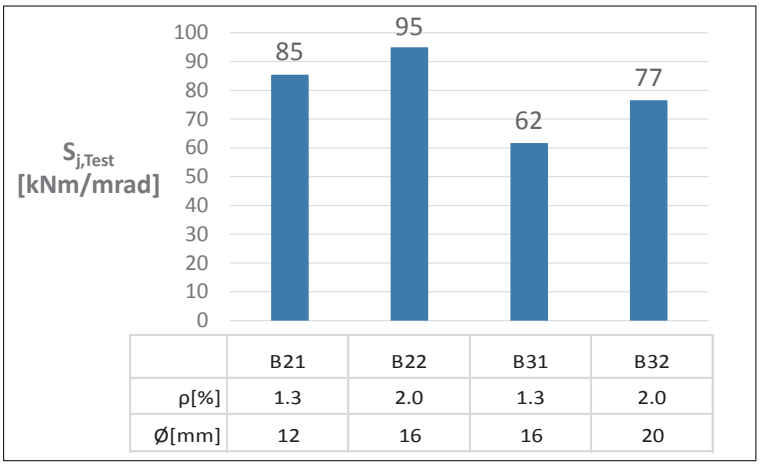

Figure 4.11: Measured joint stiffnesses in Series B

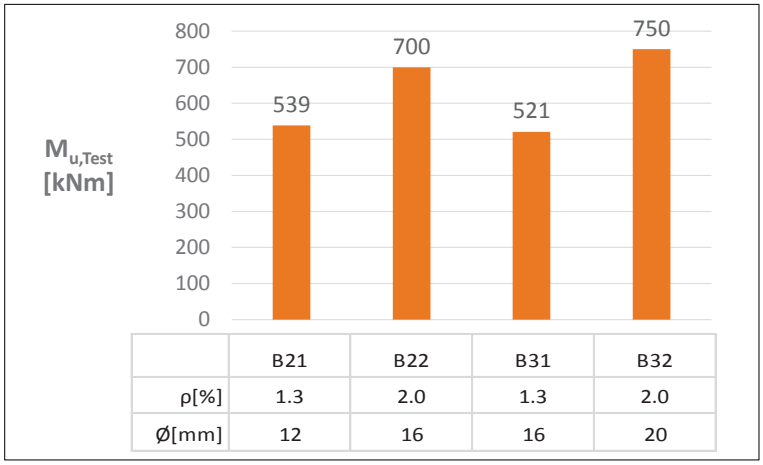

Figure 4.12: Measured joint resistances in Series B

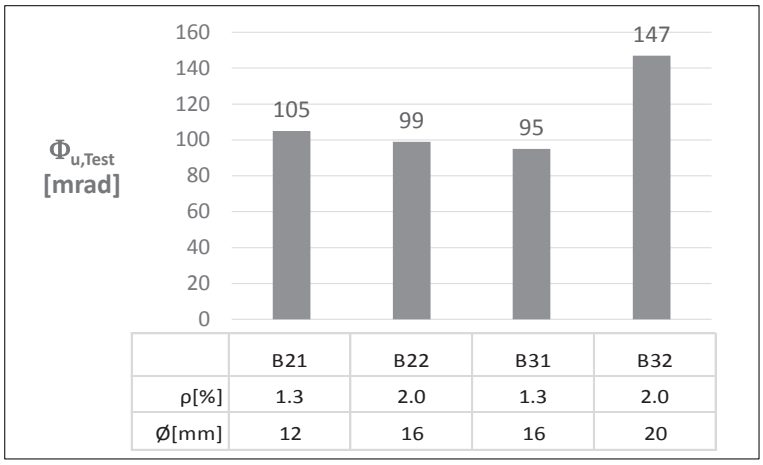

Figure 4.13: Measured rotation capacities in Series B

4.3 Test series C

Test series C consists of one single test (C14) on a bare steel joint. The steel connection was designed in such a way that the load bearing resistance of each bolt row is governed by the ductile mode of failure of the plate. This measure was essential to avoid the brittle tension failure of the bolts and to allow for the plastic redistribution of the internal forces. As desired, ductile bending of the endplate could be observed during the test performance (cf. Figure 4.14 (b)).

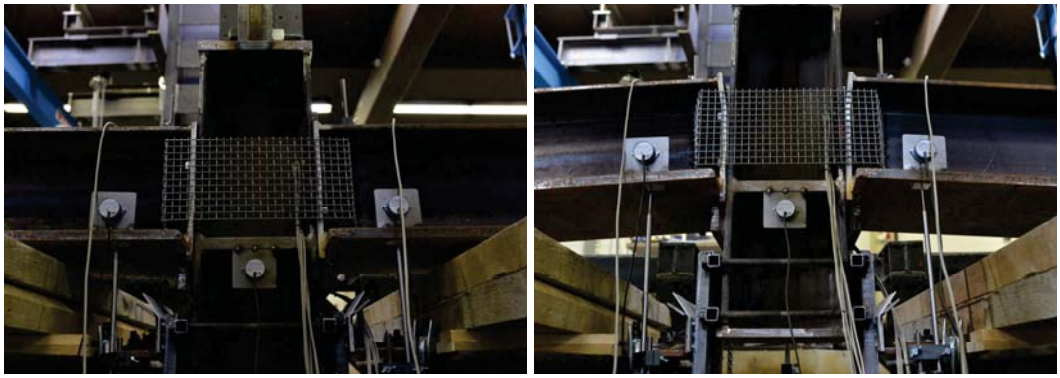

(a) Initial state (b) State at the end of the test

Figure 4.14: Test C1.4: Endplate deformation

The moment-rotation curve of specimen C14 is plotted in Figure 4.15. After an initial linear elastic response, the behaviour of the steel joint became progressively non-linear, as further load was accommodated. At the same time, the bending deflection of the endplate could be observed, confirming hereby the desired ductile failure mode.

For comparison purposes, the moment-rotation curves of test series B are also plotted in Figure 4.15. It is observed that the stiffness of the bare steel joint is significantly smaller than that of composite joints. The differences range between factors of 5 and 8 depending on the joint configuration. The larger stiffness of test series B is mainly due to the reinforced concrete component, which provides a larger internal lever arm to the compression point. It is therefore useful to take advantage of this bigger lever arm in order to increase the stiffness of beam-to-column joints and enhance the structural performance in SLS. The beneficial effect of a bigger joint stiffness on the deflection and vibration behaviour of composite beams is quantified in (Duarte da Costa et al., 2017). In terms of resistance, the greater lever arm of the reinforcement component induces a larger bending resistance of composite joints in comparison to bare steel joints. This is particularly interesting for the plastic analysis of a composite beam, since a larger joint resistance reduces the rotation requirements at the support for a full plastic redistribution of bending moments (cf. Section 2).

Test C14 was terminated at about 68 mrad, when a slight drop resistance appeared because of the stripping of the nut over the thread of the bolt (cf. Figure 4.16 and Figure 4.17). This phenomenon was extensively investigated by Steurer (1996) . From the evaluation of several bolted connections with normative nuts, he observed the occurrence of thread stripping in 90 % of the cases. Moreover, he observed a certain correlation between this failure mode and nut heights smaller than the bolt diameter. In addition, Steurer analysed also bolted

connections with bigger nut heights, where no occurrence of thread stripping was reported. Instead, tension failure of the bolts could be observed, leading to the conclusion that care should be taken in the choice of nuts.

In the present experimental campaign, standard nuts according to EN 14399-4 (2005) were used for the M24 bolts. These nuts present heights of 20 mm (cf. Figure 4.16), which according to the investigations carried out by Steurer (and test C14) is smaller than the bolt diameter and therefore not sufficient to avoid thread stripping. Although this failure mode is still preferable than the brittle failure of the bolts in tension, special attention should be paid to the size of the nuts when designing composite joints with bolted endplate connections to avoid resistance losses in the yielding plateau of the connection's response. This effect explains the smaller rotation capacity of the steel joint in the present test campaign. In Chapter 5 it is shown, that if this effect would have been avoided, the measured rotation capacity of the steel joints would have been much more substantial.

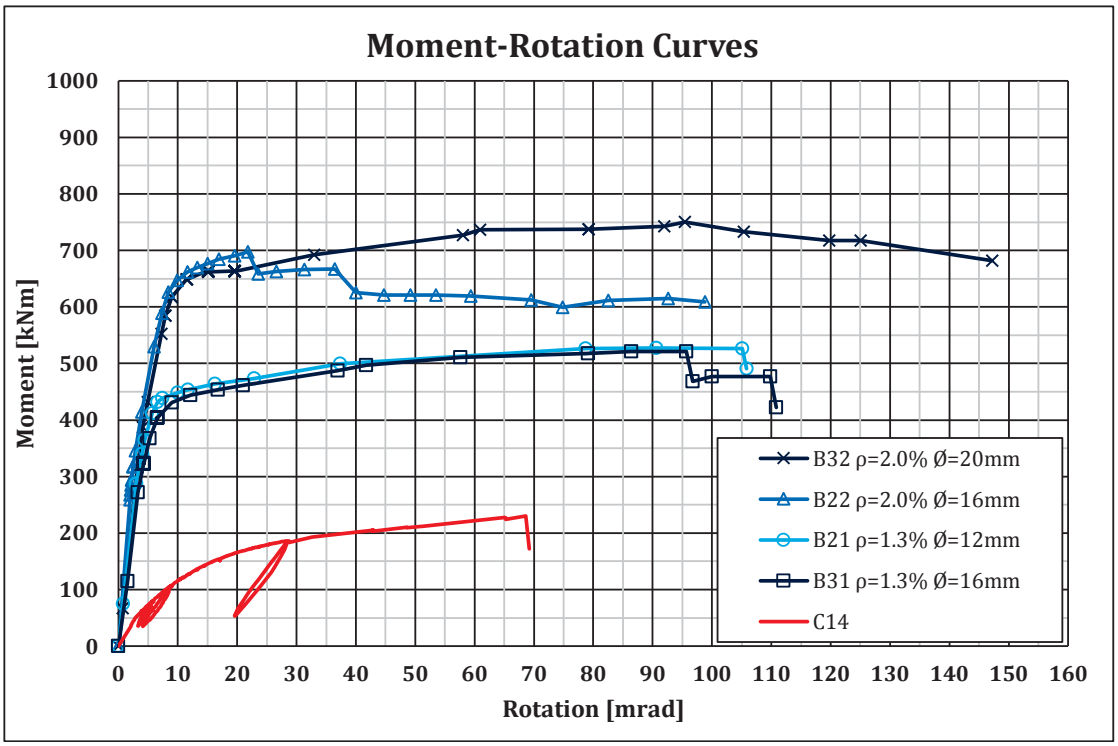

Figure 4.15: Test series C: Moment-rotation curves

Figure 4.16: Identification of thread stripping and nut/bolt dimensions

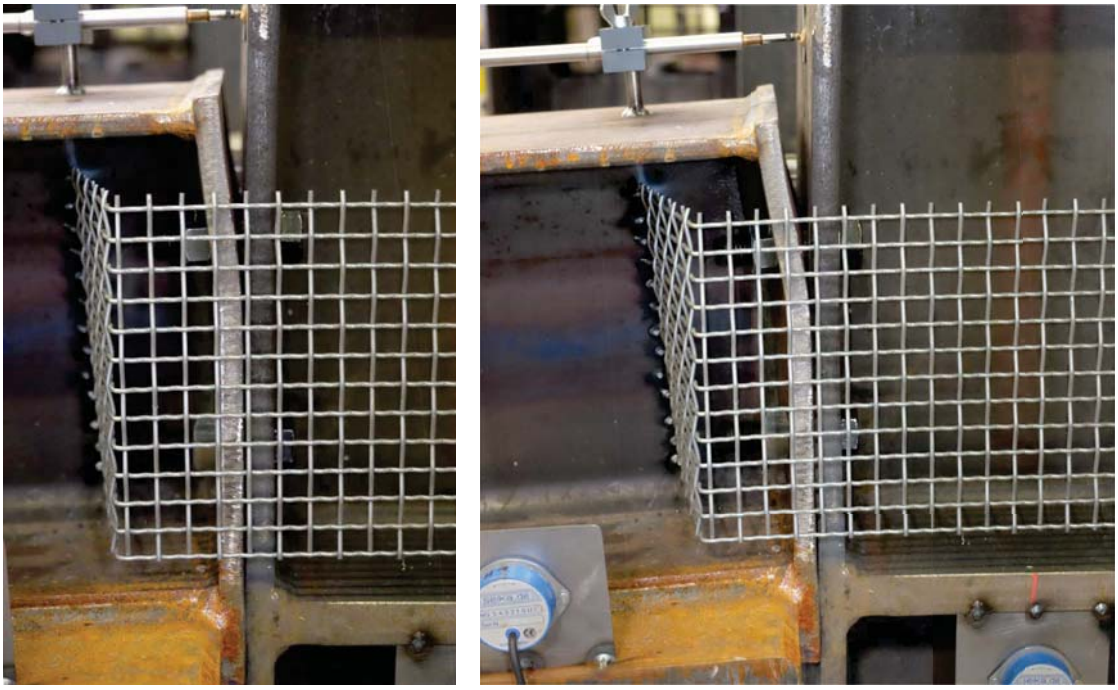

Figure 4.17: Test C14: Additional test pictures

4.4 Test series E

4.4.1 Moment-rotation curves and observations

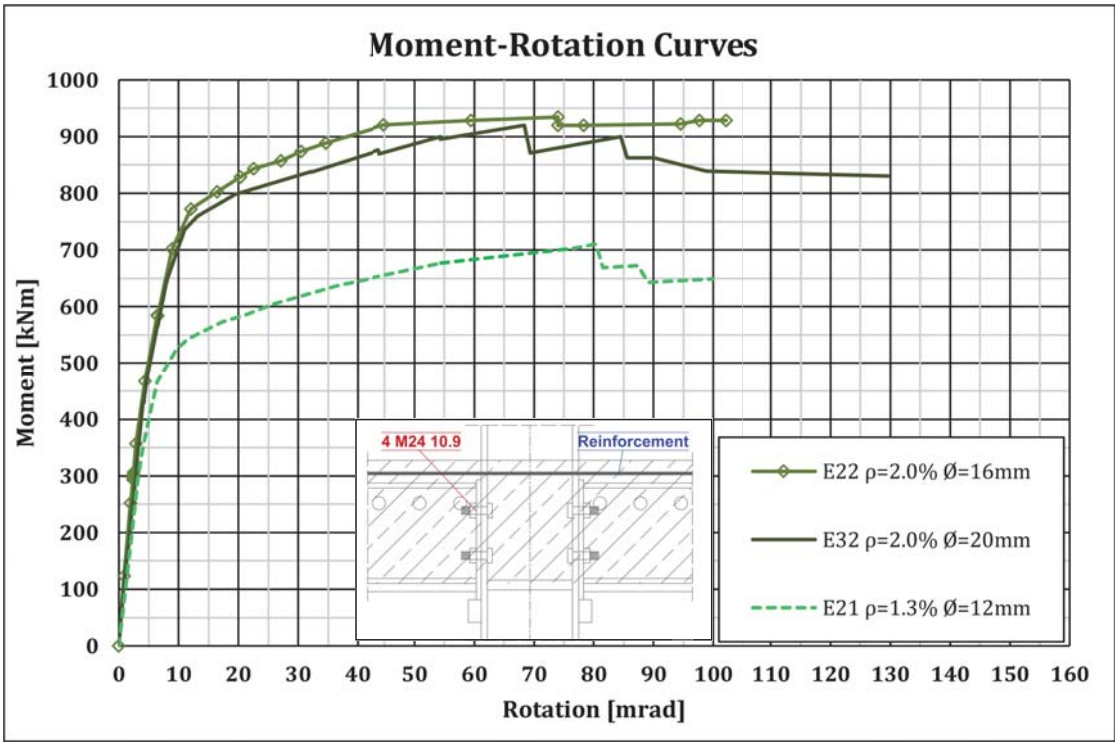

Figure 4.18: Test series E: Moment-rotation curves

The moment-rotation curves of the three tests performed within series E are illustrated in Figure 4.18. All the tests were stopped without the occurrence of a clear failure. After an initial phase dominated by the linear elastic joint response, the first signs of non-linearity initiated with a smoother transition between the elastic and plastic phase than for series B (cf. Figure 4.19). A certain shape affinity in the moment-rotation curves between series C and series E can be noticed in the plastic part of the curve. A bigger growth in resistance is observed in the plastic phase for the tests in series E in comparison to series B. It demonstrates that the steel connection is the main responsible for the increment in resistance in this phase (ca. 200 kNm). The strains measured in the bolts confirm this conclusion (cf. Appendix B). Similarly to series C, small drops of joint resistance (thread stripping) were observed at larger joint rotation.
Besides, the concrete slab of specimen E32 exhibited a remarkable transverse bending, similar to that observed in test B32. The explanation for this effect is detailed in section 4.2. In short, it is attributed to the large diameter of the longitudinal rebar used in both tests.

The moment-rotation curves of all tests are presented in Figure 4.19. The three main properties characterising the tested joints are indicated in Figure 4.20. In the following subsections, a comparison between the test series B and E is presented.

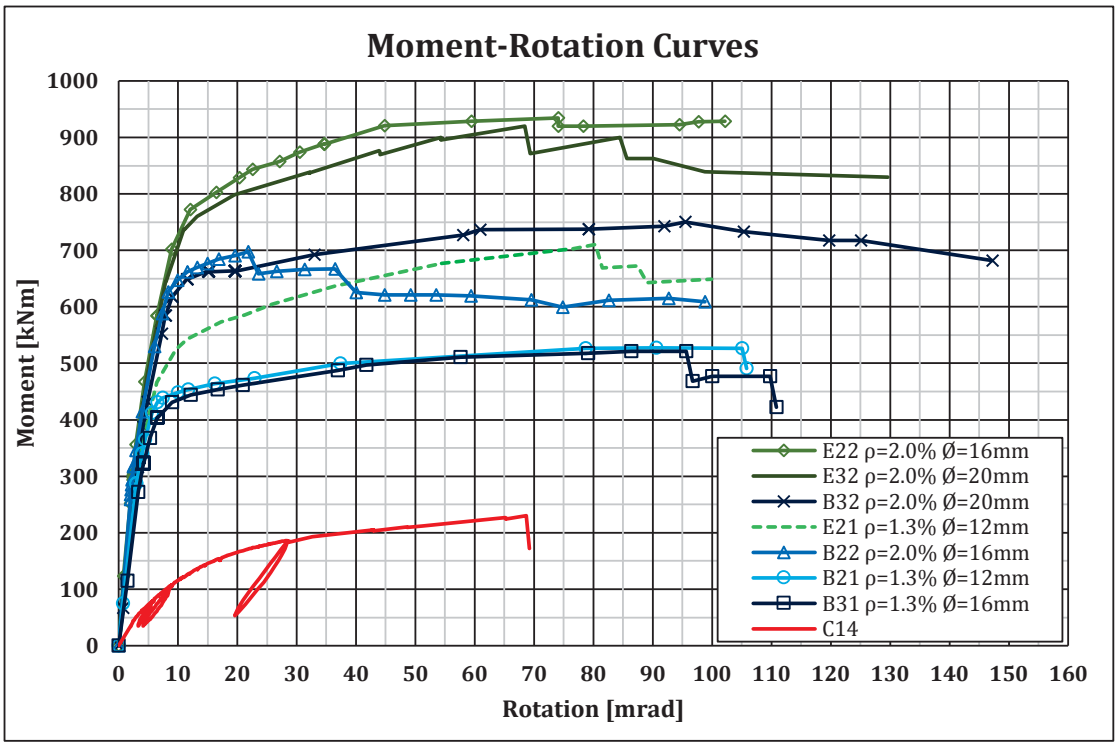

Figure 4.19: Moment-rotation curves of all tests

4.4.2 Stiffness

In Figure 4.20 (a), the joint stiffnesses $S_{j,Test}$ are compared for all tests performed in the present research. Since the influence of the parameters related to the longitudinal reinforcement was already analysed in Section 4.2.2, the present Section is focussed on the additional influence of the bolted flush endplate connections on the joint stiffness. For this purpose, specimens with equal reinforcement layout are compared, for which the only difference is related to the presence of a bolted connection.

- Test B21 vs. Test E21 (ρ = 1.3 % and $\varnothing$ = 12 mm):
  The stiffness of the composite joint with additional bolted endplate connection (test E21) is identical that of the bare composite joint (test B21). In the present case, the stiffness was therefore not influenced by the presence of a flush endplate connection.
- Test B22 vs. Test E22 (ρ = 2.0 % and $\varnothing$ = 16 mm):
  Similarly to above, no significant change in stiffness is observed between test B22 and test E22 with larger reinforcement ratio.
- Test B32 vs. Test E32 (ρ = 2.0 % and $\varnothing$ = 20 mm):
  In relation to the two previous comparisons, a bigger dimension of the longitudinal rebars is employed. The stiffness of the joint E32 is slightly larger than that of B32. The difference is equal to the stiffness of the bare steel joint C14. Thus, it can be deducted that for a larger rebar diameter, the presence of a flush endplate connection increased the stiffness of the joints. It must be however stated, that the difference is relatively small since the stiffness of the bare steel joint is in average 6 times smaller than that of the tested composite joints.

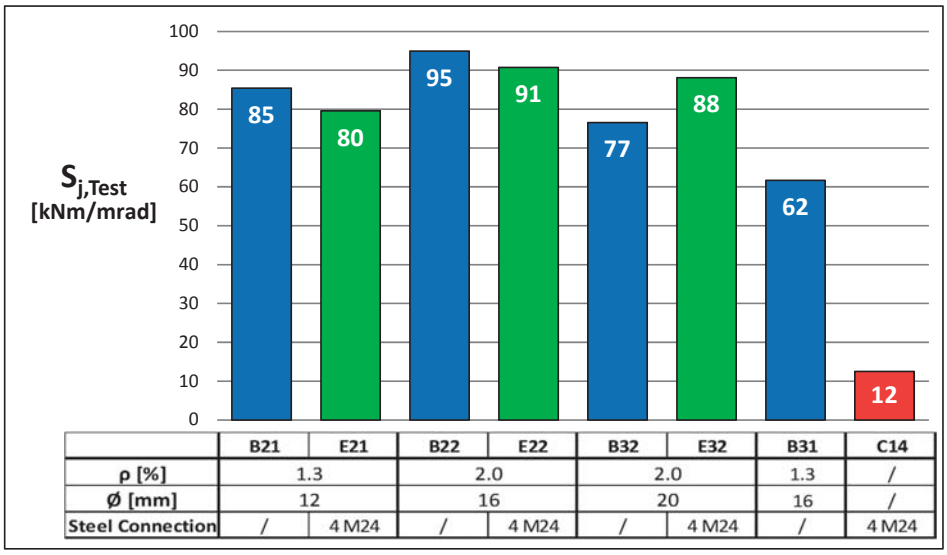

	B21	E21	B22	E22	B32	E32	B31	C14
ρ [%]	1.3		2.0		2.0		1.3	/
Ø [mm]	12		16		20		16	/
Steel Connection	/	4 M24	/	4 M24	/	4 M24	/	4 M24

(a) Comparison of measured joint stiffnesses $S_{j,Test}$

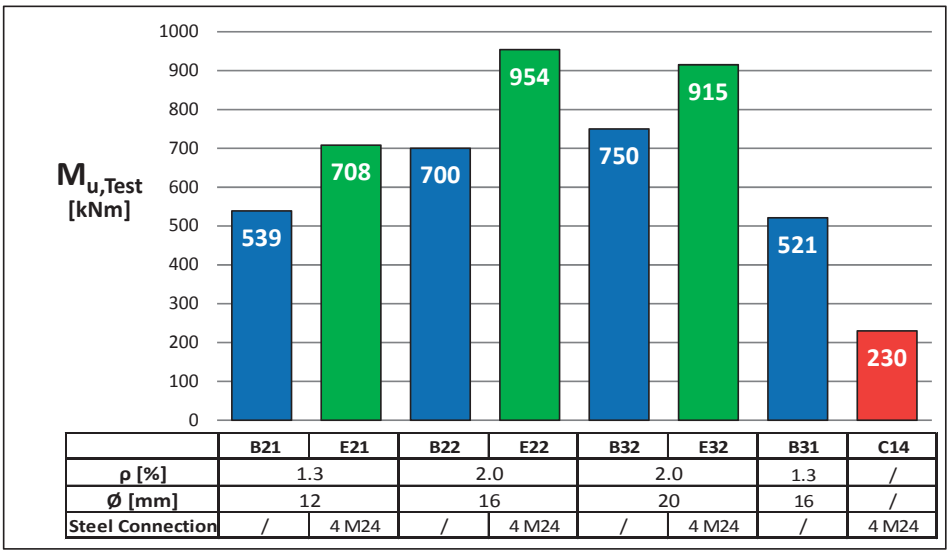

	B21	E21	B22	E22	B32	E32	B31	C14
ρ [%]	1.3		2.0		2.0		1.3	/
Ø [mm]	12		16		20		16	/
Steel Connection	/	4 M24	/	4 M24	/	4 M24	/	4 M24

(b) Comparison of measured joint resistances $M_{u,Test}$

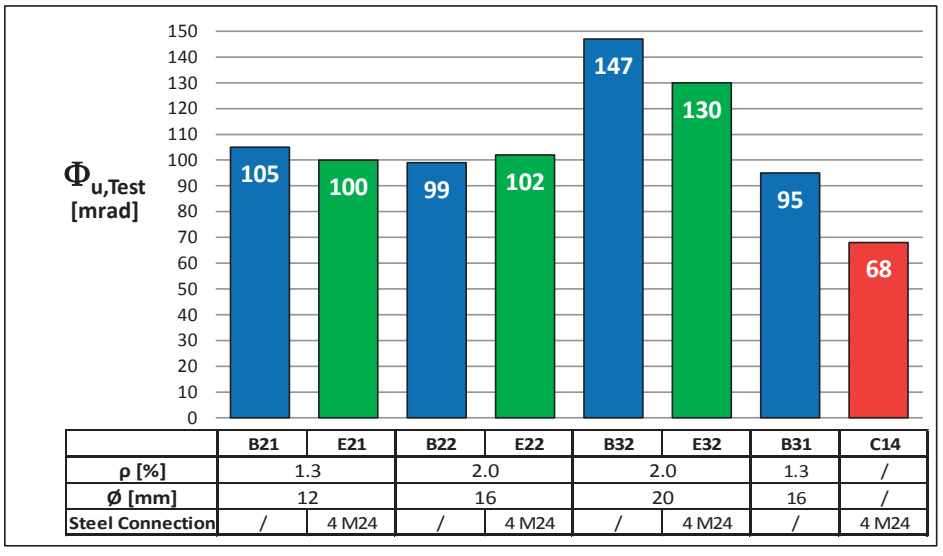

	B21	E21	B22	E22	B32	E32	B31	C14
ρ [%]	1.3		2.0		2.0		1.3	/
Ø [mm]	12		16		20		16	/
Steel Connection	/	4 M24	/	4 M24	/	4 M24	/	4 M24

(c) Comparison of measured rotation capacities $\Phi_{u,Test}$

Figure 4.20: Experimental results for the three main joint properties

4.4.3 Resistance

The ultimate joint resistance $M_{u,Test}$ of all tested beam-to-column joints are shown in Figure 4.20 (b). The influence of the steel connection is additive: the resistance of the specimen with both joint components (reinforced slab and steel connection) is equal to the sum of the resistances of the specimens with isolated components. In other words, the joint resistance of series E is equal to the sum of the resistance of series B and C. Thus, these tests prove that the resistance of a composite joint is enhanced by the presence of a bolted endplate connection:

$$M_{u,Test_E} \approxeq M_{u,Test_B} + M_{u,Test_C} \tag{4.1}$$

4.4.4 Rotation capacity

As described previously, no failure occurred in the tests of series E. Hence, the real rotation capacity of the joints tested in series E is bigger than that obtained from measurements (cf. Figure 4.20 (c)). However, these results confirm that large rotation capacities can be achieved for composite joints with ductile steel connection. This should be an essential design rule in the design of composite joints and more especially in the design of semi-continuous composite joints, for which significant rotation capacity is necessary for the plastic analysis of composite beams.

In order to design composite joint with large rotation capacities, it is therefore suggested to provide thin endplates, for which the failure of the endplate is decisive (Failure mode 1 of T-Stub model in EN 1993-1-8 (2005)). This condition ensures that the rotation capacity is limited by the ductility of the longitudinal reinforcement bars, instead of the restricted ductility of the bolts in tension.

4.5 Experimental assessment of the effective joint length

In (Gil and Bayo, 2008a), the effective joint length L_j is defined from the axis of the column and extended along the reinforcement up to the point where considerable stresses are attained in the reinforcement. This quantity represents an important property in the design of composite joints since it defines the stiffness and the rotation capacity of composite joints, as it will be seen in Chapter 6.

The objective of the present Section is to identify to what extent each investigated parameter - reinforcement ratio ρ and rebar diameter $\varnothing$ - influences the effective joint length L_j. Assuming a linear moment distribution in the vicinity of the joint, the stresses in the reinforcement decrease in longitudinal direction as illustrated in Figure 4.21. Reinforcement sections subjected to stresses below 50 % of the maximal stresses are considered beyond the effective joint region. The contribution of these parts to the overall joint behaviour is therefore neglected.

An appraisal of the effective joint length L_j on the basis of the strain measurements is given in this Section. For this purpose, the readings from the strain gauges applied on the reinforcement are illustrated in Figures 4.22 and 4.23. For clarity reason, the measured strains are converted into stresses, given in 4 sections (A-D). In the same graphs, the moment-rotation curves are additionally plotted on the secondary vertical axis.

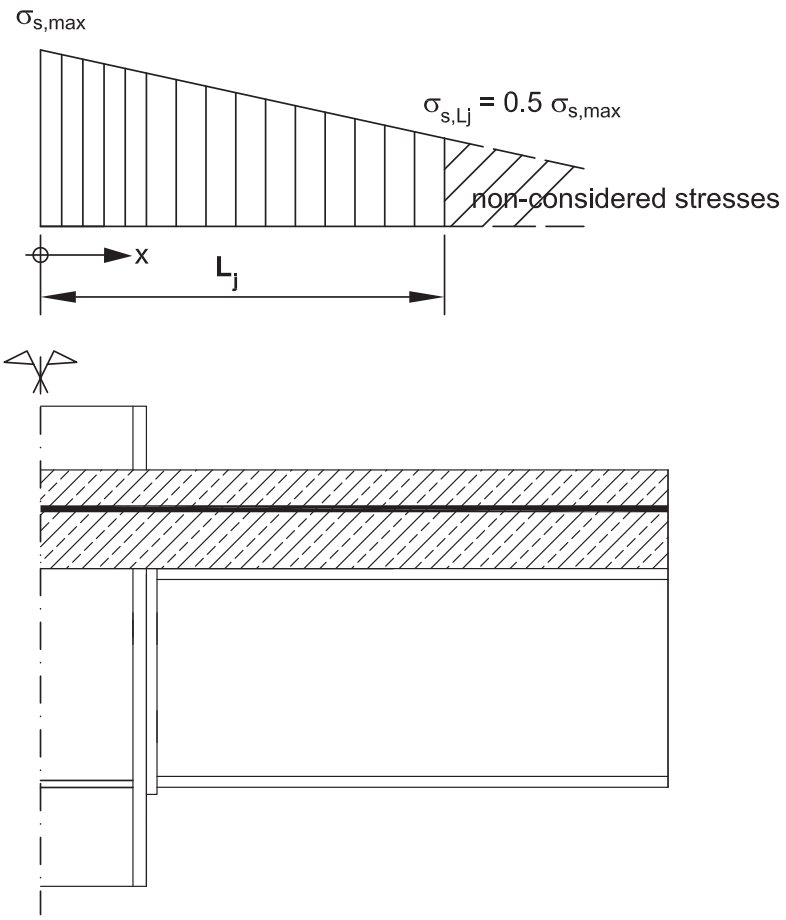

Figure 4.21: Definition of effective joint length L_j

In the initial load phase, the stresses in sections A and B increase almost equally, while for sections C and D, the development of stresses in the reinforcement is less intensive. Once the yield stress is reached in section A and B, the reinforcement stress in sections C and D increase more moderately. From this point on, the strain hardening process initiates in sections A and B (not plotted for simplification), allowing also for the accommodation of further stresses in the more remote sections C and D. This fact contradicts former research investigations, which in most cases supposed that the ductility of the reinforced slab is due to the opening of one single main crack in the vicinity of the column flange.

For the tests with higher reinforcement ratio ρ = 2.0 %, Figure 4.23 shows that at ultimate state the reinforcement is yielding at a distance of 90 cm from the column centre line, while for lighter reinforced composite joints (ρ = 1.3 %) this distance reduces to 75 cm (cf. Figure 4.22). It can be therefore deduced that **the effective joint length increases with bigger reinforcement ratio**. The same tendency can be deducted from the readings of the displacement transducers disposed on the top of the concrete slab measuring its elongation (cf. Appendix B.3).

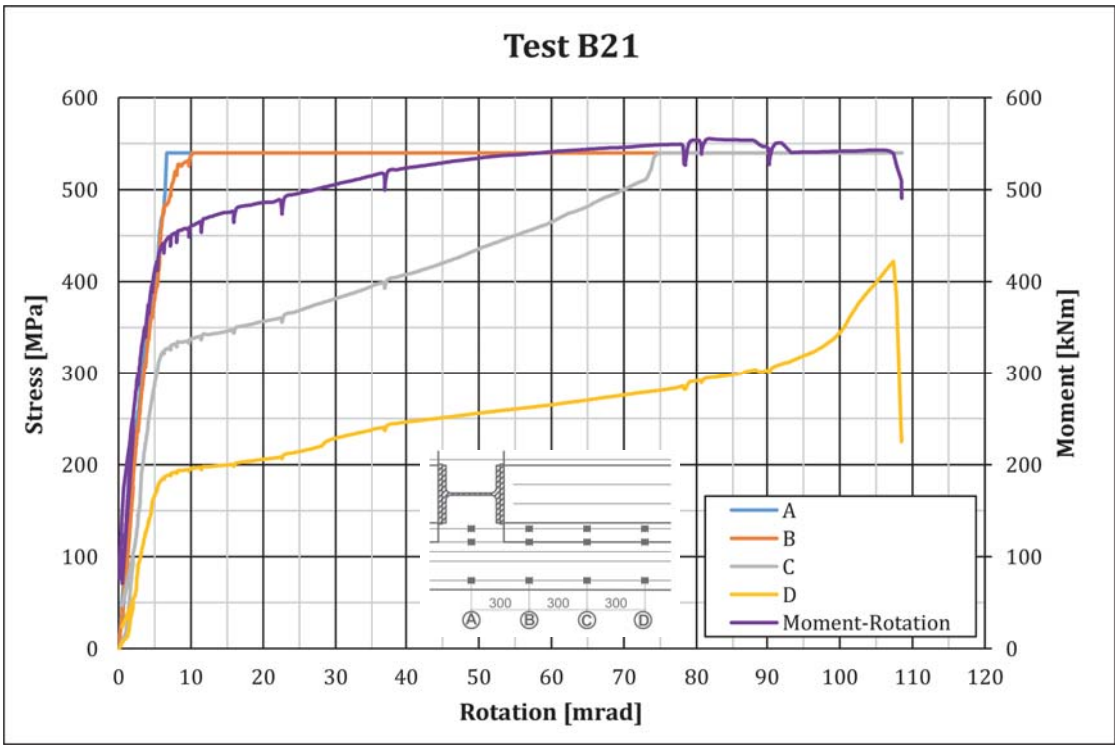

(a) Test B21 $\rho = 1.3\%$ and $\varnothing = 12mm$

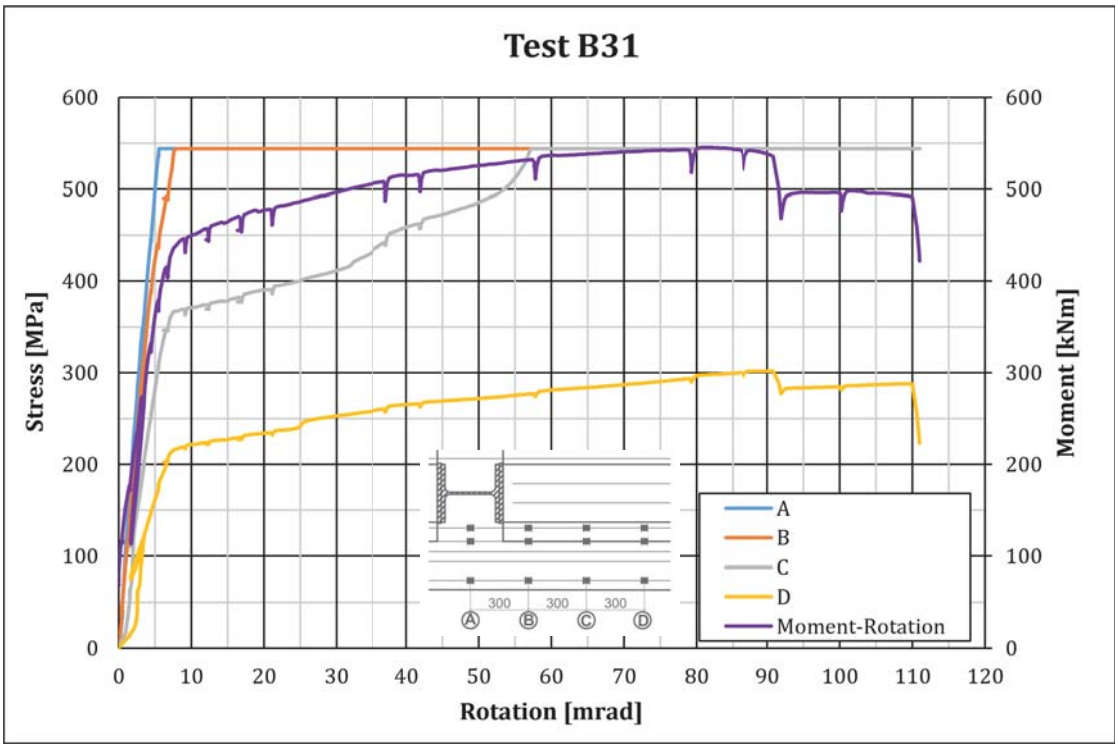

(b) Test B31 $\rho = 1.3\%$ and $\varnothing = 16mm$

Figure 4.22: Evaluation of the strain gauges in reinforcement: B21 and B31

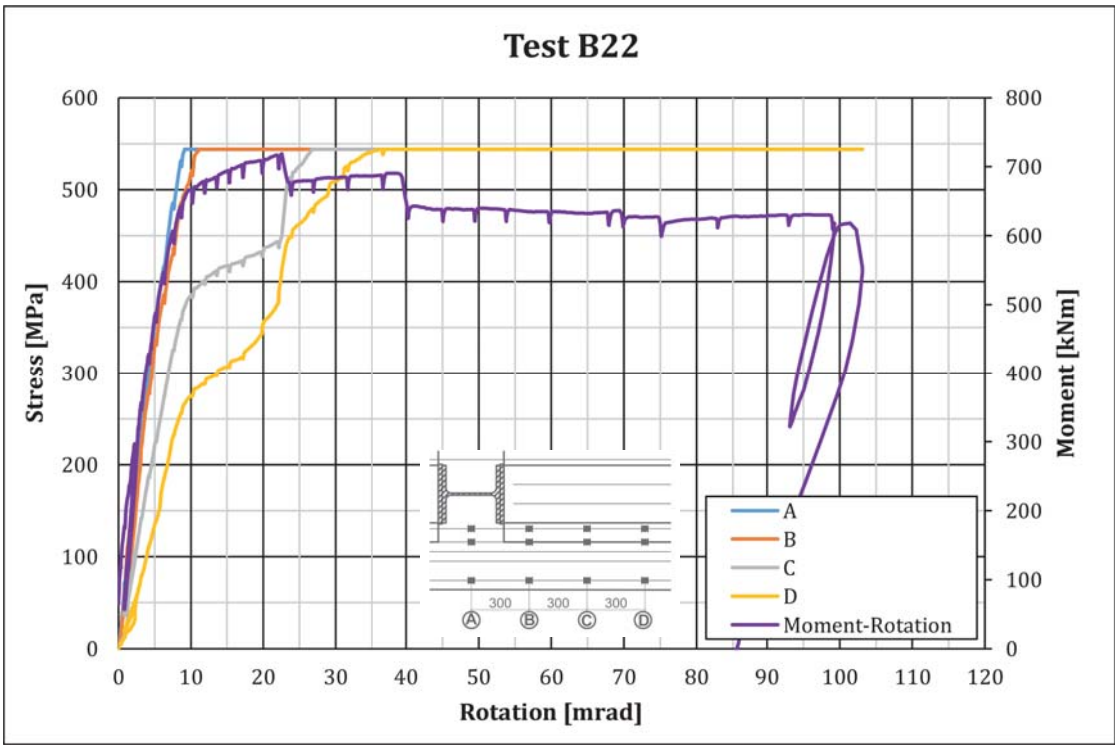

(a) Test B22 $\rho = 2.0\%$ and $\varnothing = 16mm$

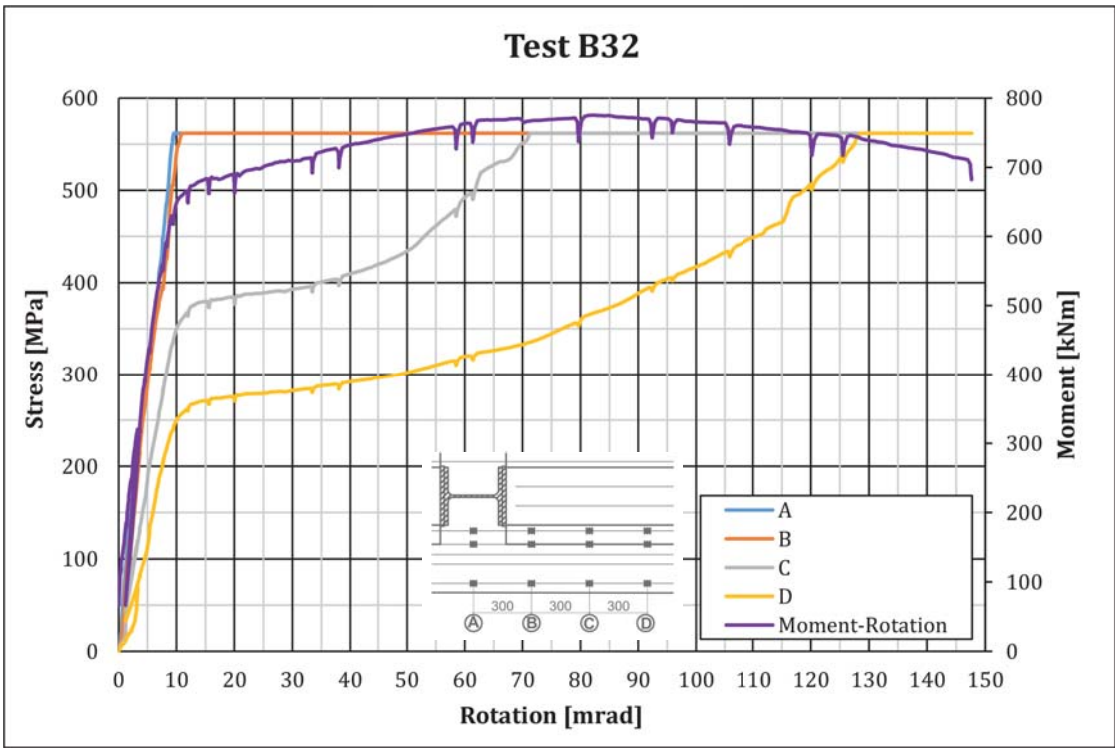

(b) Test B32 $\rho = 2.0\%$ and $\varnothing = 20mm$

Figure 4.23: Evaluation of the strain gauges in reinforcement: B22 and B32

During the performance of the tests, it was possible to observe that the formation of cracks always occurred at a very low load stage. No distinction is therefore made between the effective joint length L_j in the elastic and plastic phase ($L_{j,el} = L_{j,pl}$). This can also be seen with the strain measurements: Figures 4.24 (a) to (d) depict the joint rotation in function of the reinforcement strain for joint rotations below 10 mrad (initial load phase). At a strain of approximately $0.1‰$, a sudden increase in strain rate is recorded by the strain gauges. It coincides with the strain at which cracking of concrete occurs ($\varepsilon_{ctm} = f_{ctm}/E_{cm} \simeq 0.1‰$).

At 2/3 of the plastic bending resistance $M_{pl,cal}$, the crack development is stabilised. The ductility of the slab is accommodated by the elongation of the reinforcing bars, resulting in the opening of the existing cracks rather than in the formation of new cracks. For this reason, it can be assumed that the effective joint length is a quantity which is equal in serviceability and ultimate limit state. Thus, the crack pattern of the slab at ultimate state can be also used to visually identify the effective joint length.

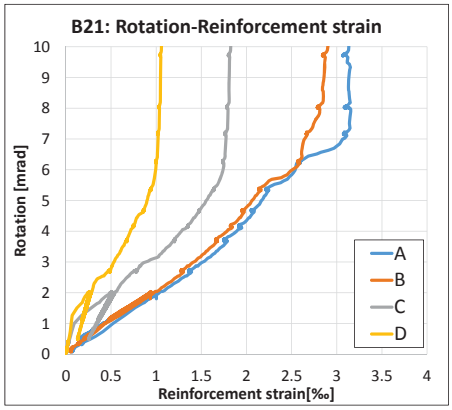

(a) Test B21 $\rho = 1.3\%$ and $\varnothing = 12mm$

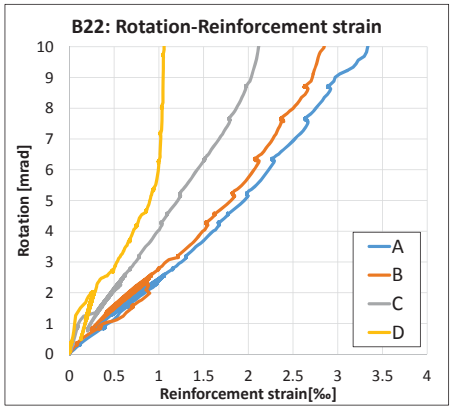

(b) Test B22 $\rho = 2.0\%$ and $\varnothing = 16mm$

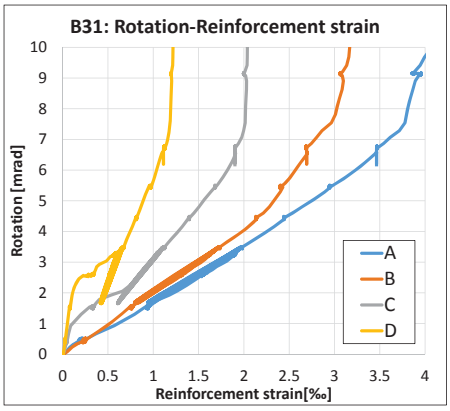

(c) Test B31 $\rho = 1.3\%$ and $\varnothing = 16mm$

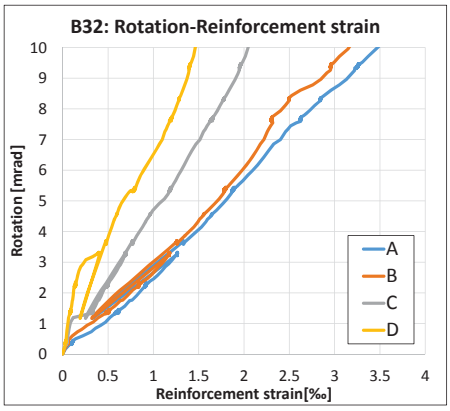

(d) Test B32 $\rho = 2.0\%$ and $\varnothing = 20mm$

Figure 4.24: Rotation-Reinforcement strain in the initial phase

The crack patterns of all tests in series B are depicted in Figure 4.25. All the pictures refer to the same joint rotation of about 100 mrad, such that the elongation of the reinforced concrete component is overall identical. The differences in the crack pattern are therefore necessarily linked to the differences in reinforcement layout. In order to facilitate the comparison, a grid is drawn on the pictures and the effective joint region marked. The latter is defined by the region in which cracks present large crack openings.

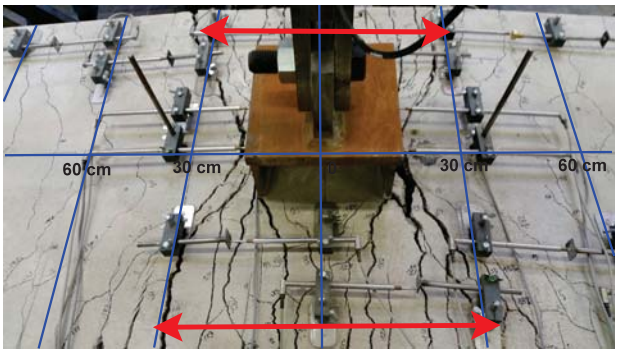

(a) Test B21 $\rho = 1.3\%$ and $\varnothing = 12mm$

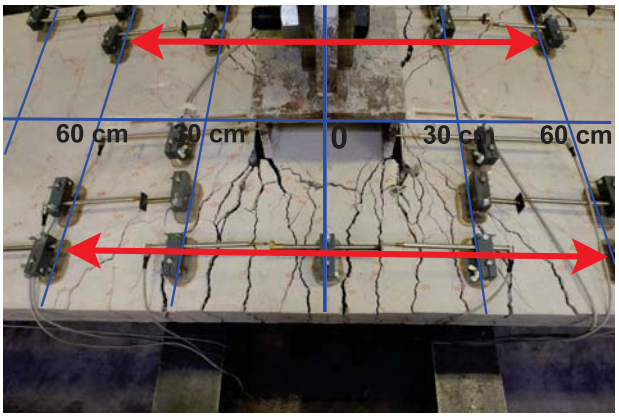

(b) Test B31 $\rho = 1.3\%$ and $\varnothing = 16mm$

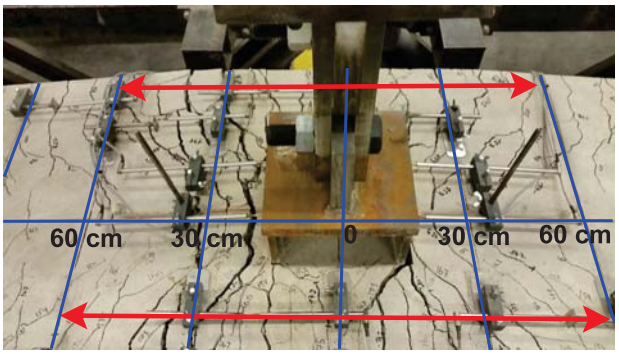

(c) Test B22 $\rho = 2.0\%$ and $\varnothing = 16mm$

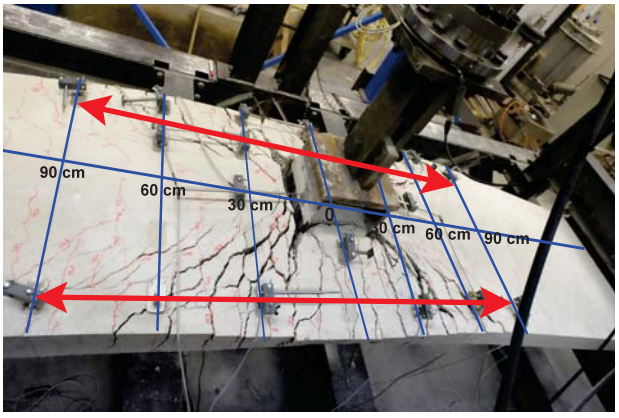

(d) Test B32 $\rho = 2.0\%$ and $\varnothing = 20mm$

Figure 4.25: Concrete cracking pattern at 100 mrad

From the pictures in Figure 4.25, different conclusions can be drawn:

1. **The effective joint length is significantly bigger than half the column depth** for the present experiments. This is in contradiction with was is proposed in EN 1994-1-1 (2004) for this type of joint configurations. Moreover, the observations carried out during the tests and the comparison between the different crack patterns demonstrate that the effective joint length is closely related to the crack behaviour of the concrete slab.
2. In order to examine and quantify the influence of the longitudinal rebar diameter, only the tests with equal reinforcement ratio are directly compared. Test B21 ($\varnothing$ = 12 mm) and test B31 ($\varnothing$ = 16 mm), for instance, have the same reinforcement ratio of ρ = 1.3 %. The only variable is the diameter of the longitudinal reinforcement bars. Comparison of the crack patterns of these specimens allows to conclude that the effective joint length is bigger for larger longitudinal rebar sections (i.e. B31). During the test performance it could be observed that the main cracks in the concrete slab of test B21 reach up to the first row of captor holders, while in test B31 large crack widths were detected up to the second row (cf. Figure 4.25 (a) and (c)).

   The same dependence between effective joint region and rebar diameter is observed in the comparison between test B22 and test B32 (same reinforcement ratio ρ = 2.0 %). It can be observed that test B32 displays a larger effective region than test B22 due to the bigger rebar diameter. For test B32 ($\varnothing$ = 20 mm), large crack widths were detected up to the third captor holder while for test B22 ($\varnothing$ = 16 mm), the length was limited to the second holder. In consequence, these two comparisons lead to the conclusion that the effective joint length L_j is proportional to the diameter of the longitudinal reinforcement bars. In other terms, **the larger the longitudinal rebar diameter, the larger is also the effective joint length** L_j.

$$L_j \sim \varnothing \tag{4.2}$$

The same outcome is obtained from the reading of the strain gauges on the reinforcement (cf. Figure 4.26). Knowing that a bigger strain in section D is synonym for a larger joint length, it can be seen that the strain at section D is larger for test B31 and test B32 (cf. Figures 4.26 (a) and (b)), confirming herewith the conclusion made above.

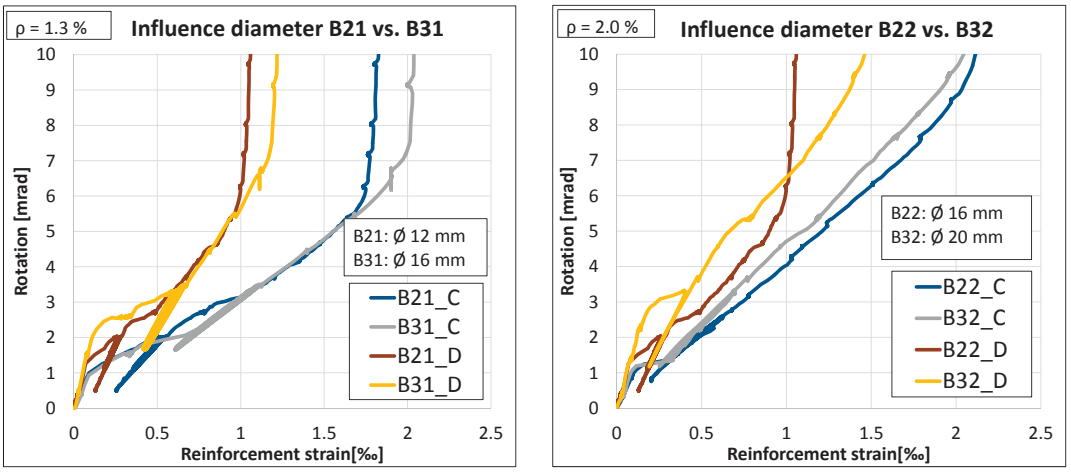

(a) ρ = 1.3 % (b) ρ = 2.0 %

Figure 4.26: Strain in reinforcement: Influence of the rebar diameter

4.6 Conclusions

Several conclusions emerged from the detailed analysis of the test results and observations elaborated in the present Section:

- The stiffness of composite joints is inversely proportional to the diameter of the longitudinal reinforcement bars. $\longrightarrow S_j \sim \frac{1}{\varnothing}$
- The stiffness of composite joints is directly proportional to the longitudinal reinforcement ratio of the concrete slab. $\longrightarrow S_j \sim \rho$
- The ultimate resistance of composite joints is directly proportional to the longitudinal reinforcement ratio. $\longrightarrow M_u \sim \rho$
- The presence of a bolted flush endplate connection affected the behaviour of the tested composite joints. Regarding the joint stiffness, the test results indicated that the stiffness of composite joints with bolted connections does not significantly differ from that of bare composite joints. The only case for which a slight increase in joint stiffness was observed, was for joints with longitudinal rebars of diameter 20 mm.
- Regarding the ultimate bending resistance, it was observed that the presence of an endplate connection increases the resistance of composite joints. Due to the ductile failure mode of the steel connection, the simple superposition principle was valid for the tested joints. $\longrightarrow M_{u,TestE} \approx M_{u,TestB} + M_{u,TestC}$
- Composite joints with a large ductility can be obtained with a conscious joint design in which the reinforcement component defines the ductility of the joint. In the present research, it was proven that, in combination with large reinforcement ratios (ρ > 1.0 %) and longitudinal rebar diameters over 12 mm, this design strategy assures large rotation capacities (over 90 mrad in the present tests). It was shown that the presence of bolted endplate connections do not diminish the rotation capacity of composite joints when the steel connection is ductile. According to the T-Stub model of EN 1993-1-8 (2005), a ductile endplate connection is guaranteed if the brittle tension failure of the bolts is avoided. The resistance of each bolt-row should be governed by the bending resistance of the endplate. In addition, the bucking failure should be prevented. When these two conditions are satisfied the reinforcement represents the weakest joint component defining therefore the overall rotation capacity.
- The phenomenon of thread stripping in the bolt-nut interface should be avoided through the use of appropriate nuts with heights bigger than the bolt diameter. $\longrightarrow h_{nut} > \varnothing_{bolt}$
- The effective joint length L_j is bigger than half the column depth h_c.
- The effective joint length L_j is related to the crack behaviour of the concrete slab.
- The effective joint length L_j increases with bigger reinforcement ratio ρ and bigger rebar diameter $\varnothing$.

The experimental measurements obtained with the different instrumentation tools are provided in Appendix B.

5 Numerical Simulations

5.1 Introduction

In this chapter the numerical model developed to simulate the behaviour of composite joints with composite slim floor beams is introduced. This FE model is validated against the experimental results obtained in the present research. It allows to analyse in detail the influence of different joint components on the global joint behaviour. It enables, for example, to determine the stress flow at different loading stages and to examine the deformation of the individual components. Therefore, a better understanding of the load bearing behaviour of composite joints can be developed on behalf of this FE model.

Moreover, this numerical model can be used to predict the behaviour of different joint configurations. It is therefore suitable to perform a parametric study to analyse the characteristic response of other composite joints.

The finite element analysis was conducted with the program Abaqus 6.14 (2014). This software offers powerful and complete solutions for sophisticated engineering problems covering a vast spectrum of applications. Abaqus allows to incorporate the effects of geometric and material nonlinearity in the analysis, which in combination with its extensive element library, provides provide a powerful set of tools for solving many different problems (Abaqus 6.14, 2014).

In the next subsections, an extensive description of the numerical model is presented. Element types, interactions and material laws are addressed. Afterwards, the numerical and experimental results are compared in order to validate the developed numerical model. The complex interactions between the joint components are examined on behalf of this model. At the end, the results of the parametric study are presented.

5.2 Description of the numerical model

5.2.1 Geometry and boundary conditions

The finite element model developed in this research work is presented in Figure 5.1 in different perspectives. Due to the symmetrical test set-up, only one quarter of the specimen was modelled in order to save on computational time. Three dimensional 8 nodes continuum elements of linear order and reduced integration (C3D8R) were used for **steel, concrete and bolt parts**. A fine mesh with hourglass control was adopted to avoid the numerical difficulties associated with the hour glassing effect (zero strain in integration point). Figure 5.2 illustrates these parts individually.

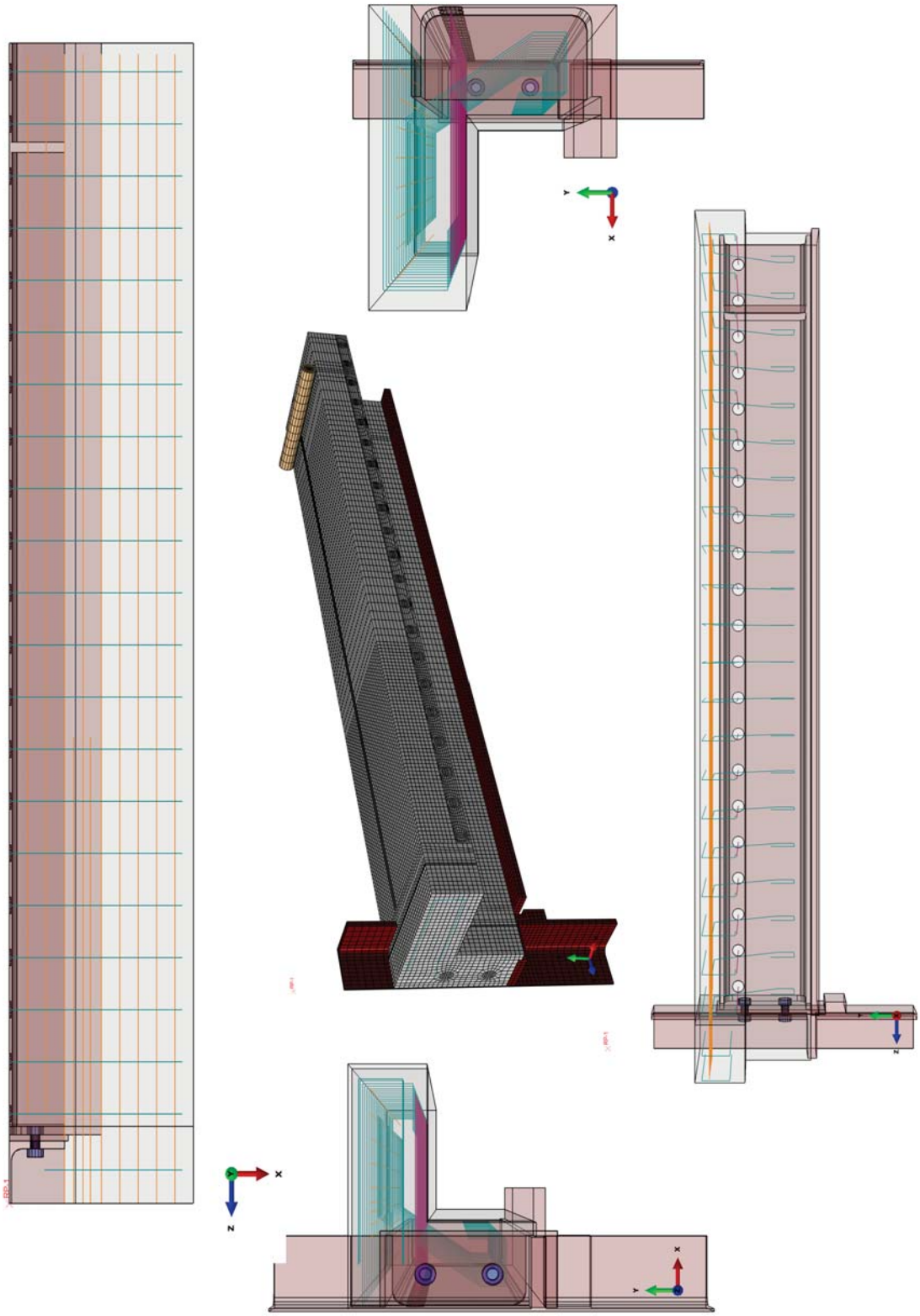

Figure 5.1: Finite element model

All the **reinforcement parts** were modelled with three-dimensional beam element types with linear interpolation (B31). A beam element is a one-dimensional line element in three-dimensional space, having a stiffness associated with the bending and axial deformation of the beam's axis and is an appropriate modelling approach if the cross-section's dimensions are small compared to the rest of the model (Abaqus 6.14, 2014). The CoSFB-dowel bars, the longitudinal reinforcement, as well as all stirrups of the specimen were therefore modelled as B31 beam elements (cf. Figure 5.1).

The geometry of all parts was detailed realistically. Hence, the holes in the web of the steel beam, in which the CoSFB-dowel bars pass through as well as the concrete between these bars and the holes have been modelled (cf. Figure 5.2).

For simplification, welded parts were modelled as rigidly connected. This had no influence on the analysis, as the welds themselves were not part of the investigations and no failure of weld was observed in the experimental tests.

All the parts were properly assembled in their correct position. Appropriate interaction and constraint conditions were then defined among these components. The mechanical interactions between steel, concrete and bolt parts were considered using general contact interaction procedure in Abaqus/Explicit. In normal direction, the contact behaviour was implemented as hard contact allowing for separation after contact, while in tangential direction, the penalty formulation with a friction coefficient of 0.4 was adopted.

The interaction between reinforcement and the surrounding concrete may be modelled using different techniques:

The *first technique* consists in modelling the reinforcement as solid elements and considering the bond behaviour between the reinforcement and concrete through cohesive elements or contact with cohesive behaviour (Henriques, 2013). This technique leads, however, to time consuming computation.

The *second strategy* consists in applying an embedded constraint between the reinforcement and the concrete. This modelling strategy is used by Abaqus to model a set of rebars (beam elements) that lie embedded in a set of solid concrete elements. It is based on master and slave regions, where the reinforcement is the embedded region (slave) and the concrete represents the host region (master). This type of formulation imposes that the nodes of the reinforcement displace by the same amount as the closest nodes of the host region, assuming thus a perfect bond between the two components. Although this behaviour is not representative for the real bond behaviour between concrete and reinforcement, Abaqus allows for certain geometric tolerances. It defines how far an embedded node can lie outside the regions of the host elements. This attenuates the approximation made by assuming a tied constraint. In comparison to the first technique, a significant reduction of computation time is obtained without loss of noteworthy accuracy. For this reason, the second technique is used to model the interactions between the reinforcement and concrete in this model.

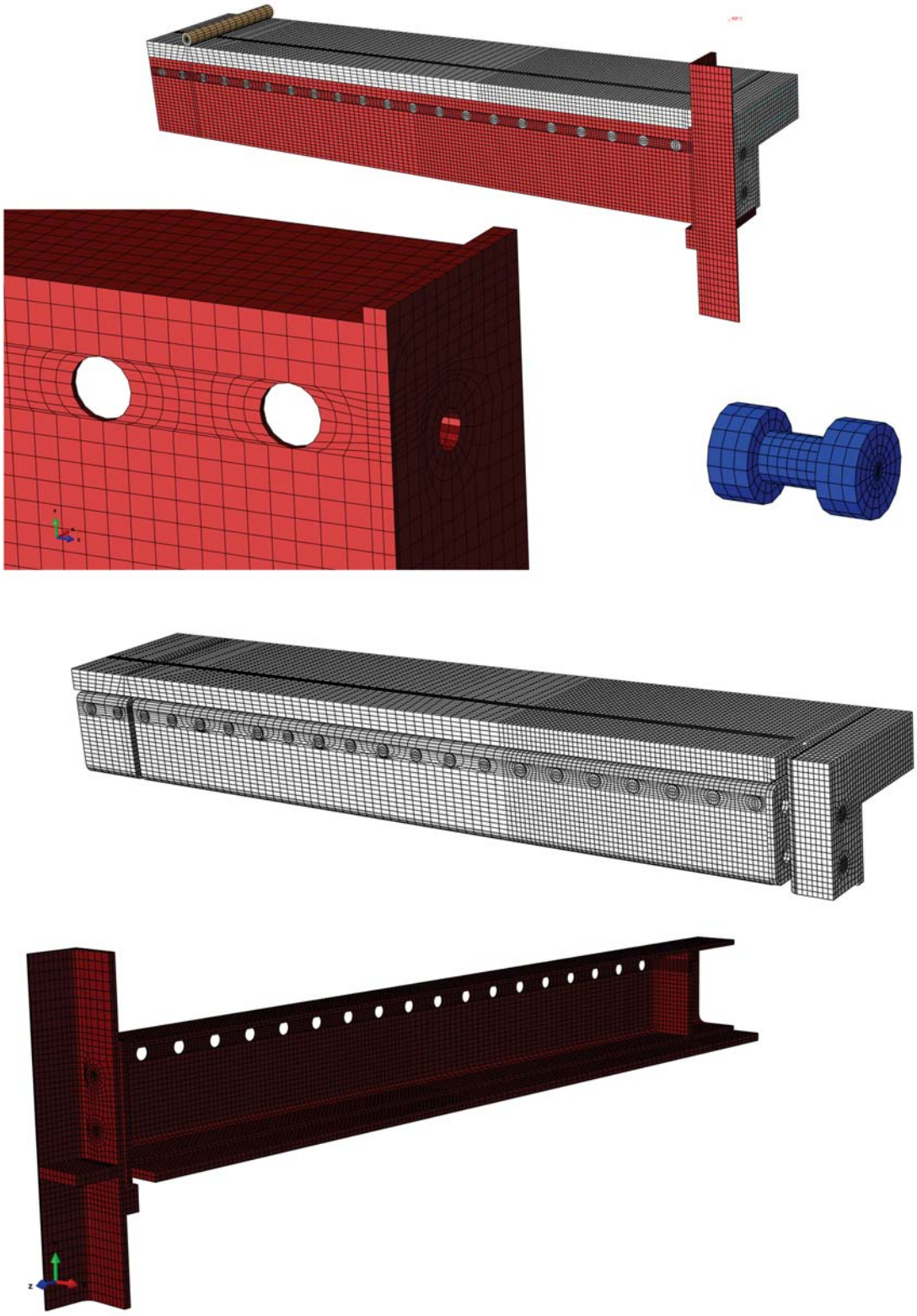

Figure 5.2: Parts modelled with C3D8R elements

As referred previously, only a quarter of the model was reproduced. Hence, double symmetric boundary conditions were applied to consider the symmetrical conditions of the specimen. At the end of the beam, an infinitely rigid roll was introduced so as to replicate the support. The translational movement of the central line of the roll nodes was fixed in the three system directions. Rotation of the roll was therefore allowed. A reference point *RP-1* representing the hydraulic jack was defined and kinematically coupled to the top nodes of the column section (X-Z plane, cf. Figure 5.3). In compliance with the experimental testing procedure, the displacement controlled loading was operated on this reference point.

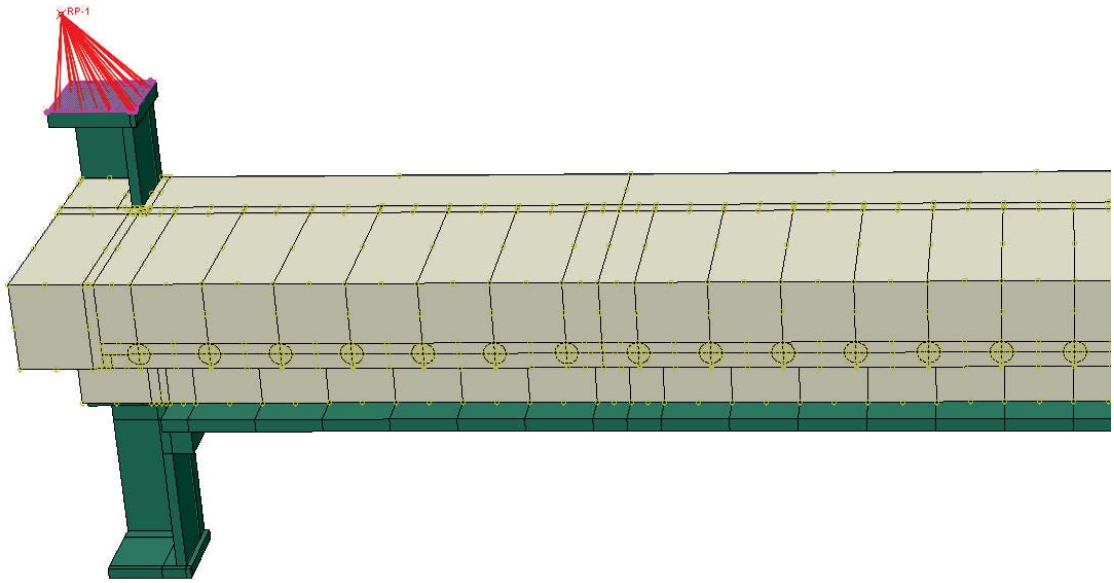

Figure 5.3: Coupling of reference point to the column section

5.2.2 Analysis method

The finite element software Abaqus provides two complementary solvers to analyse a large spectrum of problems: **static implicit** and **dynamic explicit**. According to (Abaqus 6.14, 2014), the deciding factor in the choice between both techniques is related to the degree of discontinuity in the solution. The implicit solver may encounter convergence difficulties when material degradation or failure, such as cracking of concrete is included in the solution. In order to solve highly discontinuous problems, the explicit solver constitutes therefore a more adequate tool, which facilitates convergence issues and provides an efficient solution for very large problems (Abaqus 6.14, 2014). Although the explicit technique provides a solution for true dynamic equilibrium instead of static equilibrium, it can be applied to quasi-static non-linear problems. Ideally, the process should be modelled in its natural time period, which would lead to large computational time. For this reason, the calculation time can be enhanced by artificially increasing the loading rates or by using the mass scaling method. Since, these methods tend to increase inertia forces, leading to non-static solutions, a reasonable compromise between reduced computation time and useful quasi-static results should be found.

The cracking phenomenon of concrete plays a predominant role in the load bearing behaviour of composite joints. Thus it was opted to adopt the dynamic explicit technique in the numerical model. In this context, it was important to keep the inertial effects insignificant so as to obtain a quasi-static solution of the problem. Increased loading rates were thus implemented.

The adequate loading rate was optimised in an iterative process to 0.30 mm/sec in order to achieve a satisfactory energy balance between external and internal work. In earlier numerical investigations using explicit analysis, loading rates in the same order of magnitude (0.25 mm/s) were used by other researchers (Qureshi et al., 2011).

In the initial step, all boundary conditions were defined. In the second step, a uniform displacement is applied to the reference point by means of a smooth amplitude function. This smoothing function is recommended by Abaqus for quasi-static approximations using the explicit method (Abaqus 6.14, 2014).

5.2.3 Constitutive models for materials

Concrete

Four different types of constitutive laws to model concrete structures are available in Abaqus: Brittle Cracking, Concrete Smeared Cracking, Concrete Damaged Plasticity and Drucker-Prager. Concrete Damaged Plasticity (CDP) is the most appropriate material model since, according to Gil and Bayo (2008b), it possesses the advantage of being more complete and numerically stable than the other concrete models. Due to this, Concrete Damaged Plasticity was also used in the present work as constitutive model for concrete.

Concrete Damaged Plasticity assumes two main failure mechanisms, namely compressive crushing of concrete and tensile cracking. For the compressive behaviour of concrete, the stress-strain curve ($\sigma_c - \varepsilon_c$) schematized in Figure 5.4 and defined in EN 1992-1-1 (2004) for non-linear structural analysis was implemented in the numerical model. The analytical formula for the stress-strain relationship follows to:

$$\sigma_c = f_{cm} \cdot \frac{k \cdot \eta - \eta^2}{1 + (k-2)\eta} \tag{5.1}$$

with:

$$\eta = \frac{\varepsilon_c}{\varepsilon_{c1}} \tag{5.2}$$

$$k = \frac{1.05 \cdot E_{cm} \cdot |\varepsilon_{c1}|}{f_{cm}} \tag{5.3}$$

$$\varepsilon_{c1} = 0.7 \cdot f_{cm}^{0.31} \leq 2.8 \qquad [‰] \tag{5.4}$$

$$\varepsilon_{cu1} = 3.5‰ \tag{5.5}$$

$$E_{cm} = 22000 \cdot (\frac{f_{cm}}{10})^{0.3} \qquad [N/mm^2] \tag{5.6}$$

Equations (5.1) to (5.6) are defined in EN 1992-1-1 (2004). In these equations, the concrete compressive strength f_{cm} (introduced in N/mm^2) corresponds to the values obtained in the material tests and specified in Table 3.2. The elastic properties of concrete were modelled with a modulus of elasticity E_{cm} according to equation (5.6) and a Poisson's ratio of 0.2.

The tensile behaviour of concrete can be subdivided into two domains. The first is characterised by the initial elastic behaviour of concrete until its low tensile strength f_{ctm} is fully exploited. The second is characterised by the cracking process in concrete. Due to the presence of reinforcement, the tensile stresses in concrete do not decrease sharply to zero

but are subjected to a more gradual loss of strength. As main responsible for this particular behaviour, the reinforcement exerts a tension softening effect on concrete. It can be reciprocally stated that the load bearing participation of concrete has a stiffening effect on the reinforcement. Since this effect is considered in the constitutive law of concrete, it is referred as tension softening. In the next Chapter 6, devoted to the analytical assessment of the test results, this effect is considered in the material law for the reinforcement (tension stiffening).

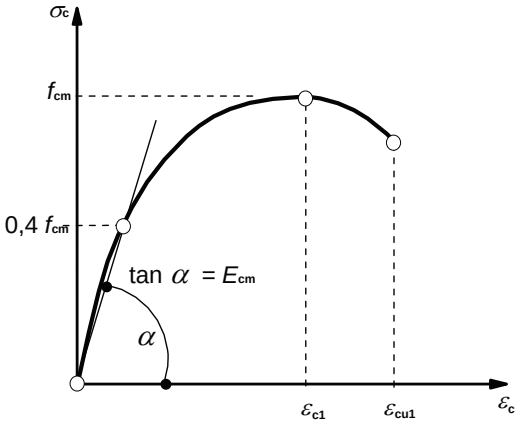

Figure 5.4: Stress-strain relation for concrete in compression (EN 1992-1-1, 2004)

According to the Abaqus Manual, the consideration of some tension softening in the constitutive law of concrete allows to model the effects associated to the rebar/concrete interface such as bond slip (Abaqus 6.14, 2014). The quantification of the softening response of concrete constitutes therefore an important aspect. The first approach dates back to Hillerborg et al. (1976), who defined a linear loss of strength after the crack initiation (cf. Figure 5.5 (a)). Since the results tend to be too stiff, Hillerborg (1985) proposed later a bilinear function to describe the gradual loss of tensile strength in concrete (cf. Figure 5.5 (b)). One year later Cornelissen et al. (1986) proposed an alternative exponential function to describe the post-failure tensile behaviour of concrete on experimental basis (cf. Figure 5.5 (c)). These three tension softening functions have in common to be characterised by the fracture energy value G_f defined in 1976 by Hillerborg. This energy may be interpreted as the energy required to open a unit area of crack and corresponds to the area under the stress-crack opening relation. According to (Abaqus 6.14, 2014), the softening response could have also been expressed in terms of stress-strain curve, which may however introduce unreasonable mesh sensitivity into the results. Moreover, the concrete's brittle behaviour is preferably characterised by a stress-displacement response using Hillerborg's fracture energy proposal (Abaqus 6.14, 2014).

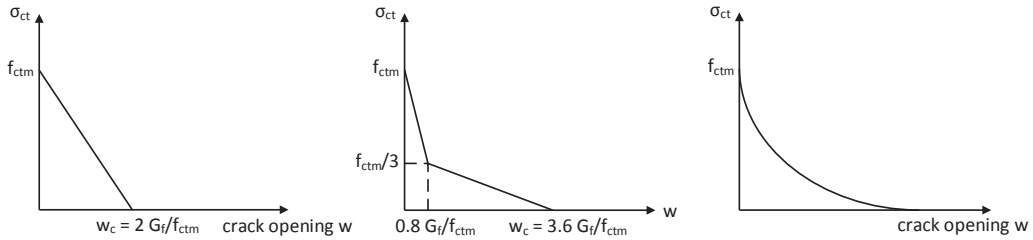

(a) Linear function (b) Bilinear function (c) Exponential function

Figure 5.5: Tension softening models for concrete

In the present numerical model, the tension softening was implemented according to the recommendations of Model Code 2010 (Comite Euro-International du Béton, 2010). It consists of a bilinear stress-crack opening relation, resembling that of the exponential approach of Cornelissen. The characteristic points of this bilinear relationship depicted in Figure 5.6 can be determined by:

$$\sigma_{ct} = f_{ctm} \cdot (1.0 - 0.8 \cdot \frac{w}{w_1}) \qquad \text{for} \quad w \leq w_1 \tag{5.7}$$

$$\sigma_{ct} = f_{ctm} \cdot (0.25 - 0.05 \cdot \frac{w}{w_1}) \qquad \text{for} \quad w_1 < w \leq w_c \tag{5.8}$$

where:

w is the crack opening in mm;

w_1 $= G_f / f_{ctm}$ in mm when $\sigma_{ct} = 0.20 \cdot f_{ctm}$;

w_c $= 5 \cdot G_f / f_{ctm}$ in mm when $\sigma_{ct} = 0$;

G_f is the fracture energy in N/mm

$= 73 \cdot f_{cm}^{0.18}$ with f_{cm} in N/mm^2;

f_{ctm} is the tensile strength in N/mm^2;

$$= \begin{cases} 0.30 \cdot (f_{cm} - 8)^{2/3} & \text{for } f_{cm} \leq 58 N/mm^2 \\ 2.12 \cdot ln(1 + (f_{cm}/10)) & \text{for } f_{ck} > 58 N/mm^2 \end{cases}$$

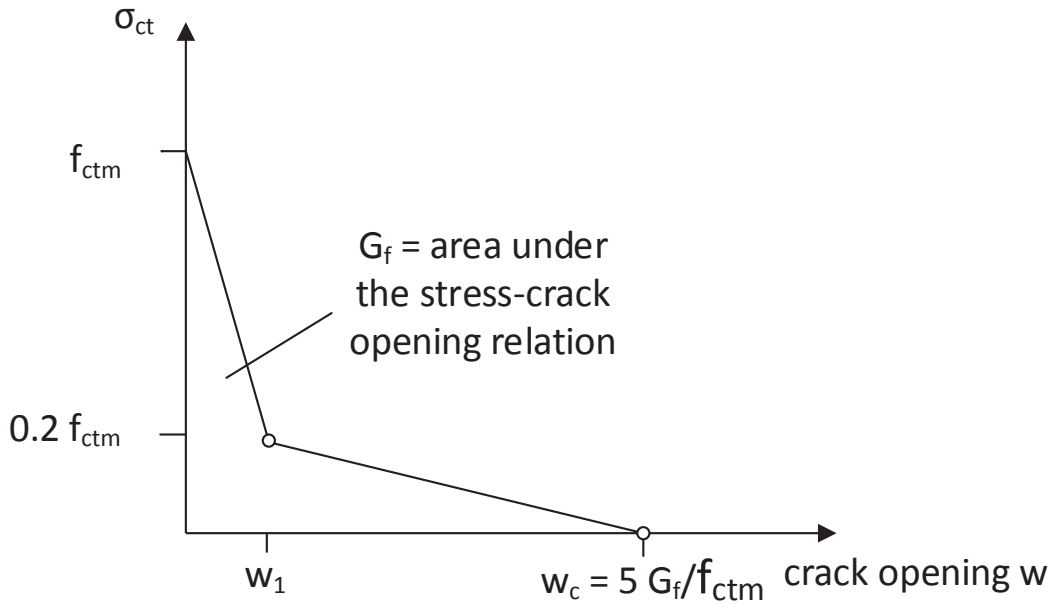

Figure 5.6: Stress-crack opening relation for uniaxial tension acc. to (Comite Euro-International du Béton, 2010)

To complete the definition of the Compression Damaged Model used in this numerical model for concrete, the five constitutive plasticity parameters required to define the shapes of flow potential and yield surfaces are presented:

- Dilation angle ψ: When concrete is subjected to high inelastic stress states, it undergoes a change in volume, which is also called dilation. An alternative interpretation of this notion is provided by Kmiecik and Kaminski (2011), who associates the dilation angle to the internal friction angle of concrete. A value of 38° was adopted in the present work.
- Flow potential eccentricity ε: According to Abaqus Manual (Abaqus 6.14, 2014), the flow potential eccentricity is a small positive value, which defines the rate at which the hyperbolic flow potential approaches its asymptote (Abaqus 6.14, 2014). The default value of 0.1 was preserved in the present model.
- Ratio f_{b0}/f_{c0}: It represents the ratio of initial equibiaxial compressive yield stress to initial uniaxial compressive yield stress. The default value of 1.16 was kept.
- Parameter K: This parameter represents the ratio of the second stress invariant on the tensile meridian to that on the compressive meridian. The values for K range from 0.5 to 1.0. According to Kmiecik and Kaminski (2011), when this value is equal to 1, the deviatoric cross-section of the failure surface becomes a circle, corresponding to the classic Drucker-Prager Hypothesis. The default value of K=2/3 was adopted.
- Viscosity parameter μ: This parameter is used for the visco-plastic regularisation of the concrete constitutive equations in Abaqus/Standard. For Abaqus/Explicit, this parameter is ignored (Abaqus 6.14, 2014). The default value is 0. Since the dynamic explicit solver was used in these simulations, this parameter does not affect the calculation.

Reinforcement

Isotropic material properties with elasto-plastic behaviour were used for the reinforcement. The Young modulus was assumed to 200 Gpa with a Poisson's ratio of 0.3. Since the main objective of the present work is to assess the rotation capacity of composite joints, the plastic material properties of the reinforcement were implemented precisely.

As explained in section 3.5, the ultimate strain elongation of the reinforcement bars was measured at ultimate strength (A_g) as well as around the fracture point, where necking of the coupons was visible ($A_{5.65}$). In this numerical model, the corresponding $A_{5.65}$ values of ultimate strain are implemented in the material definitions of the reinforcement. In the Abaqus Manual (Abaqus 6.14, 2014), it is stated that the plasticity definition in ductile metals requires the true stress and true strain relation instead of the nominal (engineering) stress and strain values, supplied by material test data. This more precise formulation of the plastic behaviour of reinforcement is needed since, in the framework of this research, the rotation capacity is defined at the rupture of the longitudinal reinforcement. Since the reinforcement undergoes large plastic deformations, necking of the bars occurs. This justifies the use of true stress-strain curves. The true stress-strain curve includes the section change of the reinforcement bars and is obtained according to (Abaqus 6.14, 2014) from the nominal stress-strain values by means of the following expressions:

$$\sigma_{true} = \sigma_{nom} \cdot (1 + \varepsilon_{nom}) \tag{5.9}$$

$$\varepsilon_{true} = \ln(1 + \varepsilon_{nom}) \tag{5.10}$$

A qualitative comparison between true and nominal stress-strain curves is shown in Figure 5.7. Damage identification is implemented in the material law through an abrupt strength loss after reaching the ultimate strain limit.

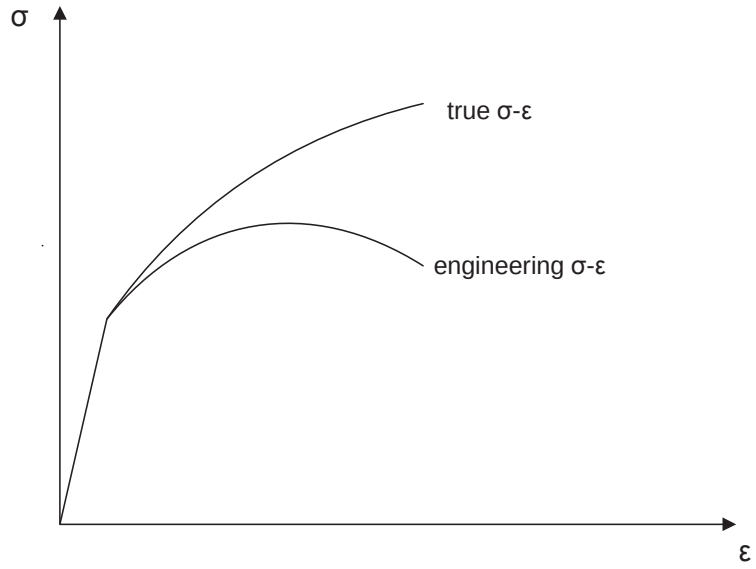

Figure 5.7: Qualitative comparison between true and engineering stress-strain relationship

Structural steel

Similarly to the reinforcement, components made of structural steel are also modelled with isotropic properties and elasto-plastic material behaviour. The modulus of elasticity was taken as 210 Gpa and the Poisson's ratio $\nu = 0.3$. Strain hardening was implemented in the material properties. The yield and tensile strength are carried over from the material tests, whose results are shown in Table 3.3. The ultimate strain limit was assumed to 0.15 and similar damage identification as for the reinforcement is introduced.

Bolt material

The elastic material properties of the bolts are identical to that of structural steel. Since no material tests were carried out on the bolt material, the yield and ultimate strength needed to be estimated on behalf of experimental investigations conducted by other researchers using similar bolt grades. In (Renner, 2015), material tests on grade 10.9 bolts were performed. It is shown that the percentage elongation after fracture ($A = 9\%$) and the tensile strength ($f_u = 1040 N/mm^2$) proposed by ISO 898-1 for 10.9 bolts are safe-sided. Thus, it was opted to rely on the results obtained in Renner (2015) rather than those suggested by ISO 898-1 (2009) for the numerical model developed herein. Similar values as in (Renner, 2015) were used for the yield and tensile strength of the bolt material. As explained above, Abaqus requires that nominal values are transformed into true stress-strain values in order to correctly account for the necking of the bolts. The values used in this model and given in Table 5.1 constitute the true stress-strain values. Damage identification was introduced over a sharp loss in strength of the bolt material at the ultimate strain of 15 %.

Table 5.1: Bolt material: Numerical input

E-Modulus $[N/mm^2]$	Poisson's Ratio [-]	True Yield Stress $[N/mm^2]$	True Tensile Stress $[N/mm^2]$	Ultimate Strain [%]
210000	0.3	1100	1250	15

5.3 Validation of numerical results

In the present section, the results of the numerical simulations are compared to the experimental results. The objective is to validate the numerical model by reproducing the results obtained in the experimental investigations. The comparison is performed on different levels. Firstly, the experimental and numerical moment-rotation curves are compared. Secondly, the numerically obtained deformations are compared to the deformations measured by the displacement captors on the experimental specimens. Finally, the development of the concrete cracks is analysed and compared to the observed cracks in the tests.

In Figures 5.8 (a) to (h), the moment-rotation curves obtained from the numerical and experimental investigations are compared. A good agreement between the numerical and experimental results is demonstrated for all tests. Similarity in joint stiffness, resistance and ductility can be observed. The same failure modes as in the experimental tests was obtained at identical joint rotations in the numerical simulations.

The numerical simulations of test series B culminated in the rupture of the longitudinal reinforcement bars. For series E the failure mode depended on the reinforcement ratio of the concrete slab. Simulation E21, for instance, failed due to the rupture of one longitudinal reinforcement bar while in simulations E22 and E32 the failure was defined by the tensile rupture of the upper bolt. These differences in load bearing behaviour can be explained by the lower amount of longitudinal reinforcement (ρ = 1.3 %) and the smaller rebar diameter ($\varnothing$ = 12 mm) used in test E21, which conveys a lower ductility to the reinforcement component of the composite joint. Numerical pictures showing the bolt or rebar failure in the individual simulations are given in Appendix D.

From the numerical and experimental analyses, it can be deducted that the larger the ductility of the reinforced slab, the larger is also the demand in bolt-row ductility. An important outcome can therefore be retrieved from this analysis: the steel connection should be designed according to failure mode 1 of the T-stub model (complete yielding of the plate), whenever large ductility is needed for composite joints.

For the bare steel joint, the FEA moment-rotation curve shows also good agreement with the experimental test curve. The failure mode of the joint was due to the fracture of the upper bolt after substantial yielding of the endplate similarly to simulations E22 and E32.

In addition to the moment-rotation curves, a comparison is furthermore performed with respect to the overall vertical deflection of the test set-up. For this purpose, the load applied vertically on the steel column is plotted against the vertical displacement of the column (cf. Figures 5.9 (a) to (h)). The numerical accuracy of the FE model is once more confirmed by the good concordance between the numerical and experimental load-displacement curves. In Appendix D, more comparisons between experimental and FEA results are provided. In particular, the good agreement between the horizontal gap between the column flange and the concrete slab is demonstrated.

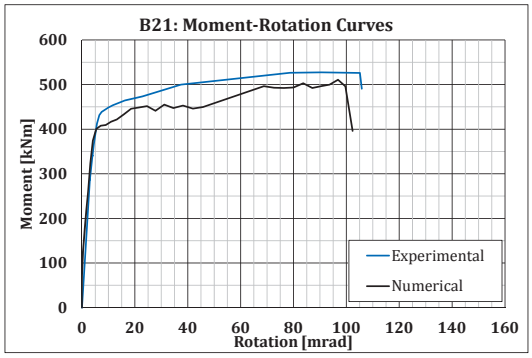

(a) Test B21

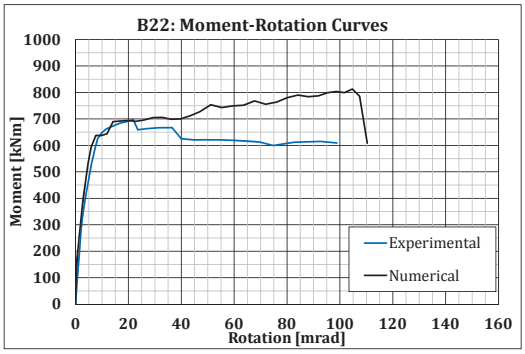

(b) Test B22

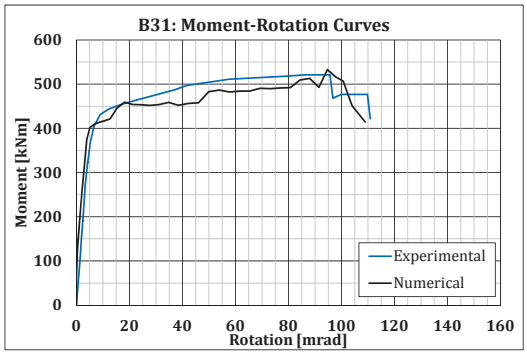

(c) Test B31

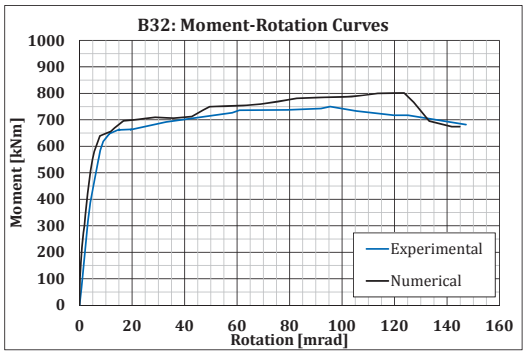

(d) Test B32

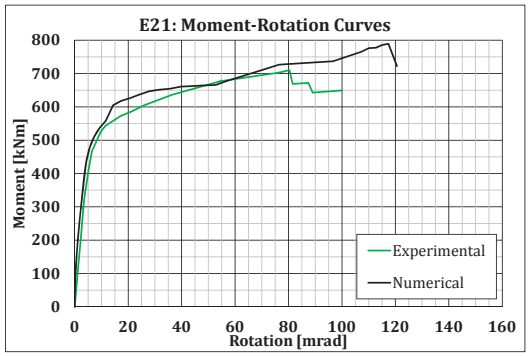

(e) Test E21

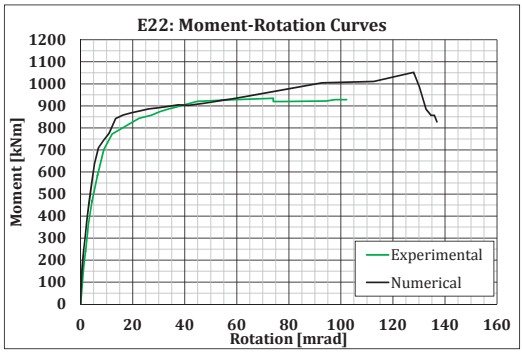

(f) Test E22

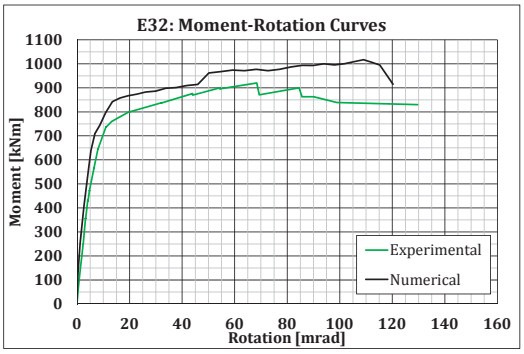

(g) Test E32

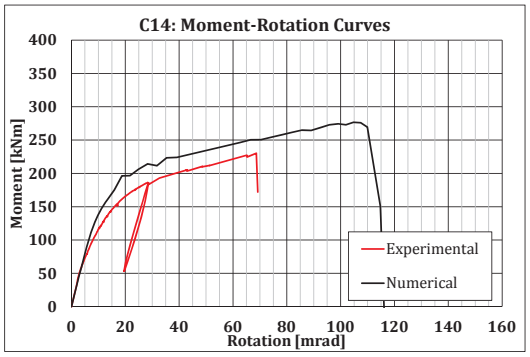

(h) Test C14

Figure 5.8: Comparison between experimental and numerical moment-rotation curves

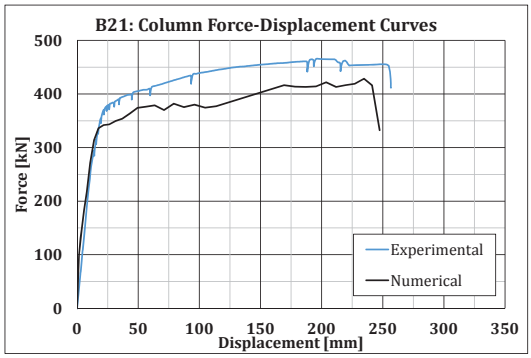

(a) Test B21

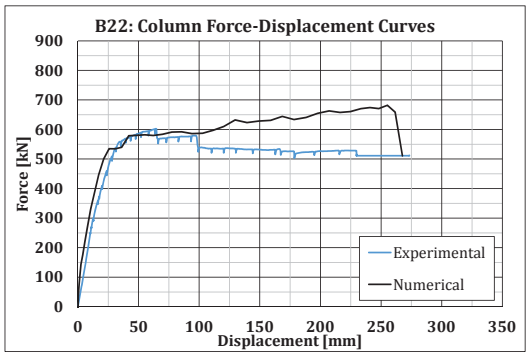

(b) Test B22

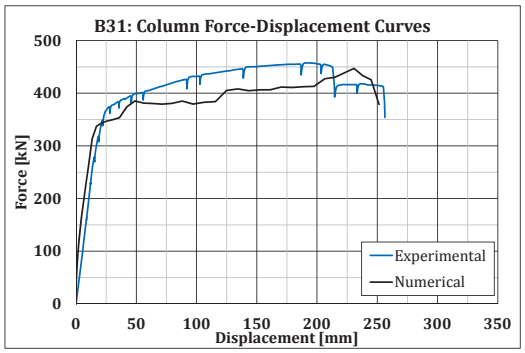

(c) Test B31

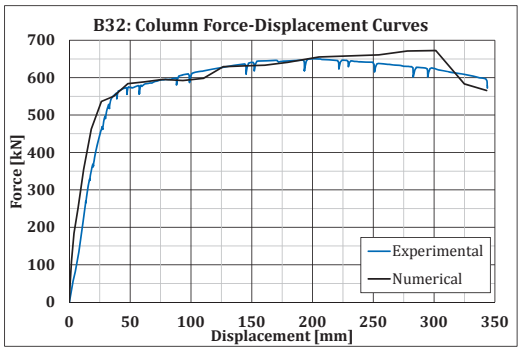

(d) Test B32

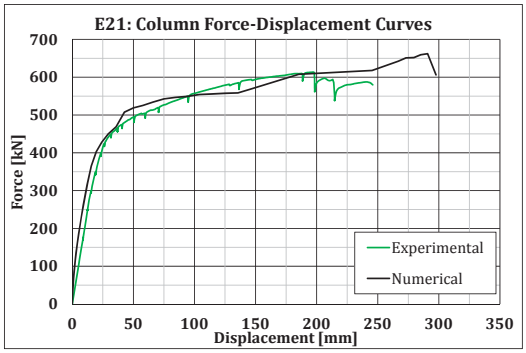

(e) Test E21

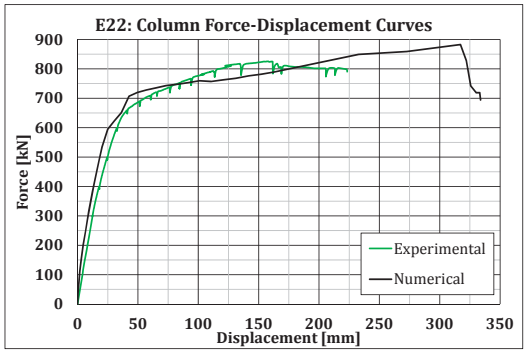

(f) Test E22

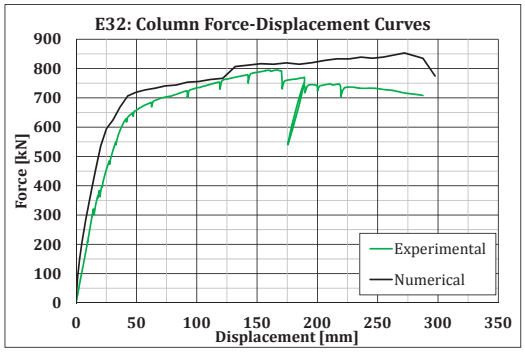

(g) Test E32

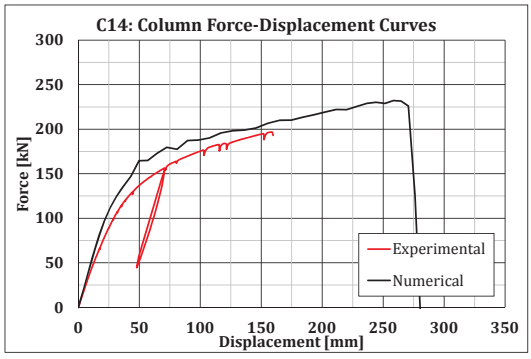

(h) Test C14

Figure 5.9: Comparison between experimental and numerical force-deformation curves

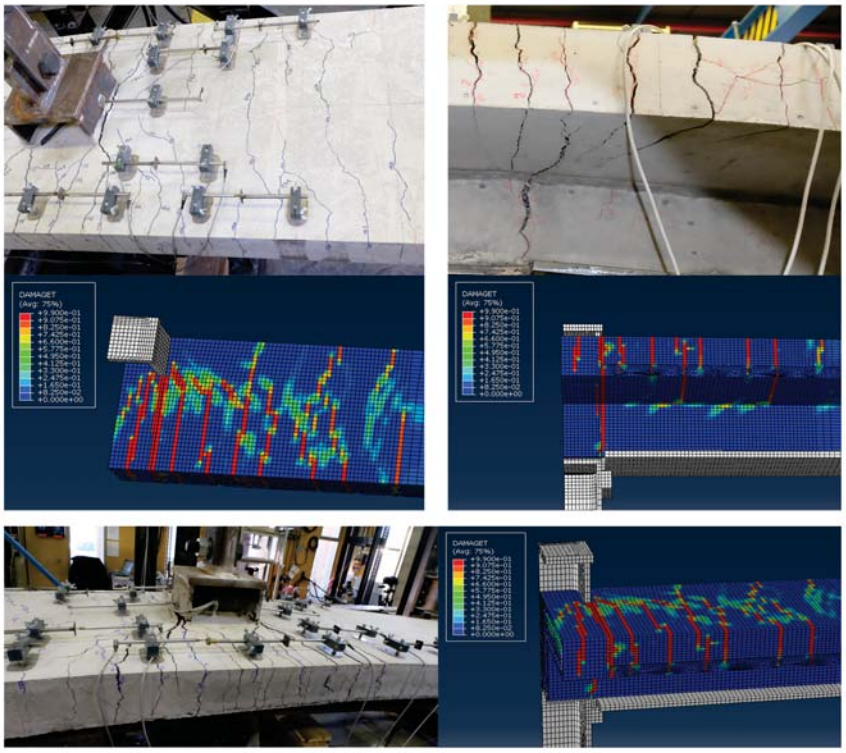

Figure 5.10: Comparison between numerical and experimental crack pattern

In Section 4.5, the importance of the crack pattern in the reinforced concrete slab is highlighted. The numerical reproduction of the crack pattern in the slab represents an additional comparison basis to verify the accuracy of the FE model. The similarity between numerical and experimental crack pattern is demonstrated in Figure 5.10. Similarly to the observations made during the experimental tests, the present numerical simulations show that after an initial stage characterised by the formation of cracks, a stabilisation occurs in the cracking phenomena.

At the end of the experimental tests, each bolt was extracted from the specimen in order to exclude bolt failure. Figure 5.11 shows the deformation of one of the bolts. The same Figure presents the bolt deformation obtained in the FEA at a load stage prior to failure. The comparison of both deformation shapes demonstrates once more the similarity between experimental and numerical results.

Due to the fact that in experimental tests of series E, the concrete encasement hides the deformation shape of the endplate, comparison can only be made for test C14. In Figure 5.12 it can be observed that the deformation shape of the endplate in the numerical analysis resembles the experimental deformation.

Although test C14 was performed without concrete, it is of interest to study how the presence of concrete encasement in the beam and column chord affects the behaviour of the steel joint. An additional numerical simulation, designated as C14b, was therefore performed on a joint model with a steel connection and concrete parts. No longitudinal reinforcement was incorporated in this model. In Figure 5.13 (a) it can be observed that after an initial discrepancy in the joint response, the moment-rotation curves of simulations C14 and C14b

rapidly converge. The initial difference in behaviour is explained by the low tensile strength of concrete. At 2/3 of the plastic bending resistance $M_{pl,cal}$, the difference in stiffness is insignificant. In terms of resistance and ductility, close FEA results are obtained for the models C14 and C14b. This leads to the conclusion that the concrete encasement does not affect the behaviour of the steel joint and that the differences observed between series B and series E are only related to bare bolted flush endplate connection and not to the concrete encasement. Comparison of the deformation shape of the endplate for simulations C14 and C14b demonstrates the insignificant influence of the concrete encasement (cf. Figure 5.14).

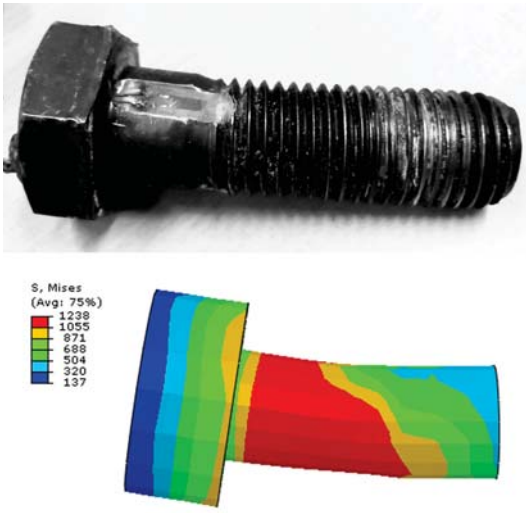

Figure 5.11: Comparison between experimental and numerical deformation shape of bolts

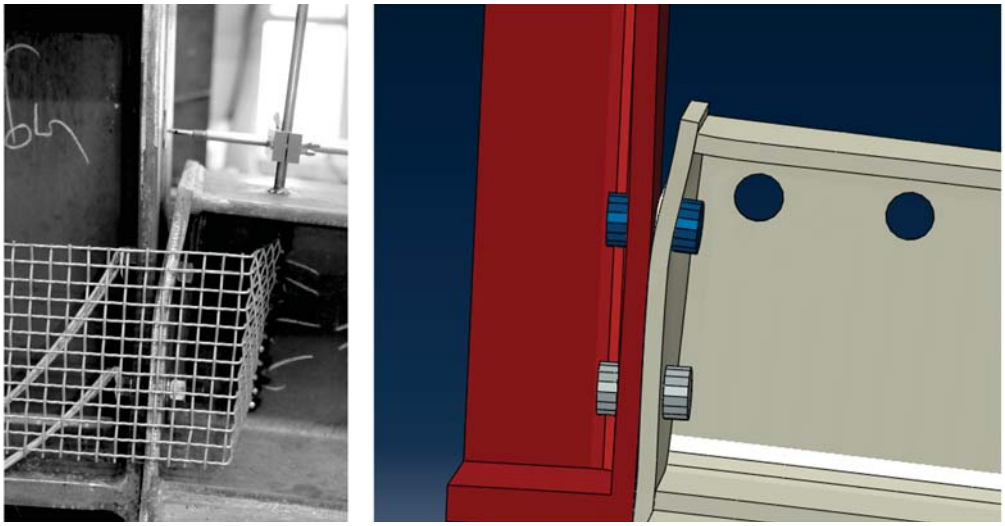

Figure 5.12: Deformed shapes of flush endplate connection (experimental and FEA)

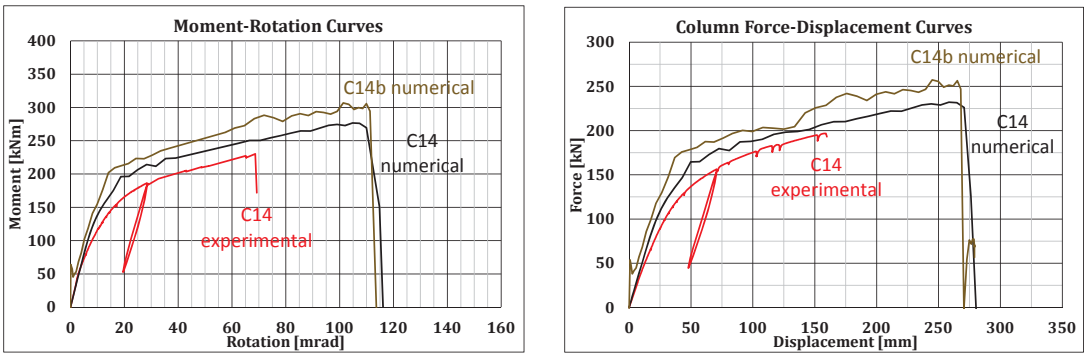

(a) Moment-rotation curves

(b) Force-displacement curves

Figure 5.13: Influence of concrete encasement on the behaviour of test C14

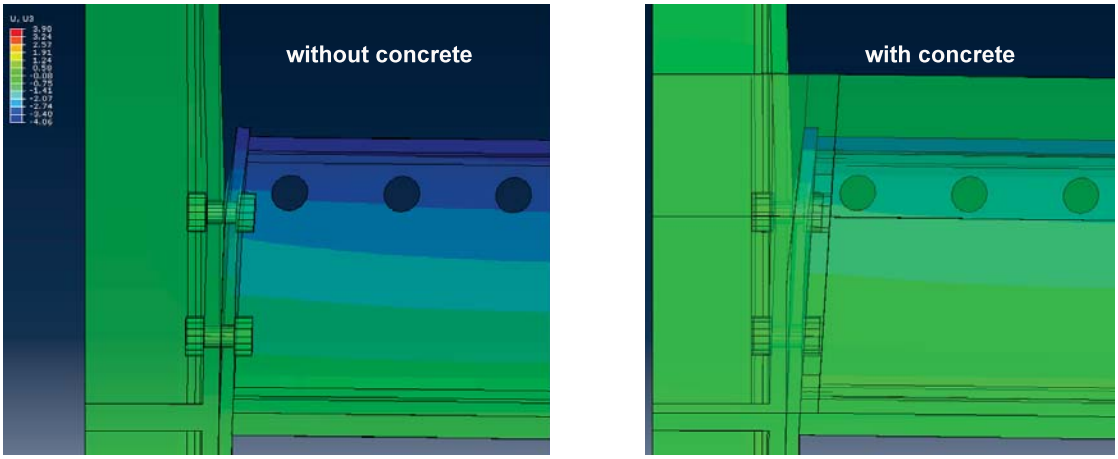

Figure 5.14: Horizontal deformation of the endplate connection for simulations C14 and C14b at the same deformation

5.4 Influence of the bolted flush endplate connection on the joint stiffness

In the previous Section 4, the influence of a bolted flush steel connection on the overall stiffness of composite joints was addressed on the basis of the experimental investigations. From Figure 4.20 (a) it can be deducted that that the presence of an additional bolted endplate connection does not necessarily increase the rigidity of a composite joint, since in test E21 and test E22, the joint stiffnesses obtained experimentally are close to those obtained in the correspondent tests of series B, namely test B21 and test B22. It should be reiterated that the only difference between tests of series E and their correspondent tests in series B is the presence of a bolted endplate type of steel connection. Since the internal lever arm between the bolt-rows and the compression point of the joint is small in comparison to that between the reinforcement layer and the compression point, the steel connection had little influence on the stiffness of the composite joints. This fact justifies the discrepancy between the experimental test on the bare steel connection C14 and that on the composite joints of series B. It must be stated that this large discrepancy was observed on a flush endplate type of steel connection. For an extended endplate, for instance, the influence of the steel connection on the joint stiffness must be investigated in further research.

Although no significant discrepancy in stiffness was found between tests E21 and B21, as well as between tests E22 and B22, a slight increment of stiffness was observed in test E32 in relation to test B32. In the next Section 6.3.1, it is shown that according to EN 1994-1-1 (2004), the stiffness of a composite joint can be taken as the simple superposition of the individual stiffnesses, namely that of the steel connection and reinforcement. This premise is confirmed by the results obtained in test E32, for which the increase in stiffness is practically equal to the stiffness of the bare steel joint. Since such an observance was not made in tests E21 and E22, it is important to determine the reason for such a difference in load bearing behaviour. In order to find out a plausible justification, the validated numerical model is used.

In Section 6.3.1 it is shown that according to EN 1994-1-1 (2004), the simple superposition principle for the joint stiffness assumes a perfectly **linear deformation plane** of the connecting zone. Even if the reliability of this assumption was shown for bare steel joints, no research investigations were found in literature on the reliability of such a premise for the specific case of composite joints. Figure 5.15 shows the scaled deformation of the connecting zone for the different tests in series B and series E in the initial elastic range. The assumption of linear deformation shape made in EN 1994-1-1 (2004) cannot be observed for the connecting zone in series E. In fact, the restraint provided by the bolted connection inhibits the linear deformation of the joint. As a consequence, the elongation of the reinforcing bars in the vicinity of the bolted connection is affected by the local restraint provided by the steel connection (cf. Figures 5.15 to 5.17 and Appendix B.3). Conversely, the elongation of the outlying rebars seems not affected by the local restraint (cf. Figure 5.17).

This particularity explains the different results obtained for test E32 and tests E21/E22 . In fact, the test specimen E32 consists of fewer rebars in the central zone where the presence of the bolted connection interferes with the elongation of the reinforced slab. For tests E21 and E22, on the contrary, the dense reinforcement arrangement in the vicinity of the steel connection magnifies the non-linear influence of the connecting zone (cf. Figure 5.17). As a consequence, the superposition principle assumed by EN 1994-1-1 (2004) for the calculation of the stiffness could not be observed in the present research.

In summary, it can be stated that the arrangement of the longitudinal reinforcement might slightly affect the stiffness of a bolted endplate composite joint. For the practical design however, these results show that the influence of the bare steelwork connection on the stiffness of flush endplate connections can be neglected. Owing to the low stiffness of this type of steel connections, this approximation provides a sufficient degree of accuracy.

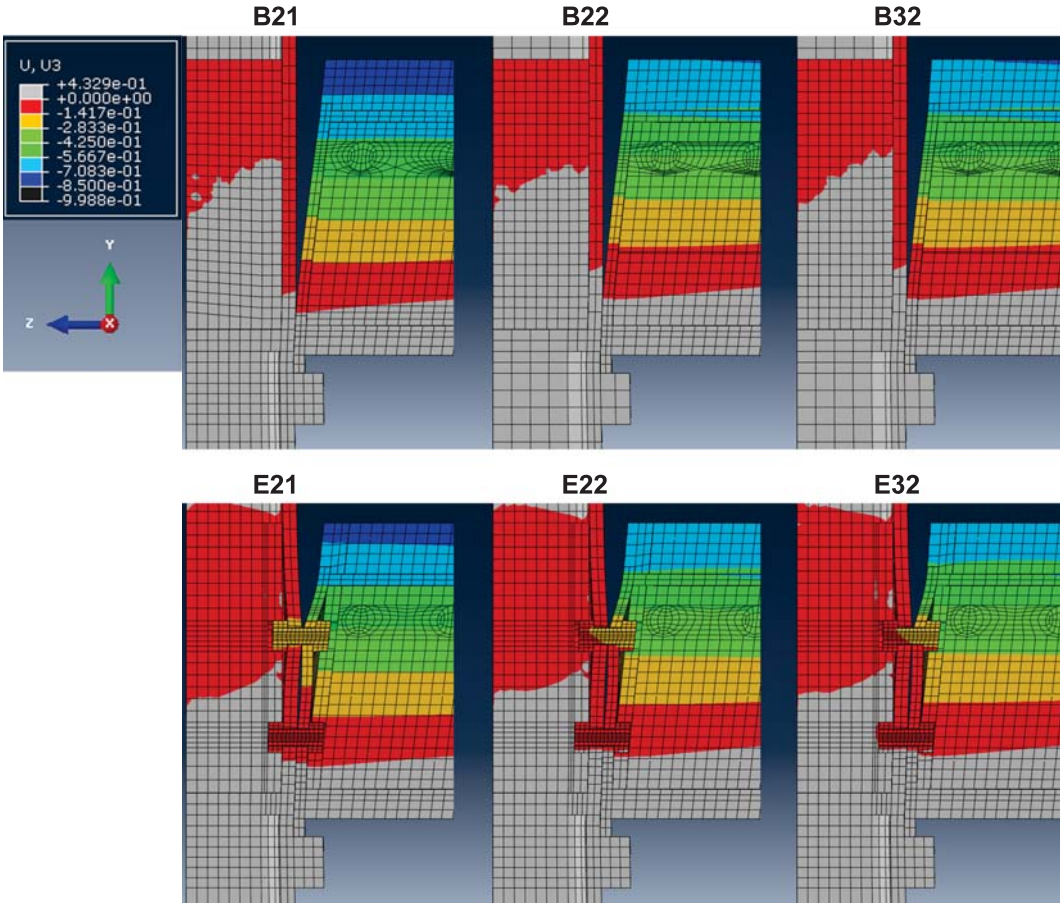

Figure 5.15: Scaled joint deformation in the elastic range for series B and E

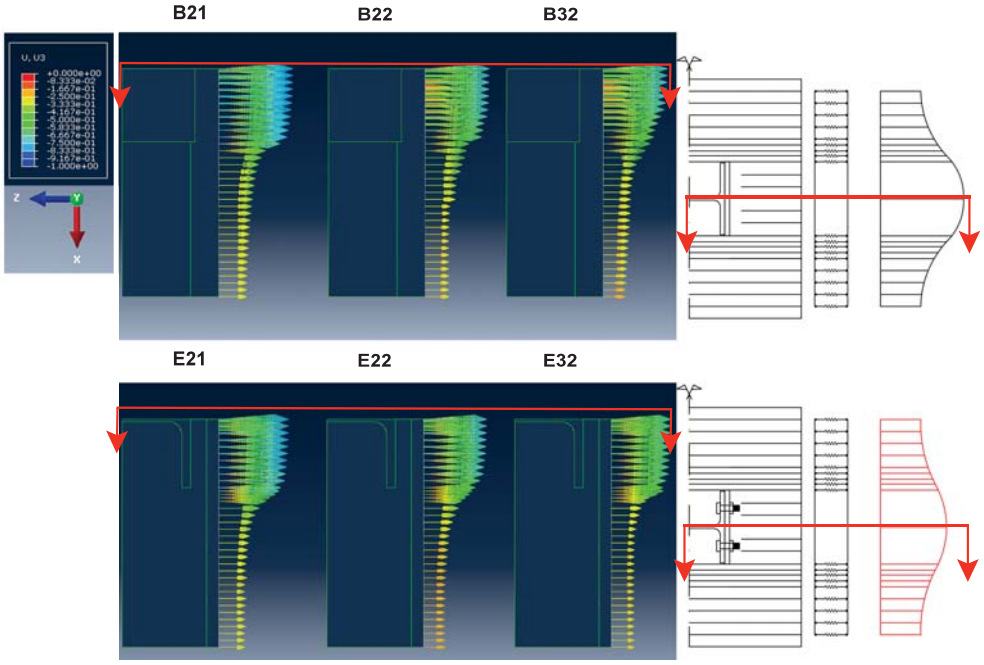

Figure 5.16: Non-uniform longitudinal elongation of reinforcement in numerical simulations

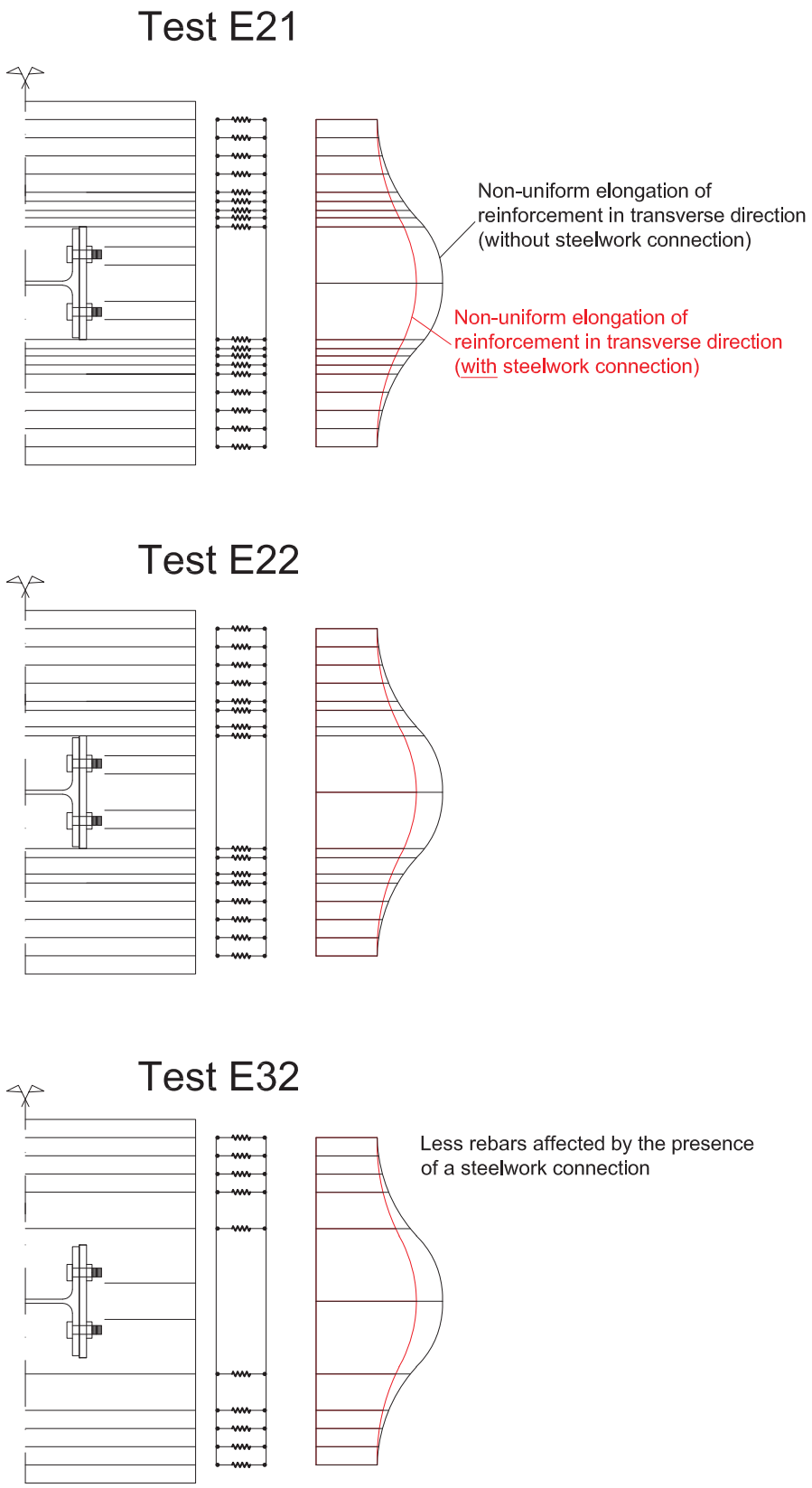

Figure 5.17: Influence of the steelwork connection on the non-uniform elongation of reinforcement in transverse direction for tests E21, E22 and E32

5.5 Parametric study

In this research, a parametric study was performed to evaluate the influence of parameters such as: **amount of longitudinal reinforcement**, **diameter of the rebars** and **maximal strain elongation** of the reinforcement. This study was carried out on the basis of the numerical model presented in this chapter. Since the intention was not to investigate the influence of the steel connection, the FE parametric study was performed on the numerical model without bolts, which corresponds to test series B. Section and material properties were kept similar to those employed in the numerical model for test B31 in order to facilitate the comparison of results obtained in this study.

The parametric study is divided into two parts. The **first part (G1)** considers the effect of variable longitudinal reinforcement ratio ρ and rebar diameter $\varnothing$ on the behaviour of composite joints. Experimental and numerical investigations have shown that these two parameters substantially influence the behaviour of composite joints. Since the experimental investigations performed in this research provided reinforcement ratios ρ ranging between 1.3 % and 2.0 %, it was opted to vary the reinforcement amount within a reasonable distance from this range. Thus, only numerical models with reinforcement ratios between 0.7 % and 2.5 % were analysed. The lower limit was determined in accordance to earlier investigations, which showed that composite joints with reinforcement ratios lower than 0.7 % present rotation capacities below 40 mrad (cf. Section 2). This is regarded as insufficient in view for a plastic global analysis. The upper limit of 2.5 % was selected in order to stay within a realistic range of practice.

In what regards the diameters of the longitudinal rebars, values between 12, 14, 16 and 20 mm were considered.

The **second part (G2)** deals with the influence of the maximal elongation capacity of the bare reinforcement on the structural properties of composite joins. Based on the FE results obtained in the first part, specific joint configurations are selected from group G1 to perform FE simulations on joints with half the maximal strain elongation of reinforcement. The objective is to determine to what extent a 50 % reduction of the ultimate strain of reinforcement affects the rotation of composite joints.

A total of 15 additional finite element simulations were analysed in this parametric study. The number of longitudinal rebars with indication of diameter as well as reinforcement ratio are specified in Table 5.2 for each individual simulation. Since the main aim of this numerical study is to investigate the rotational behaviour of composite joints, the rotation capacity is shown in the same table. As referred previously, this ultimate state of ductility is defined at the rupture of at least one reinforcement bar. This failure criterion was effectively obtained in all numerical simulations performed in this parametric study.

The moment-rotation curves of the FE analysis for group G1 are shown in Figure 5.18. The beneficial influence of large reinforcement ratios and large rebar diameters is once more demonstrated with these simulations. In group G1 it can be observed that the joint configuration with the largest reinforcement ratio and the largest rebar diameter (P12-20) is at the same time the most ductile joint with an rotation capacity of 138 mrad. It can also be observed that the composite joints with smaller rebar diameters provide typically less ductility. Nevertheless, the minimal rotation capacity obtained in these simulations was of 80 mrad, which proves the suitability of these joint configurations for a global plastic analysis. When

Table 5.2: Results of parametric study

Group	Test Ref.	No. of rebars	Rebar diameter [mm]	ρ [%]	$\Phi_{u,FEA}$ [mrad]
G1 $A_{5.65} \simeq 25\%$	P10-12	10	12	0.7	80
	P10-14	10	14	1.0	90
	P12-12	12	12	0.8	80
	P12-14	12	14	1.2	93
	P12-16	12	16	1.5	101
	P12-20	12	20	2.4	138
	P14-12	14	12	1.0	80
	P14-14	14	14	1.3	95
	P16-12	16	12	1.1	80
	P18-16	18	16	2.3	130
G2 $A_{5.65} \simeq 12.5\%$	P10-14-b	10	14	1.2	48
	P12-16-b	12	16	1.5	59
	P12-20-b	12	20	2.4	70
	P14-12-b	14	12	1.0	39
	P18-16-b	18	16	2.3	70

comparing the joints with rebar diameter of 12 mm, it can be noted that the rotation capacity stays nearly the same despite the differences in reinforcement ratio. This is explained by the small variation of reinforcement ratio for these joints. A physical interpretation of this particular behaviour is reflected in the analytical formula for the rotation capacity, presented in Section 6.5.

In Figure 5.19 the FE moment-rotation curves of group G2 are compared to the correspondent simulations in group G1. It can be observed that the strain capacity of the bar reinforcement has a significant influence on the rotation capacity of composite joints. Reducing the ultimate strain by 50 % leads to an almost equal reduction of the rotation capacity of composite joints. It is therefore a material property which should be considered in the calculation of the available rotation.

The results of these 15 additional numerical simulations are used in Chapter 6 to evaluate the accuracy of the new analytical method proposed for the rotation capacity.

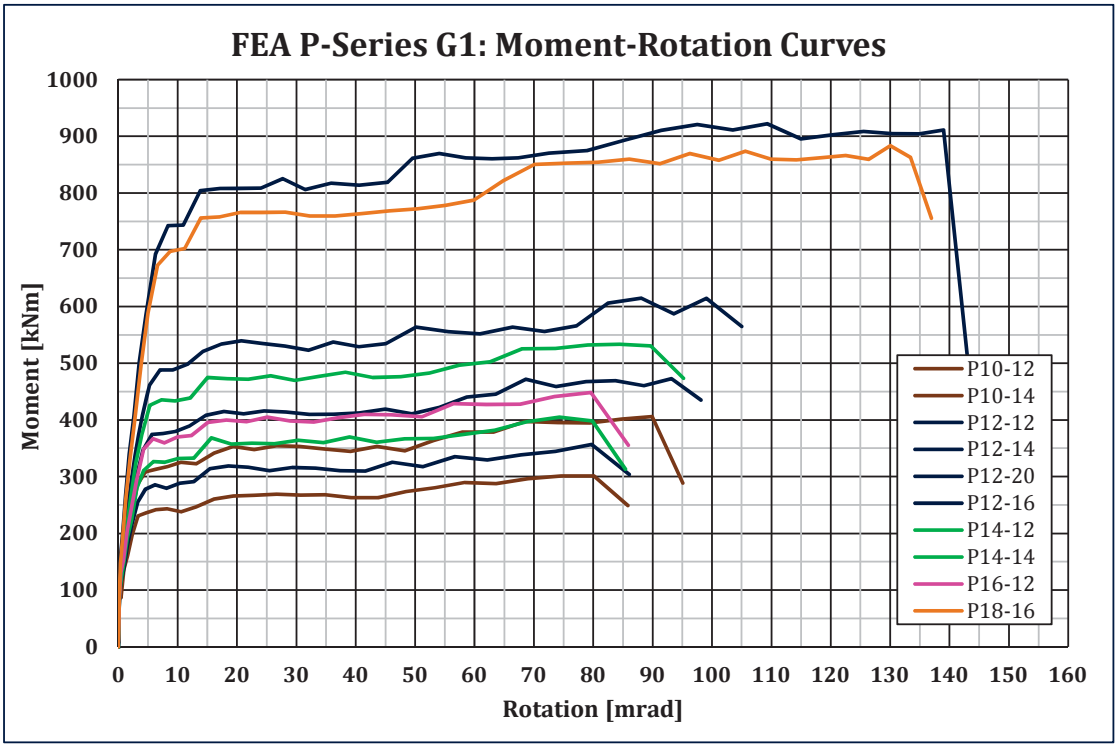

Figure 5.18: Numerical moment-rotation curves for group G1

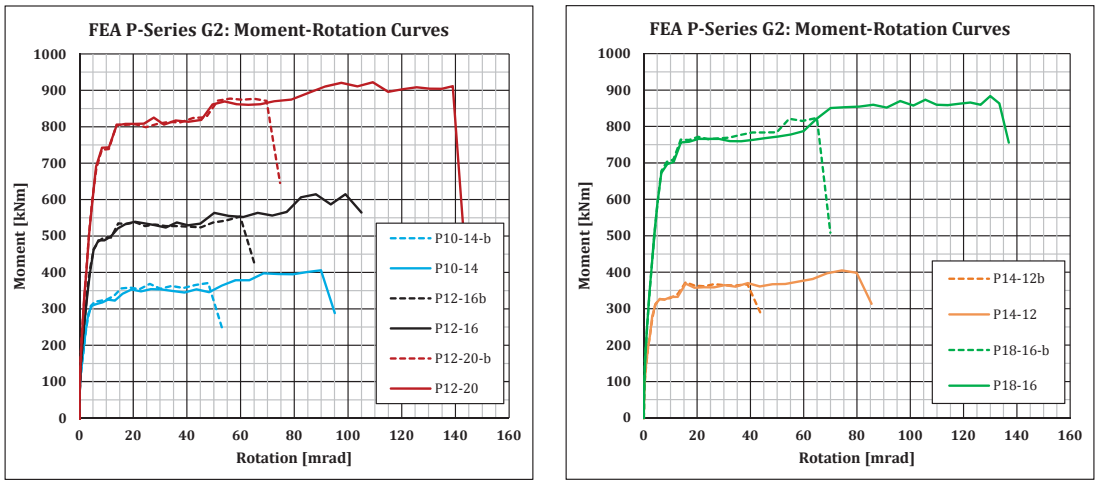

Figure 5.19: Numerical moment-rotation curves for group G2

5.6 Summary

An FE model using the software Abaqus was developed in the present work in order to assess the response of steel and composite joints. The experimental investigations described in Chapter 3 were used to validate this model. Close agreement between experimental and FEA results was obtained for the moment-rotation curves. The main joint properties (stiffness, resistance and rotation capacity) were well predicted by the numerical simulations. Similarity in force-displacement could also be observed. Besides, the concrete crack pattern was well reproduced by the numerical simulations providing similarity with the experimental results.

This validated FE model was used to predict the rotation capacity of the experimental tests, that have not been performed until failure. It was observed that for large reinforcement ratios, it is preferable to associate the failure mode of the bolt-rows to the yielding of the endplate without bolt failure (mode 1 in T-stub model of EN 1993-1-8 (2005)). This condition ensures that the rotation capacity is defined by the failure of the longitudinal reinforcement. Moreover, the influence of concrete encasement on the behaviour of the steel joint was investigated using the numerical model. It was concluded that the concrete encasement has little effect on the stiffness, resistance and ductility of the steel joint.

The objective of developing a numerical model to predict the behaviour of composite joints was accomplished and further parametric studies on the reinforcement layout and reinforcement properties were performed. It was found that the rebar diameter, reinforcement ratio and ultimate strain capacity of the reinforcement are parameters, which must be considered in the calculation of the rotation capacity.

6 Analytical assessment of the structural properties of composite joints

6.1 Introduction

The behaviour of composite joints can be assessed with the following approaches:

- experimental approach (cf. Chapter 4)
- numerical approach (cf. Chapter 5)
- analytical approach

From these three approaches, the **experimental** one is the most realistic one because the behaviour of composite joints is simulated by means of full-scale tests. This approach constitutes therefore a firm foundation on which research investigations can be based. For this reason, an experimental test campaign was projected in the present research in which seven different composite beam-to-column joints and one steel joint (cf. Chapter 3) were investigated.

In addition to the experimental investigations, a **numerical model** capable of characterising the behaviour of composite joints was developed. To validate this model, a comparison of experimental and numerical results was conducted. In comparison to the experimental approach, the numerical analysis presents the advantage of being less costly and time consuming allowing to simulate a large set of different joint configurations much more efficiently.

However, neither the experimental nor the numerical approach represent practical solutions for every-day-design. In this context, the **analytical approach** appears as the most appropriate tool for practitioners to determine the behaviour of composite joints. The principal objective of the present chapter is therefore to elaborate an analytical procedure to determine the **rotation capacity** of composite joints. This objective emerged from the lack of analytical guidance in EN 1994-1-1 (2004), where a calculation method is only provided for the stiffness and the resistance of composite joints. In this context, an additional objective of the present work is to verify the suitability of this calculation method provided by Eurocode for stiffness and resistance.

In order to achieve these objectives, the present chapter is organised in three Sections. **Firstly**, the theoretical background of the analytical method provided in Eurocode is presented. **Secondly**, the accuracy of this analytical solution is verified for the stiffness and the resistance based on the experiments performed within this research. The analytical calculations are done with the actual strengths of materials (cf. chapter 3.5) with partial safety factors equal to unity. The accuracy is verified by comparing the analytical results with the experimental ones. Congruent results prove the suitability of the proposed method, while for divergent results an adaptation of the analytical model is proposed on the basis of experimental observations. **Thirdly**, a new formula to predict the rotation capacity of composite joints is derived from the experiments performed. This new calculation method is then used to predict the rotation

capacities of joint configurations tested in previous research and numerical simulations.

It must be stated that the aim of present Section is not to elaborate an analytical expression reproducing the full shape of the moment-rotation curves. The aim is to provide a method, which predicts the three main structural properties of composite joints. These properties can be retrieved from the moment-rotation response of the joints.

In fact, the analysis of the experimental investigations has shown that the joint response can be subdivided into two stages. The first stage is characterised by an initial linear-elastic response and is defined by the rotational **joint stiffness** S_j. In the second stage, the behaviour is characterised by a plastic response. In this stage, the ultimate **bending resistance** M_u of the joint is reached. This stage is also characterised by the **rotation capacity of the joint** Φ_u. The precise analytical assessment of these three joint properties is therefore sufficient to describe the overall joint's behaviour.

6.2 Component approach

6.2.1 Introduction

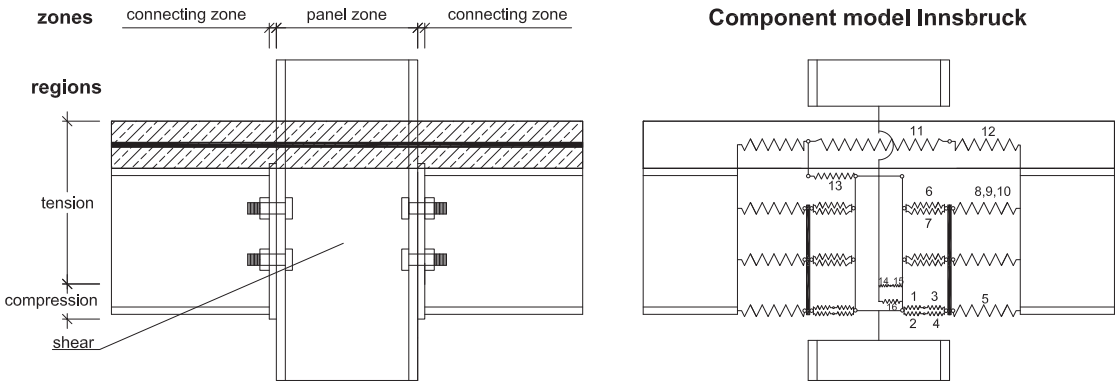

Figure 6.1: Nodal subdivision and refined component model (Huber, 2000)

The elaboration of analytical expressions for the joint's characteristics was subjected to different approaches in the past. In the very first attempts, the idea was to develop an analytical method on the basis of full-scale joints. Due to the multitude of influencing parameters within the joint area this approach was doomed to fail (Huber, 2000). Consequently, a second approach based on the decomposition of the full joint into its constitutive components was developed. In this approach, it was opted to split the global joint system into its basic subsystems, commonly called **joint components**. The idea was to reduce the complexity of the overall joint to the level of its basic components. Instead of testing the joint as a whole, the different joint components were tested in isolation in cheaper testing configurations. The purpose of this component tests was to extract the non-linear behaviour of the individual components. The general procedure of this analytical approach is subdivided into three steps:

- component identification:
  The decomposition of the complex joint into logical parts/components must account for all sources of deformations. Figure 6.1 presents the nodal subdivision of a composite joint. In horizontal direction, the joint is divided into two **zones**: the panel zone and the

connecting zone, whereas in vertical direction three different **regions** are distinguished according to the nature of the inner forces in the components: compression, tension or shear region. The first step consists therefore in identifying the components participating in the load transfer mechanism between the connecting parts. These components are then modelled as translational springs in the spring model depicted in Figure 6.1.

- component characterisation:
  Once all the contributing components are defined, their individual force-deformation responses are determined by means of component tests, finite element simulations or analytical models.
- component assembly:
  The last step consists in the appropriate assembly of the individual translational component springs into an overall rotational spring, characterising the moment-rotation behaviour of the whole joint. This assembly procedure is based on equilibrium and compatibility conditions.

The aforementioned analytical procedure was developed at the University of Innsbruck in collaboration with other research centres and is nowadays widely recognised as the Innsbruck component model. Due to the non-linear force-deformation curves of the individual components and the complex interplay of the several components, the general solution for the non-linear moment-rotation curve can only be gained by an iterative procedure (Huber, 2000). This iterative process raises difficulties in the application of this method for practitioners. Conscious of this hurdle, a simplified component model (without iteration processes) was introduced in the Eurocodes. The difference resides in the missing separation between panel and connecting zone in the Eurocode component model (cf. Figure 6.2), which may lead to a non-straight deformation of the column front. This simplification lies, however, in contradiction with existing test experiences, for which the centre line of the column front always remained plane (Huber, 2000). In addition, Eurocode allows for two levels of precision since the full shape of the resulting $M - \Phi$ curves can be simplified to bi- or trilinear curves. The aim of the present work is therefore not to predict the full non-linear moment-rotation curve of a composite joint but to determine instead the key properties characterising composite joints. For this reason, the following considerations are based on the simplified version of the component model as presented in Eurocode.

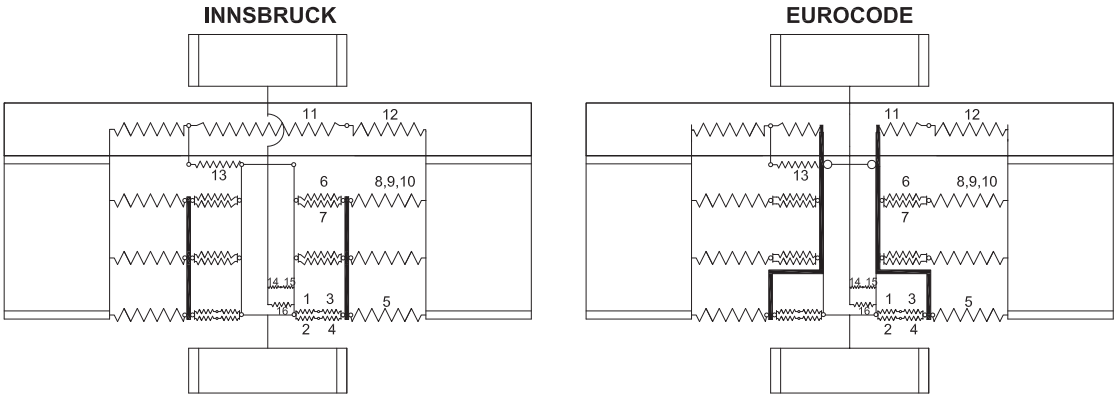

Figure 6.2: Comparison between Innsbruck and Eurocode component model (Huber, 2000)

6.2.2 Component identification

The first step in the application of the component method consists in the identification of the basic components, which contribute to the overall joint behaviour. A macroscopic inspection of the complex finite joint is necessary. The decomposition of the joint into its basic components is a crucial part of the analytical procedure. In Table 6.1 all the potential joint components are enumerated for a beam-to-column endplate connection. Their respective positions within the spring model can be found in Figure 6.2.

Table 6.1: Basic joint components

spring no.	basic component	joint zone	joint region
1	interior steel web panel	panel	compression
2	concrete encasement	panel	compression
3	exterior steel web panel	panel	compression
4	effect of concrete encasement on exterior spring	panel	compression
5	beam flange, contact plate, end plate	connecting	compression
6	steel web panel	panel	tension
7	stiffener in tension	panel	tension
8	column flange in bending	connecting	tension
9	end plate in bending, beam web in tension	connecting	tension
10	bolts in tension	connecting	tension
11	reinforcement in tension	panel	tension
12	slip of composite beam	connecting	tension
13	redirection of unbalanced forces	panel	tension
14	steel web panel in shear	panel	shear
15	steel web panel in bending	panel	shear
16	concrete encasement in shear	panel	shear

6.2.3 Component characterisation

The second step of the analytical method consists in the determination of the non-linear force-deformation curve of each basic component modelled as translational spring. Even though the most accurate way of component characterisation would be to define the whole $F - w$ curve, the most practical way, according to the philosophy adopted in Eurocode, is to linearize the curve for the considered joint property. In this sense, the elastic range of the $F - w$ curve is defined by the initial translational stiffness of the spring component and the plastic range by its resistance and ductility. These three main characteristics of the translational spring are specified in Sections 6.3, 6.4 and 6.5 respectively for the stiffness, resistance and ductility of the components.

6.2.4 Component assembly

The third and last step of the component method is the so-called assembly procedure. This procedure can be subdivided into the following sub-steps:

- Combination of basic components into translational spring groups:
  The basic components, previously identified, are assembled into groups of translational springs. In other words, springs in direct interplay are collected to equivalent

translational springs. The **grouping of springs** is not arbitrary and is subjected to well-defined rules, depending whether the springs are acting parallel or serial. For **parallel springs**, the $F - w$ curves of the individual springs are superposed in vertical direction. Hence, the resistance and the stiffness of the equivalent spring is equal to the sum of these properties in the individual springs. The deformation capacity of the parallel springs is however limited to the minimum deformation capacity of the contributing components. In contrast, for **serial springs** the $F - w$ curves of the individual springs are superposed in horizontal direction. In terms of ductility, the deformation capacity of the equivalent spring is equal to the sum of the individual deformation capacities. For the resistance however, the weaker component is defining the resistance of the group, whereas the stiffness is smaller than the minimum of the individual components. These assembly principles are summarised in Figure 6.3.

- Forming of rotational spring for the joint:

  The second step of the assembly procedure is to transform the equivalent translational springs into rotational springs based on geometric considerations. These are then finally assembled to one single rotational spring in a process fulfilling equilibrium and compatibility conditions. The so obtained rotational spring is then the final product of the analytical component method.

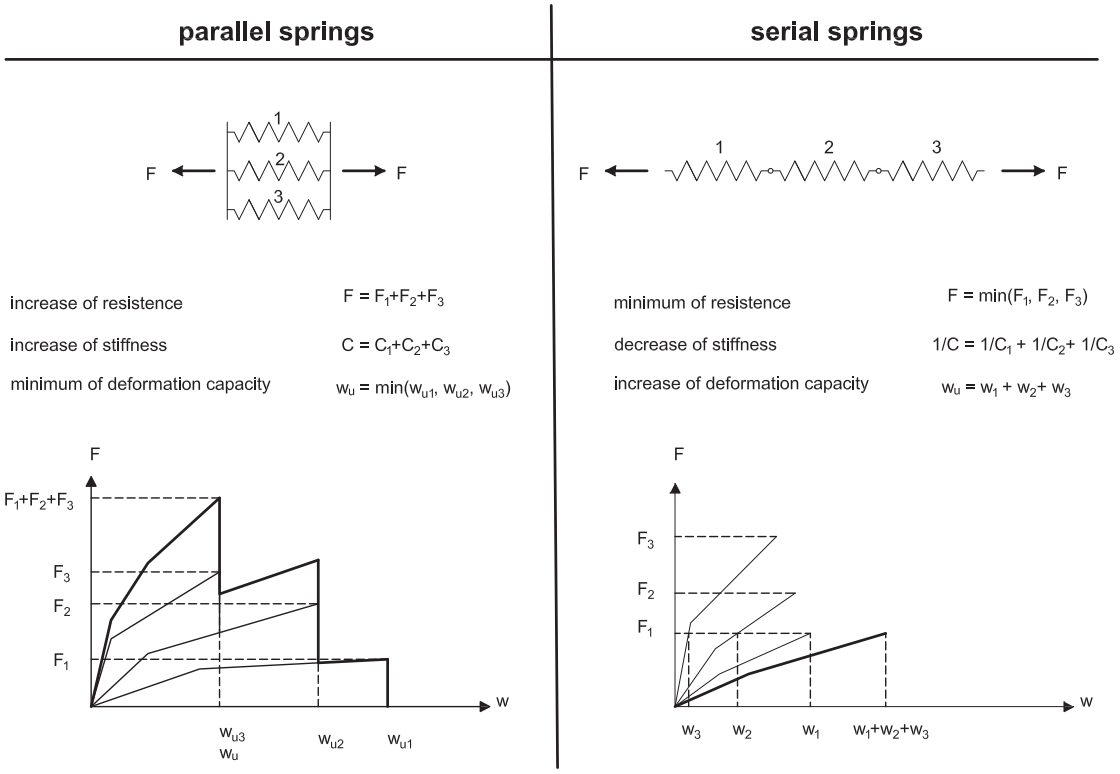

Figure 6.3: Assembly of parallel and serial springs (Huber, 2000)

6.3 Joint stiffness

6.3.1 Eurocode

According to the component method, the initial stiffness of a joint $S_{j,ini}$ is derived from the elastic stiffness of its constitutive components. In the elastic range, the force-deformation curve $F_i - w_i$ of a spring "i" obeys the well-known Hook's law and is therefore mainly characterised by its stiffness c_i. However, EN 1993-1-8 (2005) and EN 1994-1-1 (2004) do not provide the spring stiffness c_i of a component "i" as such. Instead, the latter is reformulated over the steel young modulus E_s to a stiffness coefficient k_i according to equation (6.1).

$$F_i = c_i \cdot w_i = E_s \cdot k_i \cdot w_i \tag{6.1}$$

Once the active components are identified and their stiffness coefficients defined, the different components can be assembled according to the assembling rules exposed in Figure 6.3. By means of this assembly procedure, the refined component model of Eurocode is reduced to a much simpler model as represented in Figure 6.4.

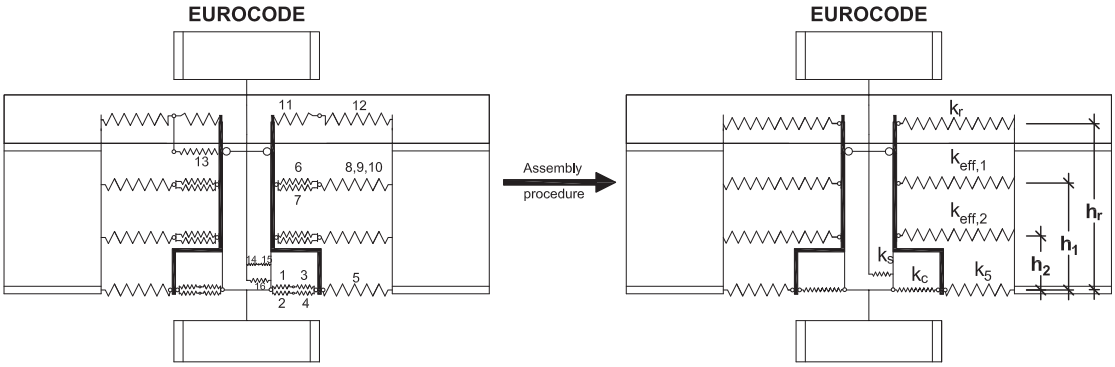

Figure 6.4: Eurocode component model after assembly procedure

The analytical description of the individual stiffness coefficients of all the components listed in Table 6.1 is beyond the scope of the present work. Reference is made to EN 1993-1-8 (2005), Table 6.11 and EN 1994-1-1 (2004), Annex A, where analytical formulas for these components are provided.

According to EN 1994-1-1 (2004), the reinforced concrete slab can be treated as a bolt-row. By assembling the reinforcement/bolt rows to an equivalent spring k_{eq} acting at an equivalent lever arm z_{eq}, the simplified component model of Figure 6.4 can be further simplified to the final model shown in Figure 6.5. Assuming a **linear deformation shape** of the joint, EN 1993-1-8 (2005) provides the following formula to determine the location z_{eq} and the stiffness coefficient k_{eq} of the equivalent spring:

$$z_{eq} = \frac{\sum_j k_{eff,j} \cdot h_j^2}{\sum_j k_{eff,j} \cdot h_j} \tag{6.2}$$

$$k_{eq} = \frac{\sum_j k_{eff,j} \cdot h_j}{z_{eq}} \tag{6.3}$$

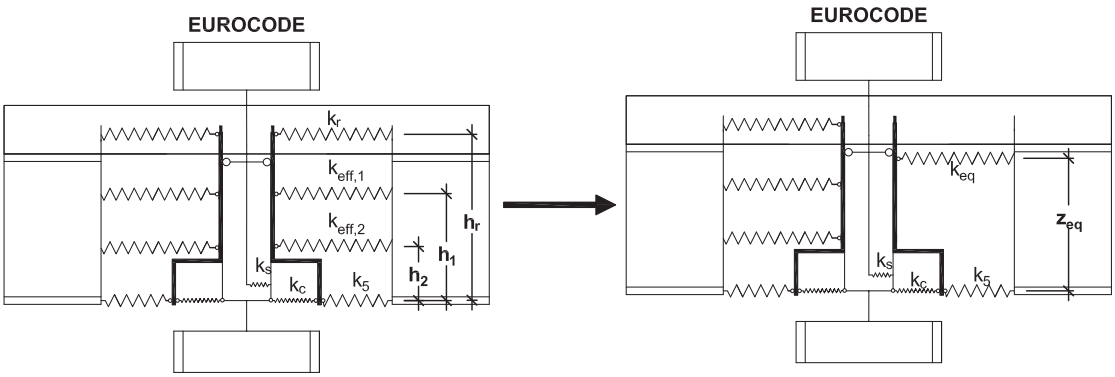

Figure 6.5: Final component model

The analytical formula provided by EN 1993-1-8 (2005) for the joint stiffness has been derived from the model illustrated in Figure 6.5. For equilibrium reasons, the springs in the tension and compression regions must be subjected to the same force F. Thus, the joint bending moment M_j results to $F \cdot z_{eq}$. Since a linear deformation shape is assumed in the joint, the joint rotation Φ_j is obtained by dividing the sum of the deformations in each spring $\sum_i w_i$ by the equivalent lever arm z_{eq}. The initial stiffness S_j is derived to:

$$S_j = \frac{M_j}{\Phi_j} = \frac{F \cdot z_{eq}}{\frac{\sum_i w_i}{z_{eq}}}$$

$$\overset{Eq.(6.1)}{\Longrightarrow} S_j = \frac{F \cdot z_{eq}^2}{\frac{F}{E_s} \cdot \sum_i \frac{1}{k_i}} = \frac{E_s \cdot z_{eq}^2}{\sum_i \frac{1}{k_i}} \tag{6.4}$$

The final expression for the initial joint stiffness is obtained in equation (6.4). It corresponds to the formula given in EN 1993-1-8 (2005). In order to evaluate the stiffness of the composite joints tested in series B and E with this equation, it must be first identified which joint components are effectively active. The composite joints were tested under symmetric loading conditions leading to fully balanced hogging moments. The translational spring k_s considering the shear deformation in the panel zone can therefore be ignored. Due to the presence of a stiffener in the compression region of the column, the spring k_c can also be assumed infinitely stiff. The same assumption can be made for the spring k_5 representing the lower beam flange in the connecting zone, according to EN 1993-1-8 (2005). For composite slim-floor beams, this assumption is even more justified because of the additional welded bottom plate in the lower beam flange. Gathering all these assumptions, the initial stiffness of composite joints can be given as:

$$S_j = \frac{E_s \cdot z_{eq}^2}{\sum_i \frac{1}{k_i}} = \frac{E_s \cdot z_{eq}^2}{\frac{1}{k_{eq}} + \cancel{\frac{1}{k_5}}^{0} + \cancel{\frac{1}{k_c}}^{0} + \cancel{\frac{1}{k_s}}^{0}} = E_s \cdot z_{eq}^2 \cdot k_{eq} \tag{6.5}$$

Introducing successively equations (6.3) and (6.2) in equation (6.5), the initial joint stiffness is formulated in function of the individual stiffness coefficients of each bolt/reinforcement row:

$$
\begin{aligned}
S_j =& E_s \cdot z_{eq}^2 \cdot k_{eq} \\
\overset{eq.(6.3)}{=\!=}& E_s \cdot z_{eq}^2 \cdot \frac{\sum_j k_{eff,j} \cdot h_j}{z_{eq}} = E_s \cdot z_{eq} \cdot \sum_j k_{eff,j} \cdot h_j \\
\overset{eq.(6.2)}{=\!=}& E_s \cdot \frac{\sum_j k_{eff,j} \cdot h_j^2}{\sum_j k_{eff,j} \cdot h_j} \cdot \sum_j k_{eff,j} \cdot h_j \\
\Longrightarrow S_j =& E_s \cdot \sum_j k_{eff,j} \cdot h_j^2
\end{aligned} \tag{6.6}
$$

From equation (6.6), it can be concluded that the analytical calculation method presented in Eurocode presumes that the rotational stiffness of the joints tested in this work is equal to the sum of the individual rotational stiffnesses of each component in the tension region. The latter can therefore be interpreted as parallel acting rotational springs.

For test series B, the only component effectively transmitting tension forces is the reinforced concrete slab. Thus, the initial joint stiffness is only defined by the component associated to the reinforcement (cf. Table 6.1). For test series C, the joint stiffness is only characterised by the bolt-rows in tension, while in test series E, the joint stiffness results from the sum of the series B and series E, according to equation (6.6).

$$S_{j,B} = E_s \cdot k_r \cdot h_r^2 \tag{6.7a}$$

$$S_{j,C} = E_s \cdot (k_{eff,1} \cdot h_1^2 + k_{eff,2} \cdot h_2^2) \tag{6.7b}$$

$$S_{j,E} = S_{j,B} + S_{j,C} = E_s \cdot (k_r \cdot h_r^2 + k_{eff,1} \cdot h_1^2 + k_{eff,2} \cdot h_2^2) \tag{6.7c}$$

In order to evaluate these formulae, the equivalent spring coefficient $k_{eff,j}$ associated to each bolt-row "j" can be determined from EN 1993-1-8, Table 6.11 in combination with the principles of parallel and serial springs. The stiffness coefficient k_r corresponds to the equivalent spring acting at the level of the reinforcement and combines the springs no. 11, 12 and 13 as represented in Figure 6.2. In the present case, the joints are under balanced loading such that spring no. 13 can be neglected. As explained in Section 3.3, the occurrence of slip in steel-concrete interface of the composite beam was prevented by a stiffener in the beam. Since the slip measurements confirmed the negligible slip, its effect can be ignored in the evaluation of the stiffness. The stiffness coefficient of spring no.12 is therefore assumed infinitely large. Hence, the only mechanical flexibility in the reinforced slab component results from the elongation capacity of the reinforcement bars embedded in concrete, which is considered in spring no.11 (cf. Table 6.1).

$$\rightarrow k_r = k_{11} \tag{6.8}$$

In EN 1994-1-1 (2004), the stiffness coefficient of the embedded reinforcement neglects the participation of concrete in tension. Its value can be derived from the model of axially loaded steel reinforcement bar of cross sectional area A_s and length L_j. It is assumed that this bar is subjected to the same tension force F on each side of the bar. Owing to the initial linear-elastic behaviour of steel, the elongation Δ of the bar follows to:

$$\Delta = \varepsilon \cdot L_j = \frac{F}{E_s \cdot A_s} \cdot L_j \Longrightarrow F = \frac{E_s \cdot A_s}{L_j} \cdot \Delta \tag{6.9}$$

Applying Hook's law $F = c_{11} \cdot \Delta$ and equation (6.1), the stiffness coefficient k_{11} of component no.11 becomes:

$$k_{11} = \frac{A_s}{L_j} \tag{6.10}$$

In EN 1994-1-1 (2004) Table A.1, it is suggested to take the length L_j as half the column depth $h_c/2$ for the particular case of double-sided joints with balanced hogging moments:

$$k_{11} = \frac{A_s}{h_c/2} \tag{6.11}$$

In order to verify the accuracy of the method provided by Eurocode, the latter was applied to predict the stiffness of the joints tested in the present research. Figure 6.6 compares the calculated stiffnesses $S_{j,EC}$ to the experimental values $S_{j,Test}$. This comparison shows that the analytical expression given in Eurocode **overestimates the stiffness** of the composite joints tested in the present research. For test B32, for instance, the analytical value is almost 7 times bigger than the measured stiffness in experiments. On the contrary for the steel joint C14, the analytical procedure proposed by EN 1993-1-8 (2005) provides a satisfactory concordance with the experimental results. This indicates that the discrepancies obtained for composite joints can only emanate from the inaccurate assessment of the stiffness coefficient of the reinforcement component k_{11}. It should be noted that other researchers similarly concluded that the above model overestimates the stiffness of composite joints (cf. Anderson and Najafi (1994), Bode and Kronenberger (1998), Malaska (2000) and Gil and Bayo (2008a)).

Considering equation (6.10), an overestimation of the stiffness coefficient can either arise from an overestimated section of the reinforcement bar A_s or from an underestimated effective joint length L_j. Since th global section of reinforcement is defined by the number of longitudinal rebars, the only questionable quantity is the effective joint length, which is roughly given to half the column depth in EN 1994-1-1 (double-sided and symmetric joints). In Section 4.5, it was shown that this simplification does not correspond to the observed behaviour in the experimental tests, since the observed effective joint length was always bigger than half the column depth.

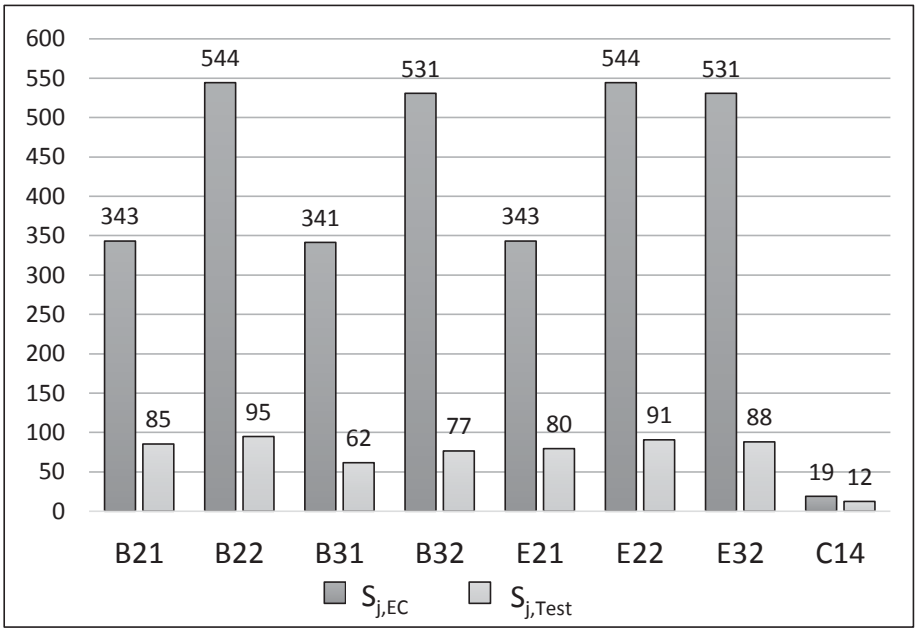

Figure 6.6: Calculated $S_{j,EC}$ and measured joint stiffness $S_{j,Test}$

6.3.2 Effective joint length

In the previous Section, it was shown that effective joint length represents an essential quantity for the correct assessment of the joint stiffness. The aim of the present chapter is to present the different approaches found in literature to determine this effective joint length L_j.

Anderson and Najafi (1994), for example, proposed to increase the effective joint length up to the first row of shear connectors, in case the flexibility of the latter is taken into account:

$$L_j = \frac{h_c}{2} + p_0 \tag{6.12}$$

Ren (1995) derived a semi-empirical formula taking into account the cohesive behaviour between concrete and steel reinforcement (factor $\eta = 0.35$), the spacing between the reinforcement bars (factor s) and the bending of the concrete slab (factor k):

$$L_j = 2 \cdot \eta \cdot (60 + 1.3 \cdot k \cdot s) \tag{6.13}$$

Ahmed and Nethercot (1997) concluded that a better agreement between the analytical and the experimental joint stiffness is achieved when the effective joint length is increased up to the second row of shear connectors:

$$L_j = \frac{h_c}{2} + p_0 + p_1 \tag{6.14}$$

More recently in 2008, Gil and Bayo performed an extensive parametric study based on FE simulations of composite joints with Abaqus. A total of 16 different composite joints with variable load conditions, steel profiles, bolts and reinforcement ratios were simulated. The purpose of this study was to identify the influence of these parameters on the effective joint length (Gil and Bayo, 2008a). From this analysis it was concluded that the effective length is a function of the column's height h_c and of the distance between the centre of the beam bottom flange to the centroid of the reinforcement h_r:

$$L_j = \frac{h_c}{2} + 0.8 \cdot h_r \tag{6.15}$$

The number of existing approaches to determine the effective joint length L_j proves that it is a key aspect in the analytical assessment of the structural properties of composite joints. From the experimental analysis described in Section 4.5, the following findings have been deducted:

- L_j is not dependant on the loading stage $L_{j,el} = L_{j,pl} = L_j$
- L_j is directly proportional to the diameter of the longitudinal rebars $L_j \sim \varnothing$

Implementing these findings in the analytical expression for the joint stiffness provided by the Eurocode, it can be concluded that the stiffness is inversely proportional to the rebar diameter from equation (6.16). In other words, small rebar diameters induce large joint stiffnesses. The interesting fact about this finding is that it corroborates the conclusion made on the basis of the measured stiffnesses (cf. Section 4.2.2). These findings constitute therefore a coherent explanation for the experimental measurements.

$$\left.\begin{array}{l} S_{j,B} = E_s \cdot h_r^2 \cdot \frac{A_s}{L_j} \\ L_j \sim \varnothing \\ \rho = \frac{A_s}{A_c} \end{array}\right\} \Longrightarrow S_{j,B} \sim E_s \cdot h_r^2 \cdot \frac{\rho}{\varnothing} \tag{6.16}$$

6.3.3 Cracking of concrete

Test observations have shown that the stiffness of composite joints is influenced by the rebar diameter and the reinforcement ratio. The correlation found between the crack pattern of the reinforced concrete slab and the joint stiffness, presented in Section 4.5, was of particular interest since it emerged that the stiffness of composite joints is strongly correlated to the cracking mechanism occurring in the slab. This correlation is not included in EN 1994-1-1 (2004), explaining the large discrepancies between analytical and experimental results. At the light of this, a new formula for the determination of the stiffness coefficient k_{11} of the reinforced concrete component in tension is provided in the present research. The elaboration of the new stiffness coefficient is based on established concrete cracking theories and experimental observations. A short introduction into the background of concrete cracking theory is therefore firstly presented in this Section.

In principle, the cracking vulnerability of concrete structures is related to its low tensile strength. Due to this vulnerability, steel reinforcement bars are embedded in concrete in order to increase the resistance, stiffness and ductility of concrete members subjected to tensile stresses. Moreover, an appropriate choice of reinforcement bars allows to control the crack width, which constitutes an important issue in serviceability limit state.

The bond behaviour between the ribbed reinforcement bars and the surrounding concrete constitutes a major factor influencing the crack pattern of concrete members. The influence of the bond strength is shown on the example of Figure 6.7 representing a reinforced concrete member subjected to a tension force F.

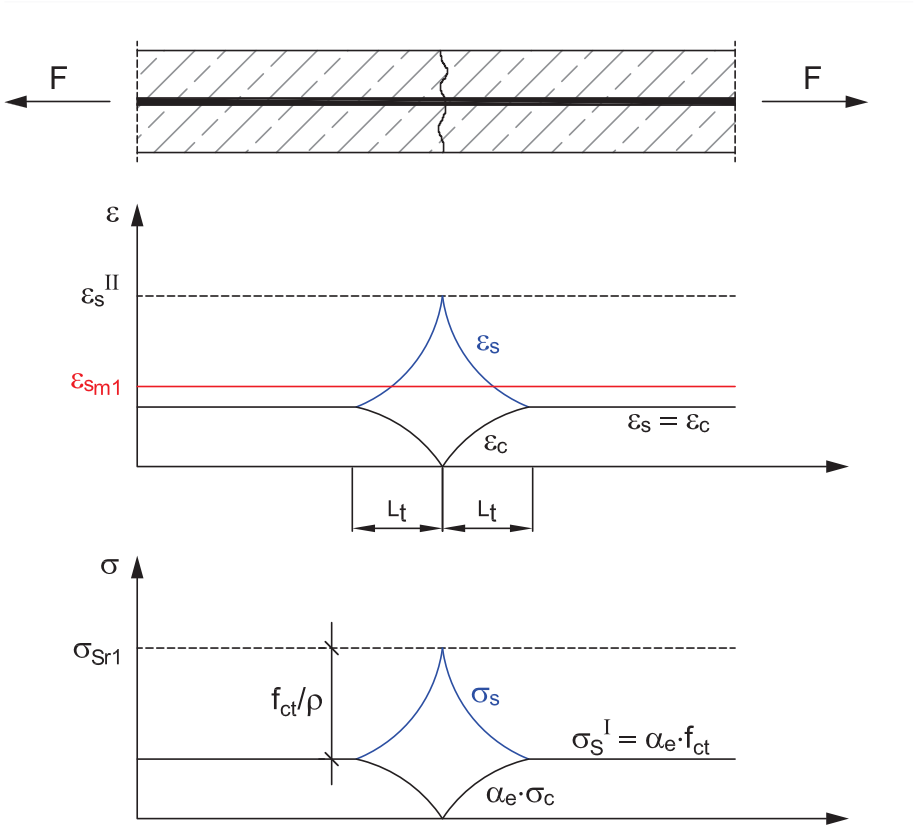

Figure 6.7: Definition of transmission length L_t

At low tensile forces, no cracks occur in the composite member such that full composite action between both materials can be assumed. At this stage, the reinforcing steel bars and concrete share the same strain ε. Thus, the total force F is proportionally distributed over both components according to their stiffnesses. At a given force F_{cr} the tensile capacity of concrete is fully exploited; the logical consequence is the occurrence of a first crack in the reinforced concrete member. It is not possible to determine the precise position of this crack because of the large scattering of concrete tensile strength f_{ct}. In reality, it will occur at the weakest point of the member. At this cracking point the part of the force that was previously in the concrete member is released and relocated to the reinforcement bar, inducing a stress increase $\Delta\sigma_{sr}$ in the reinforcement. The total force F_{cr} is therefore carried solely by the reinforcement in this precise point. The magnitude of the stress jump in the reinforcement $\Delta\sigma_{sr}$ depends on the amount of reinforcement in the concrete member. The lower the reinforcement ratio, the bigger is the stress increment in the reinforcement. The development of a further crack requires that concrete reaches again its tensile strength at a certain distance L_t, commonly called **transmission length**. This is only possible if tensile stresses can be transferred again from the reinforcement to the surrounding concrete over bond stresses. Concrete crack pattern and bond behaviour are thus directly related.

Many theories were developed to accurately quantify the bond strength τ between the ribbed reinforcement and concrete. Most of them presuppose a slip dependant bond strength. Even though in reality the bond properties are not constant over the transmission length L_t, an average bond strength τ_{bm} is assumed over this length according to Model Code 2010 (Comite Euro-International du Béton, 2010) and EN 1992-1-1 (2004). Per definition, at the end of the transmission length the mean concrete tensile strength f_{ctm} is attained. The corresponding force must be then equal to the bond force transmitted over the circumferential area of the reinforcement bar:

$$\begin{aligned} &F_{bond} = F_{concrete} \\ &\tau_{bm} \cdot \pi \cdot \varnothing \cdot L_t = f_{ctm} \cdot A_c \\ &\implies L_t = \frac{f_{ctm} \cdot A_c}{\tau_{bm} \cdot \pi \cdot \varnothing} \end{aligned} \tag{6.17}$$

Introducing the reinforcement area $A_s = \pi \cdot \varnothing^2/4$ and the definition of the reinforcement ratio $\rho = A_s/A_c$, the final expression for the transmission length becomes:

$$L_t = \frac{f_{ctm} \cdot \varnothing}{4 \cdot \tau_{bm} \cdot \rho} \tag{6.18}$$

Kreller (1989) observed that the spacing between two consecutive cracks a_{cr} scatters between one and two times the transmission length. This range is confirmed by other experimental investigations, e.g. (Elz, 2000).

$$1 \cdot L_t \leq a_{cr} \leq 2 \cdot L_t \tag{6.19}$$

In the framework of the present research, the maximal value in this range is assumed as final crack spacing. It represents nowadays a widely accepted value.

$$a_{cr} = 2 \cdot L_t = \frac{f_{ctm} \cdot \varnothing}{2 \cdot \tau_{bm} \cdot \rho} \tag{6.20}$$

Hereafter, the parameters involved in the final expression for the transmission length L_t are described individually.

Tensile strength of concrete f_{ctm}:

For a concrete member in pure tension, the mean tensile strength is given by f_{ctm}. In a composite beam under negative bending, however, the concrete slab is additionally stressed in bending. Hanswille (1986) showed that the bending tensile strength $f_{ctm,fl}$ of a concrete member in bending is higher than that of a member purely subjected to tensile forces. The difference between f_{ctm} and $f_{ctm,fl}$ decreases with larger member height (cf. Figure 6.8).

Given the general large scattering of the the concrete tensile strength, the differentiation between f_{ctm} and $f_{ctm,fl}$ is consciously omitted in the following considerations. According to EN 1992-1-1 (2004) the mean tensile strength is calculated in function of the characteristic value of the compressive cylinder strength f_{ck} of concrete to:

$$f_{ctm} = \begin{cases} 0.30 \cdot f_{ck}^{2/3} & \text{for } f_{ck} \leq 50 N/mm^2 \\ 2.12 \cdot ln(1 + (f_{cm}/10)) & \text{for } f_{ck} > 50 N/mm^2 \end{cases} \tag{6.21}$$

$$\text{with: } f_{cm} = f_{ck} + 8 \; [N/mm^2] \tag{6.22}$$

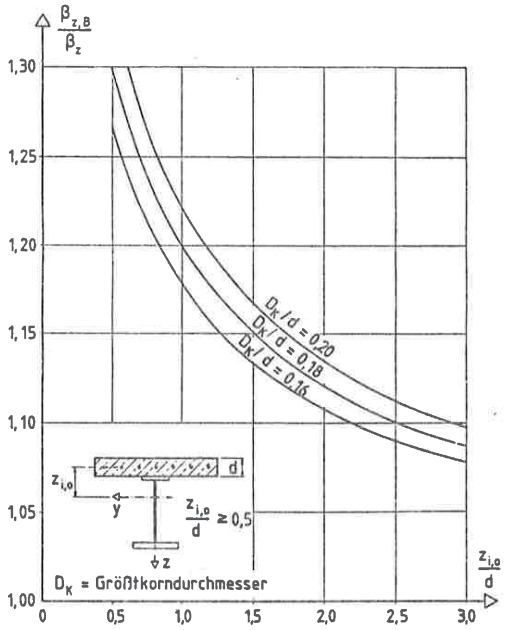

Figure 6.8: Flexural tensile strength of concrete in function of aggregate diameter and cross-section properties (Hanswille, 1986)

Mean bond strength between reinforcement and concrete τ_{bm}:

In (Schober, 1984) a model to characterise the bond behaviour between the reinforcement bar and surrounding concrete was developed. The bond is caused by three effects: the adhesion force between both materials, the friction force due to the surface roughness and the mechanical indentation provided by the reinforcement ribs. Theoretically, the bond strength is a function of the slip between both materials. A differentiation between the crack formation stage and the stabilised cracking stage is suggested in MC 2010 (cf. Figure 6.9).

	Crack formation stage	*Stabilized cracking stage*
Short term, instantaneous loading	$\tau_{bms} = 1.8 \cdot f_{ctm}(t)$ $\beta = 0.6$ $\eta_r = 0$	$\tau_{bms} = 1.8 \cdot f_{ctm}(t)$ $\beta = 0.6$ $\eta_r = 0$
Long term, repeated loading	$\tau_{bms} = 1.35 \cdot f_{ctm}(t)$ $\beta = 0.6$ $\eta_r = 0$	$\tau_{bms} = 1.8 \cdot f_{ctm}(t)$ $\beta = 0.4$ $\eta_r = 1$

Figure 6.9: Mean bond strength acc. to MC 2010 Table 7.6-2 (Comite Euro-International du Béton, 2010)

For the stabilised cracking stage, the Model Code provisions suggest the following mean bond strength τ_{bm}:

$$\tau_{bm} = 1.8 \cdot f_{ctm} \tag{6.23}$$

Alternatively, EN 1992-1-1 (2004) proposes the following formula for good bond conditions and diameter of the reinforcement bars smaller than 32 mm:

$$\tau_{bm} = 2.25 \cdot f_{ctk,0.05} = 1.6 \cdot f_{ctm} \tag{6.24}$$

Diameter of reinforcement bar ⌀:

A smaller diameter of the reinforcement bars induces smaller crack spacing according to equation (6.20). The crack pattern is thus denser and crack widths smaller, justifying the preferable use of smaller rebar diameters to reduce the crack widths. The influence of the reinforcement diameter on the transmission length L_t is shown in Figure 6.14. For the same reinforcement ratio, the transmission length increases with bigger rebar diameter.

Reinforcement ratio ρ_{eff}:

Leonhardt (1978) stated that for the purpose of crack control, it is wrong to arbitrary define the reinforcement ratio as the ratio between reinforcement area and the total concrete area. In view of crack spacing and crack width, the effect of reinforcement is in reality limited to a restricted area around the reinforcing bar, which is directly linked to the bond behaviour and the spatial dispersion of the concrete tensile stresses. According to Leonhardt, only a concrete area $A_{c,eff}$ limited to 7⌀ around the reinforcement participates effectively in the crack distribution. This restricted area is therefore defining the crack pattern of the reinforced concrete slab (cf. Figure 6.10). This proposal was later introduced in the Model Code 1978.

Aware of the importance of this effect for the crack control of reinforced concrete structures, many researchers intensified the investigations on the correct assessment of the effective concrete area. König and Tue (1996) published the background document for EN 1992-1-1 (2004), in which the original mechanical model of $A_{c,eff}$ is presented on the basis of the research conducted by Fischer (1993) and Bergner (1997). The comparison of the crack pattern of thin and large members demonstrated that this effect gains in importance as the thickness of the member increases. In fact, for thin members, the upper and lower reinforcement layers are so close to each other, that at the end of the transmission length L_t, the concrete tensile stresses are homogeneously distributed over the thickness of the member (cf. Figure 6.11). In contrary, for thick members, the reinforcement layers are located

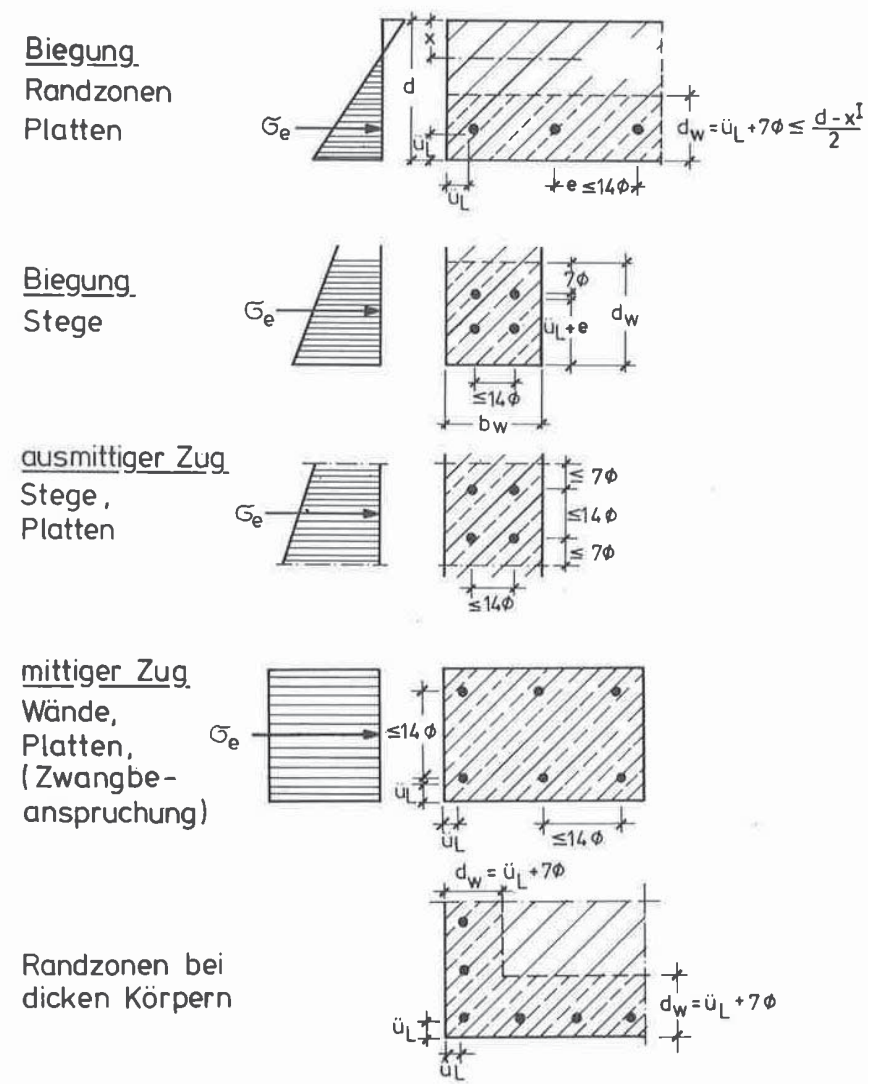

Figure 6.10: Initial proposal for the effective concrete area $A_{c,eff}$ by Leonhardt (1978)

apart. At the end of the transmission length no constant stress distribution is available over the cross-section. Secondary cracks occur at the end of the transmission length within the effective concrete area $A_{c,eff}$ around the reinforcement. It was noted that this effective area is correlated to the spatial dispersion of the concrete tensile stresses (angle of spread of 1:2).

The equation (6.25) for the effective concrete height is given in EN 1992-1-1 (2004) of which an extract is shown in Figure 6.12. This formula is only valid for concentrative reinforcement layers and thin members in bending with $h/(h-d) \leq 10$.

$$h_{c,ef} = min \begin{cases} 2.5 \cdot (h-d) \\ (h-x)/3 \\ h/2 \end{cases} \tag{6.25}$$

For larger member heights in pure tension or bending, König and Tue (1996) provides a more precise formulation for the effective reinforcement area (cf. Figure 6.13). The German national annex of EN 1992-1-1 (2004) only partially includes this formulation.

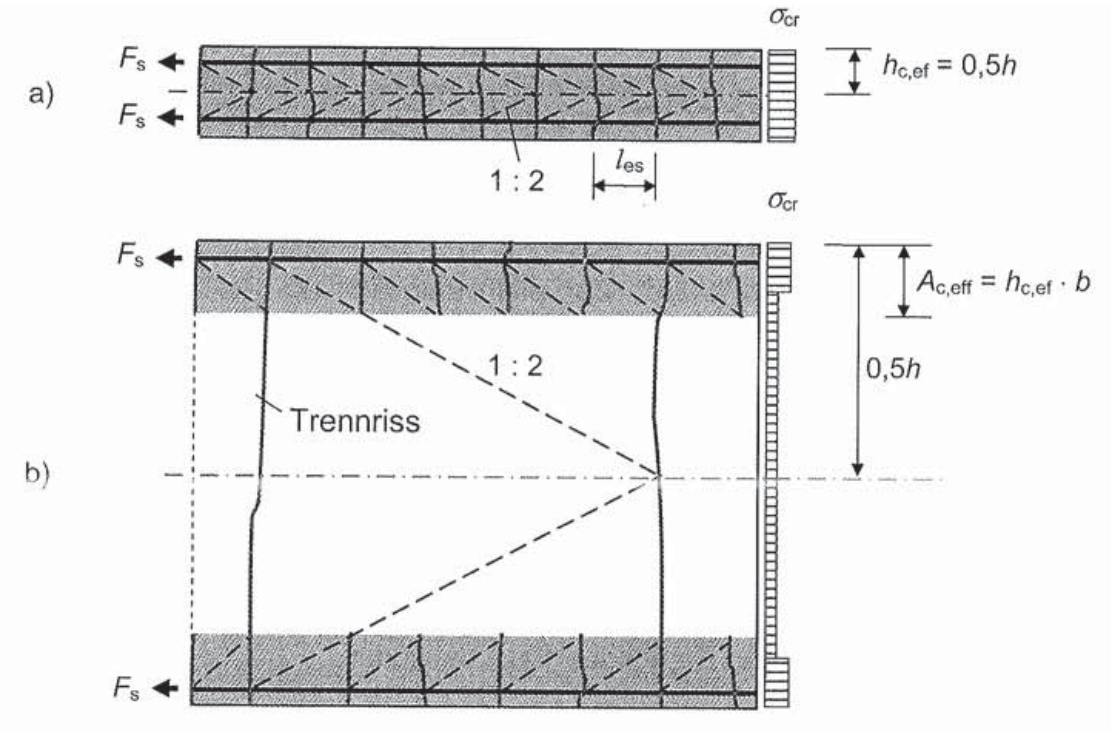

Figure 6.11: Influence of member thickness on $A_{c,eff}$ (König and Tue, 1996)

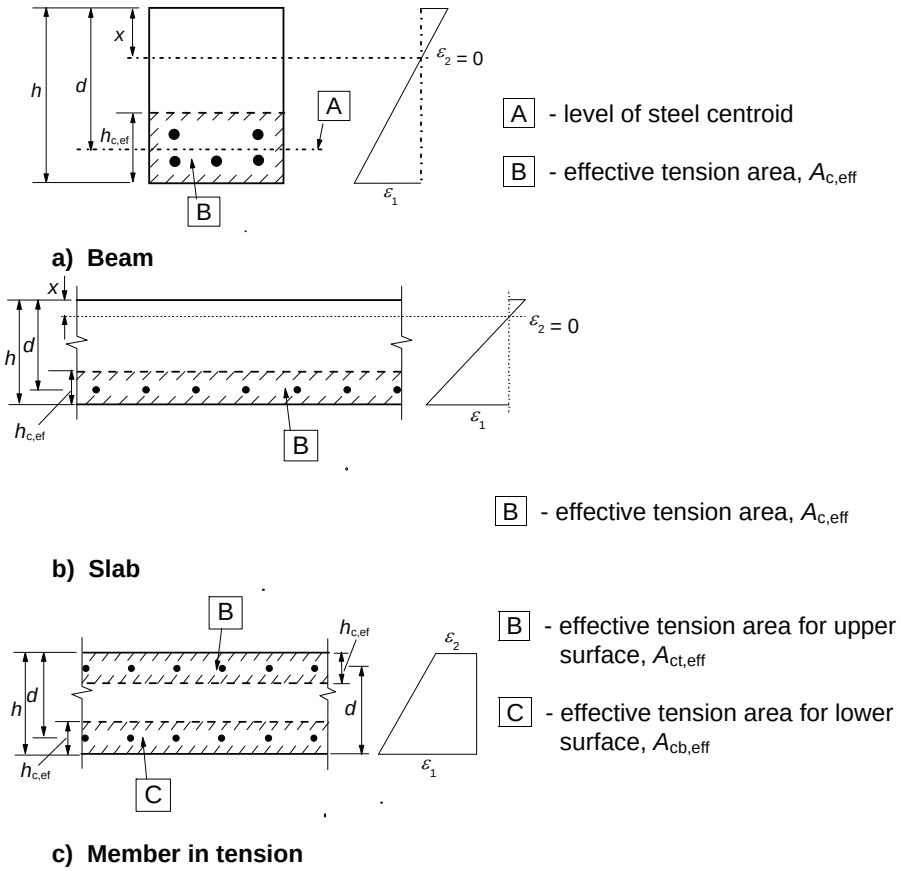

Figure 6.12: Effective tension area of concrete $A_{c,eff}$ EN 1992-1-1 (2004)

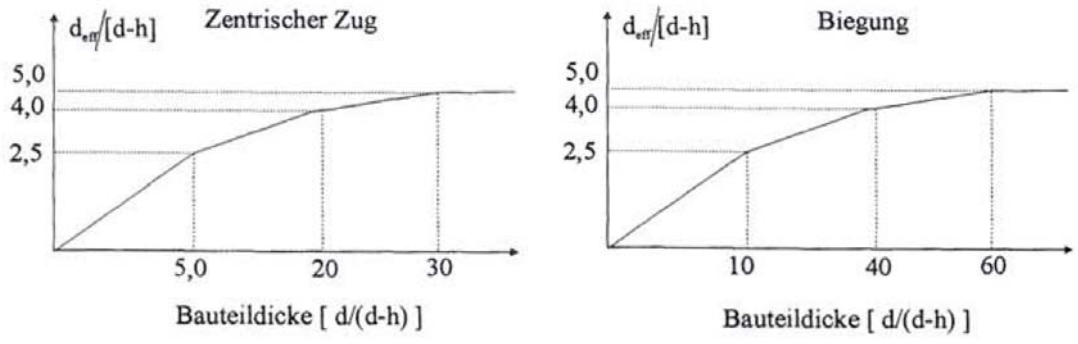

Figure 6.13: Effective height d_{eff} of concrete for pure tension and bending in function of the member height d and static height h (König and Tue, 1996)

The effective reinforcement ratio is defined as:

$$\rho_{eff} = \frac{A_s}{A_{c,eff}} \tag{6.26}$$

The parameters influencing the transmission length L_t were described above. Replacing equation (6.24) in equation (6.18), the transmission length becomes:

$$L_t = \frac{f_{ctm} \cdot \varnothing}{4 \cdot \tau_{bm} \cdot \rho} = \frac{\varnothing}{6.4 \cdot \rho} \tag{6.27}$$

Mathematically seen, the transmission length is independent of the concrete class. In Figure 6.14 a graphical representation of L_t is presented in function of the reinforcement ratio ρ and rebar diameter $\varnothing$.

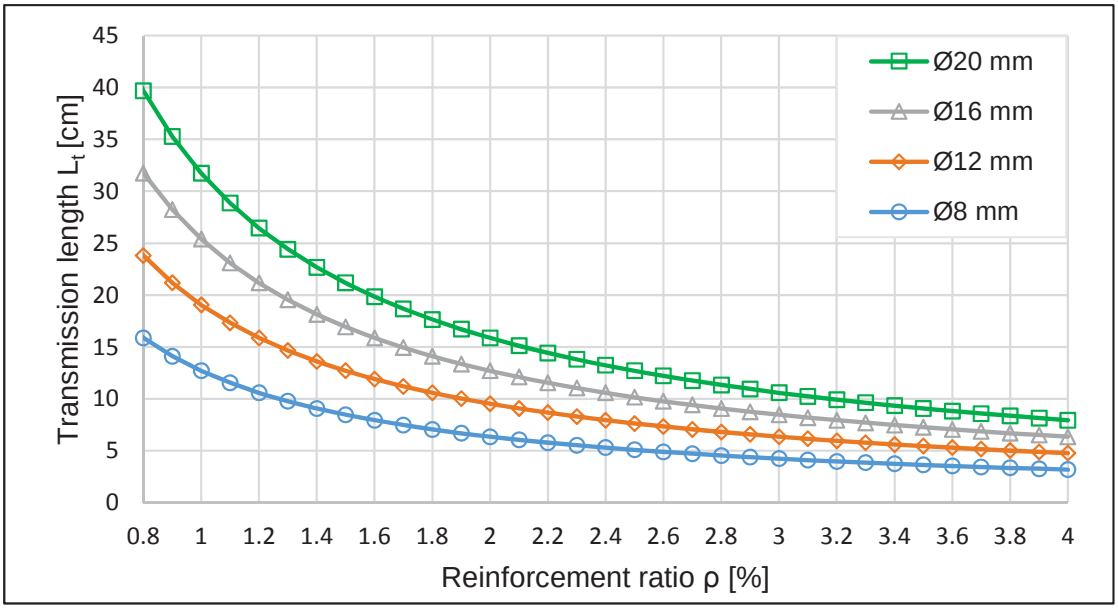

Figure 6.14: Transmission length L_t in function of rebar diameter and reinforcement ratio

6.3.4 Own proposal for the effective joint length of the reinforced concrete component

The observations made in earlier investigations as well as the own observations made during the present laboratory tests permitted to formulate the following analytical expression for the effective joint length of the reinforcement component:

$$L_j = \frac{h_c}{2} + n \cdot a_{cr} \tag{6.28}$$

with:

h_c column height
n factor considering the amount of main cracks
a_{cr} distance between two consecutive cracks

The effective joint length is determined on the basis of experimental evidence and established cracking theory of reinforced concrete members. From the tests performed in the present research, it comes out that the first crack in the reinforced slab always occurs on the level of the column flange. The same observation was made by other researchers Bode and Kronenberger (1998) and Odenbreit (2000). As the readings from the strain measurement on the reinforcement showed (cf. Section 4.5), the effective joint length increases with larger reinforcement ratio ρ. The number of wide cracks depends, therefore, on the effective reinforcement ratio ρ_{eff} of the slab component. In order to take this particular aspect into account, a factor "n" is introduced here. The following values are postulated:

$$n = \begin{cases} 1.5 & 1.0\% \leq \rho_{eff} \leq 1.6\% \\ 2.5 & 1.6\% < \rho_{eff} \leq 1.9\% \\ 3.5 & 1.9\% < \rho_{eff} \leq 2.2\% \\ 4.5 & 2.2\% < \rho_{eff} \leq 2.9\% \\ 5.5 & 2.9\% < \rho_{eff} \leq 3.5\% \end{cases} \tag{6.29}$$

Hence, the stiffness coefficient k_{11} for the reinforced concrete component in a double-sided joint configuration with symmetric hogging moments is defined as:

$$\begin{aligned} k_{11} &= \frac{A_s}{\frac{h_c}{2} + n \cdot a_{cr}} \\ &= \frac{A_s}{\frac{h_c}{2} + n \cdot 2 \cdot \frac{\varnothing}{6.4 \cdot \rho_{eff}}} \end{aligned} \tag{6.30}$$

In combination with the distance between two cracks a_{cr} defined in equation (6.20), the term $n \cdot a_{cr}$ considers the longitudinal extension of the cracked region of the slab. The effect of the rebar diameter $\varnothing$ observed in the experimental tests is included in this definition: the larger the rebar diameter $\varnothing$, the larger is also the distance between two cracks a_{cr} and the longer is consequently the effective joint length L_j according to equation (6.28). An interpretation for the factor "n" is given in more detail in Section 6.5.3. This analytical formula is only applicable within the range of validity specified in Section 6.5.6.

6.3.5 Validation of own proposal

A new analytical formula was proposed in Section 6.3.4 to assess the stiffness coefficient k_{11} representing the reinforced concrete slab. In comparison to the expression provided in EN 1994-1-1 (2004), the new proposal developed in this work includes the influence of concrete cracking in the slab. As such, the new analytical expression is not only a function of the column depth, but depends also on parameters such as longitudinal reinforcement ratio ρ and rebar diameter $\varnothing$.

In order to validate this new proposal, the stiffnesses of the composite joints tested in the present work are evaluated according to this formula and compared to the experimental values. Furthermore, additional experimental test results documented in literature and fitting in a well-defined range of validity (cf. Table 6.2 and Appendix C) are included in the evaluation of this formula. Details on the additional experimental data, such as moment-rotation curves and joint configurations can be found in Appendix C. The **good agreement** between experimental and predicted stiffnesses according to this new proposal is illustrated in Figure 6.15. In relation to EN 1994-1-1 (2004), a significant improvement in the prediction capacity for the joint stiffness is achieved with this proposal (cf. Figure 6.6).

As referred in Section 5.4, the influence of the steelwork connection on the overall stiffness of composite joints might be neglected without loss of accuracy. Thus, only the reinforcement component was considered in the calculated values.

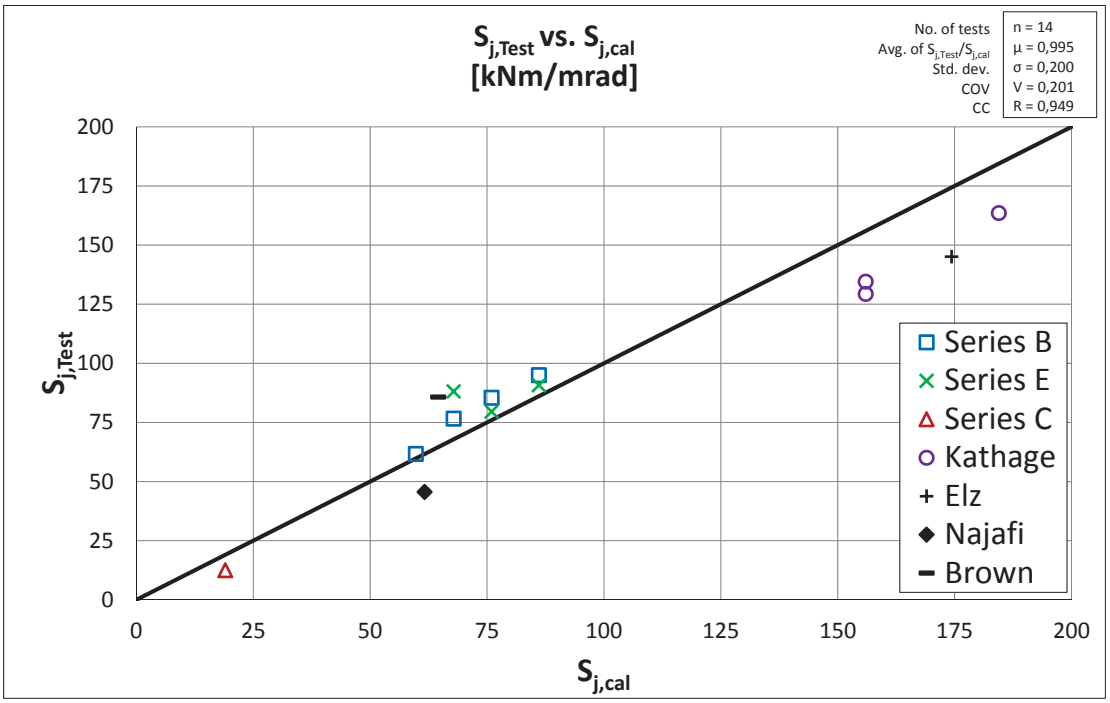

Figure 6.15: Comparison between experimental $S_{j,Test}$ and predicted $S_{j,cal}$ values
Ref.: Series B,C and E (cf. Chapter 4), Kathage (1994), Elz (2000), Najafi (1992) and Brown and Anderson (2001)

6.4 Joint bending resistance

6.4.1 Introduction

The bending resistance of a composite joint is calculated on the basis of the component model described in EN 1993-1-8 (2005) and EN 1994-1-1 (2004). According to (European Convention for Constructional Steelwork, 1999) the following aspects should be considered:

- the internal forces are in equilibrium with the forces applied to the joint
- the design resistance of each component is not exceeded
- the deformation capacity of each component is not exceeded

For the case of a boltless endplate connection, the absence of a steelwork connection leads to a simple distribution of the internal forces: the tension force is transferred at the centroid of the reinforcement and the compression force at the centroid of the beam bottom flange (cf. Figure 6.16). The joint resistance is thus associated to the resistance of the weakest joint component. For test series B for instance, the weakest component is the reinforcement because a stiffener is provided in the column web and the welded bottom plate reinforces the beam bottom flange. The bending resistance of such a type of composite joint can be written as:

$$M_j = min(F_{tr}, F_c) \cdot h_r \tag{6.31}$$

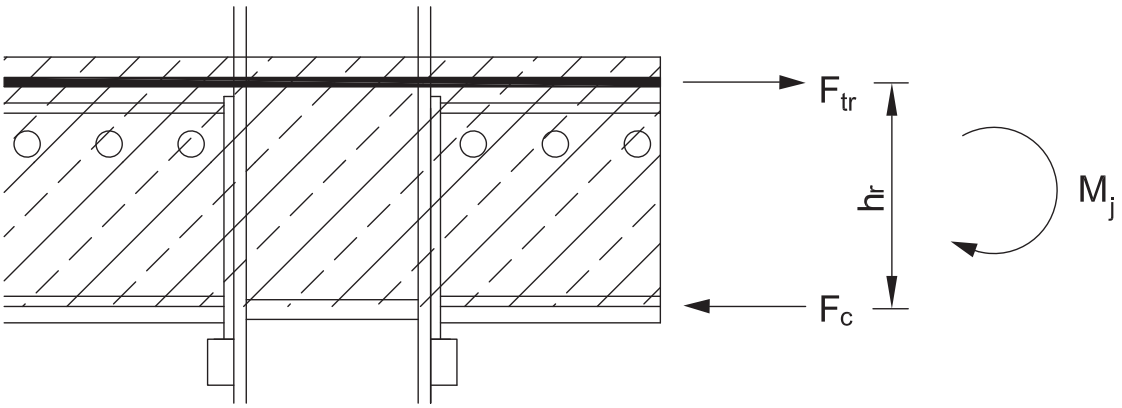

Figure 6.16: Distribution of internal forces in a boltless composite joint

For the case of a bolted endplate connection (e.g. test series E), the internal distribution of forces is not straightforward. In first approach, it seems intuitive that the resistance of a joint depends mainly on the strength of the individual components. However, under certain circumstances, the non-ductile behaviour of mesh reinforcement or bolts may restrict the bending resistance of the joint to its elastic limit. Thus, the design of ductile joint components is a principal condition to avoid such a limitation and allow for the plastic redistribution within the joint itself. In this case, the components can be used up to their ultimate resistance and provide, at the same time, a large yield plateau which favours the further distribution of moments within the system (Huber, 2000).

6.4.2 Elastic bending resistance

The elastic bending resistance of a composite joint is defined by the weakest component of the joint. If the resistance of the compression component is larger than that of tension components, the reinforcement is the first component reaching its load bearing resistance. For reinforcement with low ductility (e.g. welded wire mesh), the redistribution of internal forces is thus inhibited. The consequence is a restricted elastic resistance. In former research, Odenbreit observed that for joint typologies in which the reinforcement consists of mesh or with low compression resistance, the joint resistance was limited to its elastic bending resistance (Odenbreit, 2000).

The elastic bending resistance can be evaluated using the linear strain distribution shown in Figure 6.17. The yield strain of the weakest component is fixed, while the strain in the other components is varied until equilibrium of forces is reached. The bending resistance associated to this stress state is then called elastic bending resistance.

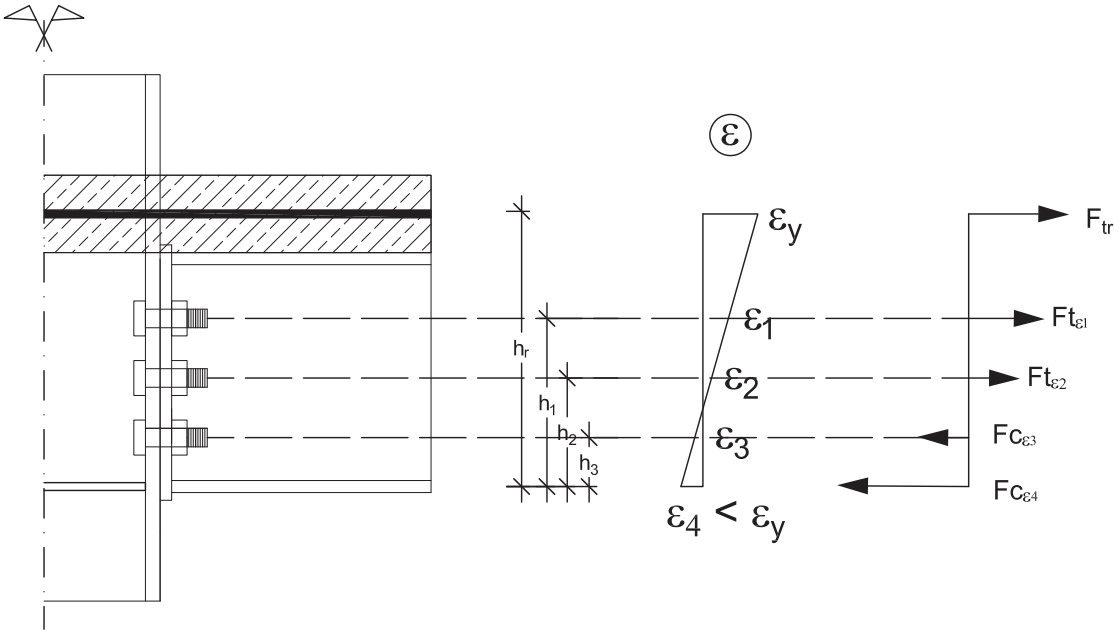

Figure 6.17: Plane strain distribution and distribution of internal forces for elastic bending resistance

6.4.3 Elasto-plastic bending resistance

Ductile reinforcement bars are not always sufficient to ensure that the joint develops its full plastic bending resistance. It requires a plastic redistribution of internal forces which is only possible if all the components in tension provide sufficient deformation capacity. A composite joint with a thick end-plate connection and several bolt-rows represents a typical case, in which only a more restricted resistance, called elasto-plastic joint resistance, can be developed. For thick endplate connections, the resistance of each bolt-row is defined by the tensile resistance of the bolts, which provides limited ductility to the connection. If the column web is stiffened and the compression resistance in the beam bottom flange is able to balance the tension forces, the joint resistance is attained as soon as the upper bolt-row attains its plastic resistance. Thus, a non-ductile tension failure of the bolt inhibits the development of the full load bearing capacity of the lower bolt-rows (cf. Figure 6.18).

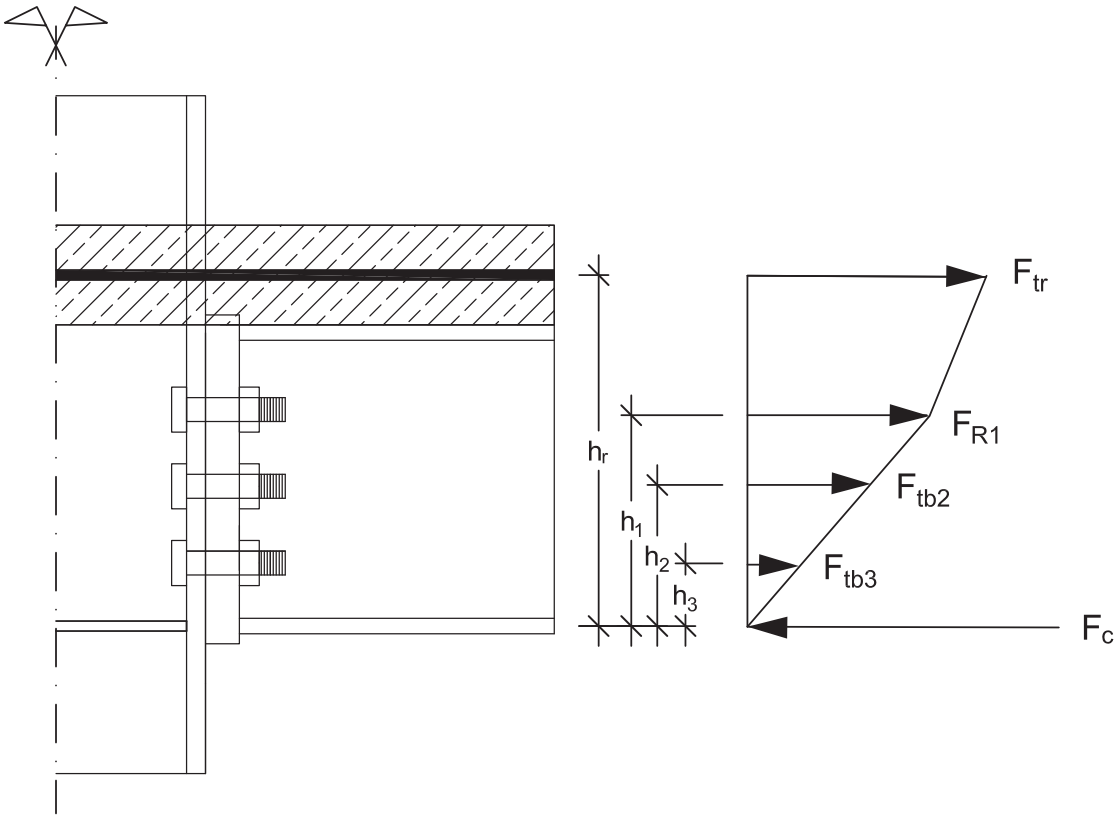

Figure 6.18: Distribution of internal forces for elasto-plastic bending resistance

6.4.4 Plastic bending resistance

In case all the tension components possess sufficient deformation capacity, the plastic redistribution of the internal forces can develop (cf. Figure 6.19). From experimental experiences, the following recommendations are proposed:

Reinforcement in tension

In (Odenbreit, 2000) and (Hahn, 2009), it was observed that composite joints with mesh reinforcement did not develop the full plastic bending resistance. Owing to the less ductile behaviour of welded wire mesh, the plastic redistribution of the internal forces is thus inhibited. It is suggested to avoid the use of mesh reinforcement or at least neglect the contribution of this component to the bending resistance of the joint.

Bolt-rows in tension

According to EN 1993-1-8 (2005), a bolt-row possesses sufficient deformation capacity to allow for a plastic redistribution of the internal forces if:

- its resistance is associated to the failure of the beam web in tension or,
- its resistance is associated to the failure of the endplate (mode 1) or bolt-plate assembly (mode 2). For the latter, it must be additionally verified that the resistance is 1.9 times smaller than the tensile resistance of the sole bolt.

Beam bottom flange

The resistance provided by the compression component F_c should be larger than the sum of the resistances of the tension components $\sum F_t$. This condition ensures that the distribution of the internal forces is not impeded by a limited compression resistance. $\longrightarrow F_c \geq \sum F_t$

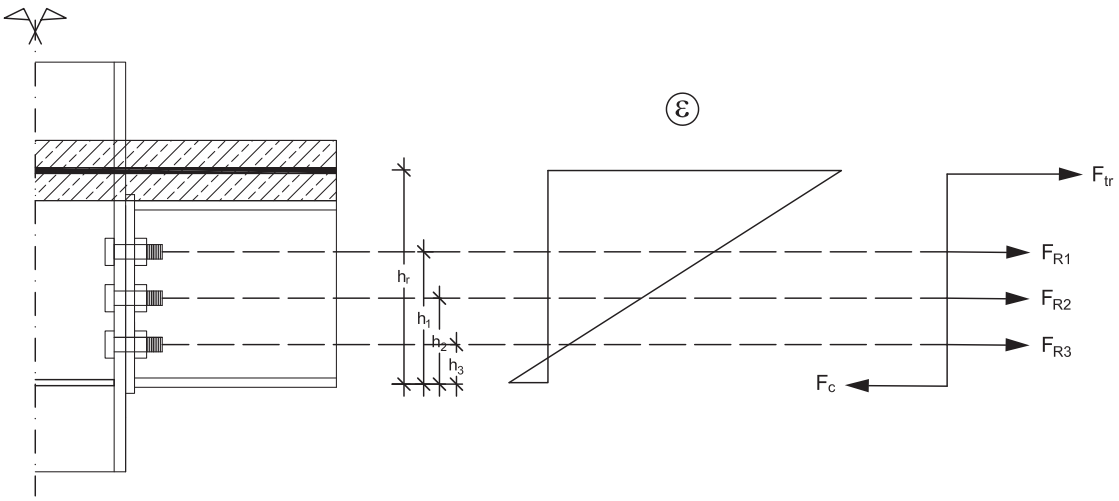

Figure 6.19: Distribution of internal forces for plastic bending resistance

6.4.5 Evaluation of the test results

The maximum bending resistance M_u of the joints tested in series B, C and E are represented in Figure 4.20 (b). As already mentioned, the endplate connection was designed to allow for the plastic redistribution of the internal forces. This fact being considered, the plastic bending resistance of the joints was calculated according to the procedure described in 6.4.4 and compared to the experimental values. Figure 6.20 shows the experimental ultimate joint resistances in comparison to the expected values.

In order to evaluate the accuracy of this analytical approach, the identity line (y=x) is plotted in the same Figure. The **good match** between expected and experimental resistances demonstrates the suitability of the method provided in EN 1994-1-1 (2004) for the present tests.

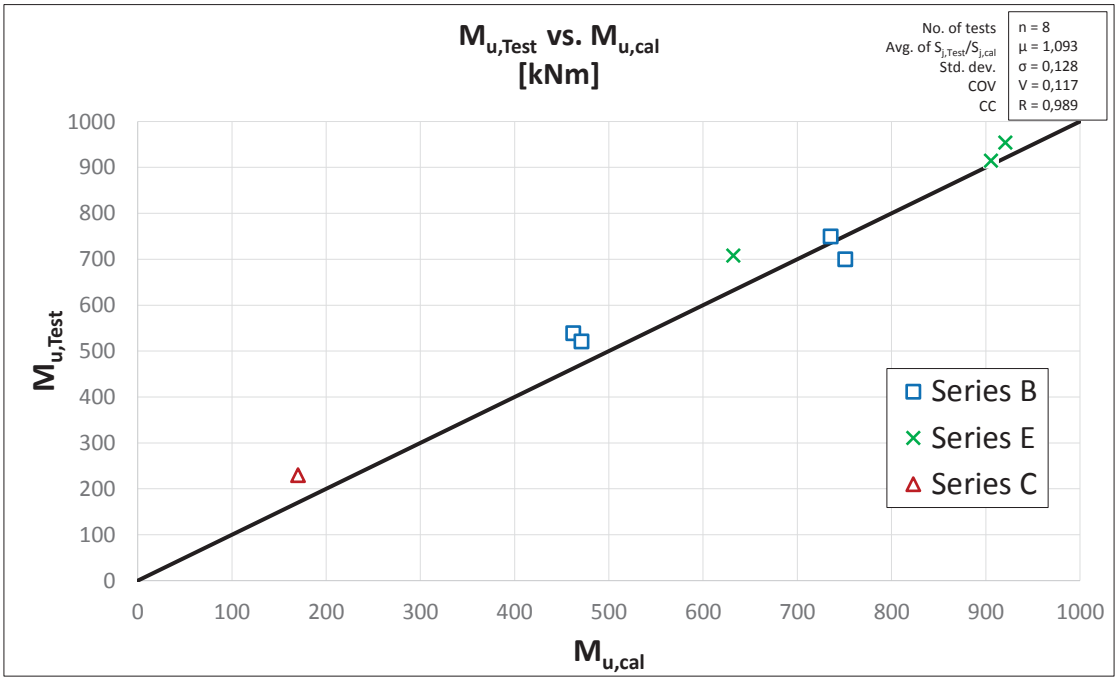

Figure 6.20: Comparison between experimental $M_{u,Test}$ expected joint resistances $M_{u,cal}$

6.5 Rotation capacity

6.5.1 Introduction

The ductility of a composite joint is defined by the ductility of its components. Thus, a beam-to-column joint with a thick endplate connection is rather non-ductile owing to the limited ductility accommodated by the bolts. Conversely, a composite joint with a thin endplate connection tends to be ductile since the load bearing capacity of each bolt-row is governed by the yielding of the end-plate, which is more ductile than the bolt failure in tension (thick endplates). If on top of that, the compression force in the beam bottom flange is transferred to the column without occurrence of buckling in the column web or beam bottom flange, the ductility of the composite joint is then limited by that of the reinforced concrete component. The deformation capacity of this component must therefore be accurately addressed in order to assess the rotation capacity of composite joints. Although the behaviour of this component is mainly influenced by that of the bare reinforcement bars, the **tension stiffening effect** of concrete between the cracks must be also considered.

6.5.2 Tension stiffening effect

The behaviour of a reinforced concrete member subjected to tensile forces lies between that of the unreinforced concrete and bare reinforcement. Due to its low tensile strength, concrete tends to crack at small stresses. The presence of reinforcement has a crack distributing effect on the concrete slab. Thus, instead of one main crack, several cracks occur at discrete positions such that between the cracks some concrete parts remain uncracked. The participation of these uncracked concrete parts in the load bearing mechanism of the reinforced concrete member is generally known as **tension stiffening effect**.

Due to this effect, the stiffness of a reinforced concrete member is larger than that of the bare reinforcement. From the experimental investigations performed by Kreller (1989), it could be observed that it also affects the ductility, or in other words the ultimate strain capacity of the reinforced concrete component. Kreller demonstrated that the ultimate strain elongation of a reinforced concrete member is smaller that that of the bare reinforcement. In the present research, the same observation could be verified in the experimental investigations since the elongation measured by the displacement captors on the top of the concrete slab recorded averaged strains under 10 %. This value is smaller than the elongation capacity of the bare reinforcement (cf. Appendix B.3).

On behalf of an ideal reinforced concrete block subjected to a tension force F (cf. Figure 6.21), Kreller developed a theoretical background model to quantify the effect. This model is subdivided into 4 stages.

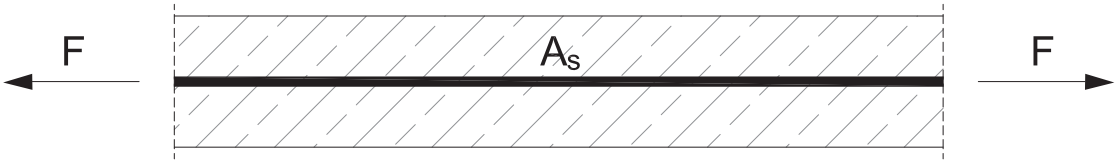

Figure 6.21: Reinforced concrete member subjected to tension force F

1^{st} stage: Uncracked concrete

For a low tensile force F the concrete block remains uncracked (cf. Figure 6.21) and the two materials - steel reinforcement and the surrounding concrete - share the same strain ε.

$$\varepsilon = \varepsilon_c = \varepsilon_s = \frac{F}{E_c \cdot A_c + E_s \cdot A_s} = \frac{F}{E_c \cdot A_c \cdot (1 + \alpha_e \cdot \rho)} \tag{6.32}$$

with:

E_c	Young's modulus of concrete
E_s	Young's modulus of steel
A_c	Cross sectional area of concrete
A_s	Cross sectional area of steel

and:

$$\alpha_e = \frac{E_s}{E_c} \tag{6.33}$$

$$\rho = \frac{A_s}{A_c} \tag{6.34}$$

2^{nd} stage: Crack formation

At a relatively low load stage, the tensile resistance of concrete f_{ct} is reached and the first crack appears. Consequently, all the tensile load is carried by the reinforcement at the crack. This induces a considerable increase in stress in the reinforcement at the cracked section (cf. Figure 6.22).

Prior to the crack, the stress in the reinforcement σ_s^I is equal to:

$$\sigma_s^I = \alpha_e \cdot f_{ct} \tag{6.35}$$

After the crack is formed, the stress in the reinforcement σ_{sr1} becomes:

$$\sigma_{sr1} = \frac{F_{cr}}{A_s} = \frac{f_{ct} \cdot (A_c + \alpha_e \cdot A_s)}{A_s} = \frac{f_{ct}}{\rho} \cdot (1 + \alpha_e \cdot \rho) = \sigma_s^I + \frac{f_{ct}}{\rho} \tag{6.36}$$

As it is perceptible from equation (6.36), the incremental jump in reinforcement stress at the crack increases with lower reinforcement ratio ρ.

Due to the high degree of statistical variance of the tensile strength of concrete, it is difficult to predict the exact position of the first crack. A confirmed design method taking into account the variance of this parameter is presented in (Kreller, 1989). This method consists in associating the whole crack formation stage to the statistical variance of the concrete tensile resistance. According to Kreller, the first crack occurs when the 5 %-fractile value of the concrete tensile strength $f_{ctk;0.05}$ is attained. The crack formation phase is concluded when its 95 %-fractile $f_{ctk;0.95}$ is reached (cf. Figure 6.23).

3^{rd} stage: Further crack development

In the previous stage, the spacing between the cracks is relatively large due to the low bond stresses between the reinforcement and the surrounding concrete. For load levels above the cracking formation stage, the bond stresses between reinforcement and concrete increase allowing for shorter transmission lengths between the cracks. Due to this, more cracks arise between already existing cracks which induces a smaller spacing between the cracks. When the yield strength of the reinforcement is reached, the cracking stage is stabilised and the strain differences between concrete and reinforcement are substantial as shown in Figure 6.24. From this stage on, the development of cracks in the reinforced concrete member is concluded and the ductility of the members is only accommodated by the opening of the existing cracks.

4^{th} stage: Post-yielding

The plastification process of the reinforcement takes place in this stage. This plateau lasts until the ultimate tensile resistance is reached in the reinforcement. Due to the effect described here, the final ductility of the reinforced concrete member ε_{smu} is smaller than that of the bare reinforcement ε_{su}.

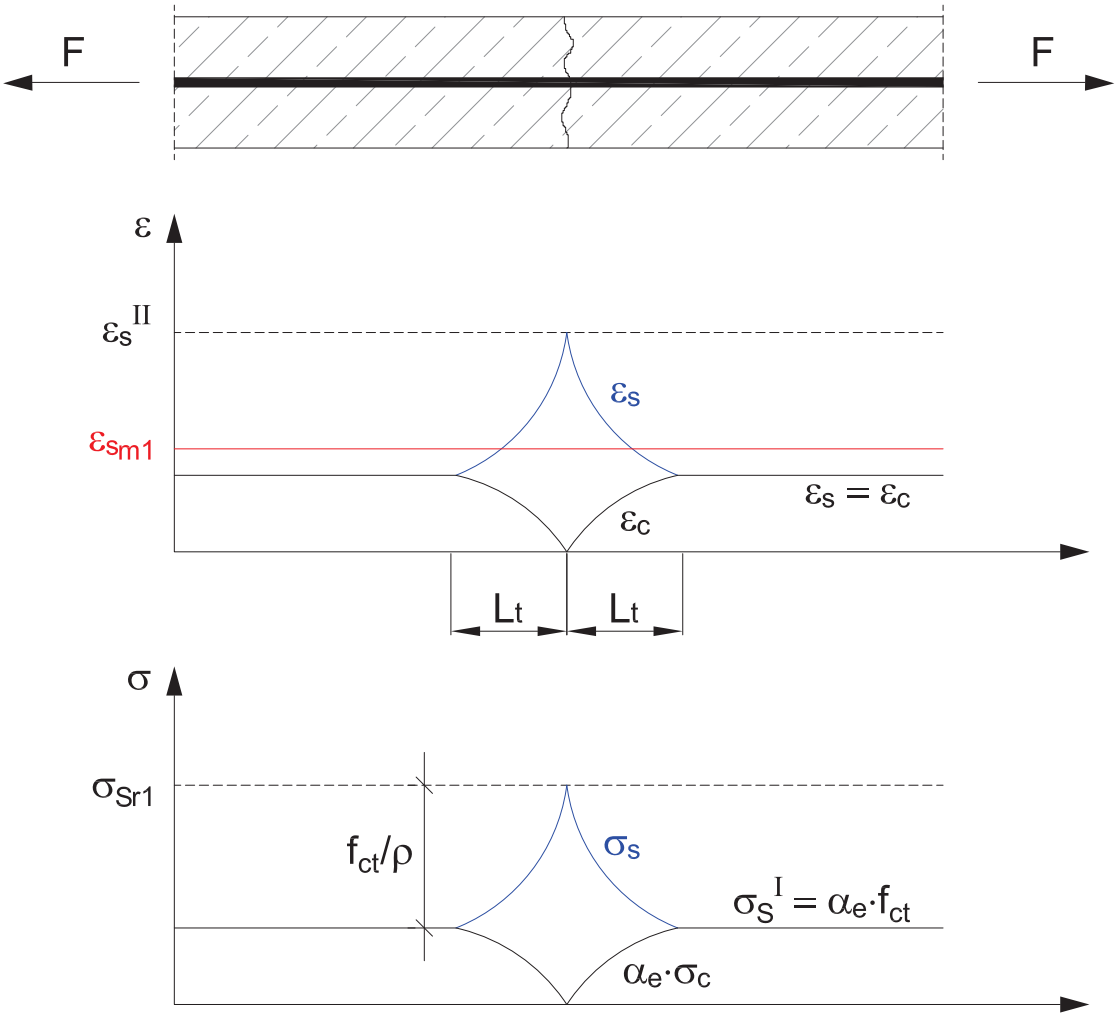

Figure 6.22: Stress and strain distribution in reinforcement around crack at first crack occurrence

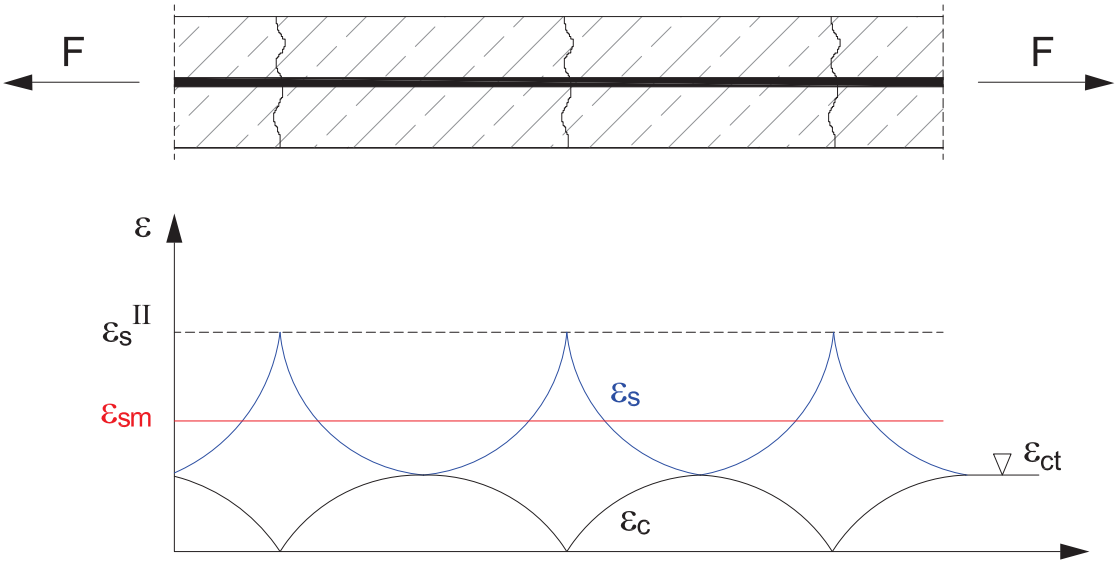

Figure 6.23: Strain distribution in reinforcement at crack formation stage

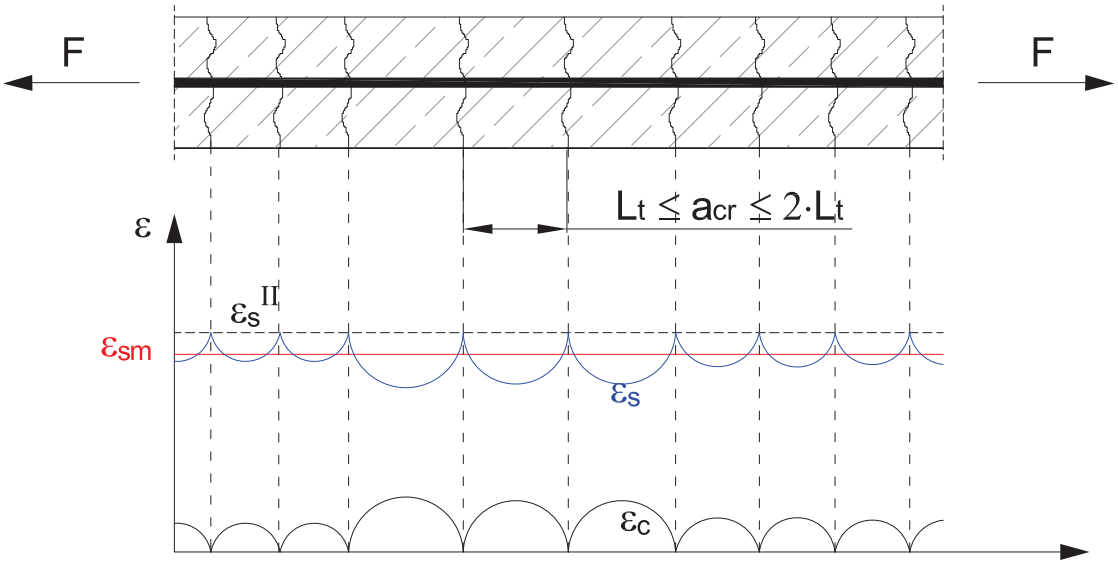

Figure 6.24: Strain distribution in reinforcement at stabilised cracking stage

In (Kreller, 1989), the tension stiffening effect of concrete is incorporated in a modified material law for the reinforcement (cf. Figure 6.25). In this context, a smeared stress-strain curve ($\sigma_s - \varepsilon_{sm}$) for the reinforcement was proposed. With this simplified model, the characteristic festoon shape of the reinforcement strain ε_s with peaks in the cracked sections is replaced by an averaged strain ε_{sm} (cf. Figure 6.24).

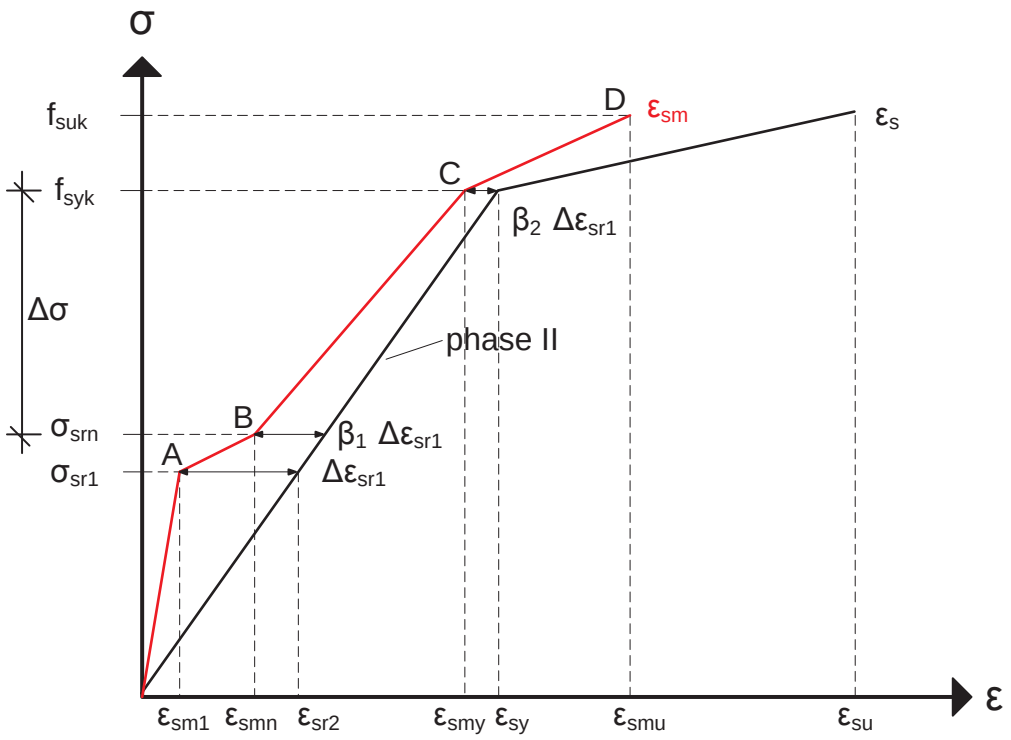

Figure 6.25: Consideration of tension stiffening in a modified material law for reinforcement

The characteristic points on the $\sigma - \varepsilon_{sm}$ curve shown in Figure 6.25 are specified below:

Point A

$$\sigma_{sr1} = \frac{f_{ctk;0.05}}{\rho} \cdot (1 + (\alpha_e - 1) \cdot \rho) \approx \frac{f_{ctk;0.05}}{\rho} \tag{6.37}$$

$$\varepsilon_{sm1} \approx 0.01\% \tag{6.38}$$

Point B

$$\sigma_{srn} = \frac{f_{ctk;0.95}}{\rho} \cdot (1 + (\alpha_e - 1) \cdot \rho) \approx \frac{f_{ctk;0.95}}{\rho} \tag{6.39}$$

$$\varepsilon_{smn} = \frac{\sigma_{srn}}{E_s} - \beta_1 \cdot \Delta\varepsilon_{sr1} \tag{6.40}$$

Point C

$$\sigma_s = f_{syk} \tag{6.41}$$

$$\varepsilon_{smy} = \varepsilon_{sy} - \beta_2 \cdot \Delta\varepsilon_{sr1} \tag{6.42}$$

Point D

$$\sigma_s = f_{suk} \tag{6.43}$$

$$\varepsilon_{smu} = \varepsilon_{smy} + \beta_3 \cdot (1 - \frac{\sigma_{sr1}}{f_{syk}}) \cdot (\varepsilon_{su} - \varepsilon_{sy}) \tag{6.44}$$

with:

$$f_{ctk;0.05} = 0.7 \cdot f_{ctm}$$
$$f_{ctk;0.95} = 1.3 \cdot f_{ctm}$$
$$\Delta\varepsilon_{sr1} = \frac{\sigma_{sr1}}{E_s} - \varepsilon_{sm1}$$
$$\varepsilon_{sy} = \frac{f_{syk}}{E_s}$$
$$\beta_1 = 0.4$$
$$\beta_2 = 0.2$$
$$\beta_3 = 0.8$$

6.5.3 Influence of longitudinal reinforcement ratio

One major factor influencing the rotation capacity of composite joints is the longitudinal reinforcement ratio of the reinforced concrete slab. The beneficial effect of this parameter has **two different causes**.

One cause emanates from the tension stiffening effect described in the previous Section. As it can be seen in equation (6.37), a larger reinforcement ratio causes a smaller first crack stress σ_{sr1} in the reinforcement which induces also a **bigger ultimate elongation** capacity ε_{smu} of the reinforced concrete slab as can be deducted from equation (6.44). A larger ductility of this component is thus available. In Figure 6.26, the ultimate strain of an embedded reinforcement bar ($f_{syk} = 500N/mm^2$ and $\varepsilon_{su} = 100‰$) is evaluated for different reinforcement ratios and concrete classes according to equation (6.44). The beneficial effect of the reinforcement ratio is demonstrated. A good strategy to increase the rotation capacity of composite joints consists therefore in providing a big amount of reinforcement in the concrete slab.

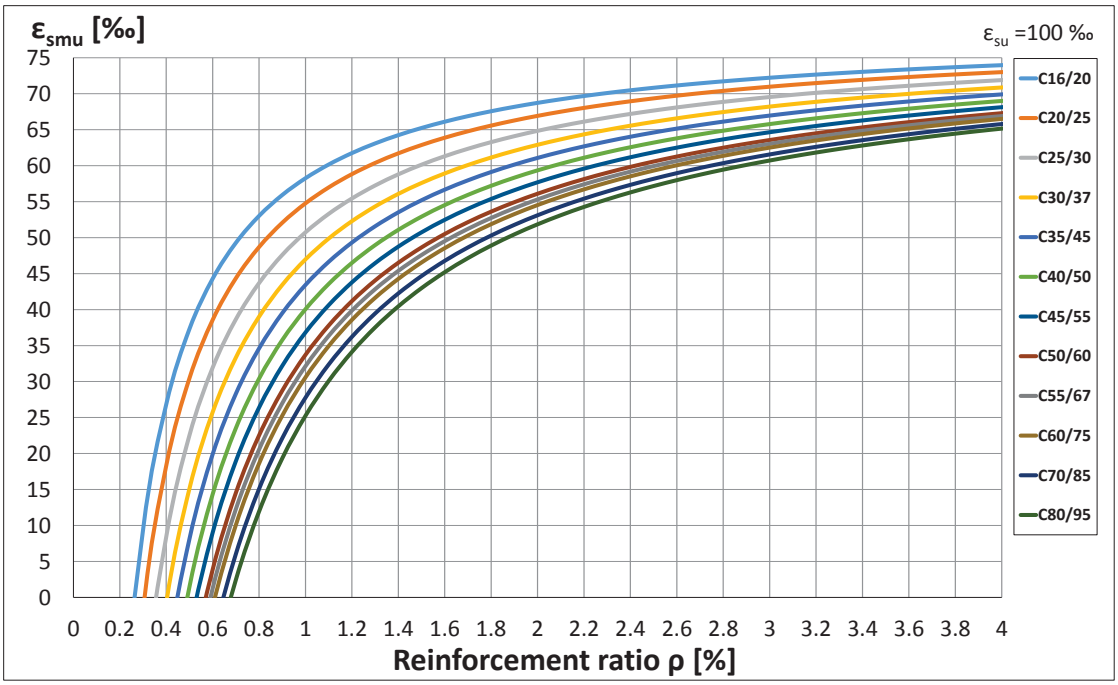

Figure 6.26: Influence of reinforcement ratio ρ on the ultimate strain capacity ε_{smu} of a reinforced concrete member in tension

The influence of the reinforcement ratio is, however, not only limited to the ultimate strain of the reinforced concrete component. It was seen in equation (6.37) that the stress in the reinforcement for the first crack occurrence increases for lower reinforcement ratio ρ of the concrete slab. In Figure 6.27 the simplified stress-strain curve according to Kreller is presented for different reinforcement ratios. It shows that the difference between yield stress and first crack stress $\Delta\sigma = f_{syk} - \sigma_{sr1}$ is bigger for slabs with a bigger amount of longitudinal reinforcement. This larger **difference** $\Delta\sigma$ is an additional cause for the bigger effective joint length observed in the experimental and numerical analysis. In order to justify this statement, two beam-to-column composite joints with different amount of longitudinal reinforcement are illustrated in Figure 6.28. For simplification, the bending moment distribution in the hogging zone is approximated by a linear shape.

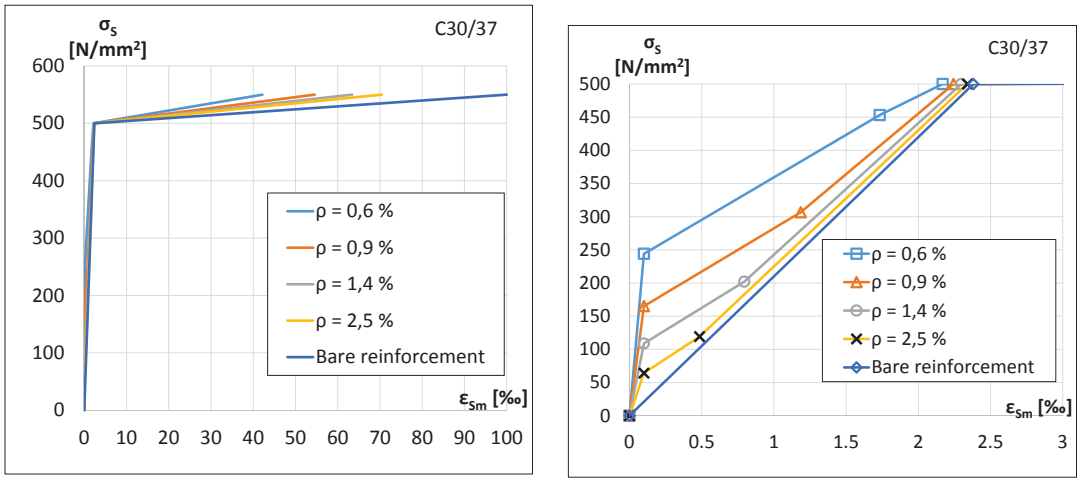

(a) Complete curve

(b) Inital curve

Figure 6.27: Simplified tensile stress-strain curve of a reinforced concrete member for different reinforcement ratios ρ

In the first case, the composite joint presents the minimum amount of longitudinal reinforcement ($\rho_1 = \rho_{min}$) necessary to ensure that the first crack stress in the reinforcement σ_{sr1} is smaller than the yield strength f_{syk}. The first crack logically arises at the maximal bending moment (cf. Figure 6.28). At this precise position the stress in the reinforcement is close to the yielding limit (i.e. $M_{cr} \simeq M_{j,pl,1}$) owing to the very low reinforcement amount (small difference $\Delta\sigma$). The load bearing capacity of the composite joint is therefore practically reached, such that practically no more load can be accommodated. At a distance $a_{cr} = 2 \cdot L_t$, at which the next crack would develop, the bending moment is lesser than the critical cracking bending resistance M_{cr}. For this reason only one single crack can develop.

In the second case, the joint presents a large reinforcement ratio ρ_2 in the slab. Thus, the first crack stress σ_{sr1} in the reinforcement is much smaller than the yielding stress f_{syk} (cf. Figure 6.28). The stress difference $\Delta\sigma$ is therefore considerably larger such that further load can be allocated in the connecting zone until the bending resistance is effectively fully exploited. The allocation of further load leads to the development of further cracks along the longitudinal axis. The consequence is a larger effective joint length L_j in which the reinforcement is subjected to considerable strains. A larger rotation capacity than in the first case is thus achieved.

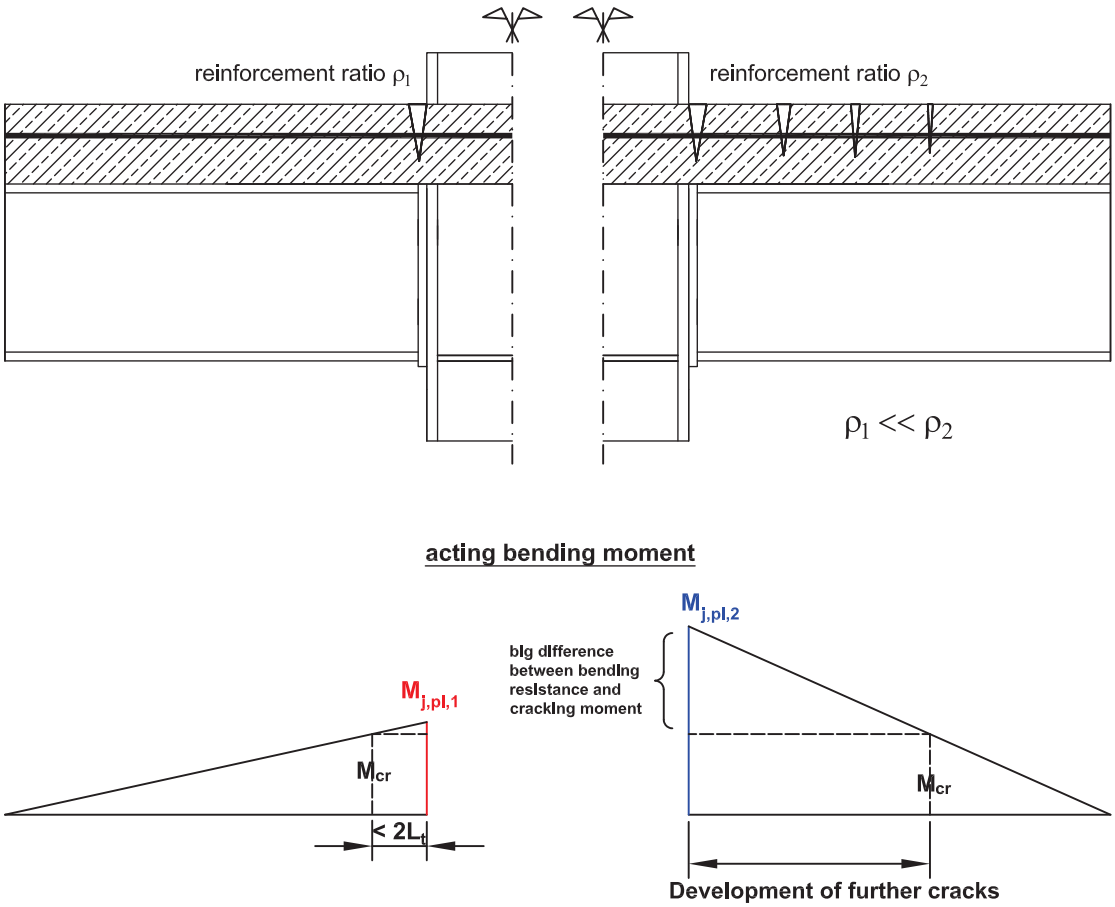

Figure 6.28: Influence of reinforcement ratio ρ on the crack pattern of a reinforced concrete slab

The same conclusion can be deducted from the numerical analysis. The FEA crack pattern of the tests performed in series B are shown in Figure 6.29. It can be observed that the larger the reinforcement ratio ρ, the longer is also the effective joint length L_j.

In Section 6.3.4 the influence of the reinforcement ratio on the **effective joint length** was implemented in the new proposal for the effective joint length by introducing a **factor n**, whose value increases for bigger reinforcement ratios. If ρ_{eff} lies for instance between 1.0 % and 1.6 % it can be assumed that a second main crack occurs in the slab. Since the distance between the first crack and the column centre line is considered in the first term of the expression for L_j, only half of the crack spacing is taken into account in the definition of the n-factor $(0.5 \cdot a_{cr})$ for this first crack. The occurrence of a second crack increases the effective joint length by a factor a_{cr} such that in this range (1.0 % $\leq \rho_{eff} \leq$ 1.6 %) the term $n \cdot a_{cr}$ is equal to $0.5 \cdot a_{cr} + 1 \cdot a_{cr} = 1.5 \cdot a_{cr}$. With the occurrence of additional cracks for the consecutive ranges of reinforcement ratio, the n-factor is successively increased by one leading to the final definition provided in equation (6.29).

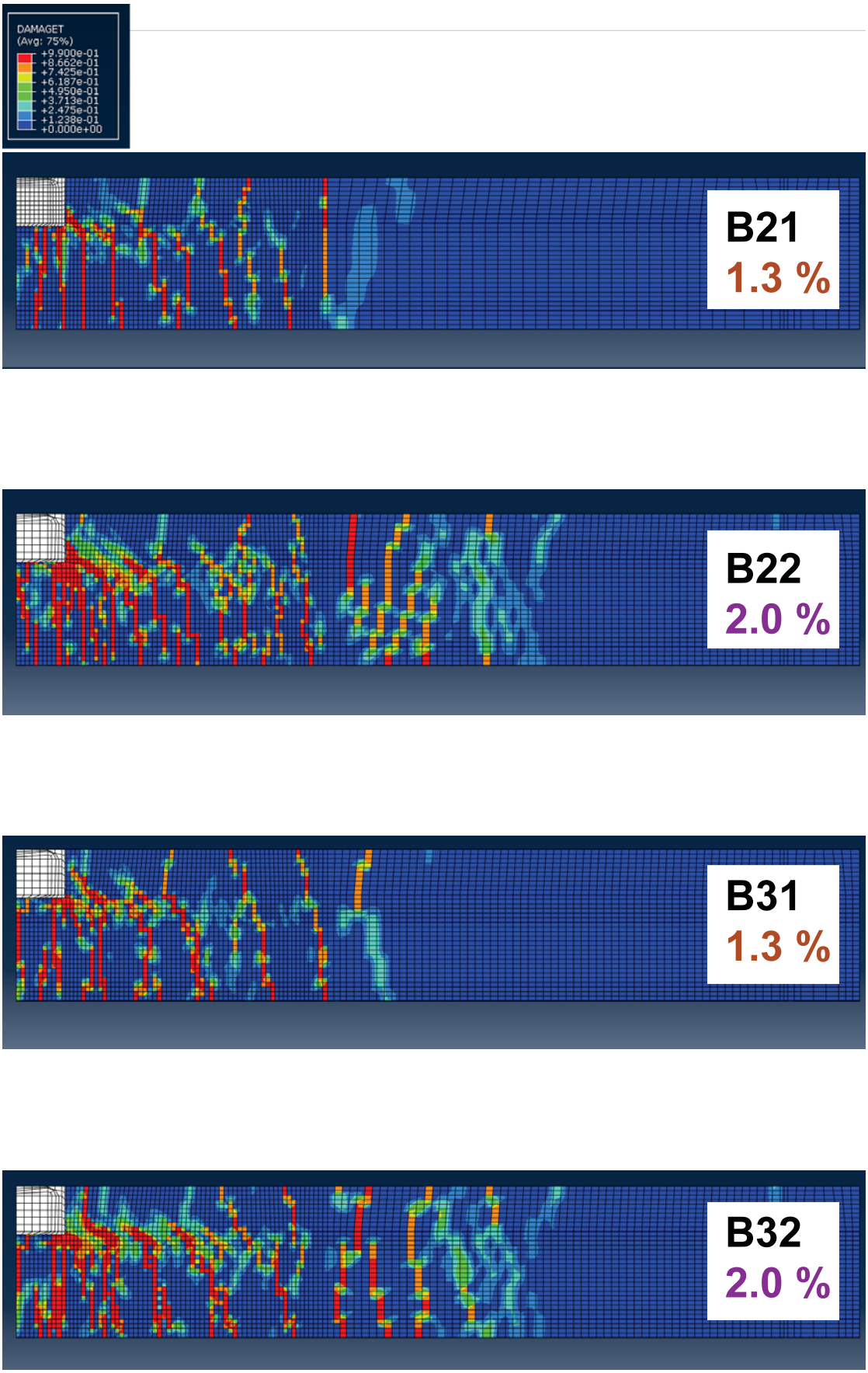

Figure 6.29: Crack pattern obtained in numerical analysis for Series B

6.5.4 Influence of the diameter of the reinforcement bars

In the present research, one of the main objectives pursued was to quantify the influence of the diameter of the longitudinal reinforcement bars on the ductility of composite joints. To achieve this objective, tests with equal reinforcement ratio were performed, for which the only difference was the diameter of the longitudinal reinforcing bars.

Due to the extremely ductile behaviour of the tested composite joints, the failure of the longitudinal reinforcing bars was only obtained for two tests B21 and B31. The other tests were stopped, for safety reasons, before any sign of evident joint failure could be detected. The large rotation capacities achieved in these tests result mainly from the big amount of longitudinal reinforcement provided, which as described previously in Section 6.5.3, activates an enlarged effective joint length L_j and allows for a bigger equivalent ultimate strain ε_{smu} of the reinforcement component. Although it is not possible to make any conclusions on the influence of the rebar diameter on the basis of the present experiments, a lower bound for the rotation capacity can be deducted from the tests. The calculation method provided in this thesis must therefore rely on these test values. Besides, the numerical analysis has shown that the rotation capacity of the tested joints is approximately that obtained in the experimental tests. This proves that the failure of the specimens was almost reached when the tests were stopped.

Although no influence can be deduced from the present experimental investigations for bar diameters of 12 mm, 16 mm and 20 mm, a former research performed at the University of Luxembourg (Hahn, 2009) confirmed the benefits of larger rebars on the rotation capacity of composite joints. It consisted of several tests on composite joints identical to the one tested in series B. The reinforcement ratio was lower and ranged between 0.7 % and 1.06 %, while the diameter of the longitudinal rebars ranged between 8 mm and 12 mm. In Figure 6.30, the moment-rotation curves of tests with different reinforcement bar diameter show that the bigger the rebars, the bigger is also the rotation capacity. It should be stated that the investigations performed by Brown and Anderson (2001) led to the same conclusion (cf. Chapter 2). The extrapolation of this conclusion to bigger reinforcement ratios and bar diameters must still be demonstrated by experimental investigations but these results provide already a first tendency on the influence of the rebar diameter.

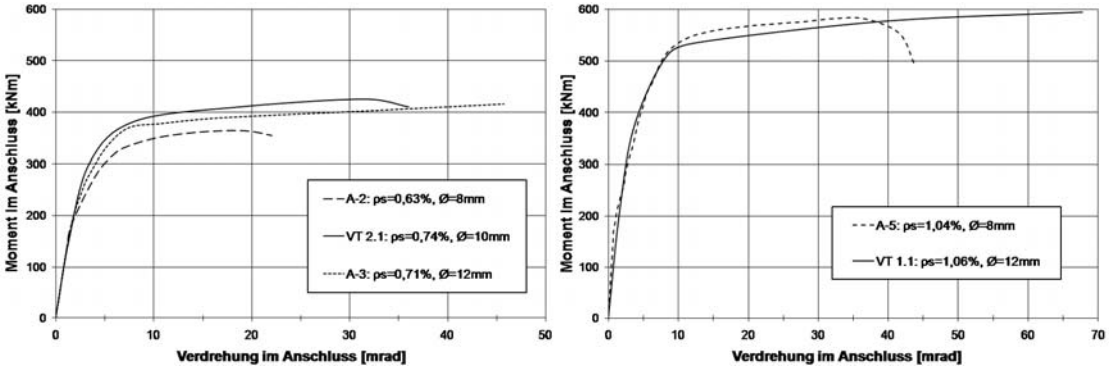

(a) Moment-Rotation curves for $\rho = 0.7\%$ (b) Moment-Rotation curves for $\rho = 1.0\%$

Figure 6.30: Influence of the rebar diameter on the rotation capacity of composite joints (Hahn, 2009)

6.5.5 Own Proposal for the rotation capacity of composite joints

The spring model presented in Section 6.3.1 is used to formulate an analytical expression for the rotation capacity of composite joints. This mechanical model is represented in Figure 6.31 for a composite joint with a bolted flush endplate connection. The presence of a stiffener in the column prevents the buckling of the column web and appoints at the same time the rotation point of the joint to the bottom flange of the beam. The deformation of this component is therefore infinitely small and can be neglected. Moreover, the resistance of the beam bottom flange against local buckling must be ensured in order to guarantee that the rotation capacity of the composite joint is defined by the components in tension.

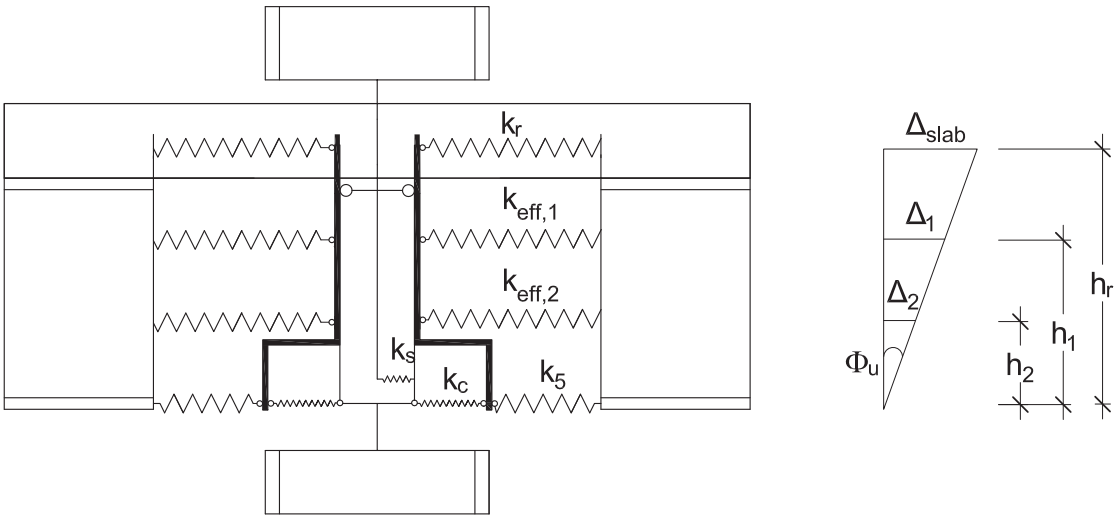

Figure 6.31: Spring model and rotation capacity

Under these conditions, the rotation capacity of the tested joints is mainly characterised by the ductility of the bolt-rows and reinforcement. Figure 6.31 shows that these components are not subjected to the same deformation; the reinforcement is the component, which endures the biggest demand (Δ_{slab}) owing to the bigger lever arm to the rotation point. For this reason, this component is in most cases defining the rotation capacity of composite joints. If however, a joint with a bolted connection presents a non-ductile failure mode (e.g. bolts in tension), the rotation capacity can be limited by the humble deformation capacity of the bolts (small values for Δ_1 and Δ_2), which "retains" the plastic elongation of the reinforcement bars. This is the only reason why the bolt-rows have been designed with relatively thin endplates. Neglecting the compressive deformation in the bottom flange (conservative assumption), and assuming that the bolt-rows do not prevent the plastic elongation of the reinforcement, the rotation capacity of the composite joints is only defined by the elongation capacity of the reinforced concrete slab:

$$\Phi_u = \frac{\Delta_{slab}}{h_r} \tag{6.45}$$

The slab elongation Δ_{slab} can be assessed by considering the tension stiffening effect presented in Chapter 6.5.2. This model, however, presupposes constant tensile forces in the concrete slab, which is not representative for the real stress condition in the slab of a composite joint. In reality, the hogging moment M_j applied to a composite joint induces a local bending moment M_c in the concrete slab, which influences the first crack stress σ_{sr1} in the reinforcement (cf. Figure 6.32). This particular behaviour was extensively described

by Hanswille (1986). The critical cracking moment M_{cr} is defined by the condition that the upper concrete fibre exceeds the tensile strength of concrete. Therefore, Hanswille introduced a geometrical factor to consider the linear stress distribution within the section prior to cracking. In EN 1994-1-1 (2004), this factor is denoted as k_c, which for consistency reasons, is re-formulated as k_b-factor in the present thesis. In (European Convention for Constructional Steelwork, 1999), this factor was similarly introduced to calculate the first crack stress in the reinforcement σ_{sr1}. There, the use of this factor was justified by the fact that the stress distribution across the thickness of the slab can be calculated with sufficient accuracy using the properties of the beam section. This interpretation avoids to consider the stiffness of the joint's components for the first crack occurrence.

The effect related to the local bending of the slab is considered in the analytical formula for the rotation capacity trough the factor k_b. Thus, when calculating the ultimate strain capacity ε_{smu} of the reinforced concrete component, the first crack stress in the reinforcement should be calculated according to equation (6.47).

$$k_b = \frac{1}{1 + \frac{d}{2 \cdot z_{i,0}}} \tag{6.46}$$

with:

d thickness of the concrete flange

$z_{i,0}$ vertical distance between the centroids of the uncracked unreinforced concrete flange and the uncracked unreinforced composite section

and:

$$\sigma_{sr1,kb} = k_b \cdot \frac{f_{ctk;0.05}}{\rho_{eff}} \cdot (1 + (\alpha_e - 1) \cdot \rho_{eff}) \tag{6.47}$$

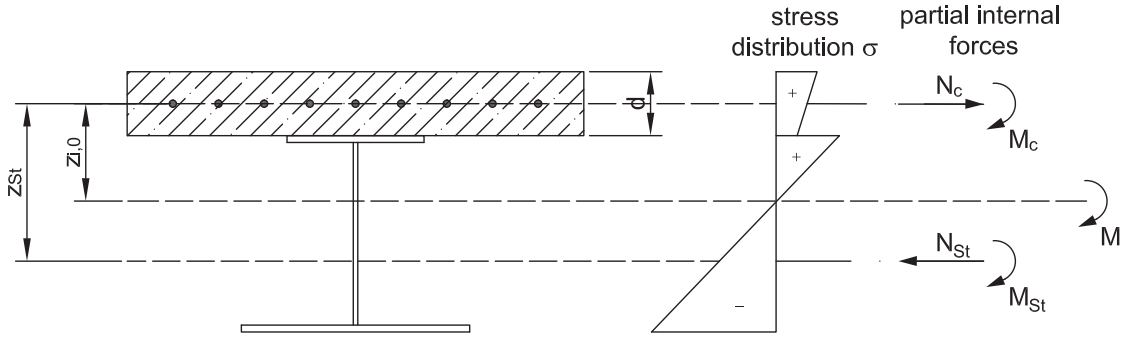

Figure 6.32: Partial slab bending moment for a composite beam in negative bending (Hanswille, 1986)

The tension stiffening model is a good approach for a reinforced concrete slab subjected to constant tension forces along its axis. For the specific case of composite joints, this model must be adapted to consider the decreasing acting bending moment along the beam axis. A major issue to be quantified is the longitudinal strain distribution in the reinforcement at failure of the joint. Just before the fracture of the reinforcement, it can be assumed that the ultimate strain capacity ε_{smu} is reached on the level of column flange. Assuming a linear decrease of the strain along the longitudinal axis of the reinforcement, it can be expected that

at the end of the effective joint length L_j, the yield strain ε_{smy} is attained (cf. Figure 6.33). Hence, the linear strain distribution $\varepsilon_{sm}(x)$ is uniquely defined along the effective joint length. The total elongation of the reinforced slab Δ_{slab} is obtained by integrating the reinforcement strains over the length L_j:

$$\Delta_{slab} = \int_0^{Lj} \varepsilon_{sm}(x) \cdot dx = \varepsilon_{smu} \cdot \frac{h_c}{2} + \frac{\varepsilon_{smu} + \varepsilon_{smy}}{2} \cdot (L_j - \frac{h_c}{2}) \tag{6.48}$$

Combining equations (6.48) and (6.45), the final expression for the rotation capacity of composite joints can be given as:

$$\Phi_u = \left[\varepsilon_{smu} \cdot \frac{h_c}{2} + \frac{\varepsilon_{smu} + \varepsilon_{smy}}{2} \cdot (L_j - \frac{h_c}{2})\right] \cdot \frac{1}{h_r} \tag{6.49}$$

with:

ε_{smu}	ultimate strain of reinforced concrete member acc. to equation (6.44)
ε_{smy}	yield strain of reinforced concrete member acc. to equation (6.42)
$\sigma_{sr1,kb}$	first crack stress to be inserted in ε_{smu} and ε_{smy} acc. to equation (6.47)
ρ_{eff}	effective reinforcement ratio acc. to regulations in EN 1992-1-1 (2004) and presented in section 6.3.3
h_c	column depth
h_r	internal lever arm between compression point and reinforcement layer
L_j	effective joint length acc. to equation (6.28)

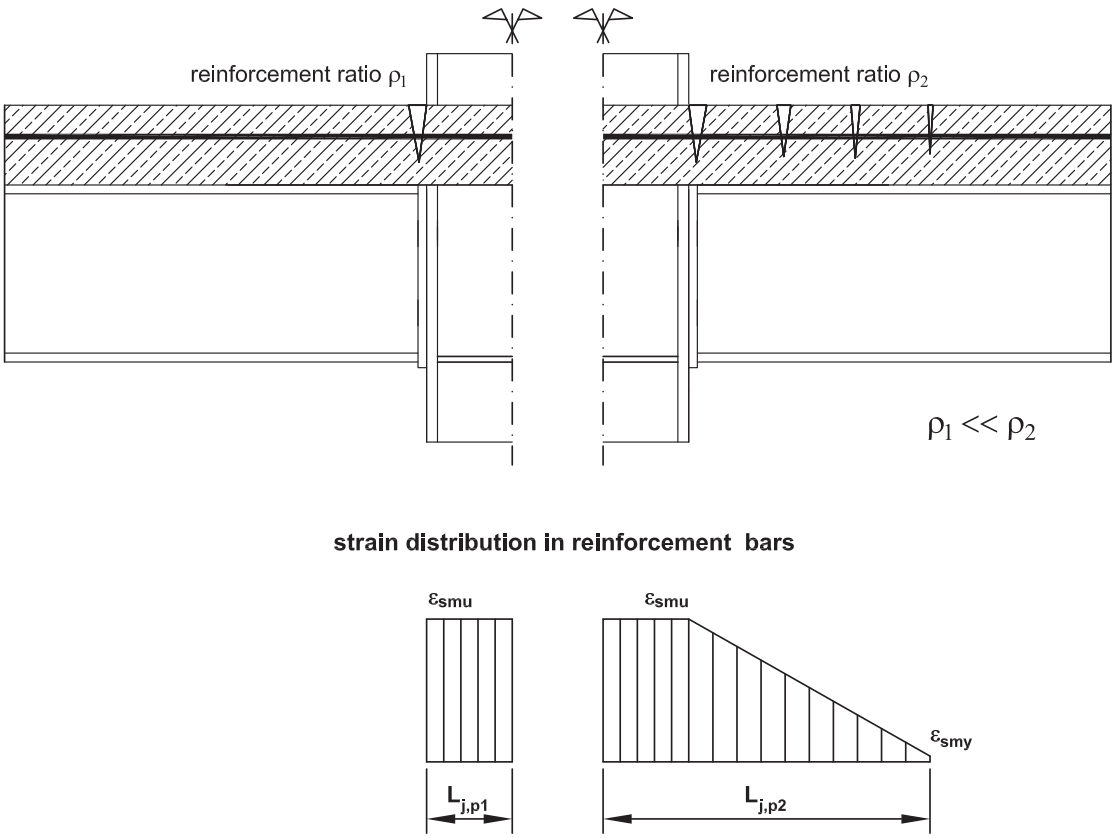

Figure 6.33: Longitudinal strain distribution in reinforcement for composite joints

6.5.6 Validation of own proposal

A set of necessary conditions to confer a larger rotation capacity to composite joints can be defined on the basis of the experimental experience assembled in all the research projects investigating the ductility of composite joints.

It was for instance demonstrated that using mesh as longitudinal reinforcement prejudices the rotation capacity of composite joints. This is due to the transverse reinforcement which creates a local damage of the bar because it is welded on the longitudinal rebars. The ultimate strain capacity in tension is therefore reduced. Moreover, the local buckling of the column web should be avoided by means of web stiffeners. This measure assigns the compression point of the connection to the beam bottom flange and ensures that the ductility of the composite joint is defined by the components in tension. Table 6.2 summarises the conditions under which the new formula for the rotation capacity Φ_u, presented in equation (6.49), can be applied.

Table 6.2: Range of validity for the stiffness and rotation capacity of composite joints

Longitudinal reinforcement	effective reinforcement ratio $\rho_{eff} \geq 1.0\%$
	diameter of longitudinal rebars $\varnothing \geq 12$ mm and $\varnothing \leq 20$ mm
	Ductility class B or C and no welded mesh reinforcement mesh
Steelwork connection	Bolted flush endplate connection: Ductile failure of endplate (mode 1 acc. to EN 1993-1-8 (2005)) must be ensured by avoiding the tension failure of the bolts or $t_{plate} < 0.36 \cdot d\sqrt{f_{ub}/f_y}$ acc. to EN 1993-1-8 (2005) and Jaspart (1991)
	Bolted finplate connection: Ductile failure of finplate must be ensured by avoiding the brittle shear failure of the bolts. To transfer the compression force in the bottom flange of the beam, a contact plate must be provided.
Compression region	If necessary, local buckling of the column web must be prevented through stiffeners or by taking the stiffening effect of concrete encasement into account.
	Compressive load bearing capacity of the beam bottom flange must be larger than the sum of the resistances of the components in tension (reinforcement and bolt-rows)
Loading	Double-sided joints with balanced bending moments
	Joints under hogging bending moments
	Non-cyclic loading

In order to verify the reliability of the analytical method presented in this thesis, a total of about 90 experiments on composite joints were examined. Not all these experiments meet the conditions mentioned above. For this reason, only those complying with these conditions were selected. More details concerning test data of the selected experiments can be found in Appendix C.

The calculation was carried out with the measured properties of the different materials used in the tests. Figure 6.34 compares the predicted rotation capacities $\Phi_{u,cal}$ with the experimental

values $\Phi_{u,test}$. An identity line is drawn in the same figure to facilitate the comparison. Close agreement between experimental and analytical values is demonstrating, showing that a confident level of accuracy is achieved with this new calculation method. The latter is furthermore used to predict the available rotation capacities obtained in the numerical simulations presented in Section 5.5. The good agreement between the results of this parametric study (P-Series) and the calculation model is demonstrated in Figure 6.35.

The statistical evaluation of the data set shows that on average, the ratio between the real and the calculated rotation capacity is close to one. In combination with the low standard deviation σ and the strong correlation factor R between the pairs ($\Phi_{u,Test}$;$\Phi_{u,cal}$), the results show that the calculated values are concentrated around the mean value.

6.6 Summary

An analytical method to calculate the stiffness S_j and rotation capacity Φ_u of composite joints was developed in the present Chapter. This method was deducted from the readings and observations made during the performance of the experimental tests. The analysis of numerical results allowed to drill deeper into these observations and contributed to the better understanding of the joint's behaviour.

The application of this method to composite joints demonstrated that this new analytical formulation is capable of predicting the measured properties of the tested joint specimens, within the range of application of Table 6.2.

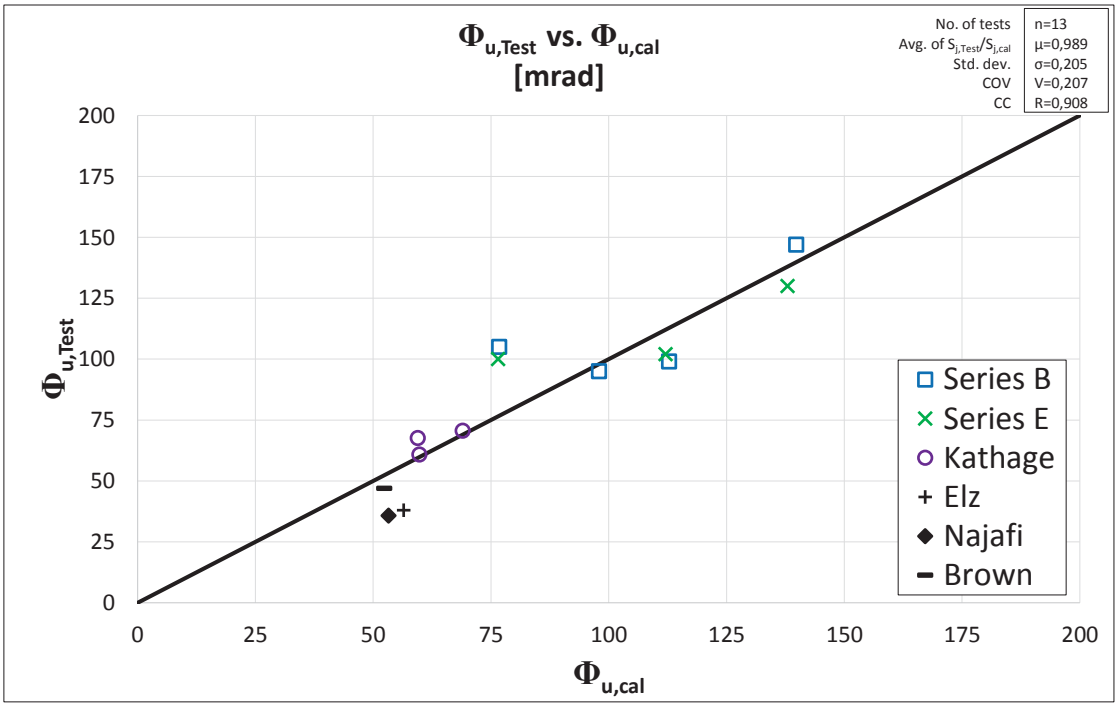

Figure 6.34: Comparison between experimental $\Phi_{u,test}$ and predicted $\Phi_{u,cal}$ rotation capacities

Ref.: Series B and E (Chapter 4), Kathage (1994), Elz (2000), Najafi (1992) and Brown and Anderson (2001)

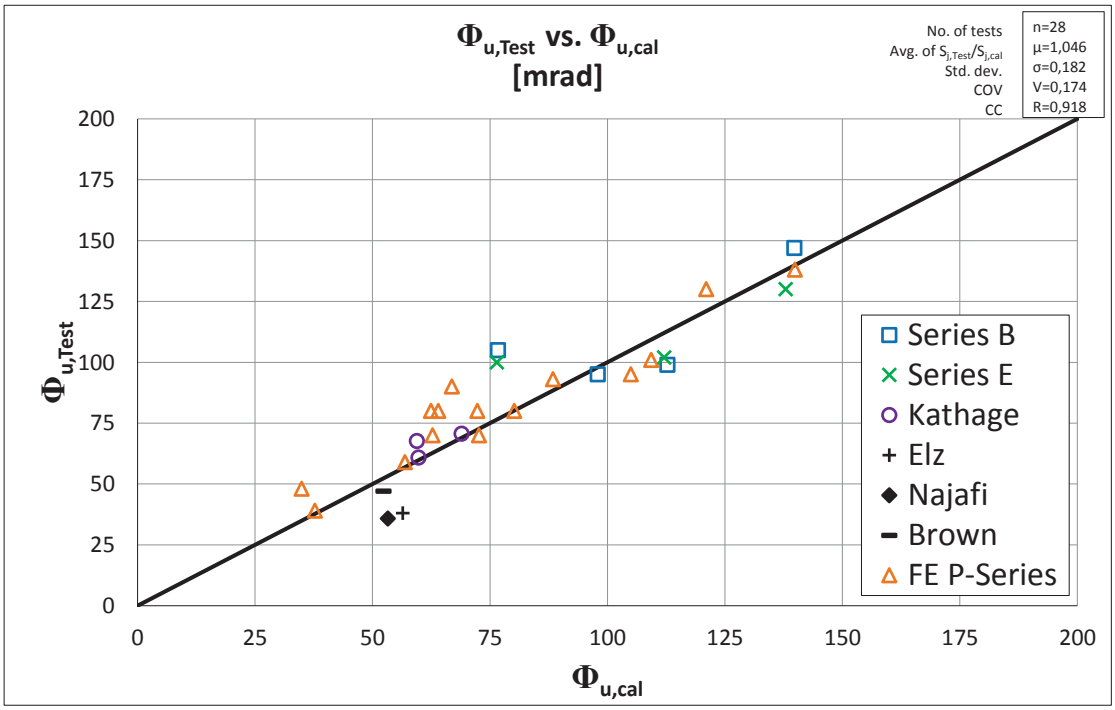

Figure 6.35: Comparison between experimental/numerical $\Phi_{u,test}$ and predicted $\Phi_{u,cal}$ rotation capacities
Ref.: Series B and E (Chapter 4), Kathage (1994), Elz (2000), Najafi (1992), Brown and Anderson (2001) and P-Series (Chapter 5)

7 Design methodology for plastic global analysis

7.1 Introduction

A design methodology allowing the application of the plastic global analysis on semi-continuous composite beams is described in this chapter. This methodology is elaborated on the basis of earlier research investigations on the required joint rotation Φ_{req} as well as on the calculation method for the rotation capacity Φ_u of composite joints.

7.2 Design principle

The plastic global analysis of semi-continuous composite beams is hampered by the fact that no analytical method is provided to calculate the available rotation capacity of composite joints in EN 1994-1-1 (2004). This difficulty is overcome with the validation of the analytical model developed in the present thesis. In order to design a semi-continuous composite beam according to the plastic global analysis, it must be verified that composite joints provide sufficient capacity of rotation to accommodate the rotation required by the structural system for the plastic redistribution of bending moments. Hence, the following condition must be fulfilled (cf. Figure 7.1):

$$\Phi_{req} \leq \Phi_u \tag{7.1}$$

In the following Sections, design aids are provided to facilitate this verification. Firstly, a simplified method is exposed to predict the required joint rotation. Then, design charts to determine the available rotation capacity are given according to the proposed analytical procedure. On this basis, a set of ductility conditions are elaborated in order to ease the application of plastic global analysis without direct verification of the rotational capacity of composite joints.

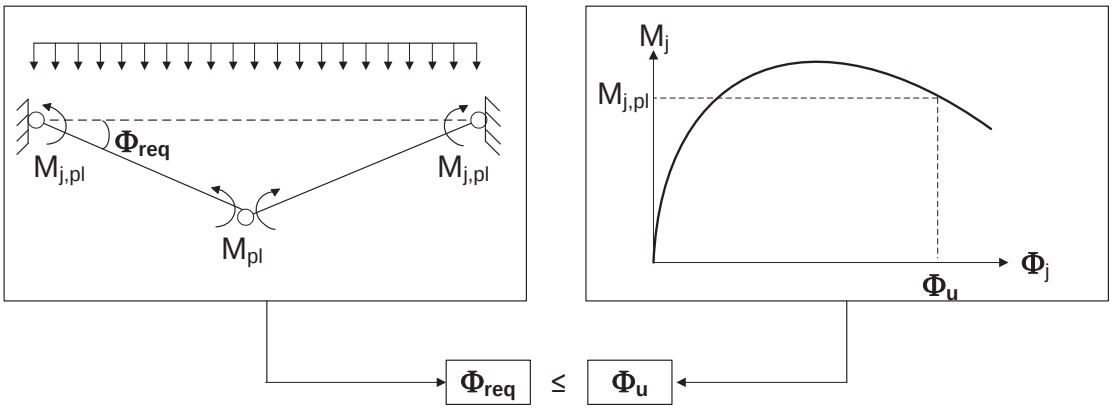

Figure 7.1: Required joint rotation Φ_{req} and available rotation capacity Φ_u

7.3 Required joint rotation

In order to provide a simplified procedure to determine the required joint rotations Φ_{req} most of the investigations carried out on this topic have been considered. All the assumptions made in this procedure are therefore based on earlier research developments.

In Section 2.3 the investigations carried out in this field were compiled. In the same Section, the upper bound of 80 mrad for the required joint rotations was derived on the basis of a composite beam with simple joints. In the perspective of a plastic global analysis, a simple joint is a joint with a moment resistance M_j smaller than 0.25 times that of the adjacent beam $M_{pl,hogg}$ according to EN 1993-1-8 (2005). As a consequence, composite joints with a resistance greater than $0.25 \cdot M_{pl,hogg}$ can be classified as semi-continuous.

The assumption for the required joint rotation of 80 mrad is not representative for a beam with semi-continuous composite joins. This is due to the fact that per definition a certain joint resistance is available for semi-continuous joints $M_j > 0.25 \cdot M_{pl,hogg}$, whereas the 80 mrad value is based on a simple supported pinned beam. This conclusion is confirmed by the research investigations carried out by Li et al. (2000), Nethercot et al. (1995) and Kattner (1999). This researchers, similarly observed that the higher the ratio between joint resistance and span moment $M_{j,pl}/M_{R,sagg}$, the smaller is the demand on joint rotation for the plastic distribution of moments.

In (Li et al., 2000) the relation between required joint rotation and the ratio $M_{j,pl}/M_{R,sagg}$ was established for different steel grades and beam slendernesses (cf. Figures 7.2, 7.3 and 7.4). The calculations assumed a full shear connection for the composite beams as well as a sagging moment $M_{R,sagg}$ equal to 95 % of the plastic moment capacity $M_{pl,sagg}$ of the composite beam using the stress-block method. This reduction in bending resistance is justified by the fact that the real strain limited bending resistance is smaller than the plastic moment capacity. From Figures 7.2 to 7.4 the following conclusions are drawn:

- The required joint rotations Φ_{req} are bigger for higher steel grades.
- For a simple composite joint with $M_{j,pl} = 0$ and S355 steel grade, the required joint rotation is about 55 mrad (cf. Figure 7.4). This finding demonstrates that the 80 mrad upper limit represents an over-conservative value within the range of application defined in (Li et al., 2000).
- The relationship between Φ_{req} and $M_{j,pl}/M_{R,sagg}$ is practically linear.
- At $M_{j,pl}/M_{R,sagg} = 1$, the required joint rotation is about 30 mrad for S355.

In (Kattner, 1999), the influence of partial shear connection, construction phase, ductility of the shear connectors as well as concrete strength were additionally investigated. Similarly to (Li et al., 2000), it was also found that the required joint rotation Φ_{req} decreases linearly as the ratio $M_{j,pl}/M_{R,sagg}$ increases. Besides, it was shown that for the same beam length, the required joint rotation Φ_{req} decreases with greater steel section. However, if the beam length is varied so as to obtain the same beam slenderness, the required joint rotation is comparable.

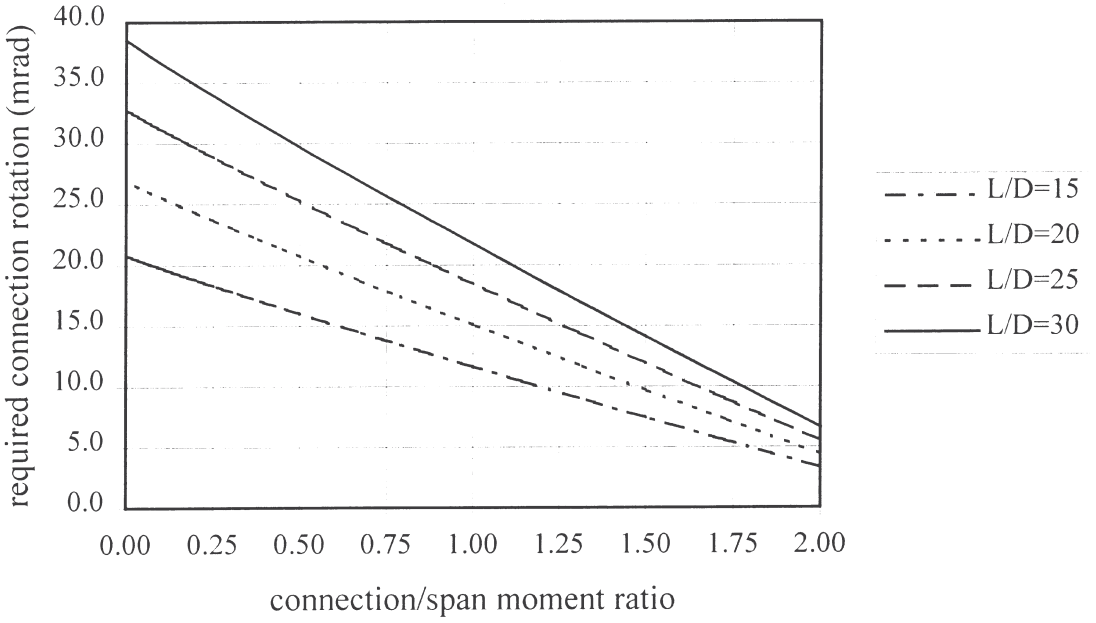

Figure 7.2: Required joint rotations for steel grade S235 (Li et al., 2000)

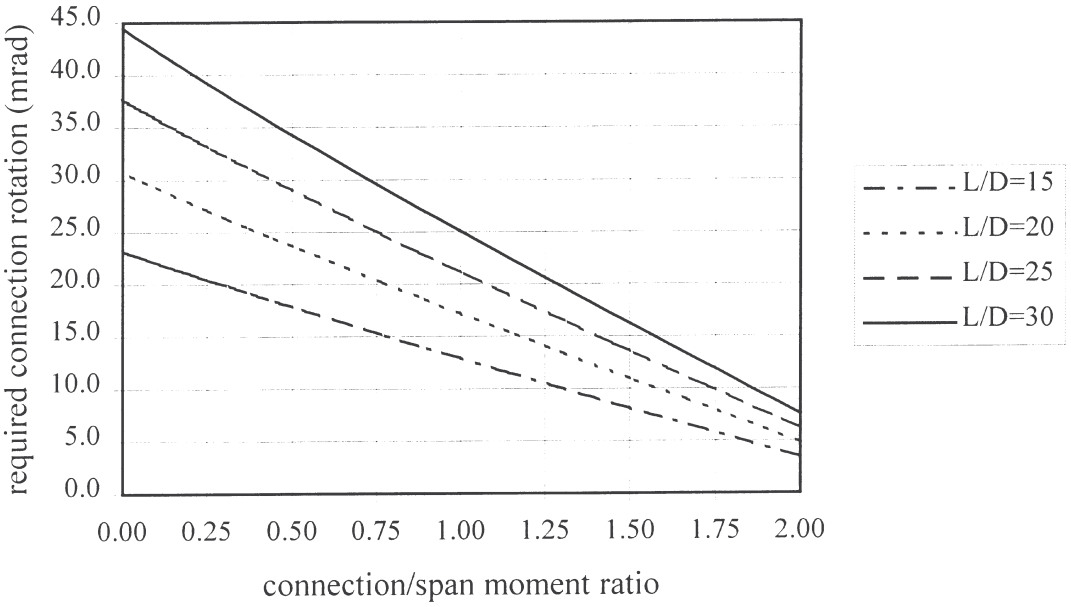

Figure 7.3: Required joint rotations for steel grade S275 (Li et al., 2000)

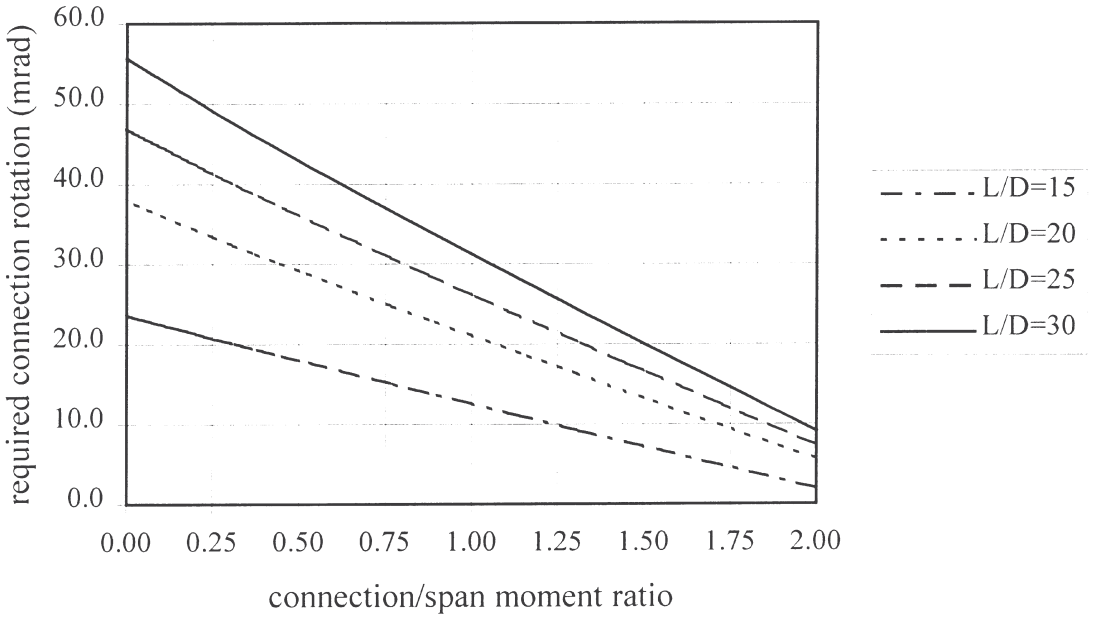

Figure 7.4: Required joint rotations for steel grade S355 (Li et al., 2000)

From the knowledge assembled with these investigations, a simplified method to estimate the required joint rotation is proposed in Figure 7.5. In this method the required joint rotation can be determined in function of the ratio between the joint resistance $M_{j,pl}$ and the span moment $M_{R,sagg}$. The following assumptions are made:

- At $M_{j,pl}/M_{R,sagg} = 0$ the required joint rotation is equal to 80 mrad.
  This proposal is safe-sided within the range of application defined in (Li et al., 2000), since the required joint rotation Φ_{req} is about 55 mrad (cf. Figure 7.4).
- At $M_{j,pl}/M_{R,sagg} = 1$ the required joint rotation is equal to 40 mrad.
  Similarly to above, a safe-sided assumption was made since according to (Li et al., 2000), the required joint rotation is less than 30 mrad.

As described earlier, different researchers concluded that the required joint rotation is linearly linked to the ratio $M_{j,pl}/M_{R,sagg}$. Thus, a linear relation between the values $M_{j,pl} = 0$ and $M_{j,pl} = M_{R,sagg}$ was assumed. The application of this simplified method is, however, subjected to the conditions of the range of application specified in (Li et al., 2000):

- uniformly distributed load
- steel grade not higher than S355
- full shear connection
- beam slenderness L/D $\leq$ 35
- equal joint configurations at each beam support
- I or H shape for steel section
- sagging moment resistance $M_{R,sagg}$ equal to the strain limited bending resistance or to 0.95 times the plastic bending capacity $M_{pl,sagg}$
- non-sway frames

As shown in Figure 7.6, the procedure proposed in this thesis is more severe than the ductility boundaries suggested by Huber (2000). Furthermore, it can be seen that the required joint rotations ensure a certain safety distance to the 30-50 mrad range defined by Nethercot et al. (1995). Thus, it can be asserted that within the range of applicability described above, this method is safe-sided and can be used to determine in a simple way the rotational requirements of composite joints in a structural frame.

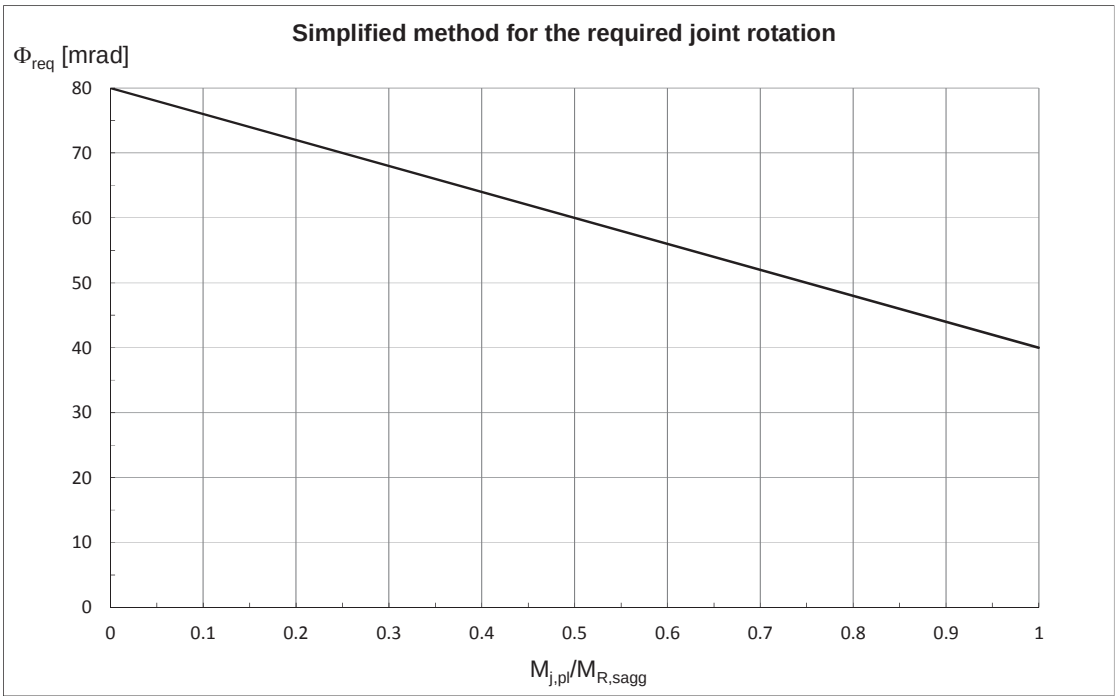

Figure 7.5: Proposed simplified method for required joint rotation Φ_{req}

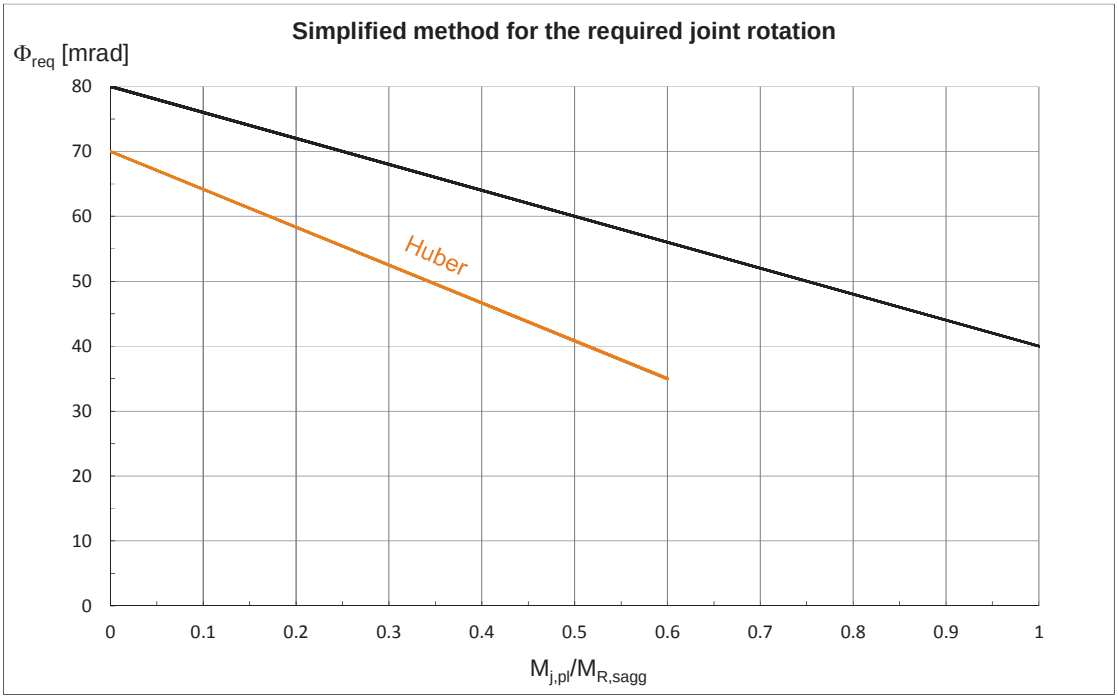

Figure 7.6: Comparison to ductility boundaries defined in (Huber, 2000)

7.4 Available joint rotation capacity

In Chapter 6, an method to calculate the available rotation capacity of composite joints was presented. The accuracy of this method was verified on the basis of experimental investigations fulfilling a defined set of conditions (cf. Section 6.3.5).

In order to ease the application of this analytical method, design charts assuming the characteristic concrete properties according to EN 1992-1-1 (2004) are given in this Section. Since only ductility class B was considered for the reinforcement the following characteristic properties have been assumed in concordance with EN 1992-1-1 (2004):

- $f_{syk} = 500N/mm^2$
- $\varepsilon_{su} = \varepsilon_{u,k} = 50‰$
- $E_s = 200000N/mm^2$

The **first step** of the analytical method consists in the determination of the ultimate ε_{smu} and yield strain limit ε_{smy} of the reinforced concrete component. As it was shown in Section 6.5, the tension stiffening effect plays a non-negligible role in the elongation capacity of this component. Hence, design charts to easily determine ε_{smy} and ε_{smu} are presented in Figure 7.7. These charts are given in function of concrete class and effective reinforcement ratio ρ_{eff}. In order to determine ε_{smu} and ε_{smy} with the help of these charts, the following steps must be followed:

1. Calculate the effective reinforcement ratio ρ_{eff} considering the effective area $A_{c,eff}$ of concrete around the longitudinal reinforcement according to EN 1992-1-1 (2004), Figure 7.1 (cf. Figure 6.13 in the present work) and derive the first stress crack σ_{sr1} with the upper chart in Figure 7.7.
2. Multiply the first crack stress σ_{sr1} obtained in the previous step by the factor k_b given in equation (6.46). This factor considers the linear stress distribution in the section prior to cracking. On this basis, determine the ultimate strain limit ε_{smu} of the reinforced concrete member with the inferior chart of Figure 7.7.
3. On the same chart, determine the yield strain limit ε_{smy} of the reinforced concrete member.

Alternatively, the yield and ultimate strain limits ε_{smy} and ε_{smu} can be calculated with the formulas given in Section 6.5.5. The explicit calculation of these values may be necessary when different material properties than those stated above for the reinforcement are provided.

In the **second step**, the effective joint length L_j according to equation (6.28) is calculated. The latter is given straightforward with the following expression:

$$L_j = \frac{h_c}{2} + n \cdot 2 \cdot \frac{\varnothing}{6.4 \cdot \rho_{eff}} \tag{7.2}$$

with:

$$n = \begin{cases} 1.5 & 1.0\% \leq \rho_{eff} \leq 1.6\% \\ 2.5 & 1.6\% < \rho_{eff} \leq 1.9\% \\ 3.5 & 1.9\% < \rho_{eff} \leq 2.2\% \\ 4.5 & 2.2\% < \rho_{eff} \leq 2.9\% \\ 5.5 & 2.9\% < \rho_{eff} \leq 3.5\% \end{cases} \tag{7.3}$$

In the **last step**, the rotation capacity of the joint is calculated with equation (7.4) by implementing the values obtained in the two previous steps.

$$\Phi_u = \left[\varepsilon_{smu} \cdot \frac{h_c}{2} + \frac{\varepsilon_{smu} + \varepsilon_{smy}}{2} \cdot (L_j - \frac{h_c}{2})\right] \cdot \frac{1}{h_r} \tag{7.4}$$

with:

h_c column depth

h_r internal lever arm between compression point and reinforcement layer

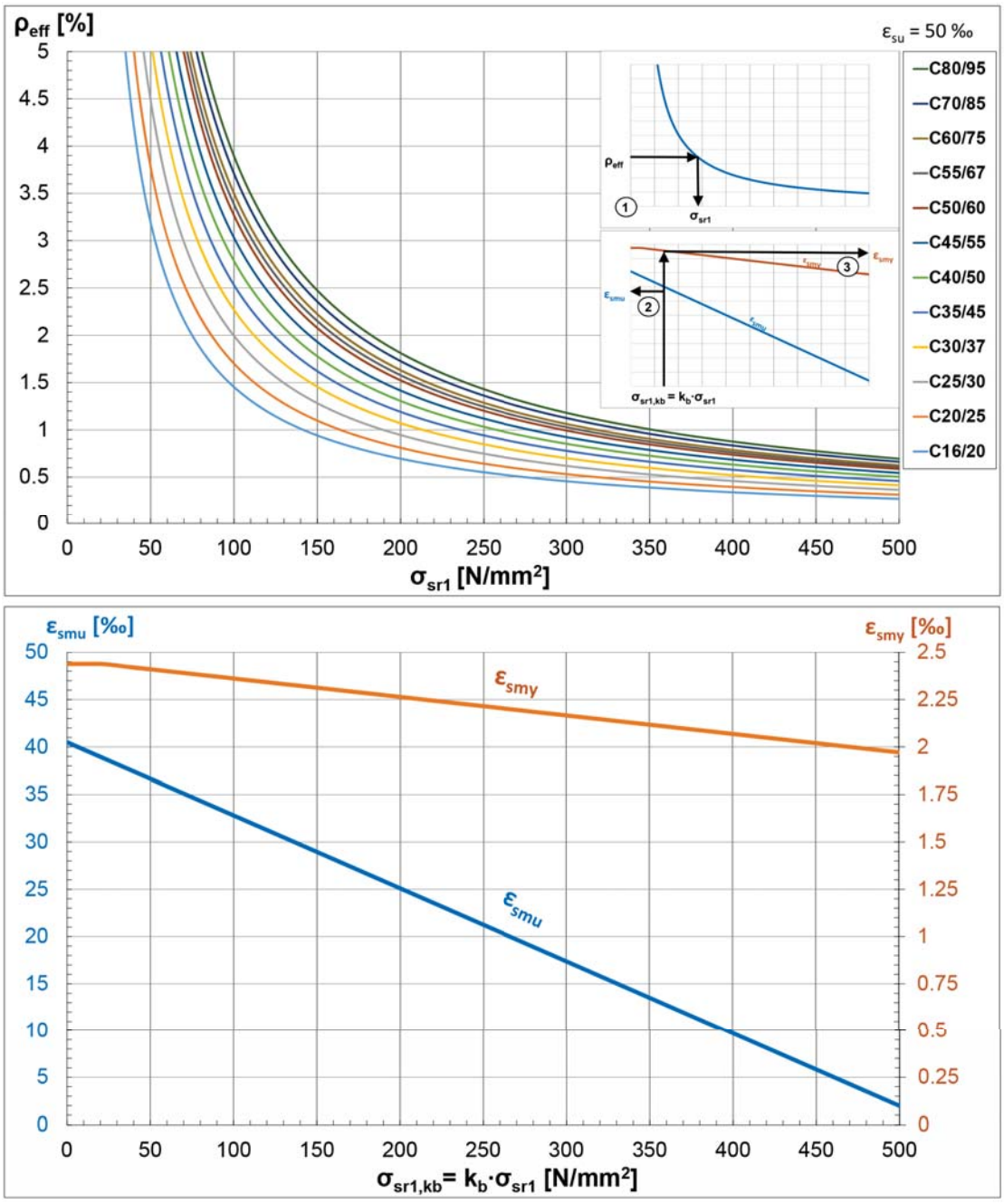

Figure 7.7: Design aids to determine ε_{smu} and ε_{smy} for the rotation capacity of composite joints

7.5 Simplified verification of joint without direct rotation analysis

The procedure described in the two previous sections allows to define a set of conditions, for which an explicit rotation verification of the joint is not necessary. These conditions can be interpreted as ductility requirements to fit in a newly defined **ductility class**.
The available rotation capacity Φ_u of a composite joint is always bigger than the required joint rotation Φ_{req} if the following ductility conditions are fulfilled:

- effective reinforcement ratio: 2.5 % $\leq \rho_{eff} \leq$ 3.5 %
- diameter of longitudinal reinforcement bar $\varnothing = 20$ mm
- ductility class B or C
- depth of column section $h_c \geq 30$ cm
- internal lever arm between reinforcement and compression $h_r \leq 40$ cm
- concrete class $\leq$ C50/60
- $k_b \leq 0.7$ or alternatively $z_{i,0} \leq d$
- $M_j \geq 0.5 \cdot M_{R,sagg}$

In addition, all the conditions specified in Section 6.5.6 must be verified in order to ensure the applicability of the analytical method for the rotation capacity. This simplified approach is furthermore subjugated to the conditions given in Section 7.3 allowing for the simple calculation of the required joint rotation.

7.6 Safety

The design verification proposed in equation (7.1) does not include any explicit safety factor because EN 1990 (2005) Annex D only provides guidance for the statistical determination of resistance models. Thus, no guidance is provided for models related to rigidity and ductility. Nevertheless, an indirect safety margin is included when determining the available rotation capacity Φ_u and the required joint rotation Φ_{req}.

The simplified method to determine the required joint rotation Φ_{req} presented in Figure 7.5 provides already a considerable safety margin to the real requirements. The values proposed in this method were intentionally raised in order to give a safe-sided approach.

As it was seen in the FE parametric study, the ultimate elongation ε_{su} of the bare reinforcement affects the available rotation capacity of composite joints. Assuming a smaller elongation ε_{su} than in reality leads to a reduced rotation capacity of composite joints. Yet, it must be stated that the characteristic values suggested by EN 1992-1-1 (2004) for reinforcing steel of class B are in principle too low in comparison to the real elongation capacity. To justify this statement, statistical evaluations of tensile tests performed on reinforcing steel have been explored in great detail. In (Comite Euro-International du Béton, 1993), Siviero and Russo exposed a statistical evaluation of tensile tests performed on B500 B reinforcement bars with different diameters. The outcome of this statistical evaluation is presented in Figure 7.8. As it can be seen, the mean value for the ultimate elongation is almost always above 10 % and the standard deviation is always smaller than 1 %. Assuming a typical normal (Gaussian) distribution for this quantity, the 5 %-fractile value would be bigger than 8 %, which is larger than the 5 % assumed by EN 1992-1-1 (2004).

In a more recent research project (Braconi et al., 2007), a similar statistical evaluation was carried out on the material properties of reinforcing steel B500 B on a big number of samples (cf. Figure 7.9). The measured ductility was even higher than in the previous statistics, which indicates again that a larger elongation capacity of B500 B rebars than that suggested by EN 1992-1-1 (2004) is in principle available. Besides, it should be added that in the earlier standard for rebars (DIN 488 Teil 1, 1984), the value suggested for ultimate elongation was of 10 %. From this observation, it results that calculating the rotation capacity of composite joints with the values proposed by EN 1992-1-1 (2004) can lead to the underestimation of the available rotation capacity. Thus, a large safety margin is also embedded in the calculation of Φ_u.

At the light of the statistical evaluation conducted in the two independent research projects, the 5 %-fractile value of the ultimate strain could be realistically estimated to 8 % without loss of significant safety. Such an estimation would relieve the two first ductility conditions allowing for the plastic analysis of semi-continuous composite beams:

- effective reinforcement ratio: 2.0 % $\leq \rho_{eff} \leq$ 3.5 %
- diameter of longitudinal reinforcement bar $\varnothing \geq 12$ mm

Following this approach, semi-continuous composite beams can be straightforwardly designed according to the plastic global analysis leading to better utilisation of the beam.

ϕ (mm)		8	10	12	14	16	18	20	22	24	26	28	30	32
	$\bar{X}$	0.32	0.36	0.42	0.39	0.48	0.47	0.50	0.49	0.51	0.54	0.57	0.60	0.64
ε_y	s	0.035	0.0216	0.033	0.031	0.100	0.02	0.02	0.02	0.010	0.021	0.29	0.018	0.21
	cv	0.11	0.06	0.08	0.08	0.21	0.06	0.04	0.05	0.02	0.04	0.51	0.03	0.33
	$\bar{X}$	12.39	11.83	10.07	10.65	12.95	9.40	10.40	10.20	13.18	12.46	10.67	13.26	11.48
ε_u	s	0.99	0.94	0.704	0.63	0.518	0.37	0.52	0.612	0.32	0.87	0.512	0.397	0.574
	cv	0.08	0.08	0.07	0.06	0.04	0.04	0.05	0.06	0.04	0.07	0.048	0.03	0.05

Figure 7.8: Statistical evaluation on the ductility of reinforcing steel by Siviero (Comite Euro-International du Béton, 1993)

A_{gt} (ε_{uk}) - Elongation at maximum load							
Diameter [mm]	Mean %	Standard Deviation %	10% percentile %	90% percentile %	Skewness	Curtosi	Sample Numerousness
14	16,15	1,80	13,80	18,60	-0,014	-0,377	1413
16	15,03	1,84	12,60	17,40	0,101	-0,348	2002
18	14,99	2,33	11,57	18,09	0,067	-0,525	88
20	16,52	1,72	14,20	18,70	-0,257	-0,047	2601
22	15,48	1,78	13,41	17,73	-0,123	-0,492	48
25	16,36	2,04	13,70	19,00	0,120	-0,211	2152

Figure 7.9: Statistical evaluation on the ductility of reinforcing steel (Braconi et al., 2007)

8 Conclusions

The structural properties of steel and concrete composite joints were studied in the present research. The **objectives** of this study were to:

1. Provide an analytical approach to assess the structural properties of composite joints, mainly focussing on the available rotation capacity,
2. Develop a method to ease the rotation verification at the joint, allowing the design of the structure according to the plastic global analysis.

The behaviour of beam-to-column composite joints was analysed with an **experimental test program**. This test program allowed to quantify the influence of the:

1. Reinforcement ratio ρ,
2. Diameter of reinforcement bars $\varnothing$ and
3. Bolted flush endplate connection,

on the structural properties of composite joints, namely stiffness S_j, resistance M_j and rotation capacity Φ_u. On the basis of the experimental observations, a new **analytical model** was developed, which realistically considers the influences of the above parameters. The accuracy of this new analytical formulation was confirmed by a set of experimental and numerical investigations conducted in the present and earlier research projects. To facilitate the application of this method, ready-to-use design charts were implemented according to the characteristic values suggested in Eurocode.

Furthermore, a **finite element model** capable of accurately replicating the behaviour of composite joints was elaborated in the present research. A close agreement between experimental and numerical moment-rotation curves was obtained with this FE model. Similarities in crack pattern, vertical deflection and deformation of individual joint components were also observed. Besides, additional numerical simulations with variable reinforcement ratio, rebar diameter and ductility of the reinforcing bars were carried out to investigate the behaviour of composite joints with other reinforcement properties than those tested in laboratory experiments.

A simplified and conservative method to determine the required joint rotation was deducted from the available literature. This method emerged from the congruent outcome of different researchers and can be applied within the range of validity defined in the present work. On this basis, a **ductility class** was defined in Section 7.5, which allows the plastic global analysis to be applied without direct rotation verification at the joint. This classification of composite joints in terms of ductility can be interpreted as the counterpart to the already existing classification system for cross-sections. It constitutes a simplified tool of which advantage can be taken, especially in the design of semi-continuous composite beams. For composite joints not fulfilling the simplified ductility conditions, a plastic global analysis can still be ensured by an explicit verification of the rotation at the joint. This requires the separate calculation of the available rotation capacity of the joint Φ_u and the required joint rotation Φ_{req}. A summarising flowchart for the design of composite joints is provided in Figure 8.1.

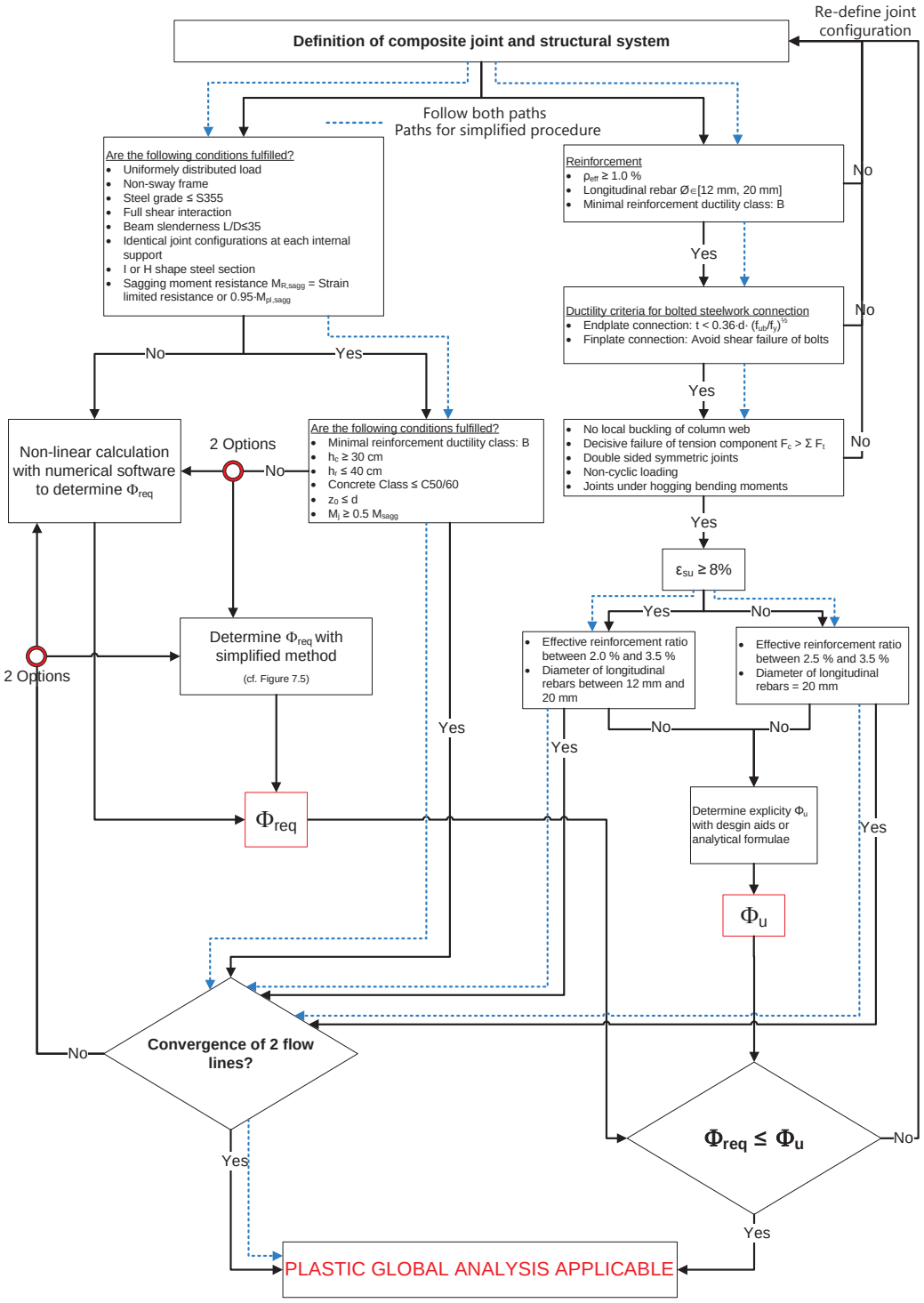

Figure 8.1: Summarizing flowchart on the procedure to verify the applicability of the plastic global analysis involving beam-to-column composite joints

9 Recommendations for further research

A lot has already been found by research on the particular behaviour of composite joints. However, more detailed investigation might be required for further optimization of the joint design. The following recommendations are proposed for further research:

1. The investigations on the required joint rotation carried out by most of the researchers were limited to S355 steel grade. It would be of interest to inquire the influence of higher steel grades on the required joint rotations. Higher concrete strength is an additional factor to be investigated.
2. The influence of higher steel or concrete grades on the structural properties of composite joints should also be examined in more detail.
3. As referred previously, a finite element model was developed and validated in the present study. Advantage could be taken of this model to perform an intensive parametric study to investigate characteristic aspects of composite joints. It is recommended to study the influence of following parameters:
    - type of steelwork connections, namely extended endplate and finplate connections
    - thickness of endplate and bolt diameter
    - degree of bolt preload
    - beam and column size
    - arrangement of longitudinal and transverse reinforcement bars
    - degree of shear connection
4. The finite element model could still be improved by implementing the longitudinal reinforcement bars as three-dimensional continuum elements and the exact consideration of bond-slip behaviour between reinforcement and surrounding concrete trough cohesive contact properties.
5. The characteristic value suggested by EN 1992-1-1 (2004) for the ultimate elongation of reinforcement of class B500 B seems to be too conservative in comparison to the elongation measured on tensile coupons of rebar samples (Braconi et al., 2007) and (Comite Euro-International du Béton, 1993). It is suggested to investigate the reliability of this value with a large set of tensile coupons allowing for an exhaustive statistical evaluation of this particular property. This investigation should consider different rebar diameters as well as origin of the rebars and manufacturing process. A standard testing procedure with equal sample sizes on identical testing equipment should be employed for a consistent comparison.
6. A reliability analysis should be performed on the design procedure proposed in the present work for the rotation verification at the joint.
7. A conclusive procedure for the required joint rotation should be developed for sway-frames and cyclic loading.
8. The behaviour of composite joints subjected to cyclic and unbalanced loading should be studied more deeply in order to derive a calculation method for the structural properties of composite joints.

Bibliography

Abaqus 6.14 (2014). *Online Documentation*. Dassault Systèmes.

Ahmed, B. and Nethercot, D. A. (1997). Prediction of initial stiffness and available rotation capacity of major axis composite flush endplate connections. *Journal of Constructional Steel Research*, 41(1):31–60.

Altmann, R., Maquoi, R., and Jaspart, J.-P. (1991). Experimental study on the non-linear behaviour of beam-to-column joints. *Journal of Constructional Steel Research*, 18.

American Institute of Steel Construction (1996). Partially Restrained Composite Connections.

Anderson, D., Aribert, J. M., and Kronenberger, H.-J. (1998). Rotation capacity of composite joints. In *Cost C1: Control of the semi-rigid behaviour of civil engineering structural connections*.

Anderson, D. and Najafi, A. A. (1994). Performance of composite connections: major axis end plate joints. *Journal of Constructional Steel Research*, 31:31–57.

Aribert, J. M. (1995). Influence of slip of the shear connection on composite joint behaviour. In *Connections in steel structures III: behaviour, strength, and design*.

Aribert, J. M. and Lachal, A. (1992). Experimental investigation of composite connection and global interpretation. In *COST C1 Workshop in Strasbourg*.

Ataei, A., Bradford, M. A., Valipour, H. R., and Liu, X. (2016). Experimental study of sustainable high strength steel flush end plate beam-to-column composite joints with deconstructable bolted shear connectors. *Engineering Structures*, 123:124–140.

Bakker, C. and Voorn, W. (1974). *Gelaste Hoekverbindingen in Raamweken*. Agon Elsevier.

Barcewicz, W. (2010). *Sztywność, nośność i zdolność do obrotu pewnej klasy węzłów w konstrukcjach stalowych ze stropami zespolonymi*. PhD thesis, Politechnika Warszawska.

Barcewicz, W. and Gizejowski, M. (2011). Evaluation of M-Phi characteristic of composite joints: Influence of the reinforcement on the behaviour if steel concrete joints. In *Eurosteel 2011: 6th European Conference on Steel and Composite Structures*, Budapest, Hungary.

Barnard, P. R. (1970). Innovations of composite floor systems: Canadian structural engineering conference.

Benussi, F., Pushali, R., and Zandonini, R. (1986). Experimental analysis of semi-rigid connections in composite frames. In *Proceedings of International Conference on Steel structures*, Buvda, Yugoslavia.

Bergner, H. (1997). *Rissbreitenbeschränkung zwangbeanspruchter Bauteile aus hochfestem Normalbeton*. PhD thesis, Technische Hochschule Darmstadt, Darmstadt.

Bode, H. and Kronenberger, H.-J. (1996). Behaviour of composite joints and their influence on semi-continuous composite beams. In *Composite Construction in Steel and Concrete III*. American Institute of Steel Construction.

Bode, H. and Kronenberger, H.-J. (1998). Zum Einfluß teiltragfähiger, verformbarer Verbundanschlüsse auf das Tragverhalten von Verbundträgern. *Stahlbau*, 67(Heft 7).

Bode, H., Michaeli, W., Sedlacek, G., and Müller, C. (1997). Forschungsbericht P 237/A 86: Weiterentwicklung der Bemessungsregeln von Anschlüssen im Stahl- und Verbundbau zur

Verbesserung der Wirtschaftlichkeit.

Braconi, A., Degee, H., Finetto, M., Oppe, M., Osta, A., Rinaldi, V., and Salvatore, W. (2007). Optimizing the seismic performance of steel and steel-concrete structures by standardizing material quality control: Six-Monthly Report.

Braun, M., Hechler, O., and Obiala, R. (2014a). Untersuchungen zur Verbundwirkung von Betondübeln. *Stahlbau*, 83(5):302–308.

Braun, M., Obiala, R., Odenbreit, C., and Hechler, O. (2014b). COSFB - Design and application of a new generation of slim-floor construction. In *Eurosteel 2014: 7th European Conference on Steel and Composite Structures*, Napoli, Italy.

Brown, N. and Anderson, D. (2001). Structural properties of composite major axis end plate connections. *Journal of Constructional Steel Research*, 57(3):327–349.

Climenhaga, J. J. and Johnson, R. P. (1972). Local buckling in continuous composite beams. *Structural Engineer*, 50(9).

Comite Euro-International du Béton (1993). Bulletin 218: Ductility of Reinforcement.

Comite Euro-International du Béton (2010). Model Code for Concrete Structures 2010.

Cornelissen, H. A., Hordijk, D., and Reinhardt, H. W. (1986). Experimental determination of crack softening characteristics of normalweight and lightweight concrete. *HERON*, 31(2).

Cost C1 (1996). Semi-rigid behaviour of civil engineering structural connections: Composite steel-concrete joints in braced frames for buildings.

Couchman, G. (1994). *Design of Continuous Composite Beams Allowing for Rotation Capacity*. PhD thesis, École Polytechnique Fédérale de Lausanne, Lausanne.

Da Silva, L. S., Simões, R., and Cruz, P. (2001). Experimental behaviour of end-plate beam-to-column composite joints under monotonical loading. *Engineering Structures*, 23.

Dabaon, M. A., El-Boghdadi, M. H., and Kharoob, O. F. (2009). Experimental and numerical model for space steel and composite semi-rigid joints. *Journal of Constructional Steel Research*, 65(8-9):1864–1875.

Davison, B., Lam, D., and Nethercot, D. A. (1990). Semi-rigid action of composite joints. *The Structural Engineer*, 68.

DIBt - Deutsche Institut für Bautechnik (2014). Allgemeine bauaufsichtliche Zulassung für den CoSFB-Betondübel.

DIN 488 Teil 1 (1984). Betonstahl: Sorten, Eigenschaften, Kennzeichen.

Duarte da Costa, J., Braun, M., Obiala, R., and Odenbreit, C. (2017). Design of single-span beams for SLS and ULS using semi-continuous beam-to-column joints: Part 2: Composite beams with variable bending stiffness and joints according to EN 1993-1-8. *Steel Construction*, 10(2):93–114.

Echeta, C. B. (1982). *Semi-rigid connections between concrete filled steel columns and composite beams*. PhD thesis, University of London, London.

Elz, S. (2000). *Untersuchungen zum Riß- und Tragverhalten des Betongurtes von Verbundträgern im negativen Momentbereich*. PhD thesis, Universität Kaiserslautern, Kaiserslautern.

EN 14399-4 (2005). High-strength structural bolting assemblies for preloading - Part 4: System HV - Hexagon bolt and nut assemblies.

EN 1990 (2005). Eurocode: Basis of structural design.

EN 1992-1-1 (2004). Eurocode 2: Design of concrete structures - Part 1-1: General rules and rules for buildings.

EN 1993-1-1 (2005). Eurocode 3: Design of steel structures - Part 1-1: General rules and rules for buildings.

EN 1993-1-8 (2005). Eurocode 3: Design of steel structures - Part 1-8: Design of joints.

EN 1994-1-1 (2004). Eurocode 4: Design of composite steel and concrete structures - Part 1-1: General rules and rules for buildings.

European Convention for Constructional Steelwork (1999). Design of composite joints for buildings.

Fischer, A. (1993). *Modelluntersuchungen zur Ermittlung des Rissabstandes dicker Bauteile aus Stahlbeton*. PhD thesis, Technische Hochschule Darmstadt, Darmstadt.

Fu, F. and Lam, D. (2006). Experimental study on semi-rigid composite joints with steel beams and precast hollowcore slabs. *Journal of Constructional Steel Research*, 62(8):771–782.

Fu, F., Lam, D., and Ye, J. (2008). Modelling semi-rigid composite joints with precast hollowcore slabs in hogging moment region. *Journal of Constructional Steel Research*, 64(12):1408–1419.

Gil, B. and Bayo, E. (2008a). An alternative design for internal and external semi-rigid composite joints. Part I: Experimental research. *Engineering Structures*, 30(1):218–231.

Gil, B. and Bayo, E. (2008b). An alternative design for internal and external semi-rigid composite joints. Part II: Finite element modelling and analytical study. *Engineering Structures*, 30(1):232–246.

Hahn, C. (2009). *Zur Rotationskapazität von Verbundanschlüssen bei der Bemessung nach dem Fliessgelenkverfahren*. PhD thesis, University of Luxembourg, Luxembourg.

Hanswille, G. (1986). *Zur Rissbreitenbeschrankung bei Verbundtragern*. PhD thesis, Ruhr-Universität Bochum, Bochum.

Henriques, J. A. (2013). *Behaviour of joints: simple and efficient steel-to-concrete joints*. PhD thesis, Universidade de Coimbra, Coimbra.

Hillerborg, A. (1985). The theoretical basis of a method to determine the fracture energy GF of concrete. *Materials and Structures*, 18(4).

Hillerborg, A., Modeer, M., and Petersson, P.-E. (1976). Analysis of crack formation and crack growth in concrete by means of fracture mechanics and finite elements. *Cement and Concrete Research*, 6.

Huber, G. (2000). *Non-Linear Calculations of Composite Sections & Semi-Continuous Joints*. Ernst & Sohn.

ISO 898-1 (2009). Mechanical properties of fasteners made of carbon steel and alloy steel - Part 1: Bolts, screws and studs with specified property classes — Coarse thread and fine pitch thread.

Jaspart, J.-P. (1991). *Etude de la semi-rigidité des noeuds poutre-colonne et son influence sur la résistance et la stabilité des ossatures en acier*. PhD thesis, Université de Liège, Liège.

Johnson, R. P. and Hope-Gill, M. (1972). Semi-rigid joints in composite frames.

Johnson, R. P., Van Dalen, K., and Kemp, A. R. (1966). Ultimate strength of continuous composite beams: British Construction Steelwork Association, Conference on Structural Steel, London.

Jones, S. W., Kirby, P. A., and Nethercot, D. A. (1983). The Analysis of Frames with Semi-Rigid Connections - A state of the Art Report. *Journal of Constructional Steel Research*, 3(2).

Kathage, K. (1994). *Beitrag zur plastischen Bemessung durchlaufender Verbundträger mit Verbundanschlüssen*. PhD thesis, Ruhr-Universität Bochum, Bochum.

Kattner, M. (1999). *Beitrag zum Entwurf von Rahmen mit Verbundknoten im Hochbau*. PhD thesis, École Polytechnique Fédérale de Lausanne.

Kmiecik, P. and Kaminski, M. (2011). Modelling of reinforced concrete structures and composite structures with concrete strength degradation taken into consideration. *Archives of Civil and Mechanical Engineering*, 11(3):623–636.

König, G. and Tue, N. V. (1996). Grundlagen und Bemessungshilfen für die Rißbreitenbeschränkung im Stahlbeton und Spannbeton. Heft 466.

Kreller, H. (1989). *Zum nichtlinearen Trag- und Verformungsverhalten von Stahlbetonstabtragwerken unter Last- und Zwangseinwirkung*. PhD thesis, Universität Stuttgart, Stuttgart.

Law, C. (1983). *Planar no-sway frames with semi-rigid beam-to-column joints*. PhD thesis, University of Warwick.

Leon, R. and Lin, J. (1986). Towards the development of an analytical model for composite semi-rigid connections. *Structural Engineer*, 86.

Leonhardt, F. (1978). *Vorlesungen über Massivbau: Nachweis der Gebrauchstrauglichkeit*.

Li, T. Q., Choo, B. S., and Nethercot, D. A. (1995a). Connection element method for the analysis of semi-rigid frames. *Journal of Constructional Steel Research*, 32(2):143–171.

Li, T. Q., Choo, B. S., and Nethercot, D. A. (1995b). Determination of rotation capacity requirements for steel and composite beams. *Journal of Constructional Steel Research*, 32(3):303–332.

Li, T. Q., Nethercot, D. A., and Choo, B. S. (1996). Behaviour of flush end-plate composite connections with unbalanced moment and variable shear/moment ratios: I. Experimental behaviour. *Journal of Constructional Steel Research*, 38(2).

Li, T. Q., Nethercot, D. A., and Lawson, R. M. (2000). Required rotation of composite connections. *Journal of Constructional Steel Research*, 56(2):151–173.

Loh, H. Y., Uy, B., and Bradford, M. A. (2006a). The effects of partial shear connection in composite flush end plate joints Part I — experimental study. *Journal of Constructional Steel Research*, 62(4):378–390.

Loh, H. Y., Uy, B., and Bradford, M. A. (2006b). The effects of partial shear connection in composite flush end plate joints Part II—Analytical study and design appraisal. *Journal of Constructional Steel Research*, 62(4):391–412.

Malaska, M. (2000). *Behaviour of a semi-continuous beam-column connection for composite slim floors*. PhD thesis, Helsinki University of Technology, Espoo.

Maquoi, R. and Chabrolin, B. (1998). Frame design including joint behaviour Report: Final Report.

Najafi, A. A. (1992). *End plate connections and their influence on steel and composite structures*. PhD thesis, University of Warwick.

Nethercot, D. A. (1995). Semirigid joint action and the design of nonsway composite frames. *Engineering Structures*, 17(8).

Nethercot, D. A., Li, T. Q., and Choo, B. S. (1995). Required rotations and moment redistribution for composite frames and continuous beams. *Journal of Constructional Steel Research*, 35(2):121–163.

Odenbreit, C. (2000). *Zur Ermittlung der Tragfähigkeiten, der Steifigkeiten und der Schnittgrößen von Verbundträgern mit halbsteifen, teiltragfähigen Verbundanschlüssen*. PhD thesis, Universität Kaiserslautern, Kaiserslautern.

Odenbreit, C., Hahn, C., and Jaspart, J.-P. (2009). Untersuchungen über das Trag- und Dehnungsverhalten des Betongurtes bei Verbundanschlüssen. *Stahlbau*, 78(1):35–41.

Piluso, V., Rizzano, G., and Tolone, I. (2012). An advanced mechanical model for composite connections under hogging/sagging moments. *Journal of Constructional Steel Research*, 72:35–50.

Qureshi, J., Lam, D., and Ye, J. (2011). Effect of shear connector spacing and layout on the shear connector capacity in composite beams. *Journal of Constructional Steel Research*, 67(4):706–719.

Ren, P. (1995). *Numerical Modelling and experimental analysis of steel beam-to-column connections allowing for the influence of reinforced composite slabs*. PhD thesis, École Polytechnique Fédérale de Lausanne.

Renner, A. (2015). *Zug-Abscher-Interaktion bei Schrauben im Stahlbau*. PhD thesis, Technische Universität Darmstadt, Darmstadt.

Schäfer, M. (2005). *Zum Rotationsnachweis teiltragfähiger Verbundknoten in verschieblichen Verbundrahmen*. PhD thesis, Universität Stuttgart, Stuttgart.

Schäfer, M. (2017). Limits of plastic design for composite beams: Requirements for slim and compact composite sections. In *Eurosteel 2017: 8th European Conference on Steel and Composite Structures*, Copenhagen, Denmark.

Schober, H. (1984). *Ein Modell zur Berechnung des Verbundes und der Risse im Stahl- und Spannbeton*. PhD thesis, Universität Stuttgart, Stuttgart.

Simões, R. (2000). *Comportamento de ligações mistas viga-pilar sob acções estáticas e cíclicas*. PhD thesis, Universidade de Coimbra, Coimbra.

Steel Construction Institute (1998). Joints in steel construction composite connection P213.

Steurer, A. (1996). *Trag- und Verformungsverhalten von auf Zug beanspruchten Schrauben*. PhD thesis, ETH Zürich, Zürich.

Van Dalen, K. and Godoy, H. (1982). Strength and rotational behaviour of composite beam-to-column connections. *Canadian Journal of Civil Engineering*, 9.

Vasdravellis, G., Valente, M., and Castiglioni, C. A. (2009). Behavior of exterior partial-strength composite beam-to-column connections: Experimental study and numerical simulations. *Journal of Constructional Steel Research*, 65(1):23–35.

Xiao, Y., Choo, B. S., and Nethercot, D. A. (1994). Composite connections in steel and concrete. I. Experimental behaviour of composite beam—Column connections. *Journal of Constructional Steel Research*, 31(1):3–30.

Xiao, Y., Choo, B. S., and Nethercot, D. A. (1996). Composite Connections in Steel and Concrete: Part 2- Moment Capacity of End Plate Beam to Column Connections. *Journal of Constructional Steel Research*, 37(1).

Zandonini, R. (1989). Semi-rigid composite joints: Stability and Strength: Structural Connections. *Elsevier Applied Science*.

Appendices

A Technical drawings of the test specimens

A.1 Steel parts

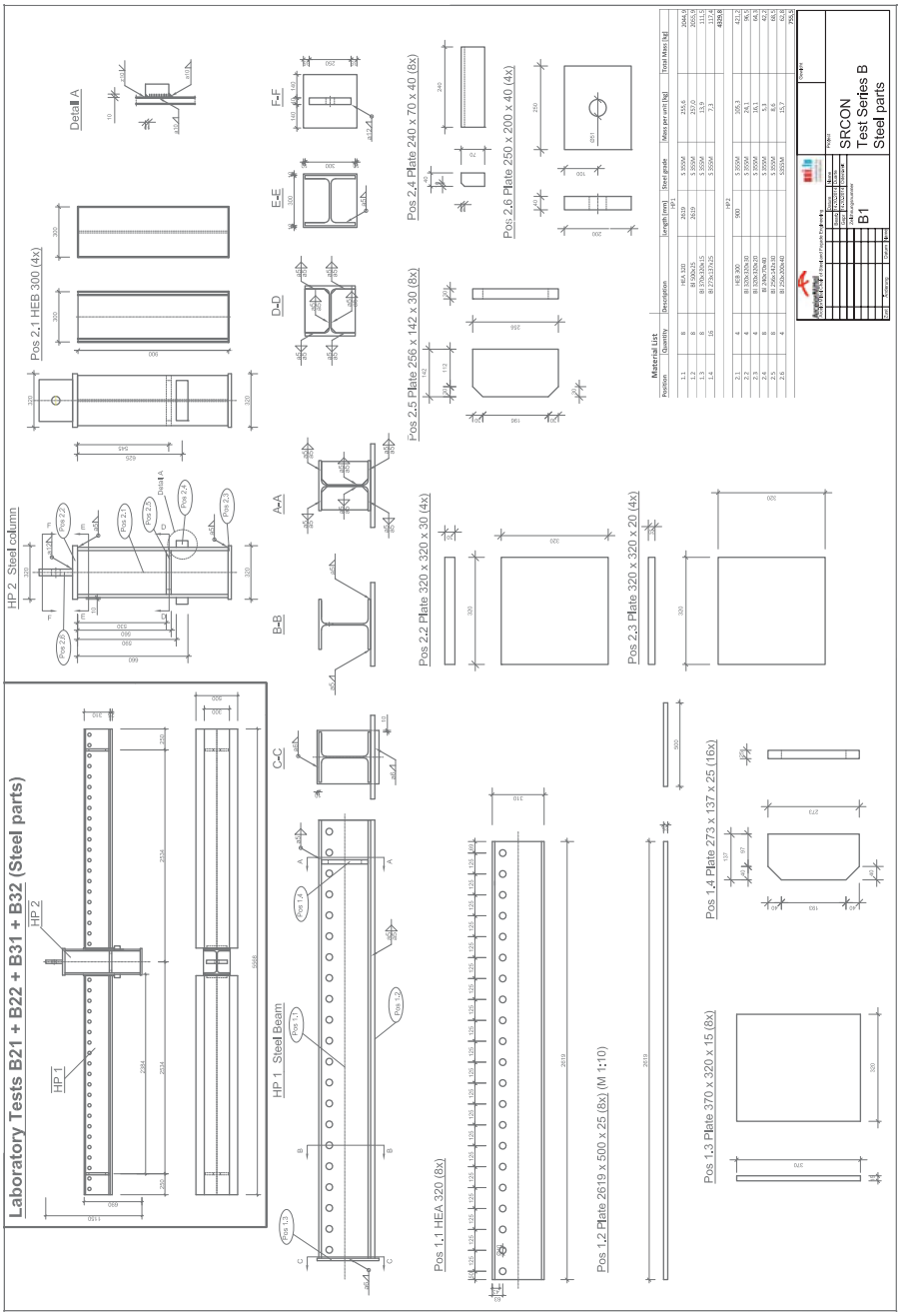

Figure A.1: Steel parts Series B

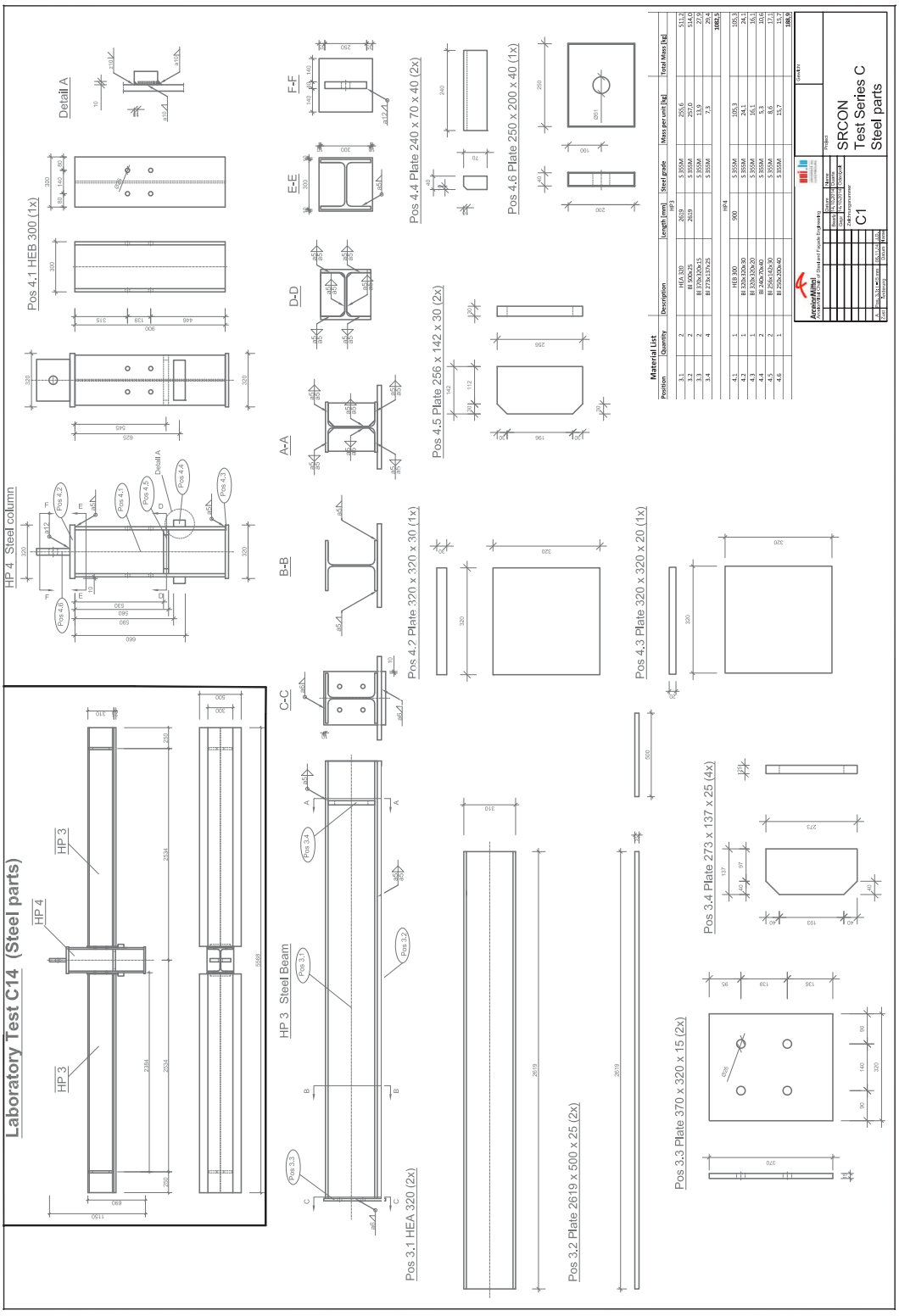

Figure A.2: Steel parts Series C

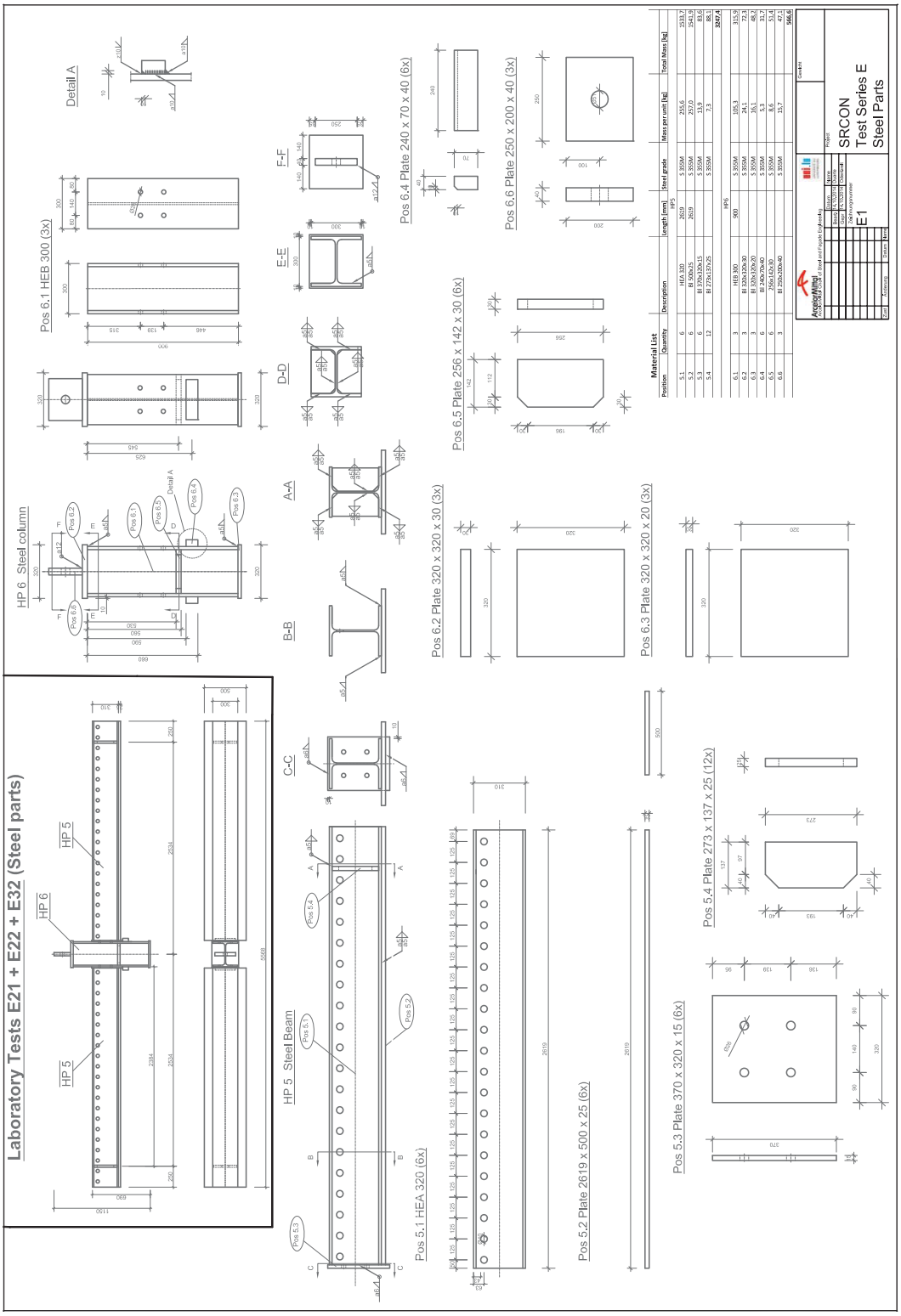

Figure A.3: Steel parts Series E

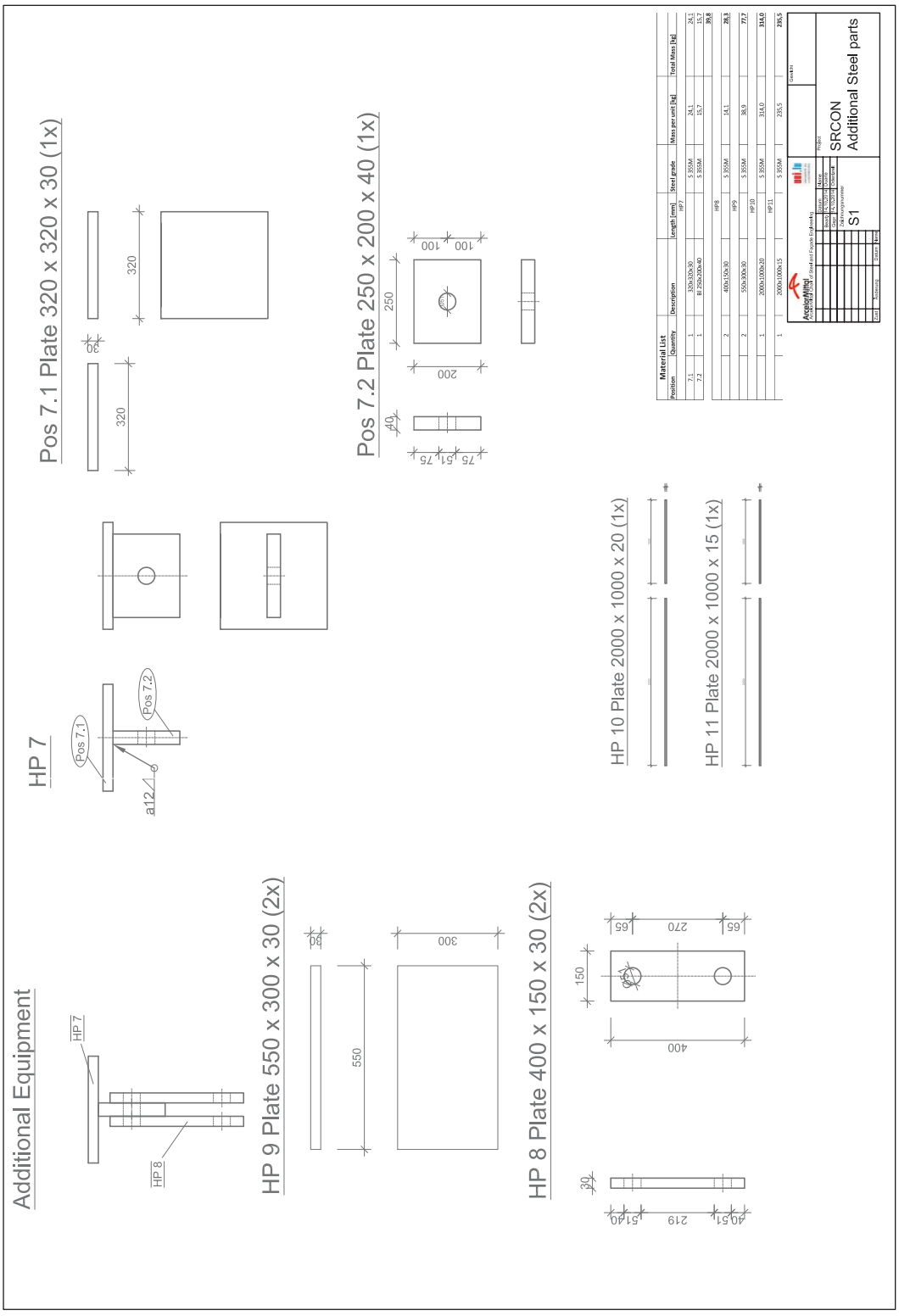

Figure A.4: Additional Steel parts

A.2 Reinforcement plans

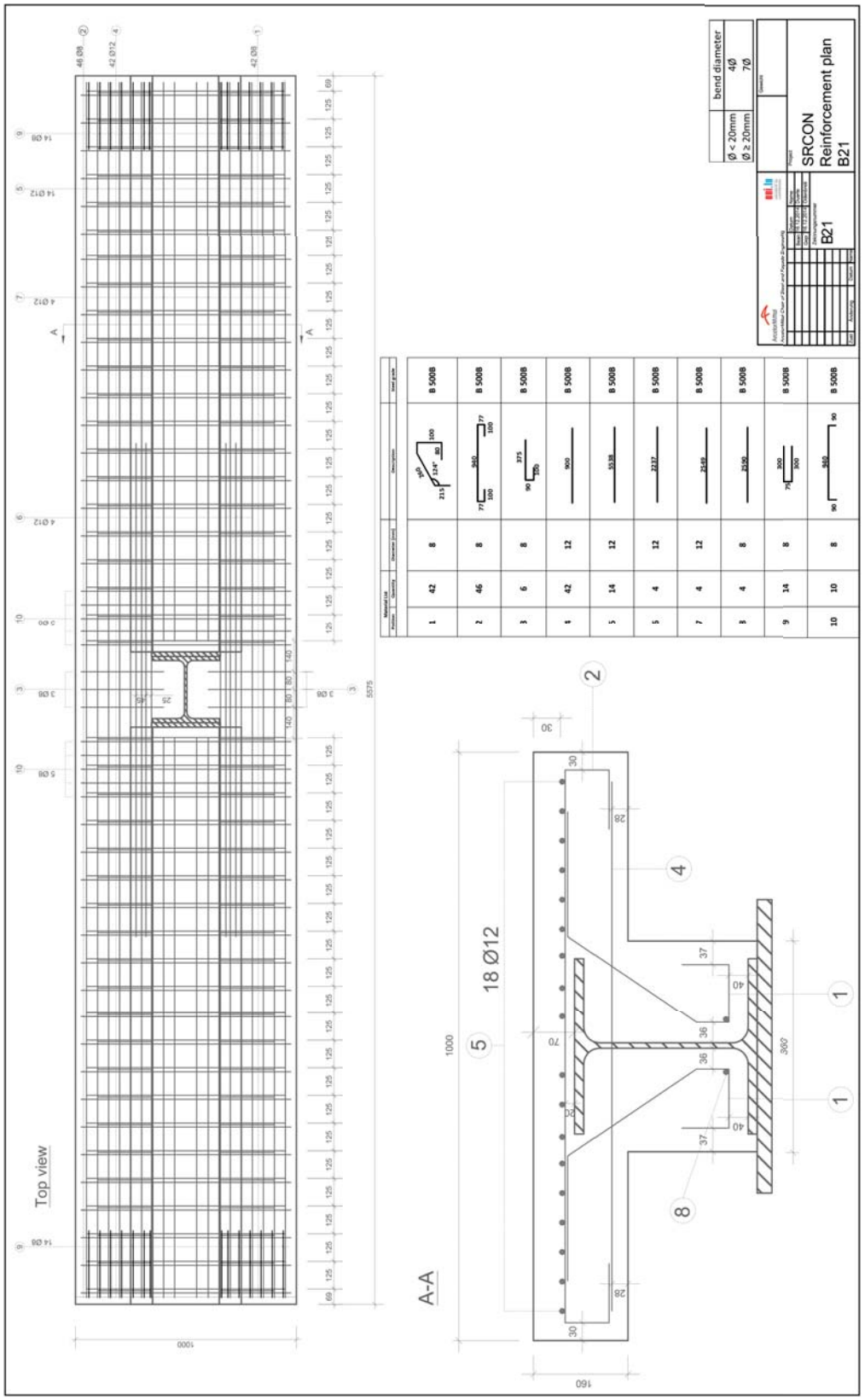

Figure A.5: B21: Reinforcement plan

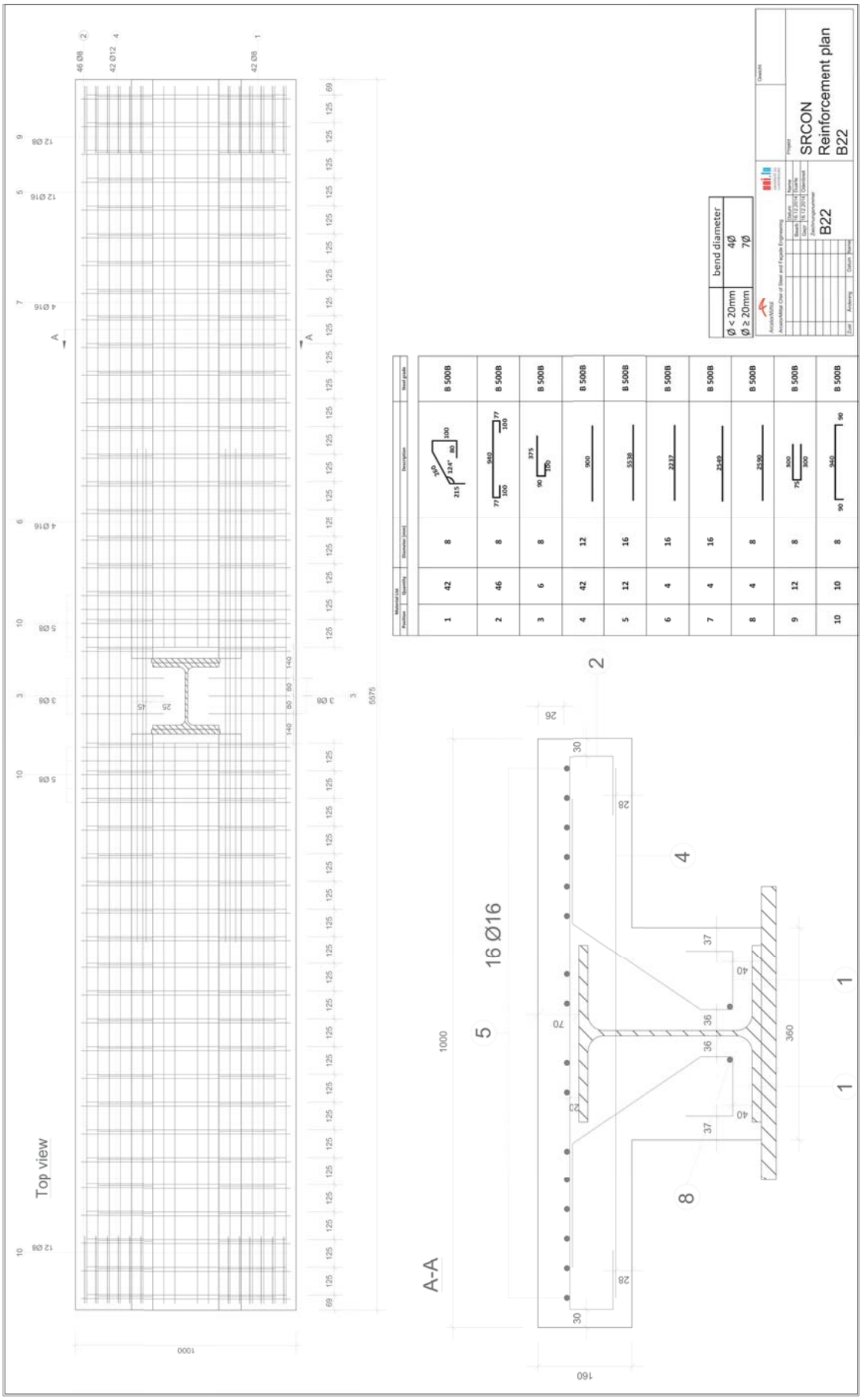

Figure A.6: B22: Reinforcement plan

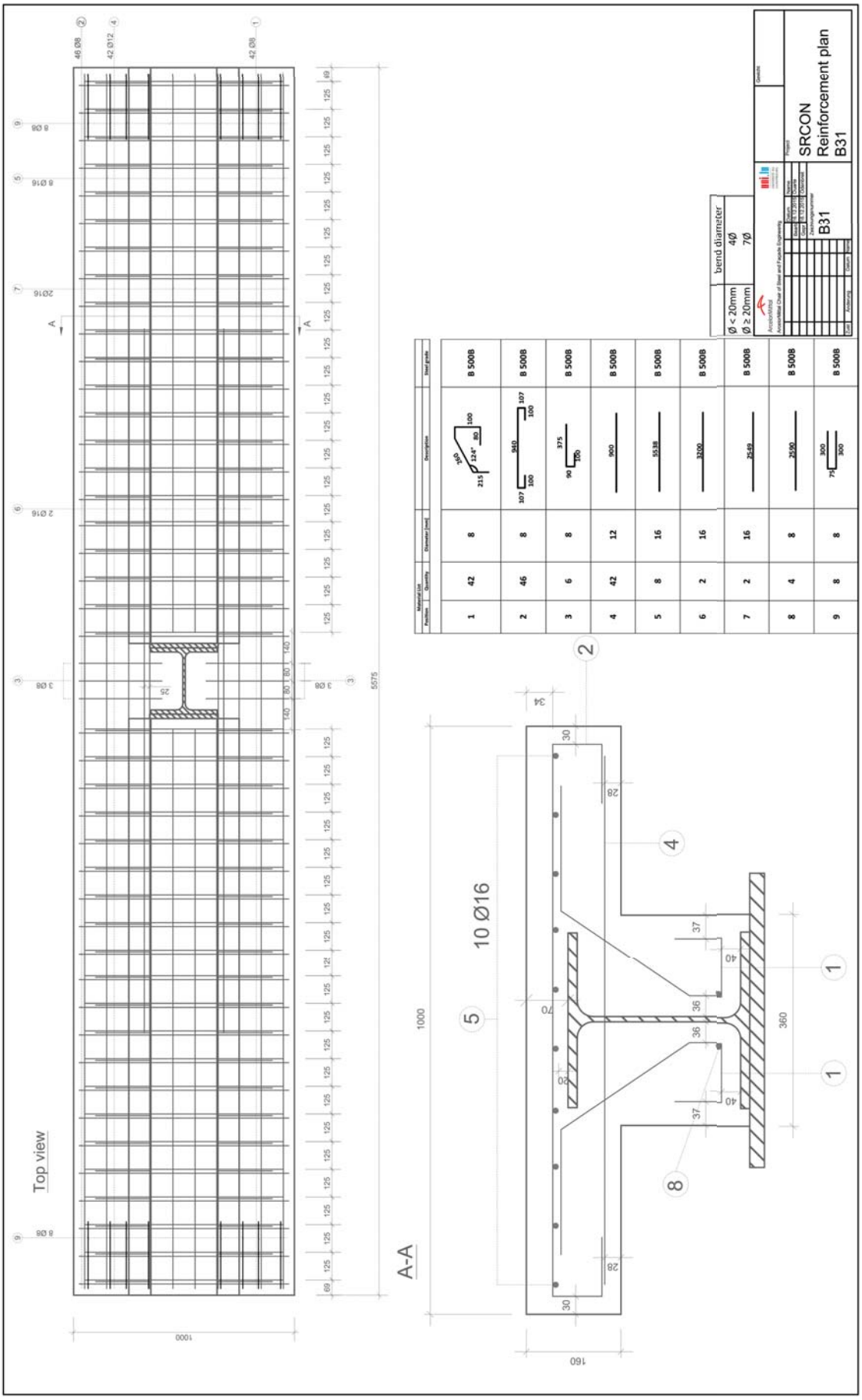

Figure A.7: B31: Reinforcement plan

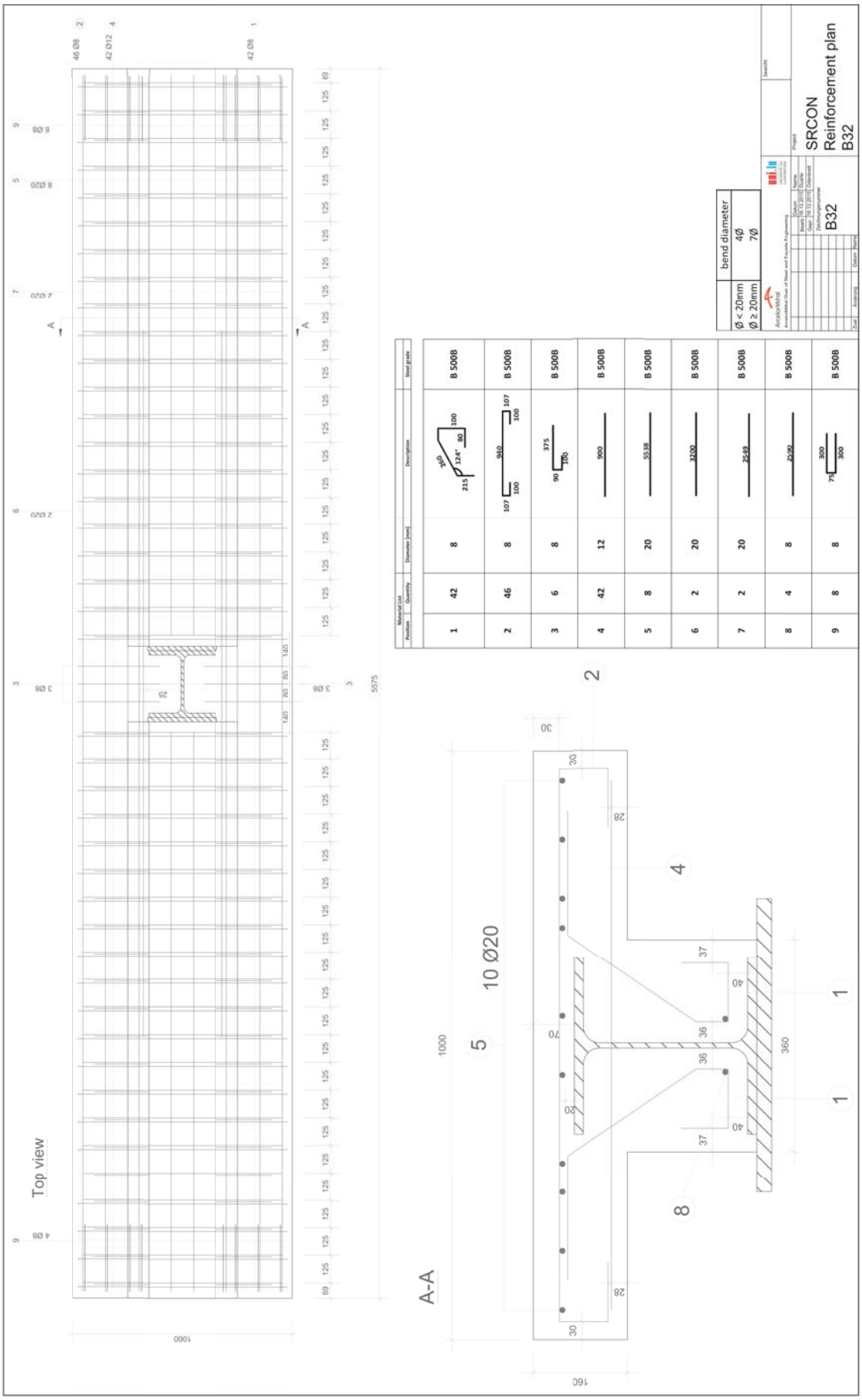

Figure A.8: B32: Reinforcement plan

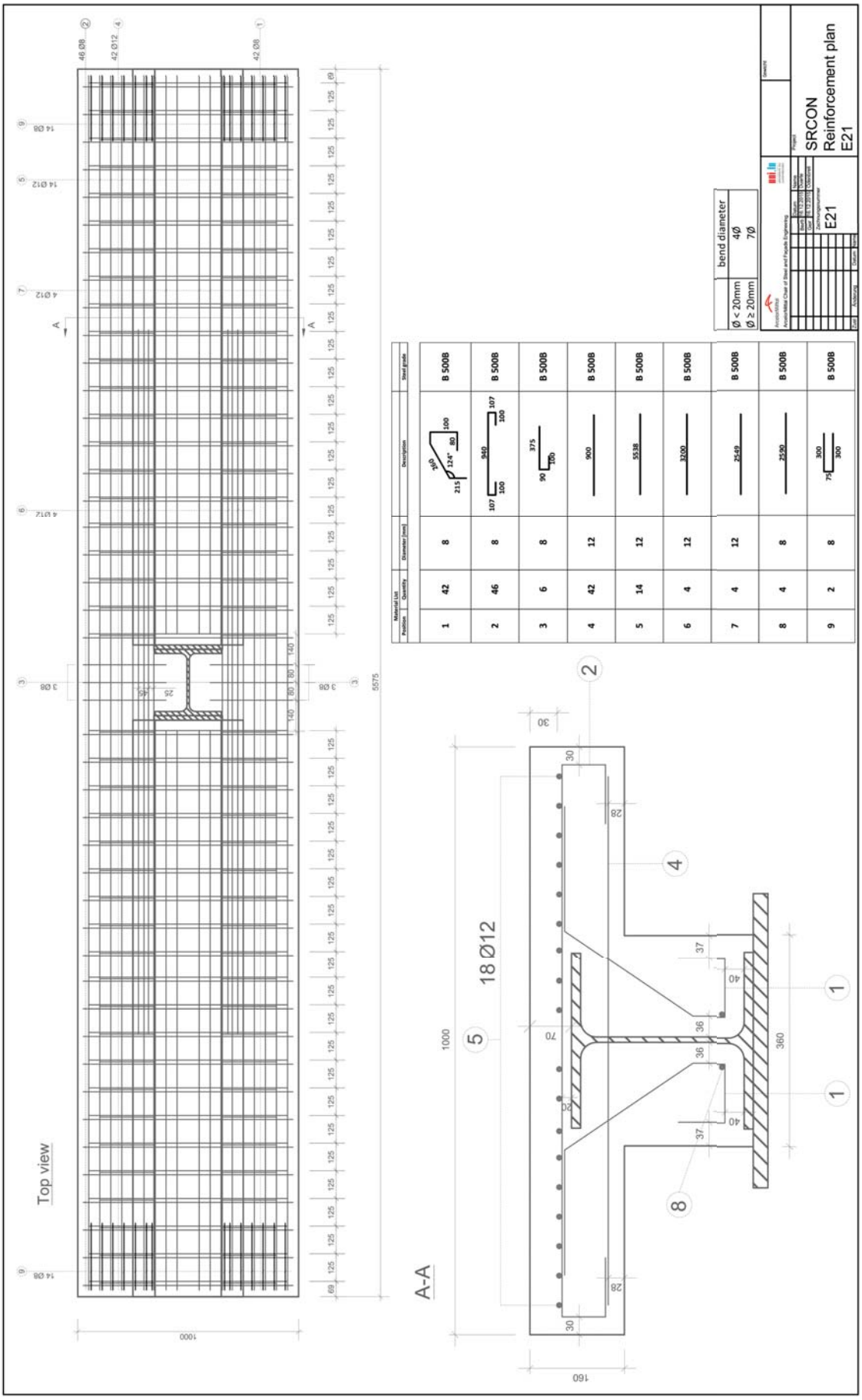

Figure A.9: E21: Reinforcement plan

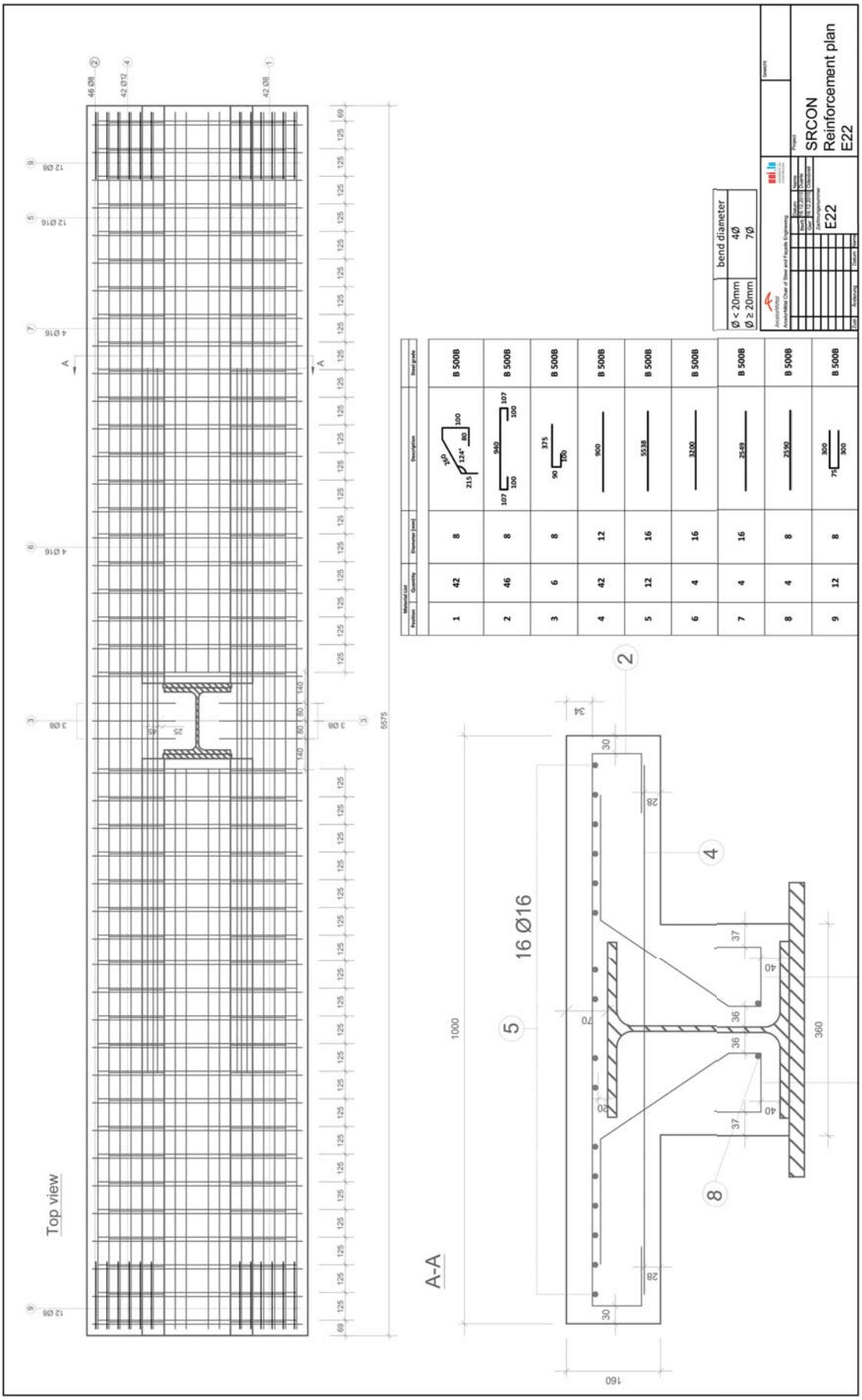

Figure A.10: E22: Reinforcement plan

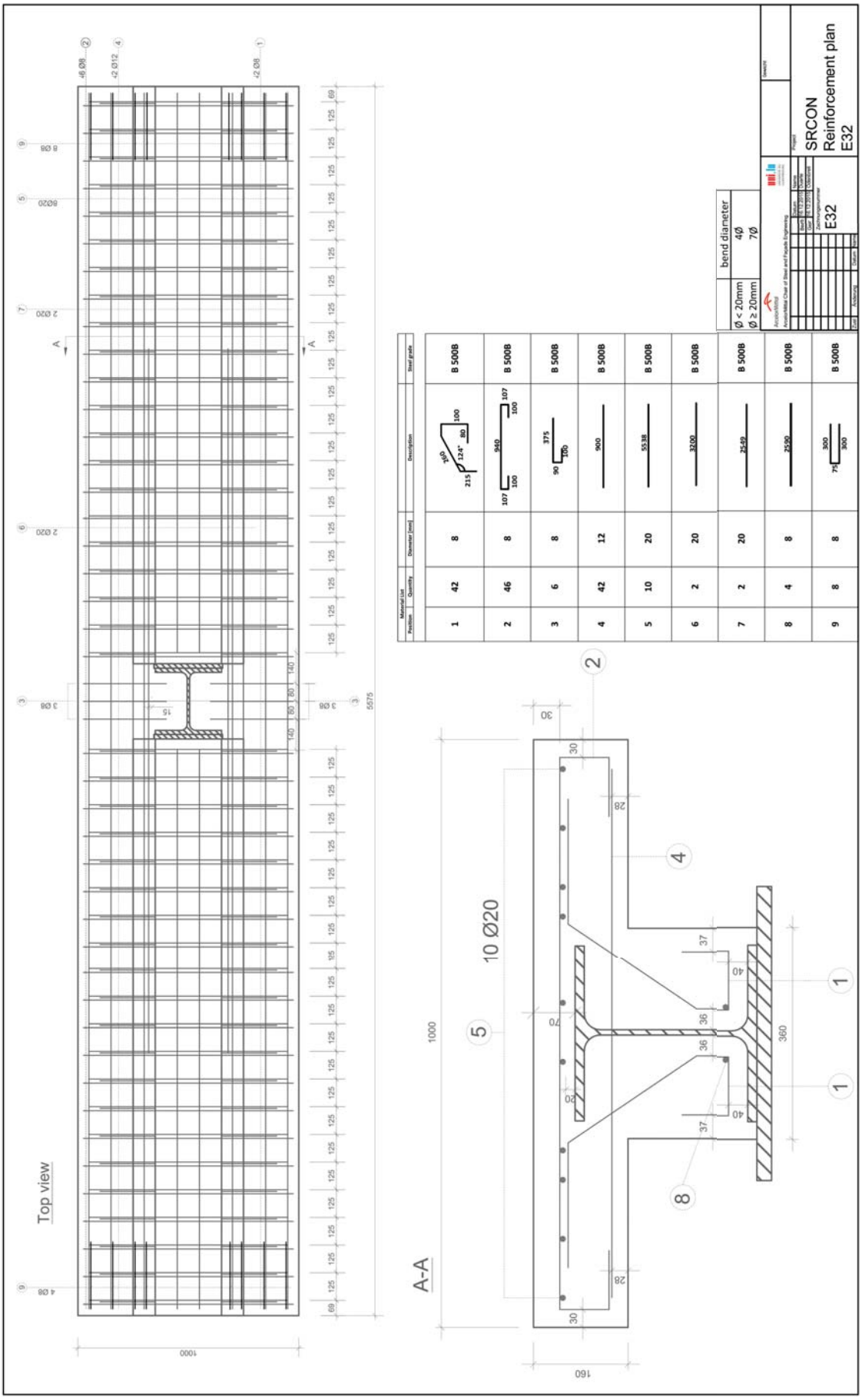

Figure A.11: E32: Reinforcement plan

A.3 Instrumentation plans

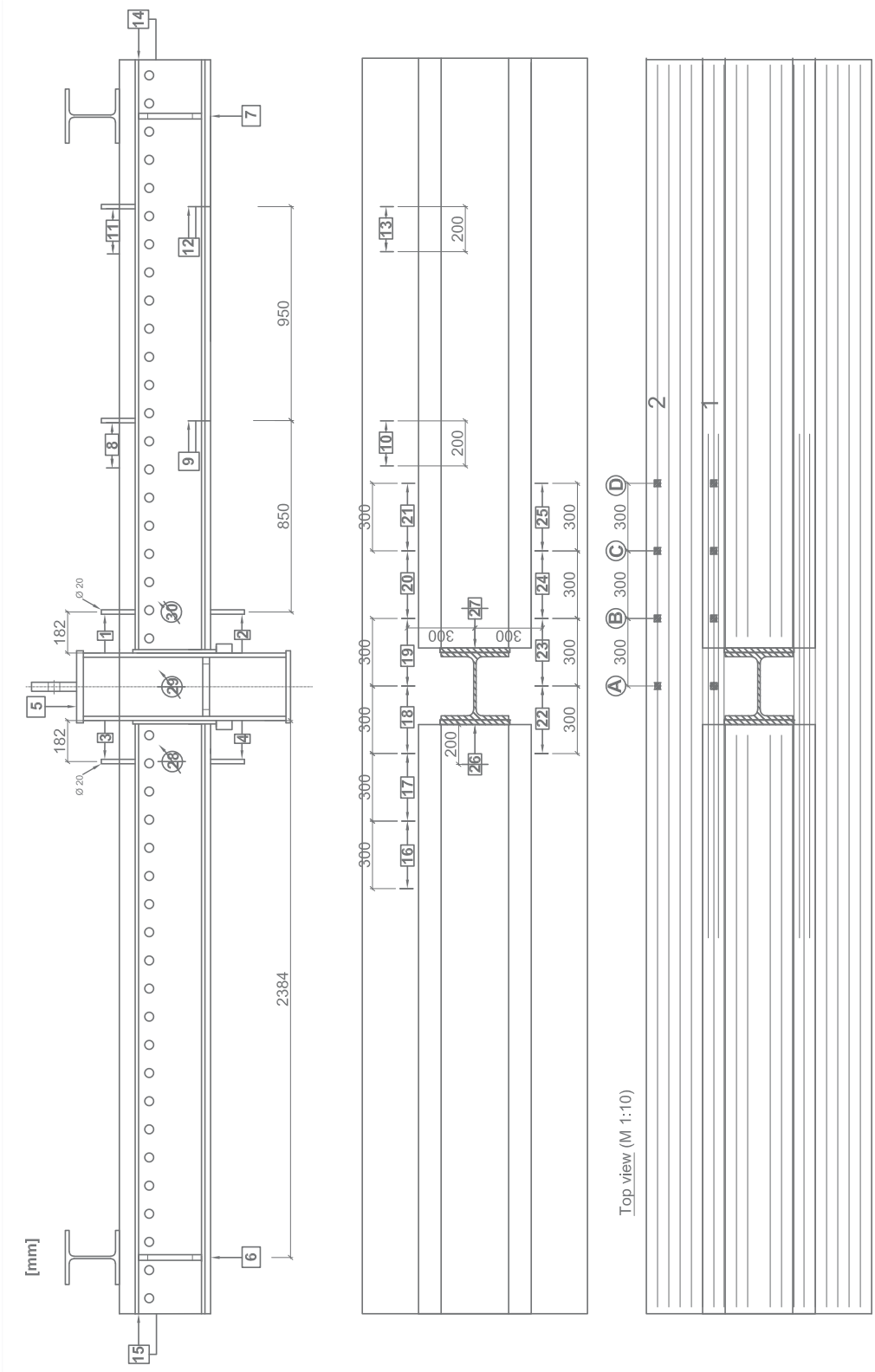

Figure A.12: Instrumentation plans for B21 and B22

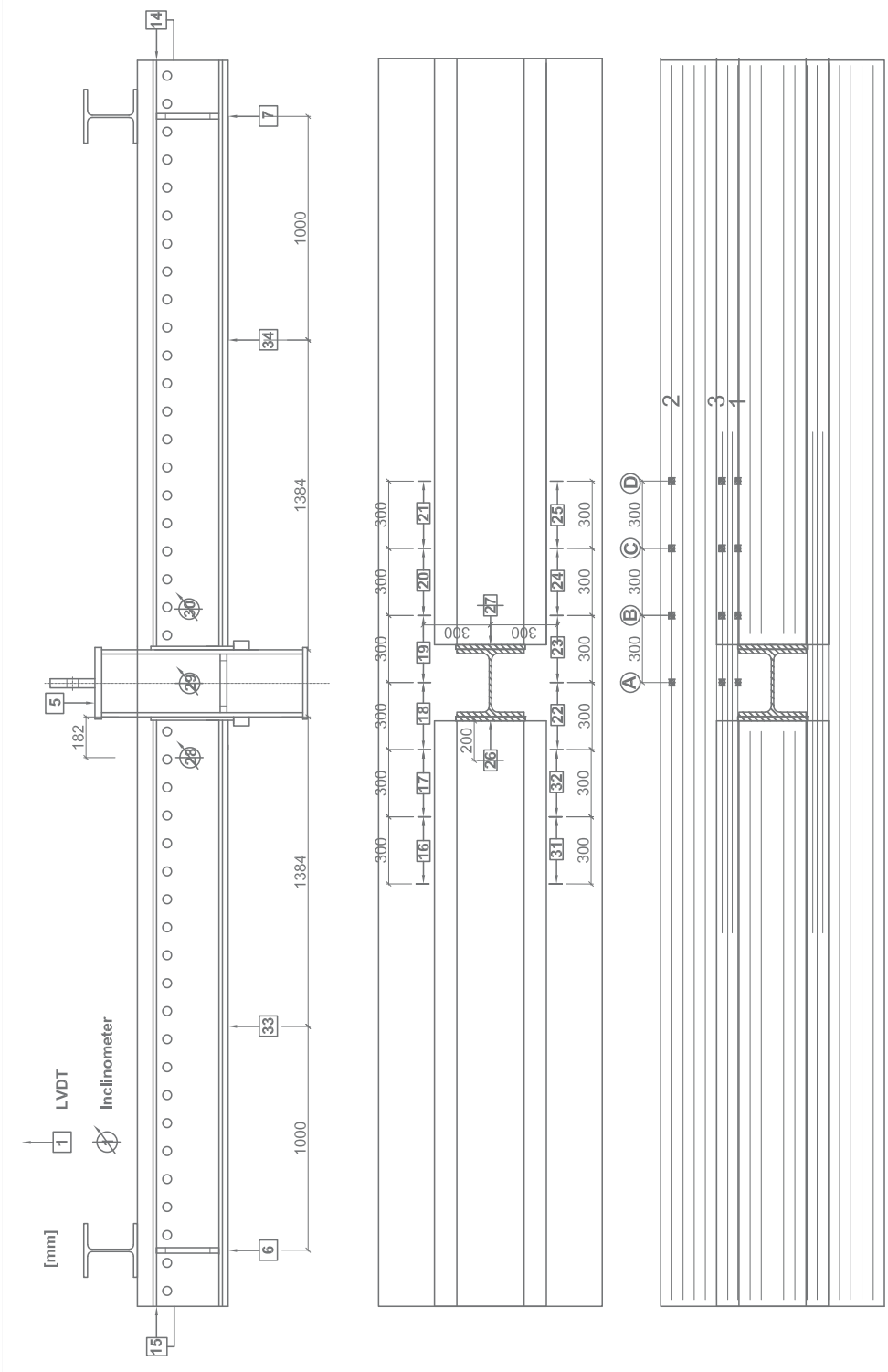

Figure A.13: Instrumentation plans for B31 and B32

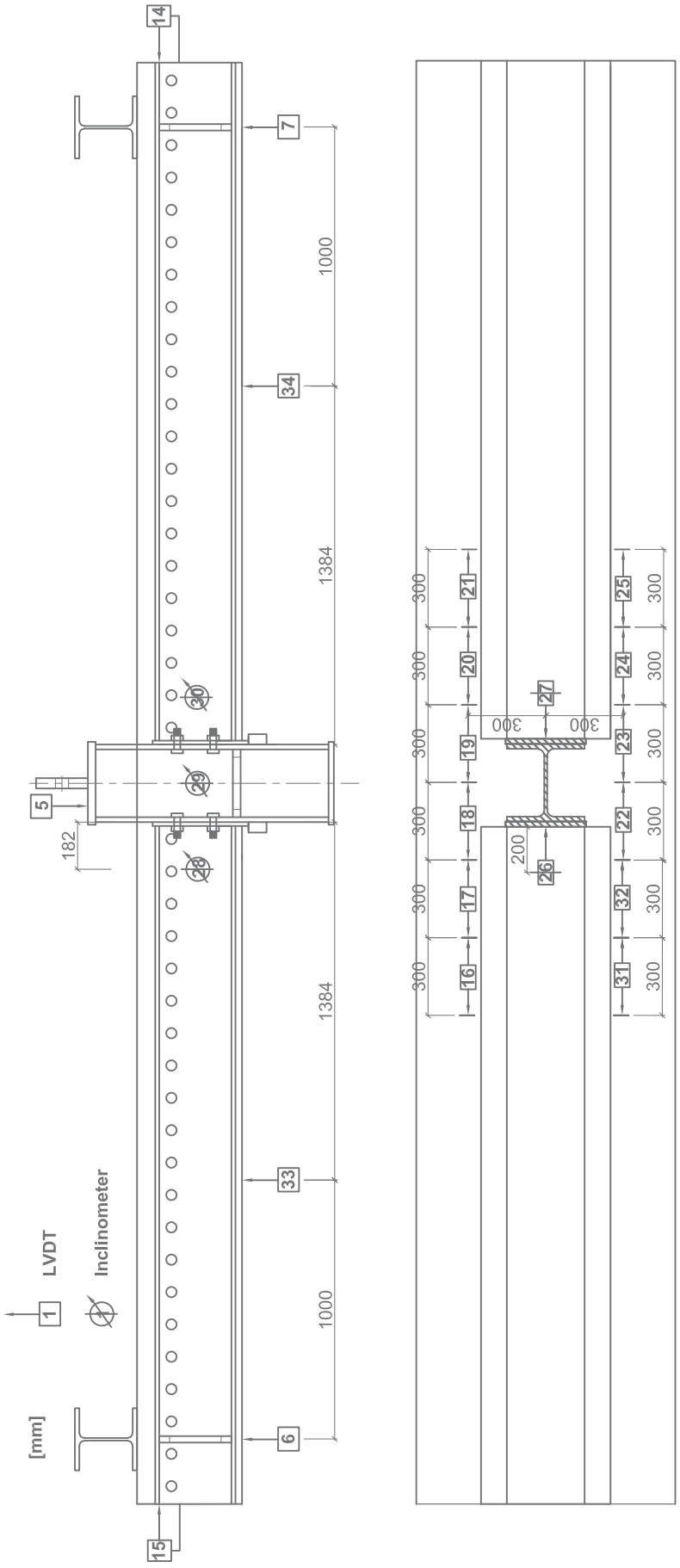

Figure A.14: Instrumentation plans for E21, E22 and E32

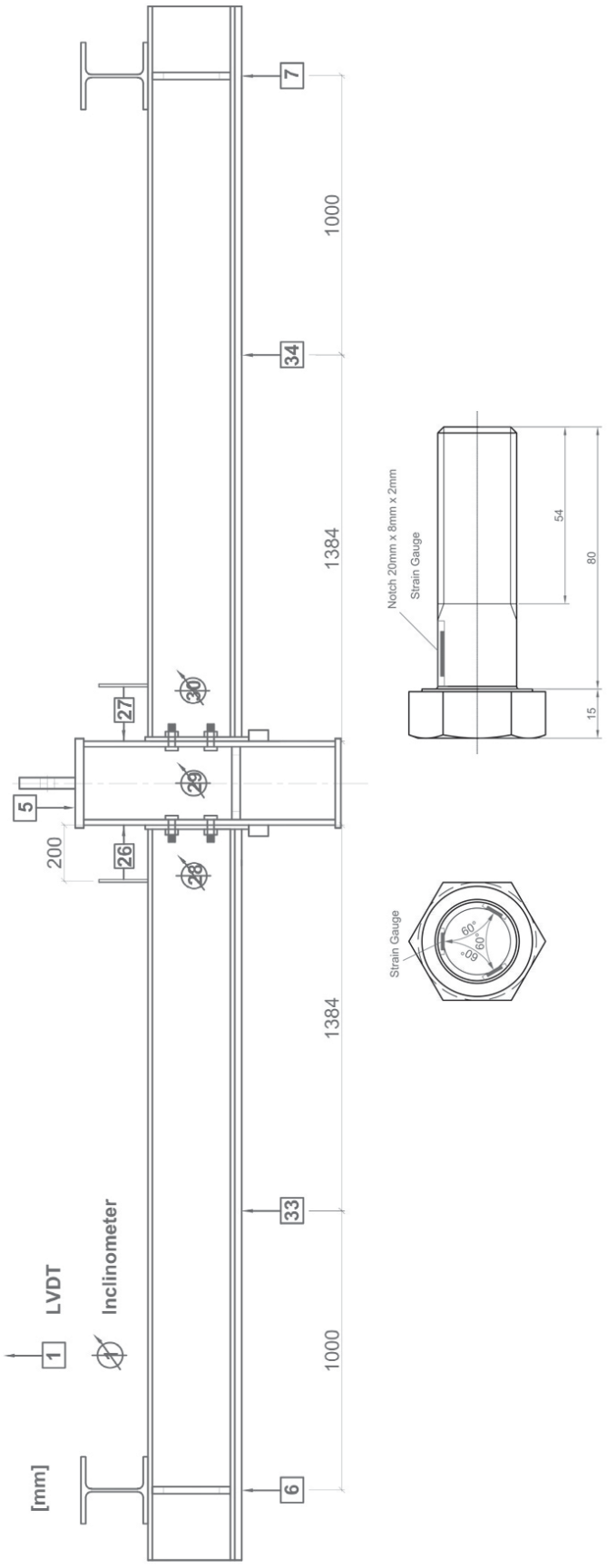

Figure A.15: Instrumentation plan for C14

B Additional experimental results

B.1 Moment-rotation curves

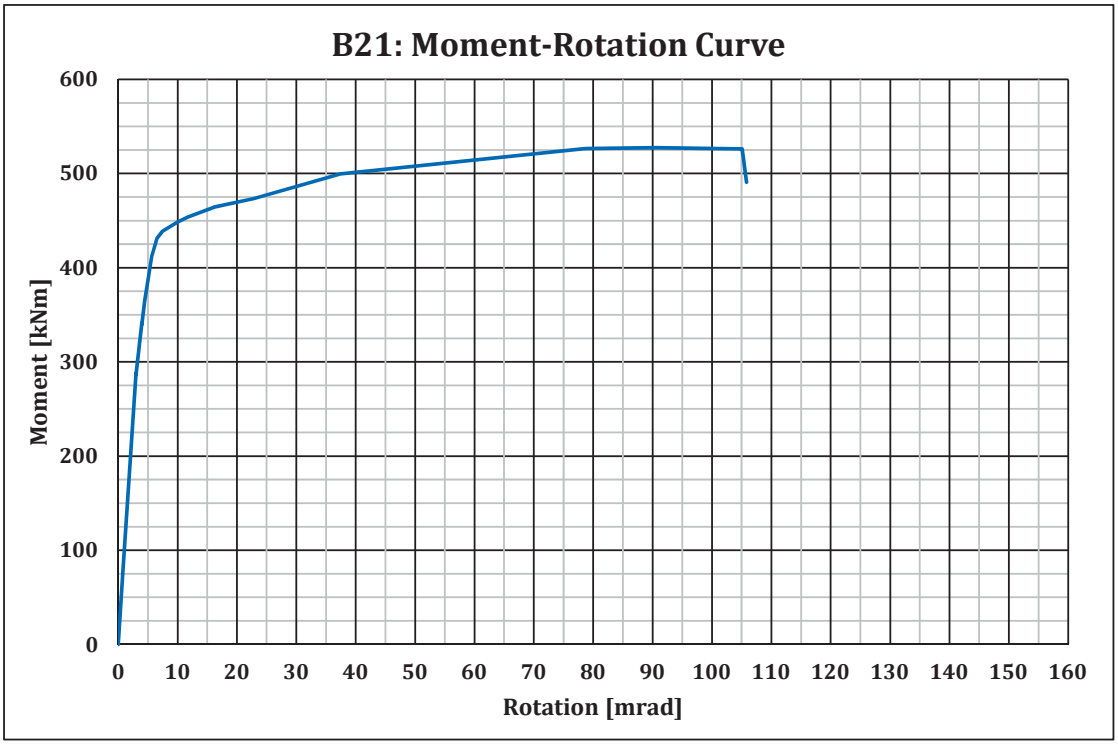

Figure B.1: B21: Moment-rotation curve

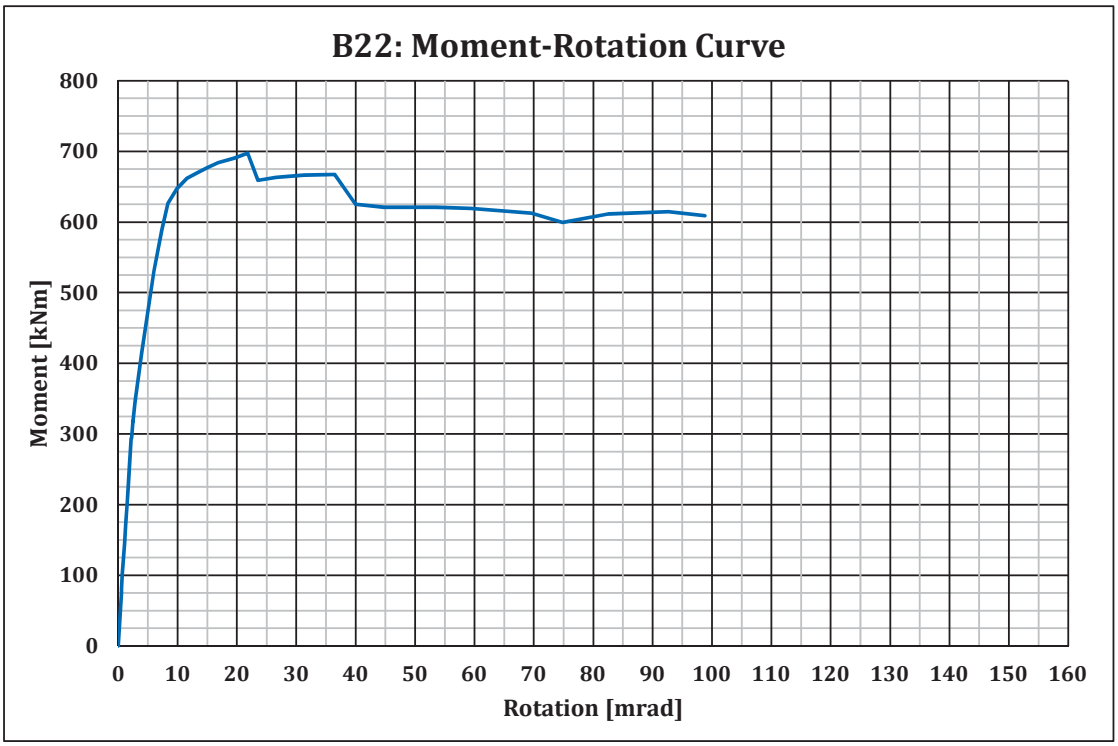

Figure B.2: B22: Moment-rotation curve

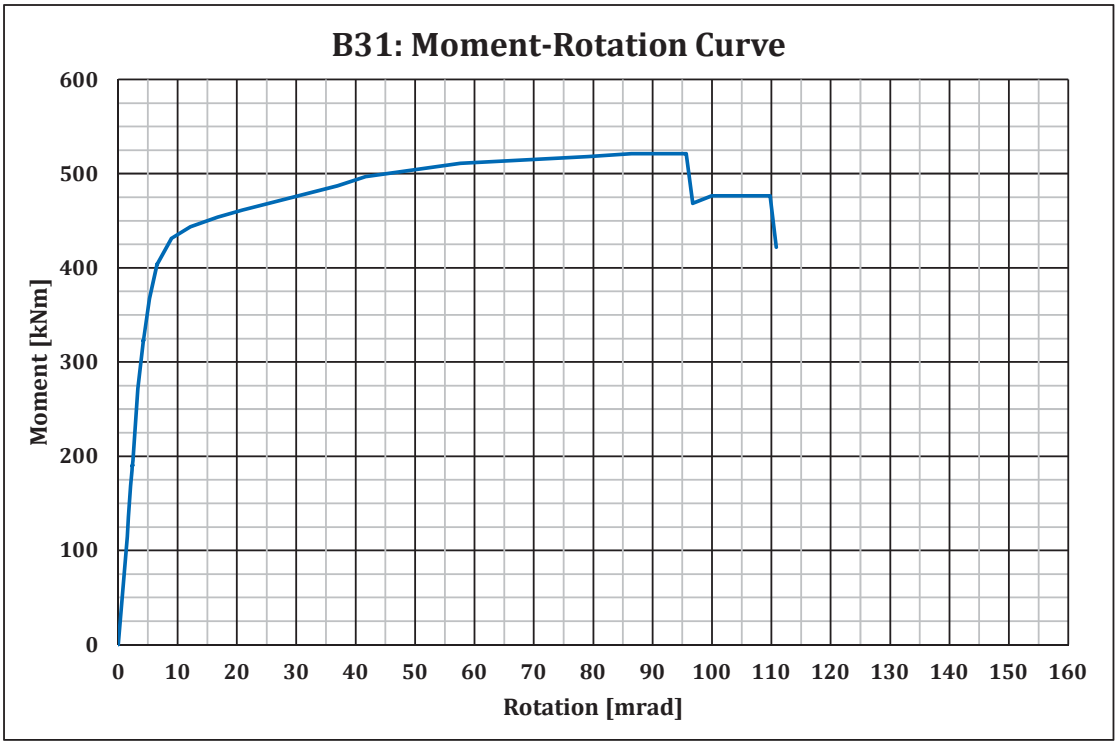

Figure B.3: B31: Moment-rotation curve

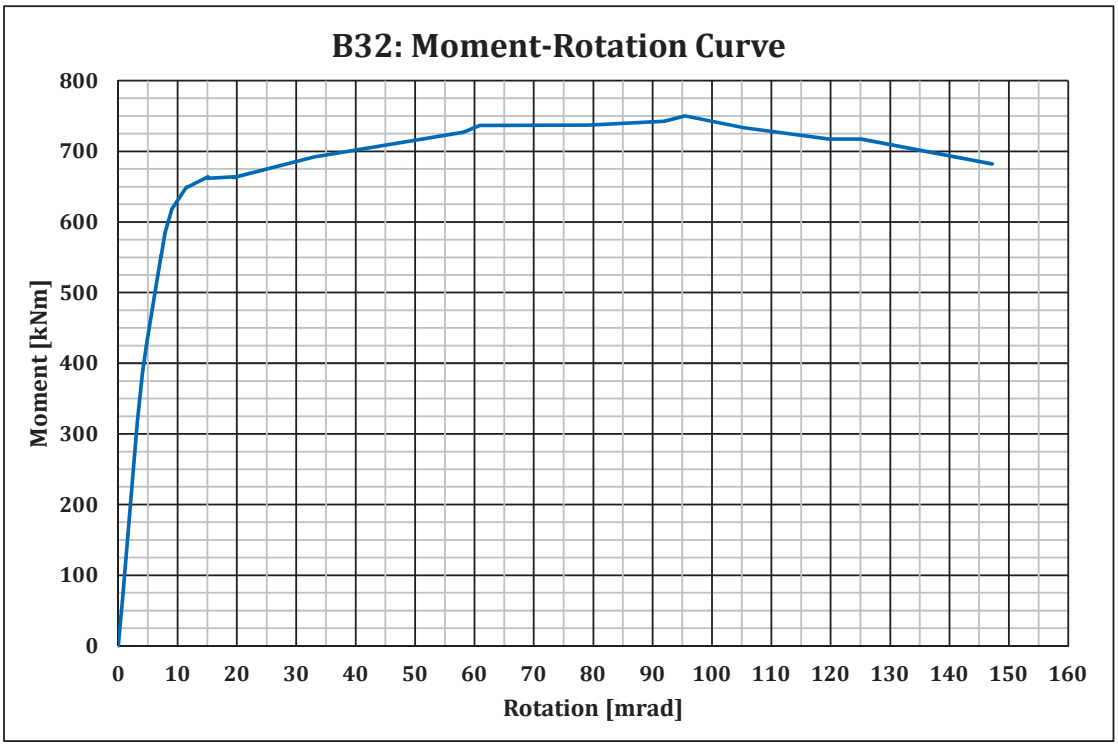

Figure B.4: B32: Moment-rotation curve

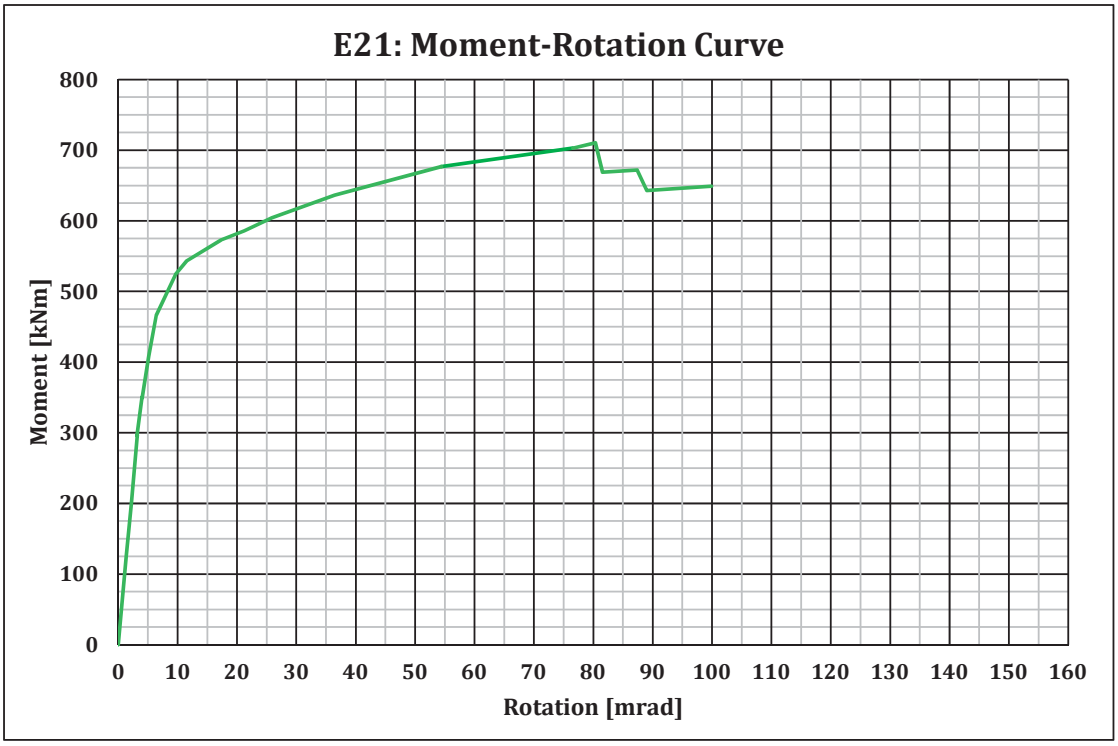

Figure B.5: E21: Moment-rotation curve

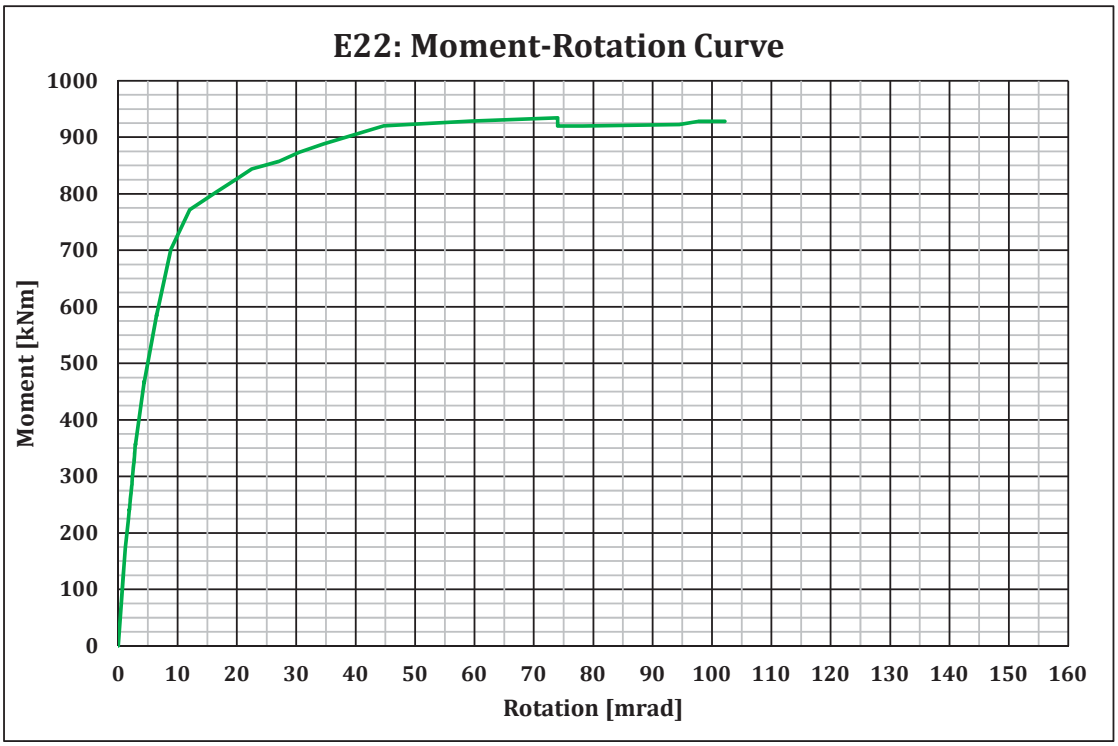

Figure B.6: E22: Moment-rotation curve

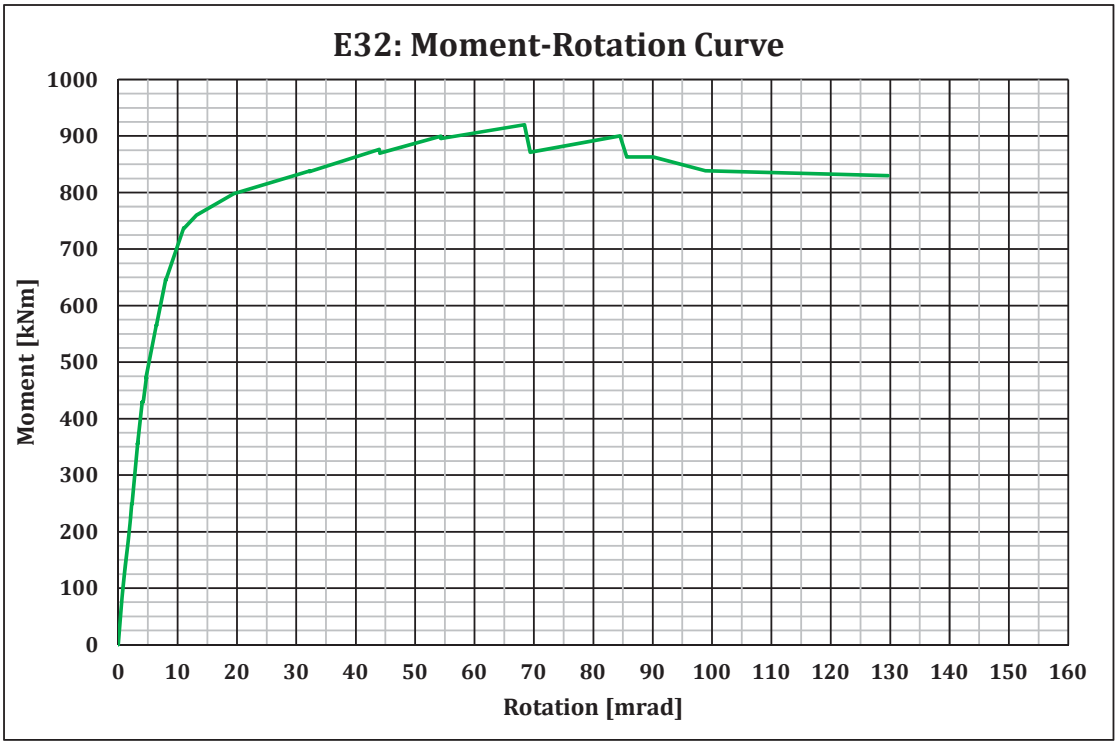

Figure B.7: E32: Moment-rotation curve

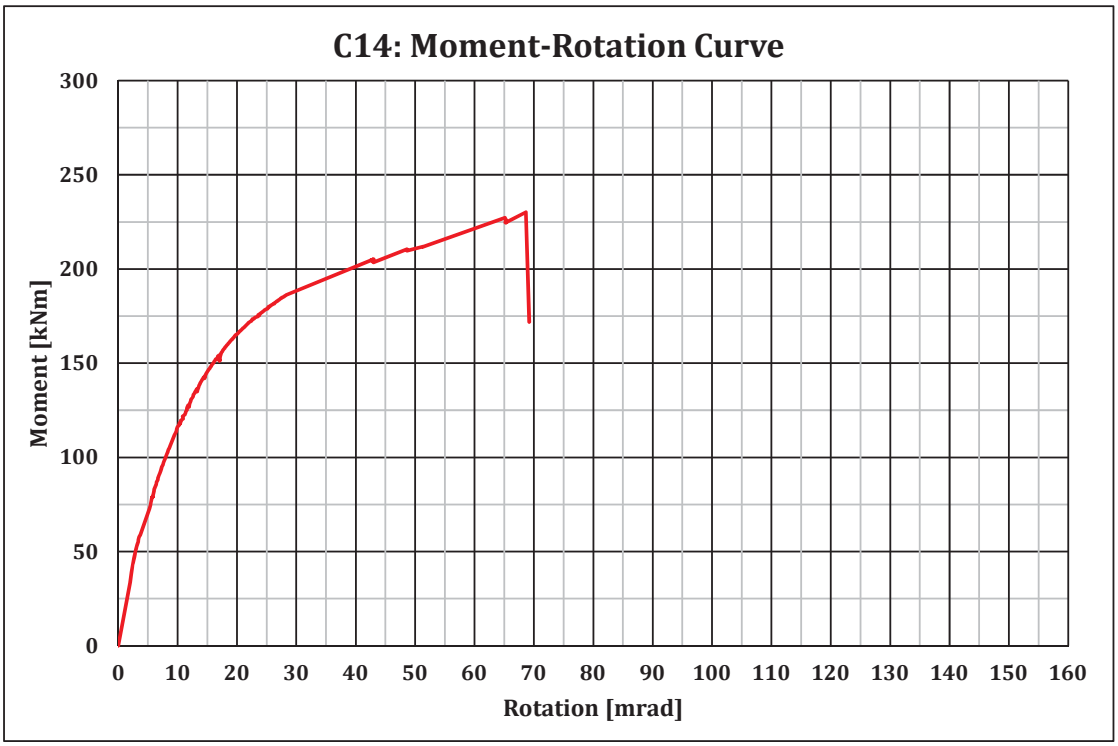

Figure B.8: C14: Moment-rotation curve

B.2 Force-Displacement curves

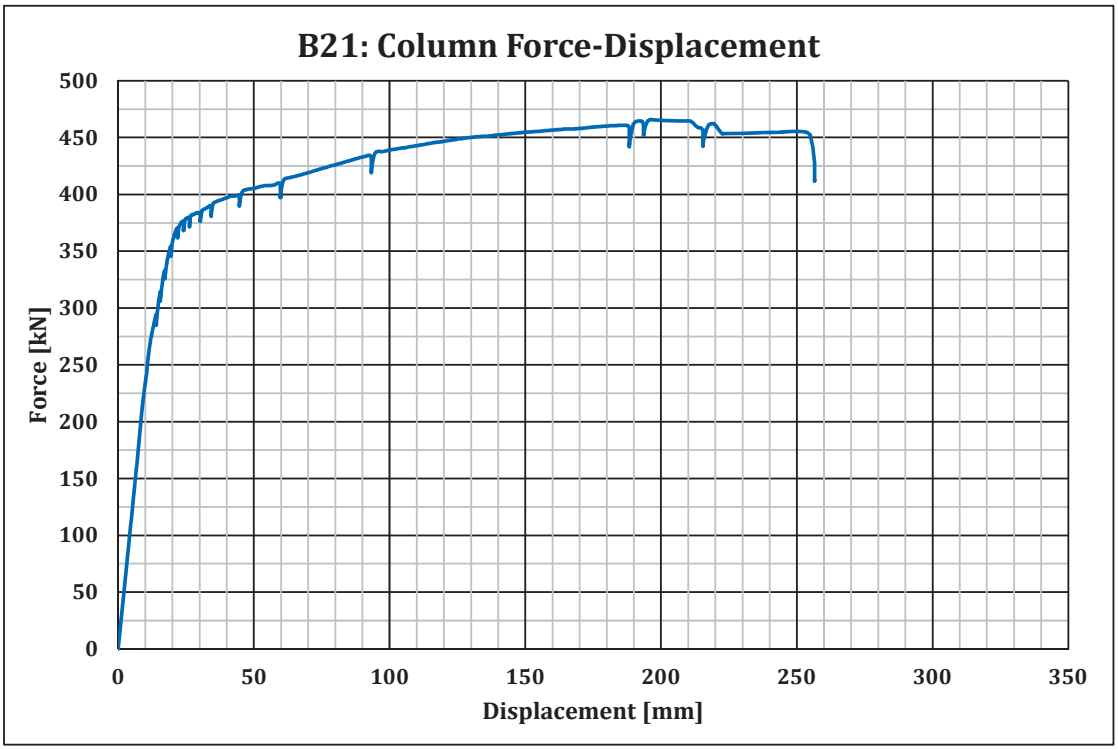

Figure B.9: B21: Force-displacement curve

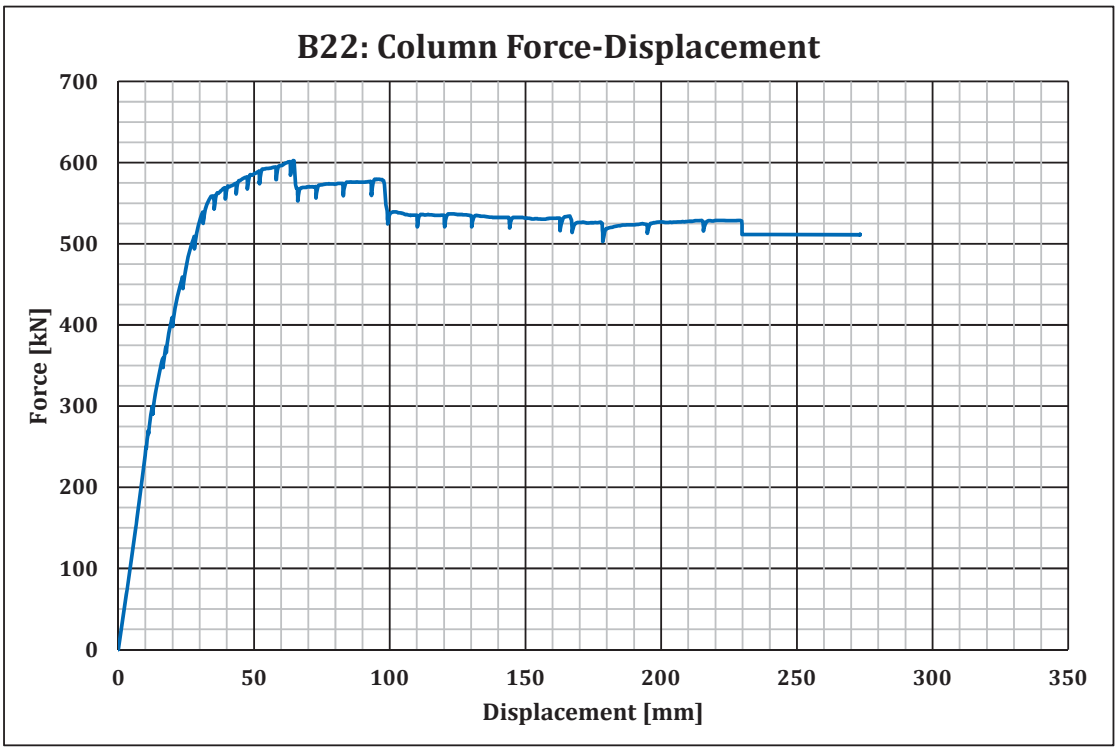

Figure B.10: B22: Force-displacement curve

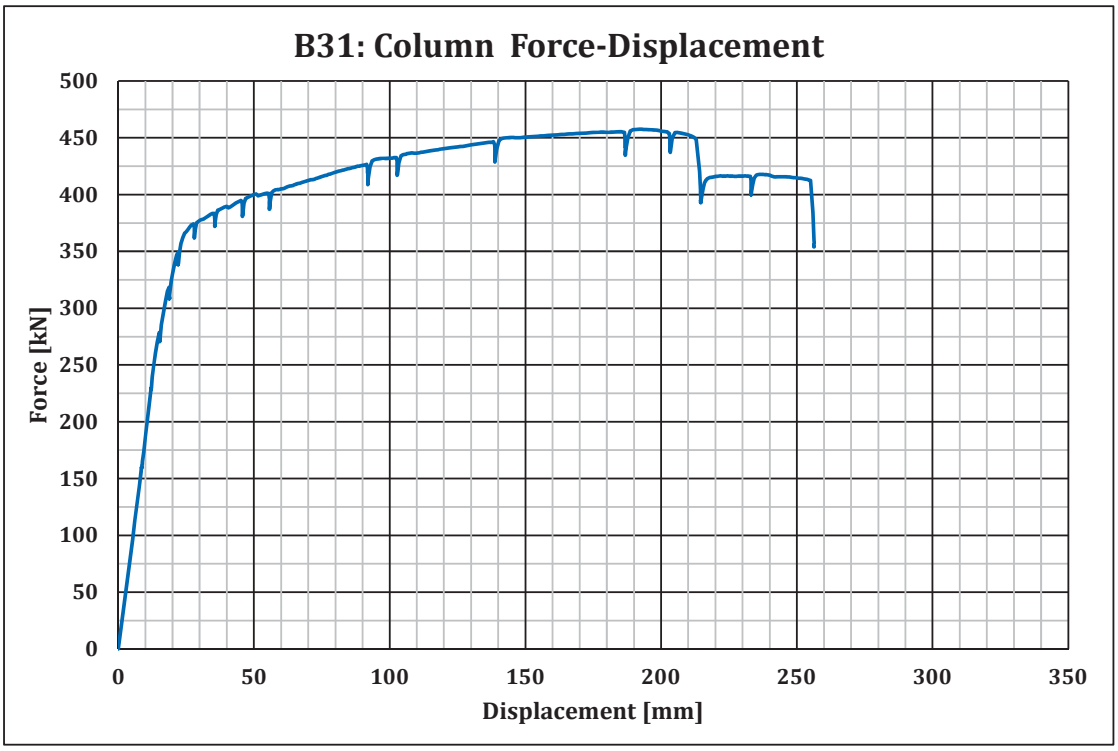

Figure B.11: B31: Force-displacement curve

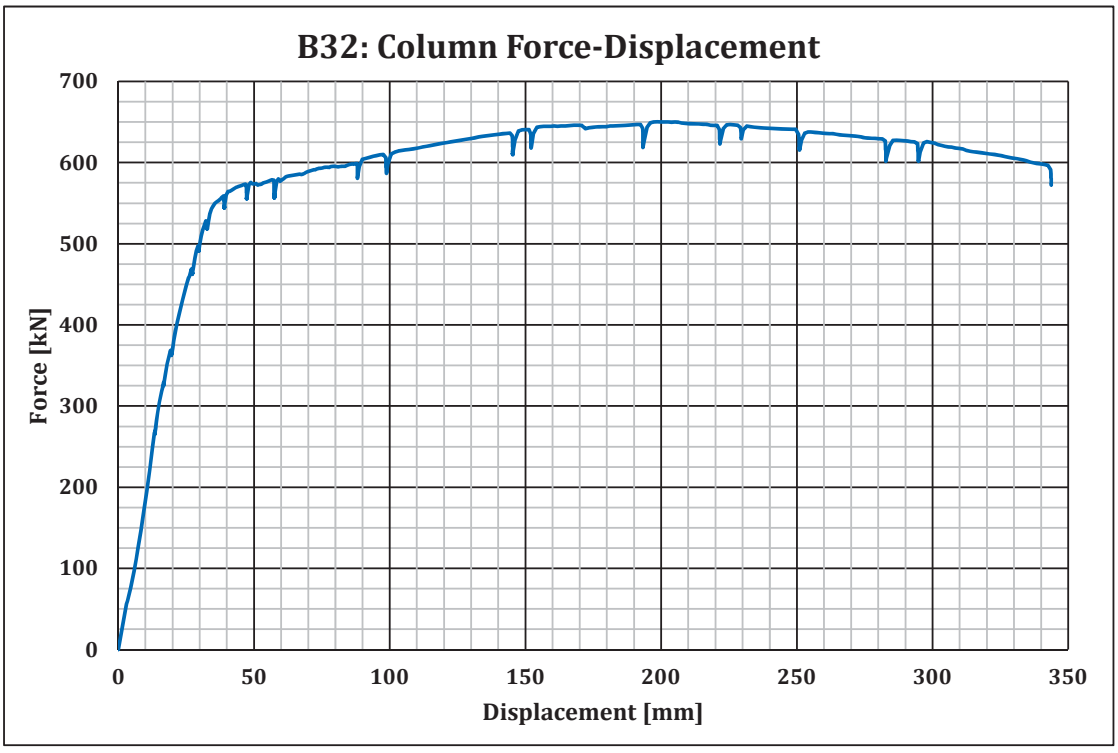

Figure B.12: B32: Force-displacement curve

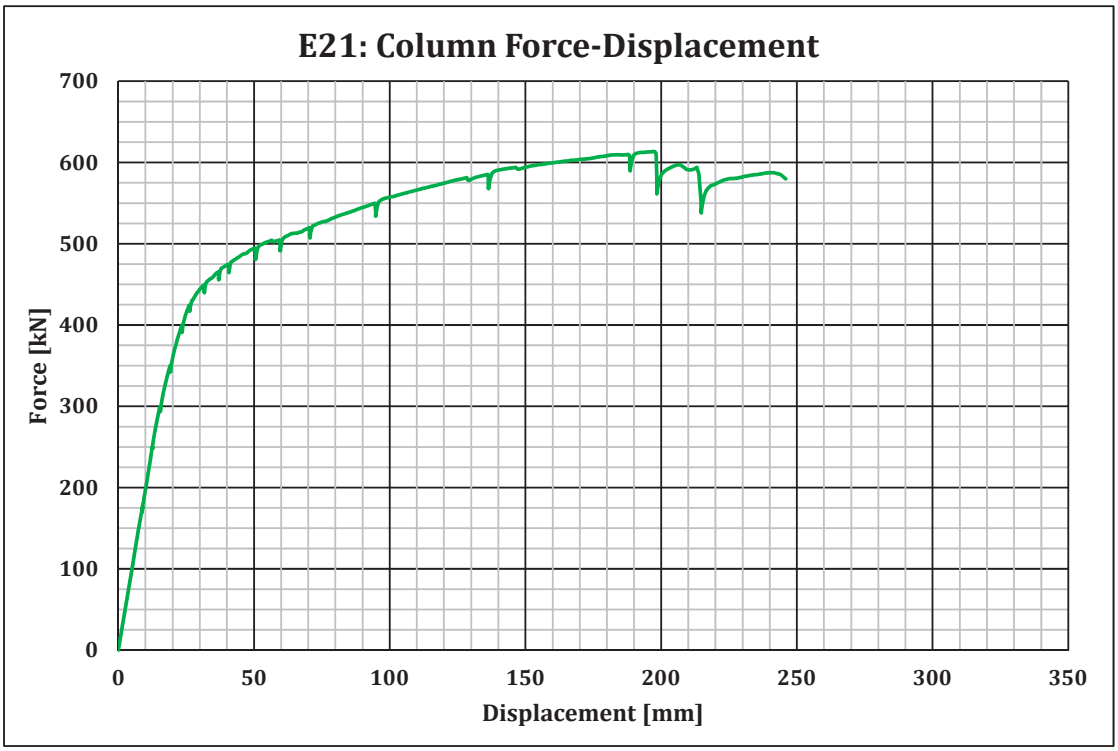

Figure B.13: E21: Force-displacement curve

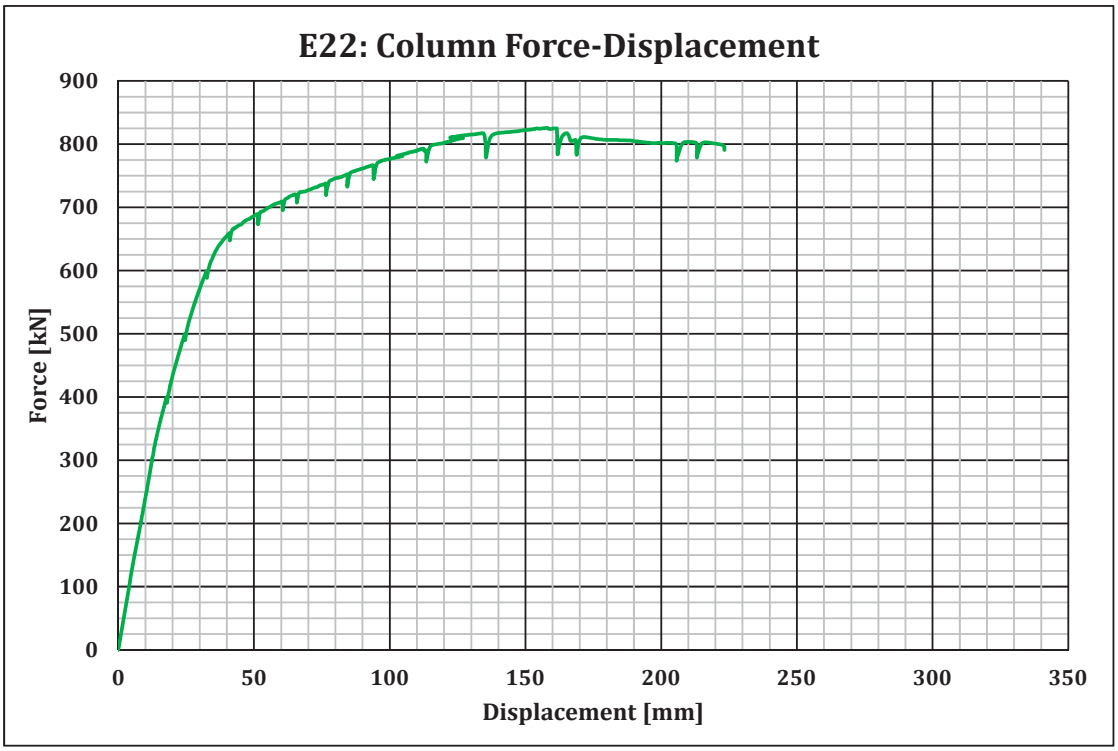

Figure B.14: E22: Force-displacement curve

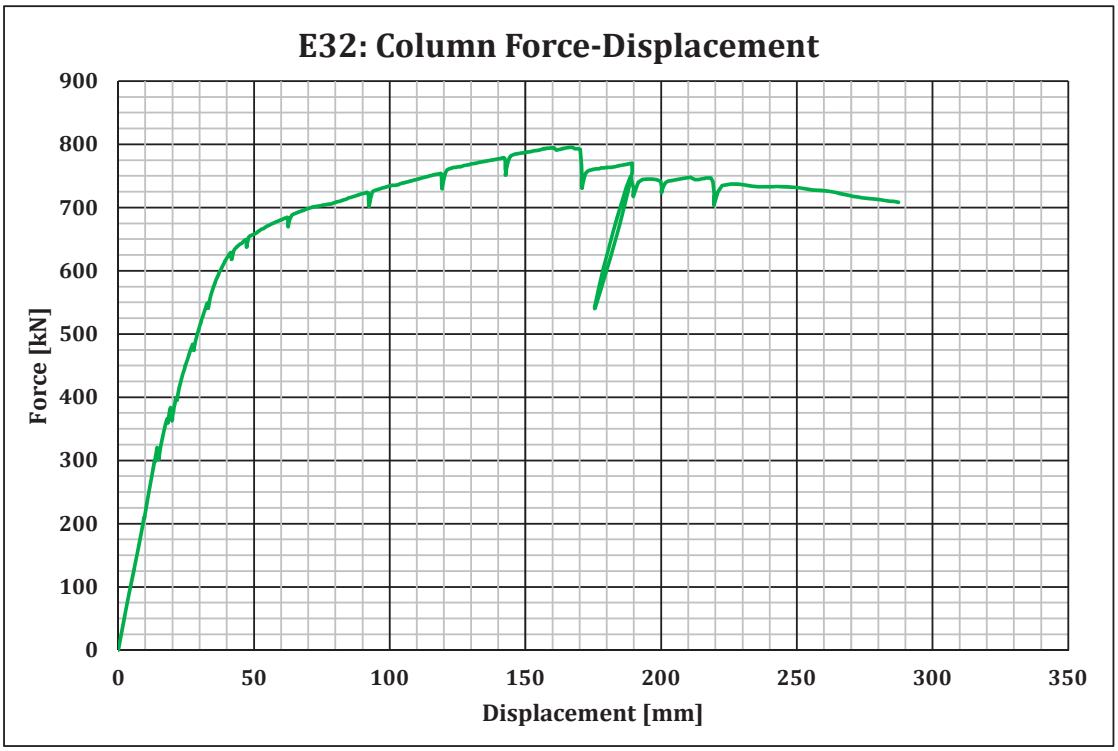

Figure B.15: E32: Force-displacement curve

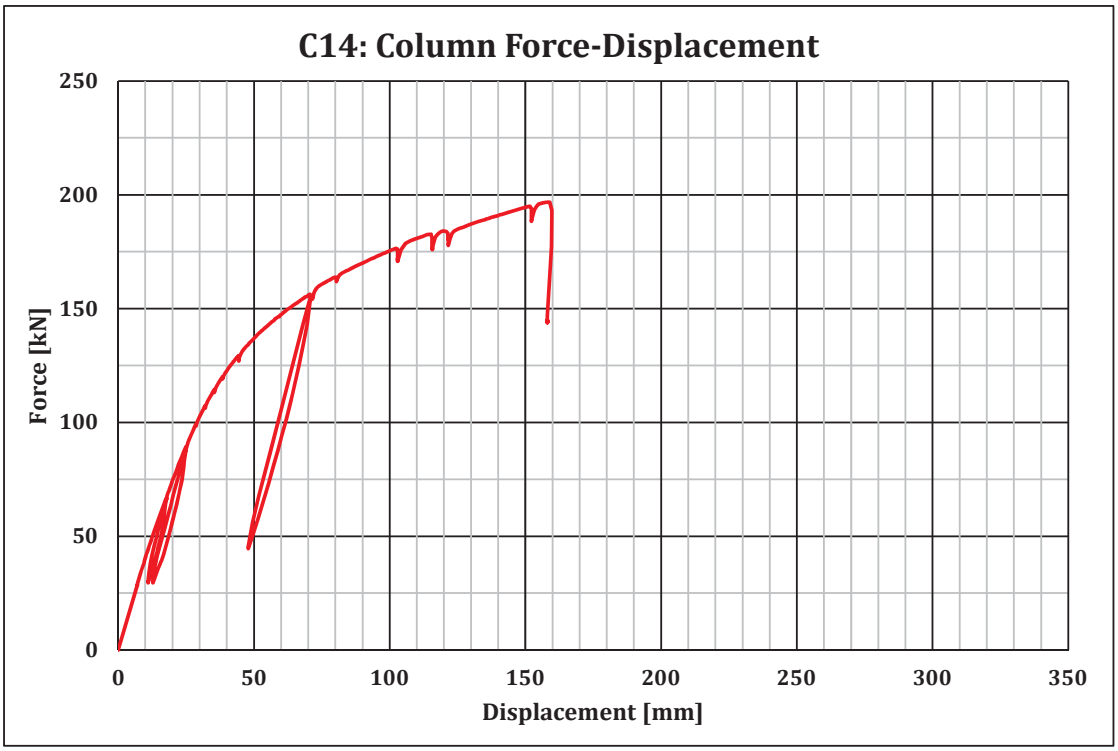

Figure B.16: C14: Force-displacement curve

B.3 Elongation of reinforced concrete slab

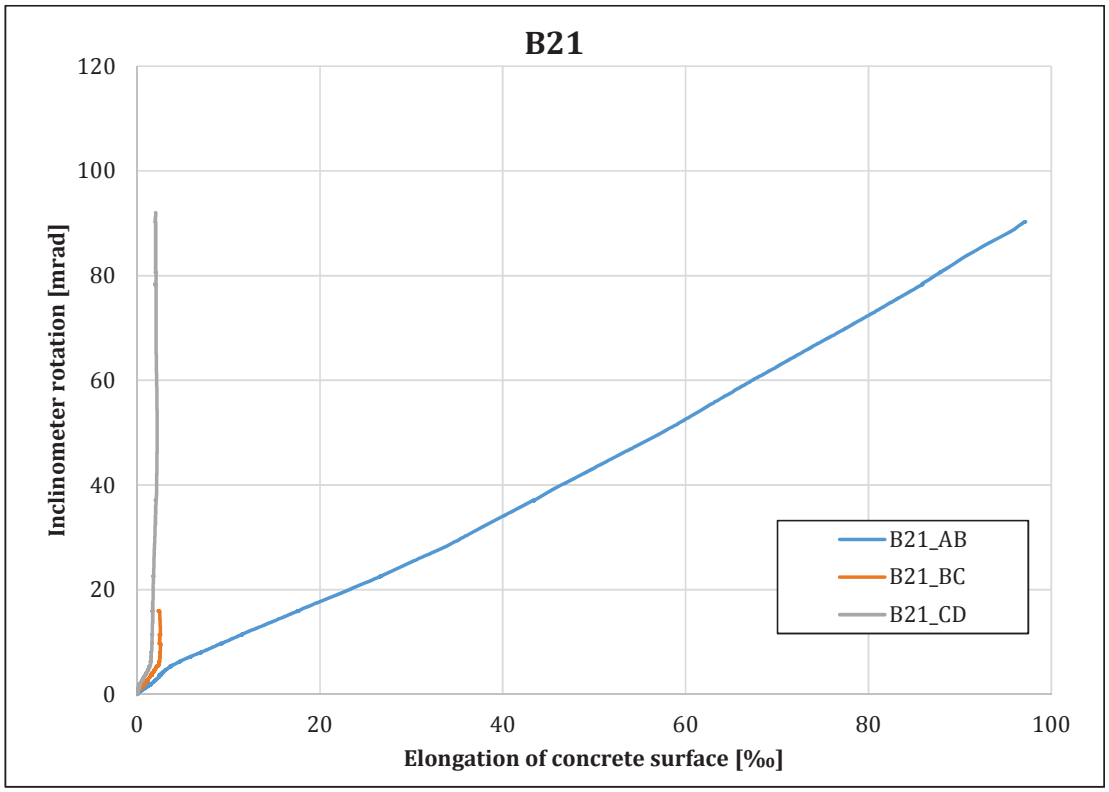

Figure B.17: B21: Slab elongation

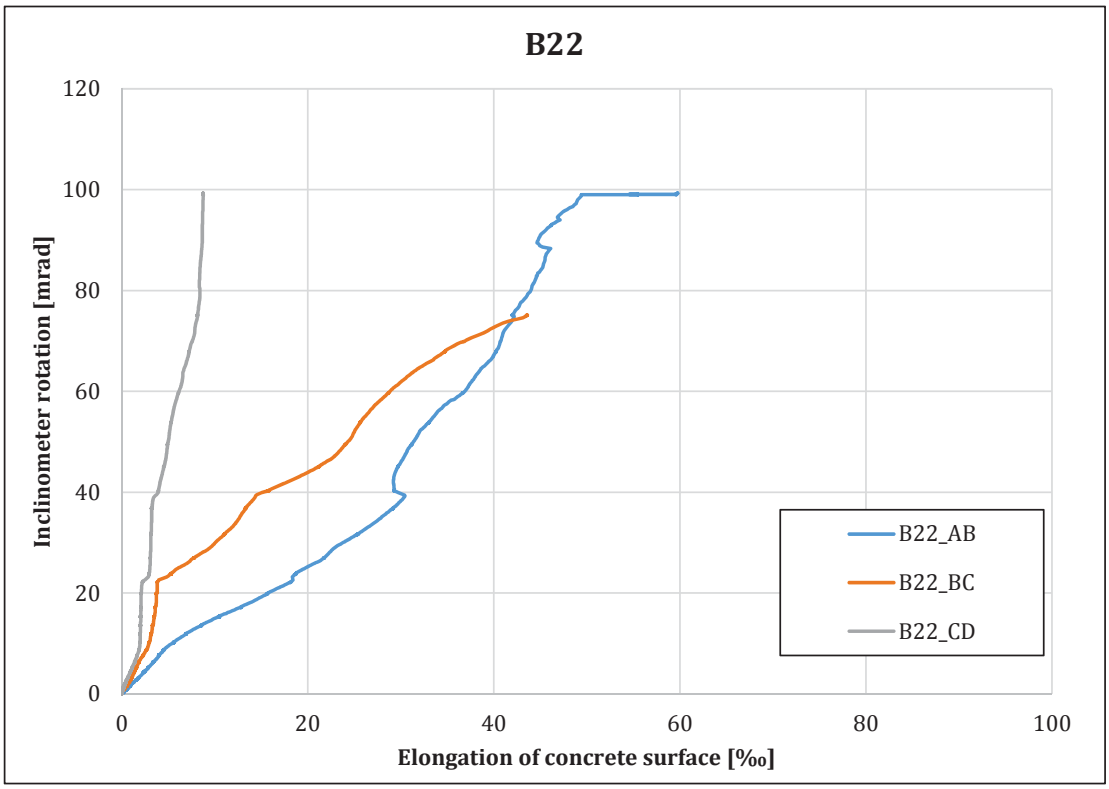

Figure B.18: B22: Slab elongation

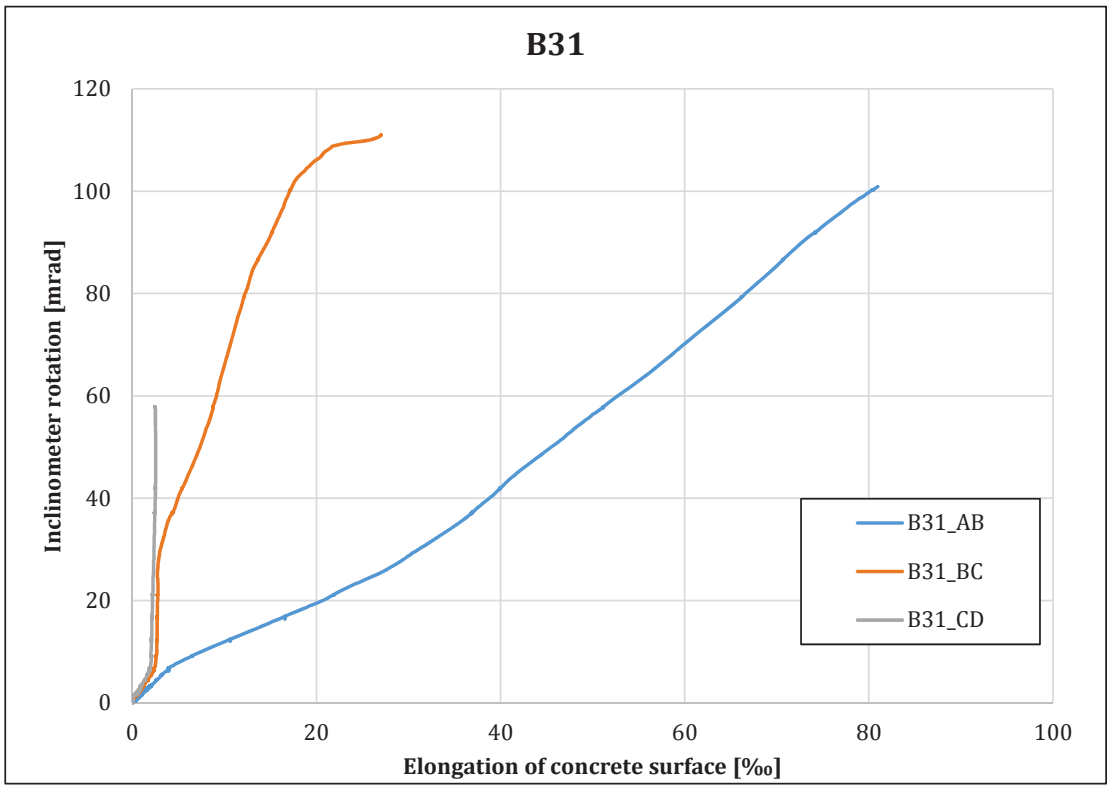

Figure B.19: B31: Slab elongation

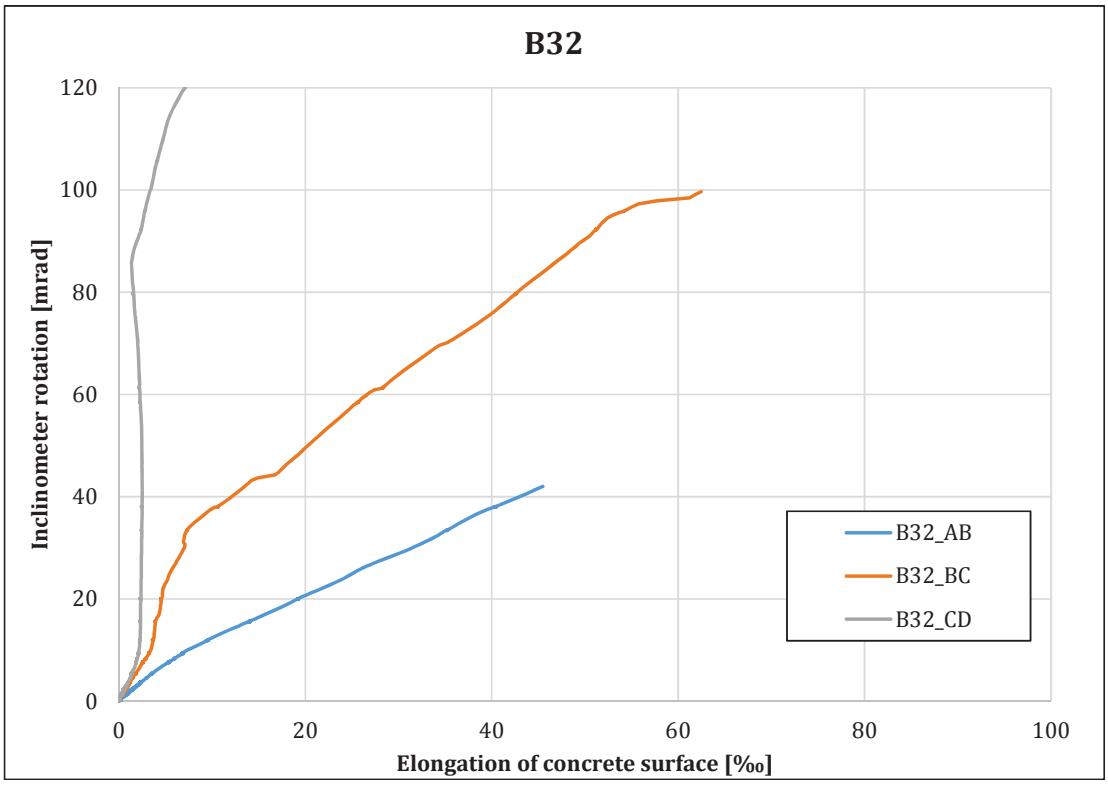

Figure B.20: B32: Slab elongation

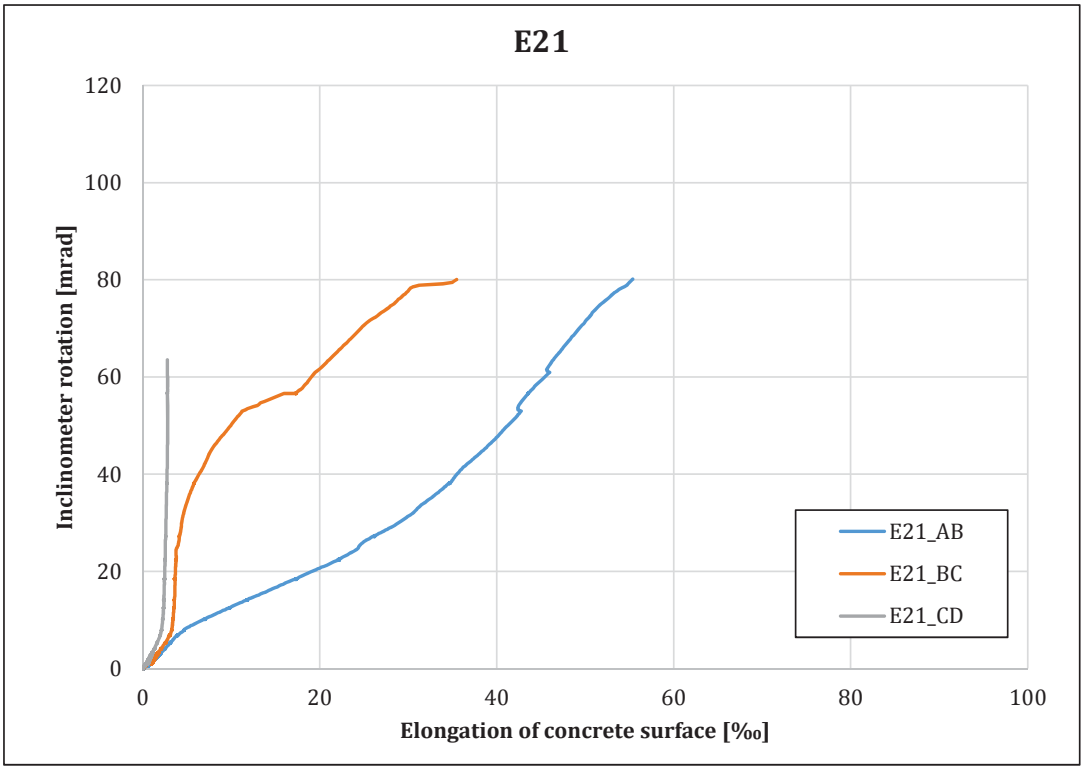

Figure B.21: E21: Slab elongation

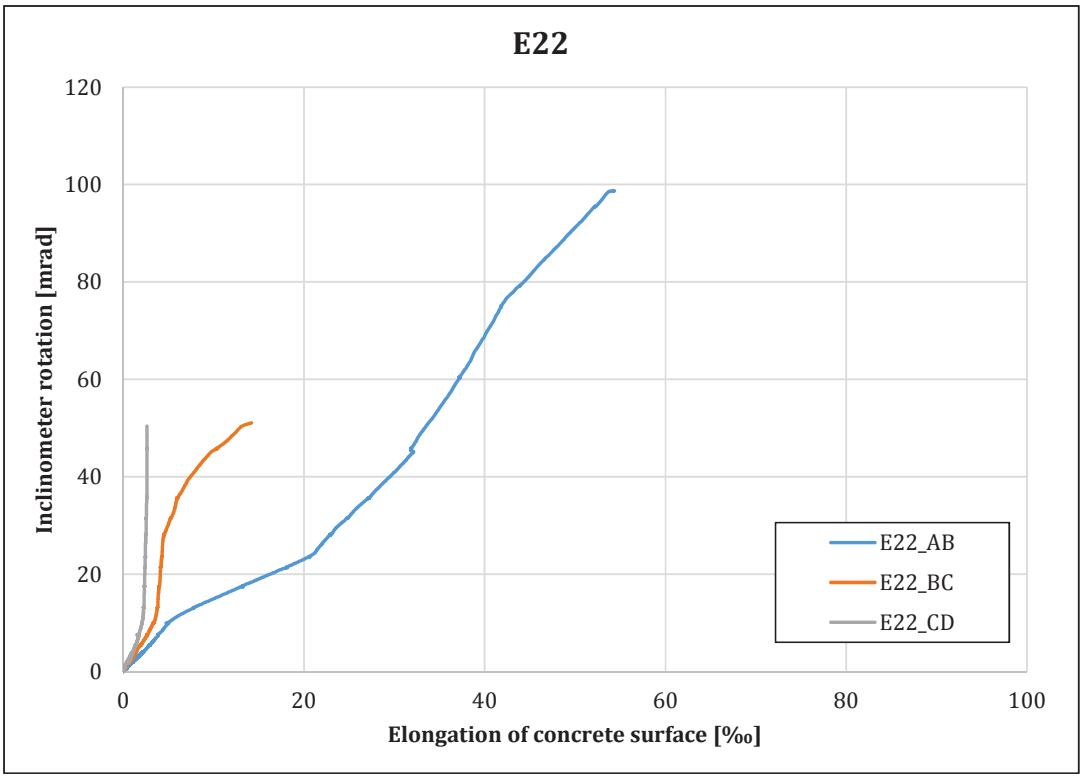

Figure B.22: E22: Slab elongation

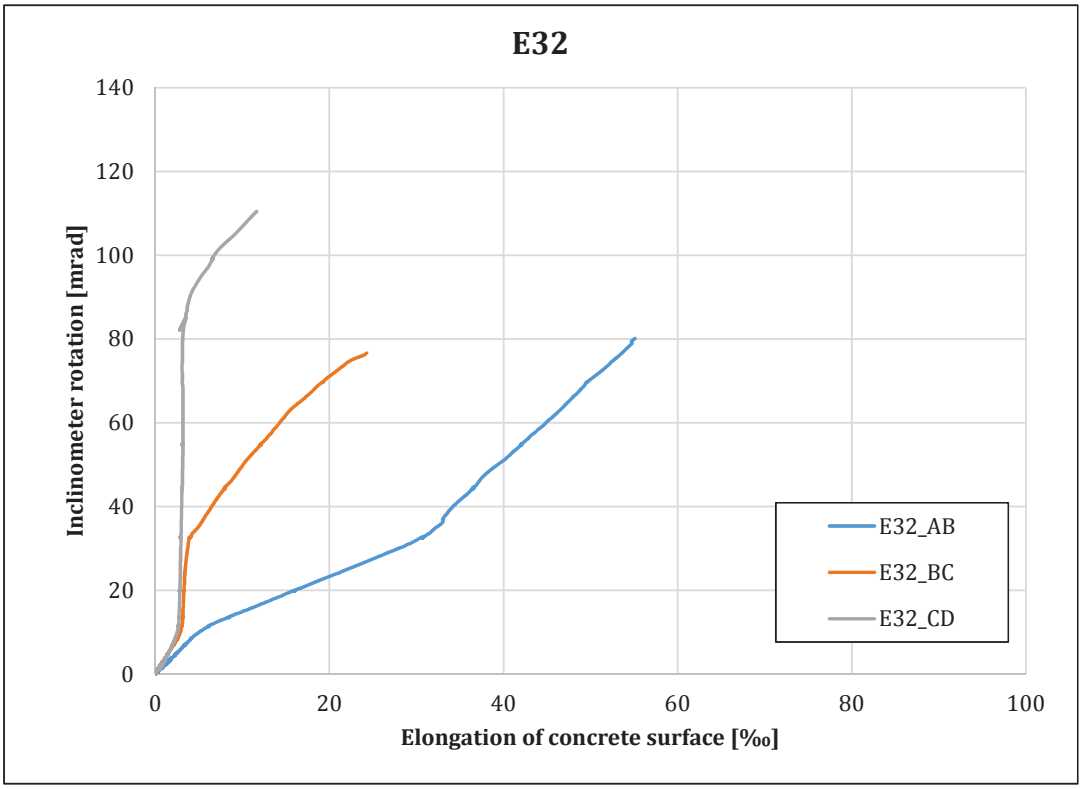

Figure B.23: E32: Slab elongation

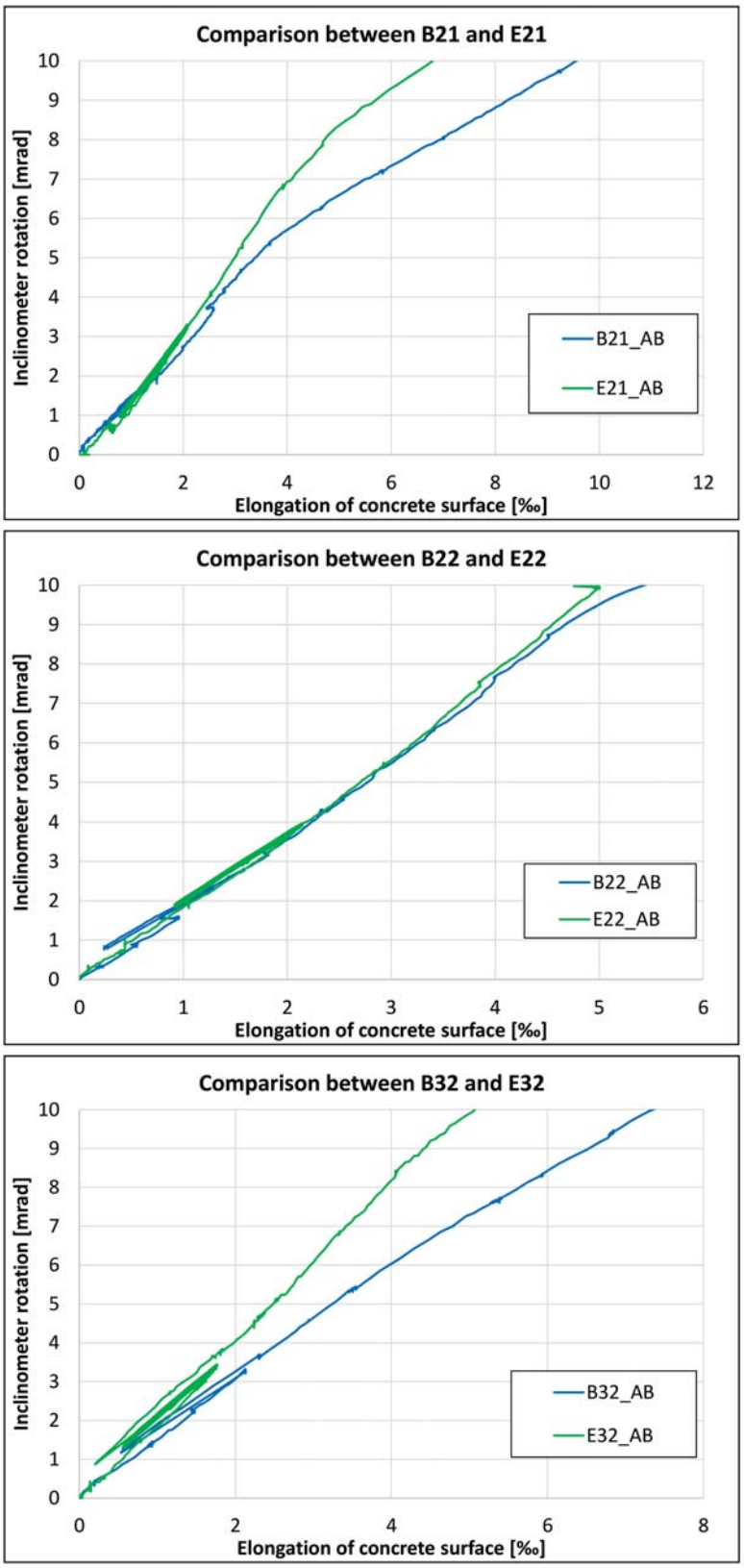

Figure B.24: Influence of steelwork connection on elongation of reinforced concrete slab in the initial state

B.4 Results from the strain gauges in the bolts

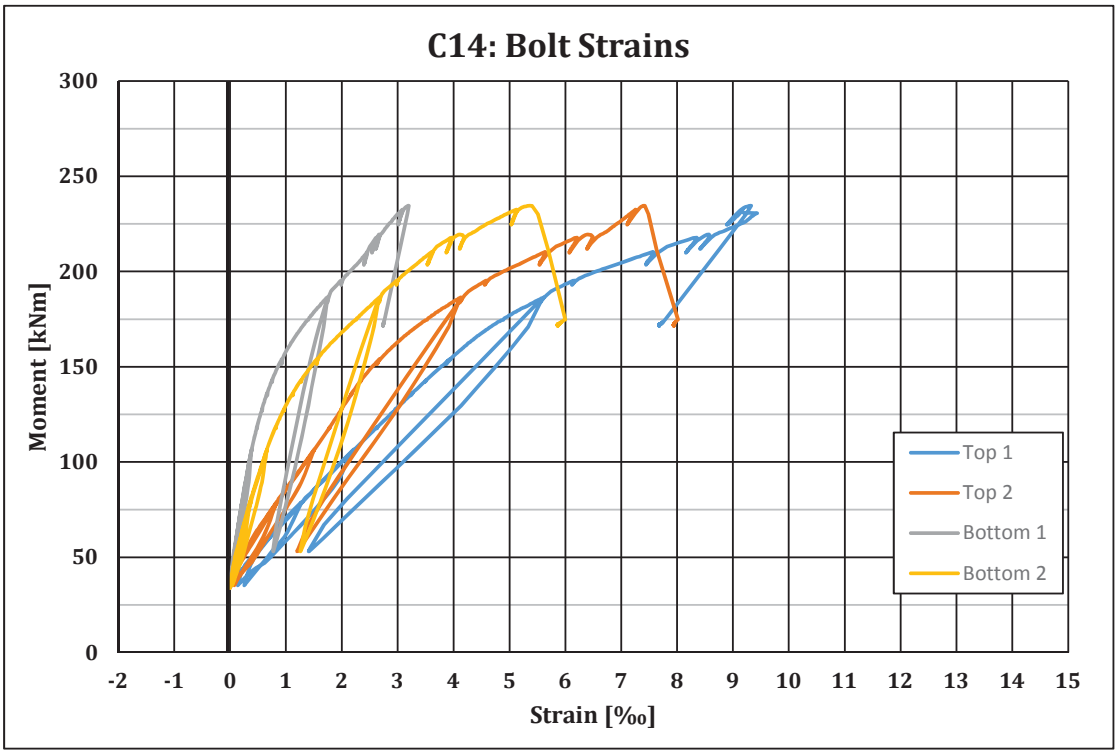

Figure B.25: C14: Measured bolt strains

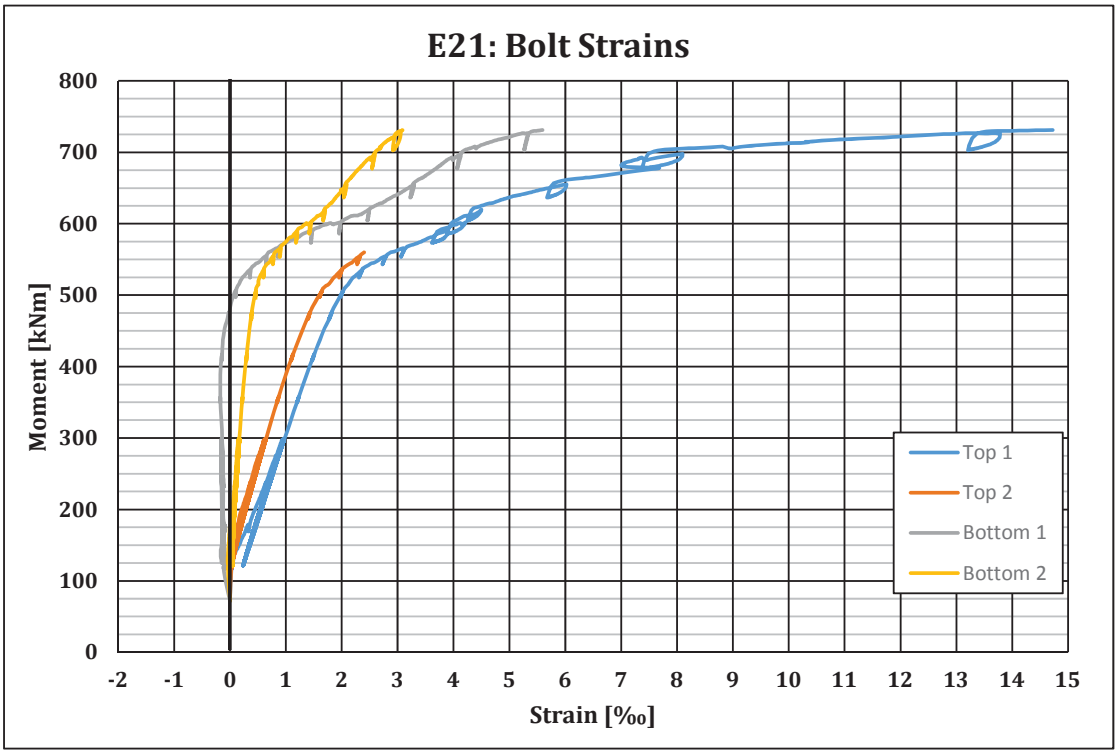

Figure B.26: E21: Measured bolt strains

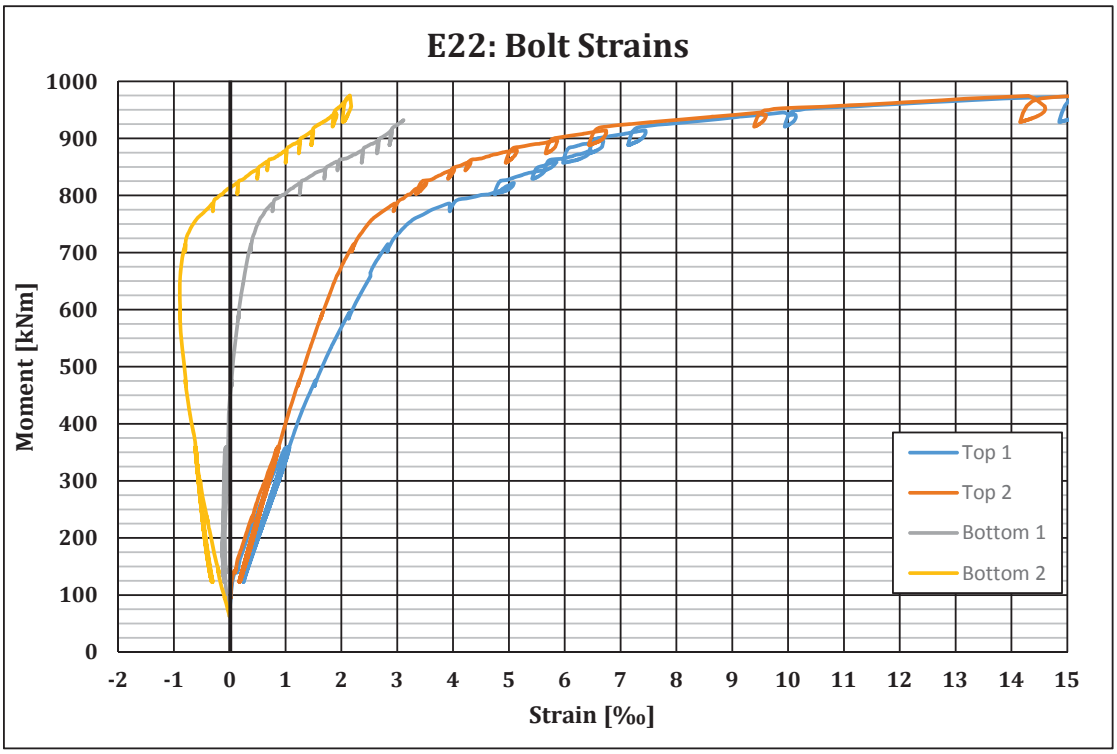

Figure B.27: E22: Measured bolt strains

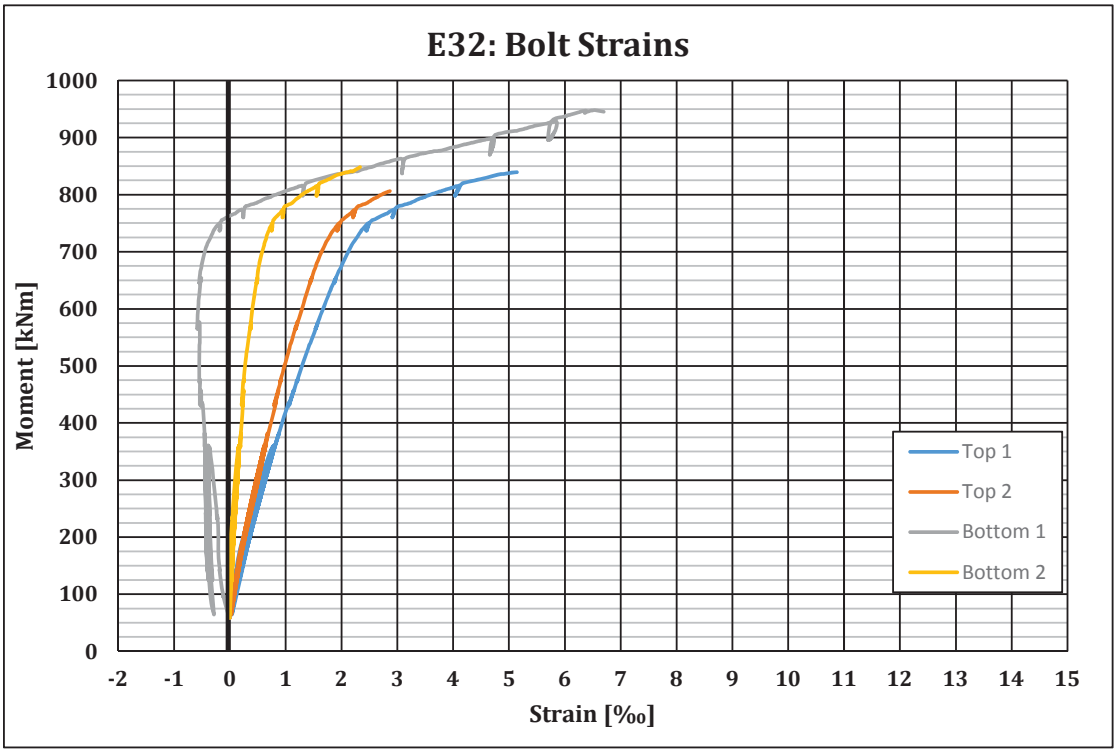

Figure B.28: E32: Measured bolt strains

C Test data of evaluated composite joints

The following composite joints tested in earlier investigations have been selected from an extensive database of about 90 composite joints. This selection is based on the following criteria:

- Only experimental tests with sufficient data have been retained in the final evaluation
- Longitudinal rebars with diameters bigger or equal to 12 mm
- Only composite beams with full shear connection
- No tests involving cycling loading
- Symmetric joints with balanced hogging moments
- Only tests with failure due to rupture of the longitudinal reinforcement
- Test performance under displacement control of jack

Reference	Test Nr.	Steel beam			Steel column		
		Profile	f_y [N/mm²]	f_u [N/mm²]	Profile	f_y [N/mm²]	f_u [N/mm²]
Najafi	S8F	306 x 165 UB 40	271	465	203 x 203 UC 52	284	484
Brown	Test 3	457 x 152 UB 52	306	N/A	203 x 203 UC 52	276	N/A
Elz	I14B1-09	HEB 360	353	446	HEA 300	400	529
Kathage	VT1.1	IPE 400	371	N/A	HEA 400	N/A	N/A
	VT1.3	IPE 400	371	N/A	HEA 400	N/A	N/A
	VT2.4	IPE 400	433	N/A	HEA 400	N/A	N/A

Reference	Test Nr.	Concrete slab			Steel decking/solid slab		Longitudinal reinforcement					
		b [mm]	d [mm]	f_c [N/mm²]	Type	h_p [mm]	Ø [mm]	f_{sy} [N/mm²]	f_{su} [N/mm²]	$z_{l,top}$* [mm]	$z_{l,bottom}$* [mm]	degree of shear connection
Najafi	S8F	1100	120	33	PMF CF46	46	A142+8 Ø 12	486	557	31	---	100%
Brown	Test 3	1100	120	36	PMF CF 46	46	A142+ 4 Ø 16	504	611	33	---	100%
Elz	I14B1-09	2000	140	34	solid slab	---	22 Ø 12	510	587	35	---	100%
Kathage	VT1.1	1200	160	38	solid slab	---	2 x 9 Ø 12	491[a]	565	25	135	100%
	VT1.3	1200	160	36	solid slab	---	2 x 9 Ø 12	491[a]	565	25	135	100%
	VT2.4	1200	160	41	solid slab	---	2 x 12 Ø 12	489[a]	562	25	135	100%

Reference	Test Nr.	Steelwork connection							Test Failure
		Type	t_e [mm]	bolts	z_{i1} [mm]	z_{i2} [mm]	z_{i3} [mm]	z_{i4} [mm]	
Najafi	S8F	FE	15	4 M20 8.8	170	374	---	---	Reinforcement
Brown	Test 3	FE	15	6 M20 8.8	170	430	480	---	Reinforcement
Elz	I14B1-09	FP	14	3 M27 10.9	240	320	400	---	Reinforcement
Kathage	VT1.1	---	---	---	---	---	---	---	Reinforcement
	VT1.3	---	---	---	---	---	---	---	Reinforcement
	VT2.4	---	---	---	---	---	---	---	Reinforcement

N/A Data not available
FE Flush endplate connection
FP Finplate connection with contact plate between the compression flange of the beam and the column
a Estimated yield strength $f_{sy}=f_{su}/1.15$
* Measured from the top of the concrete surface

Figure C.1: Test data of evaluated composite joints
Ref.: Najafi (1992), Brown and Anderson (2001), Elz (2000) and Kathage (1994)

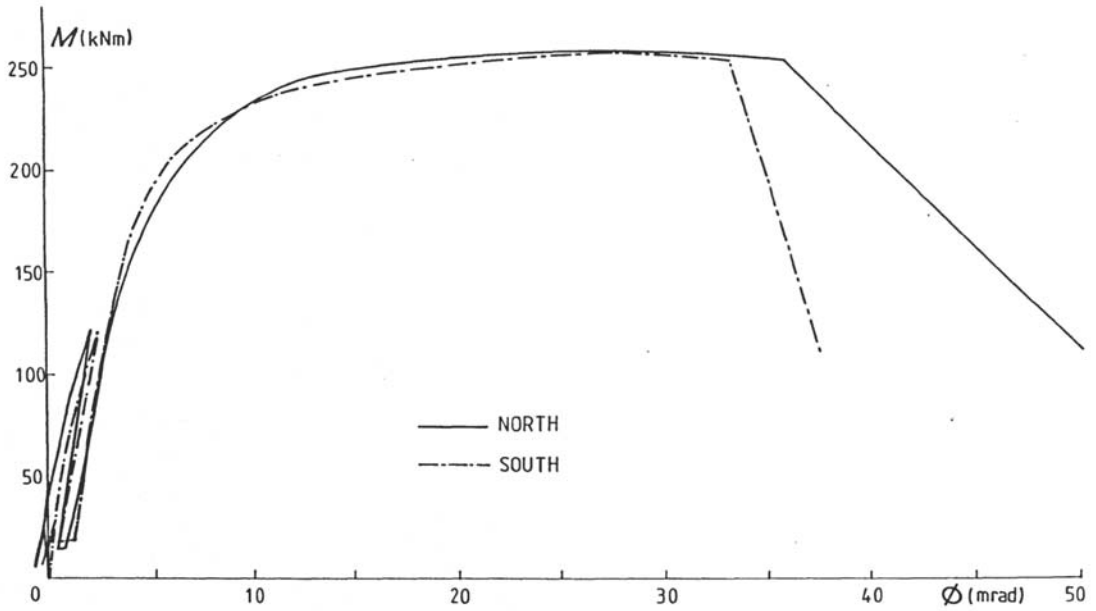

Figure C.2: Moment-rotation curve from Najafi (1992)

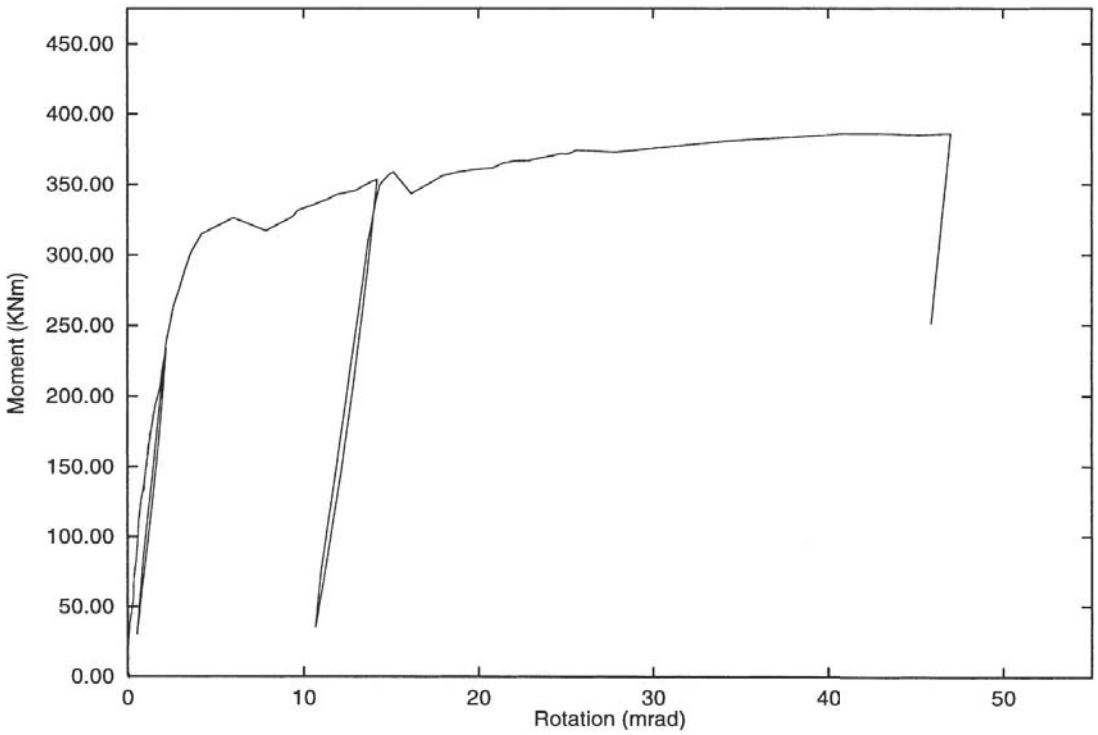

Figure C.3: Moment-rotation curve from Brown and Anderson (2001)

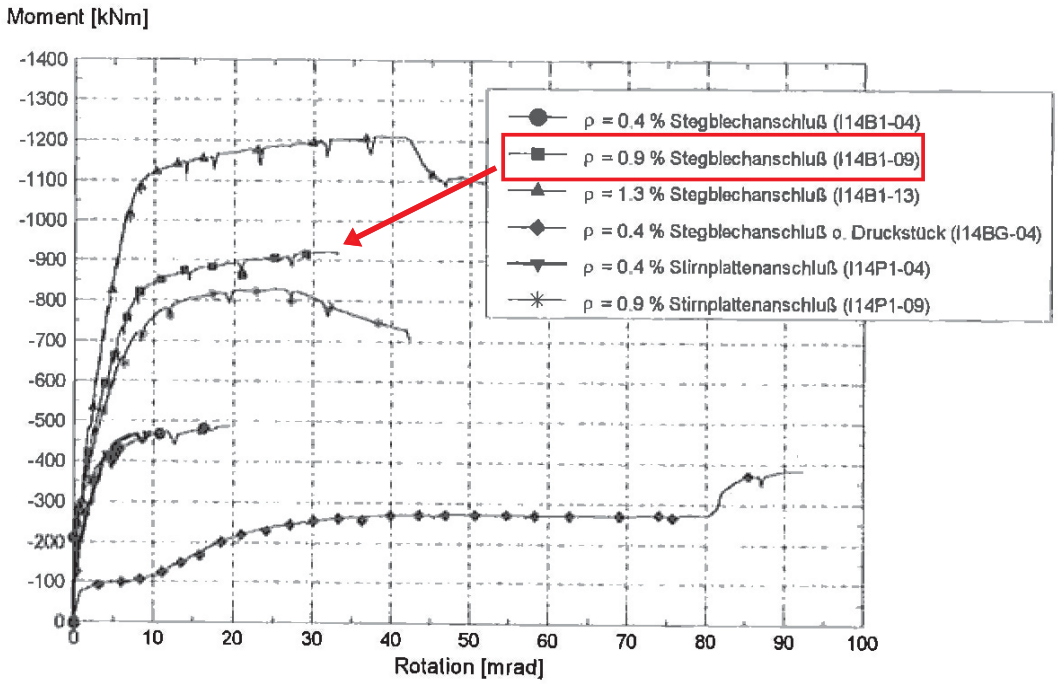

Figure C.4: Moment-rotation curve from Elz (2000)

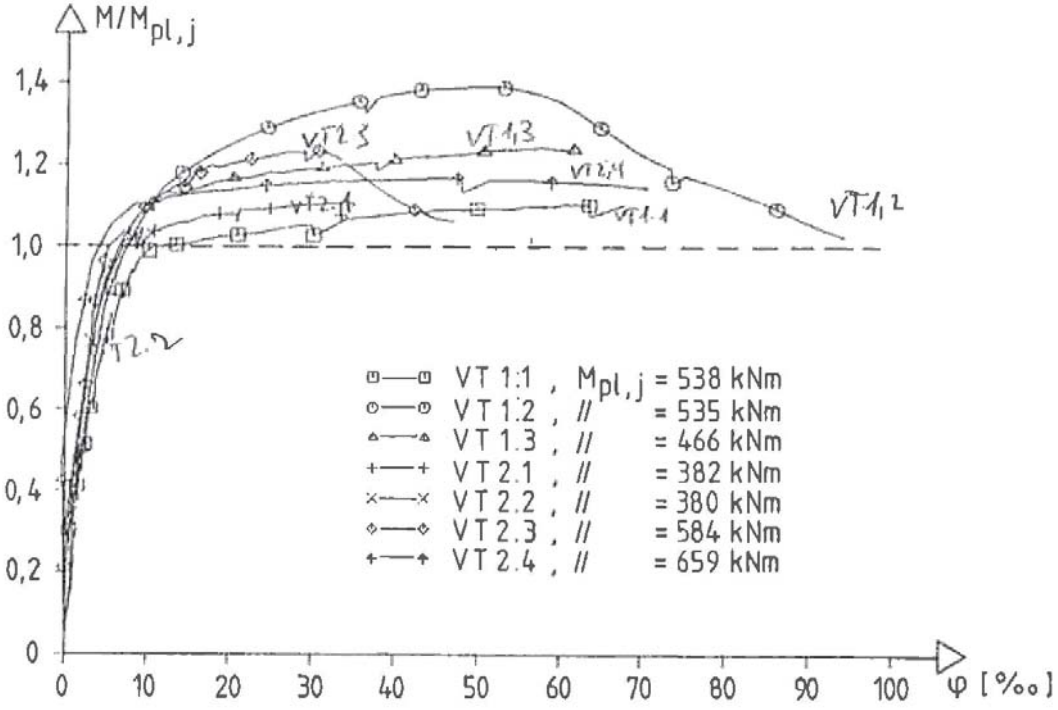

Figure C.5: Moment-rotation curve from Kathage (1994)

D Additional numerical results

D.1 Gap between column flange and concrete slab

The gap between the column flange and the concrete slab was measured in the laboratory tests with the displacement captors no. 26 and 27. The captors are shown in Figure D.1. The values obtained with these captors are compared to those obtained numerically in accordance to Figure D.1. Great agreement is achieved between experimental and FEA results, especially for small joint deformations justifying the correct assessment of deflections in the numerical approximation. At large specimen deformation, the FEA results provide smaller values because during the test performance the gap was measured at a specific vertical distance from the concrete surface. Since the numerical results are given for a point on the concrete surface (steel surface for test C14), the results diverge for large specimen deformations. Besides, the action line of the mentioned captors deviated from the horizontal z-axis for large specimen deformations. Consequently, a larger value than that obtained in the numerical results was measured. The reason for this, is the significant inclination experienced by the captors at ultimate state as shown in Figure D.1. For these reasons, comparison should be primarily made in the initial state for which the above-mentioned effects remain insignificant. The comparison is made in the form of moment-gap rotation curves.

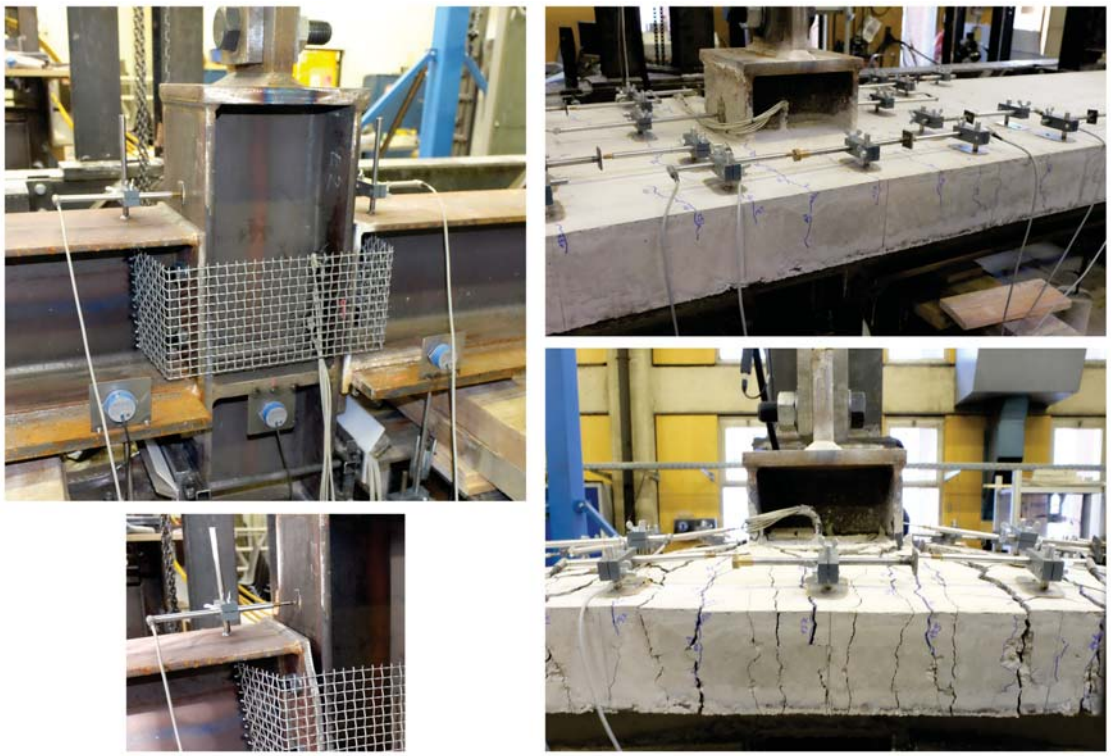

Figure D.1: Displacement captors to measure the gap at initial and ultimate state

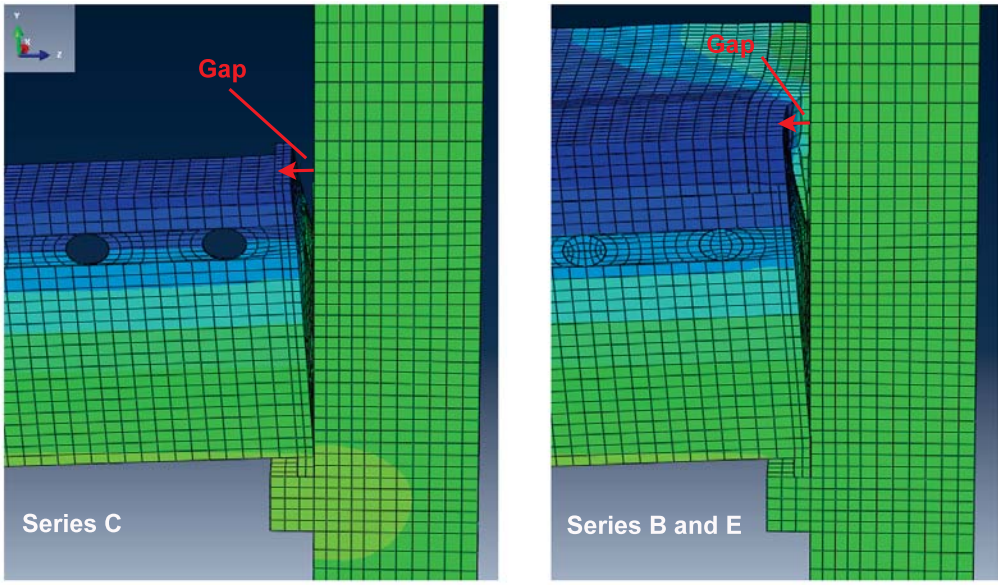

Figure D.2: Gap definition in the numerical model

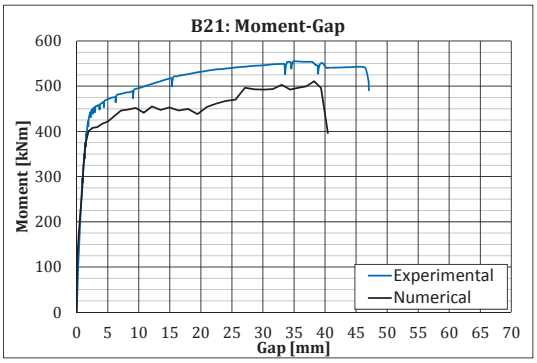

Figure D.3: B21: Moment-gap curve

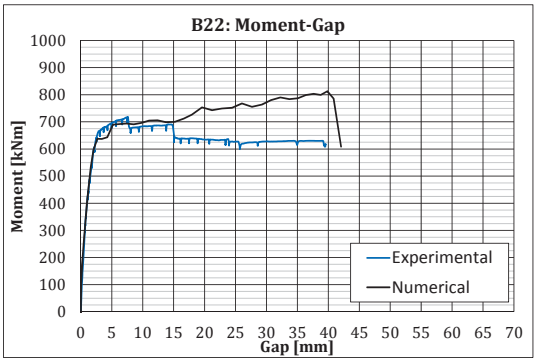

Figure D.4: B22: Moment-gap curve

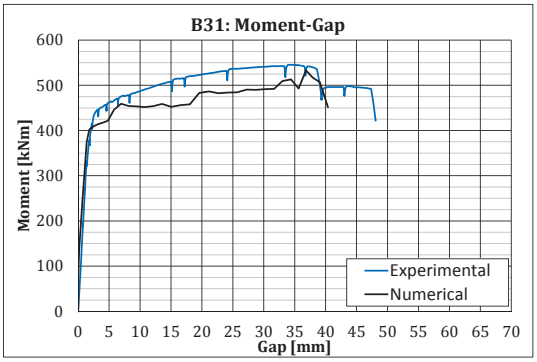

Figure D.5: B31: Moment-gap curve

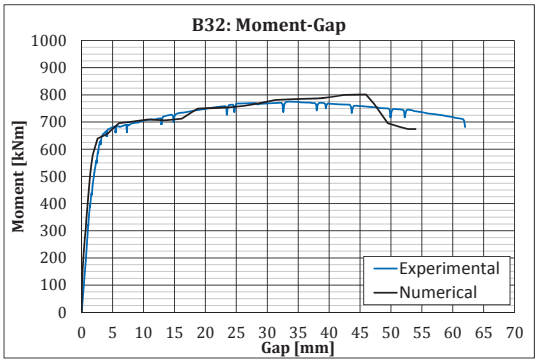

Figure D.6: B32: Moment-gap curve

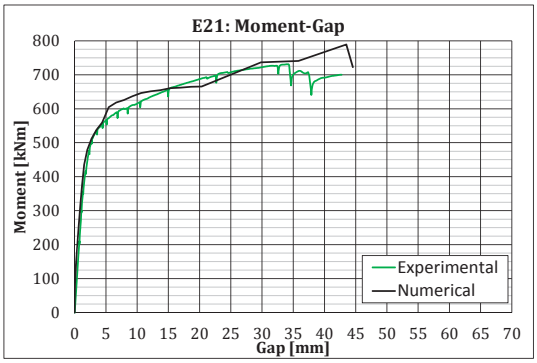

Figure D.7: E21: Moment-gap curve

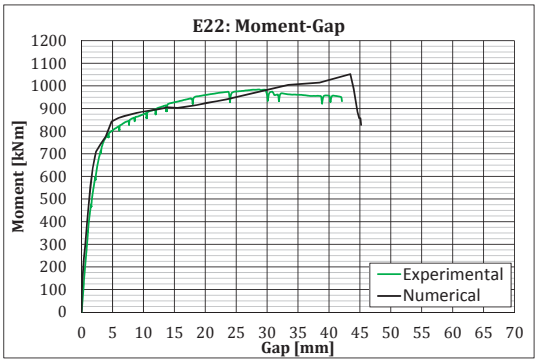

Figure D.8: E22: Moment-gap curve

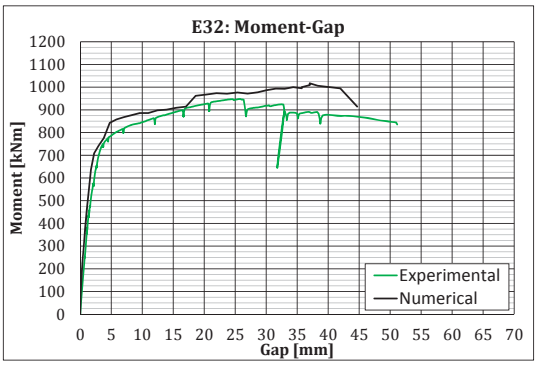

Figure D.9: E32: Moment-gap curve

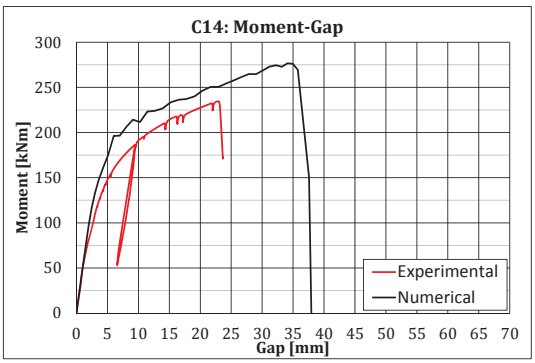

Figure D.10: C14: Moment-gap curve

D.2 Failure recognition

Test B21

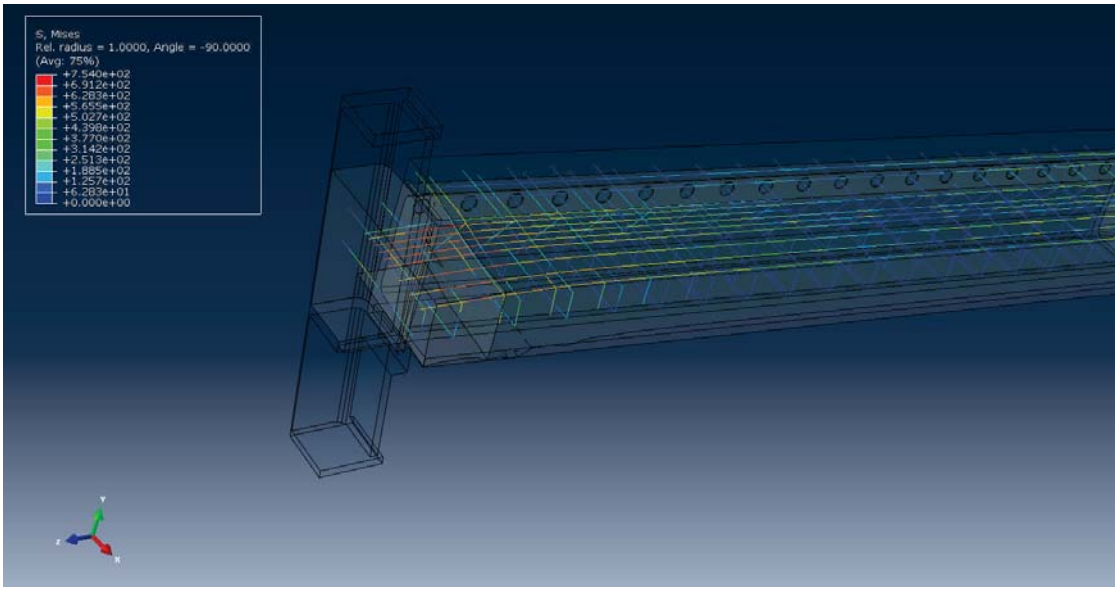

Figure D.11: Failure recognition in B21

Test B22

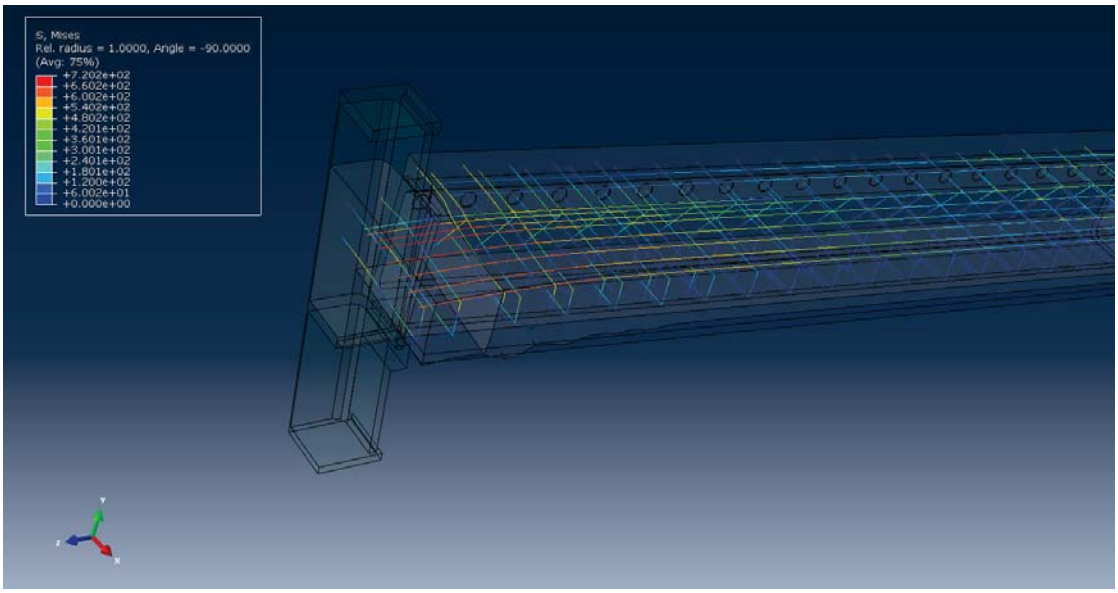

Figure D.12: Failure recognition in B22

Test B31

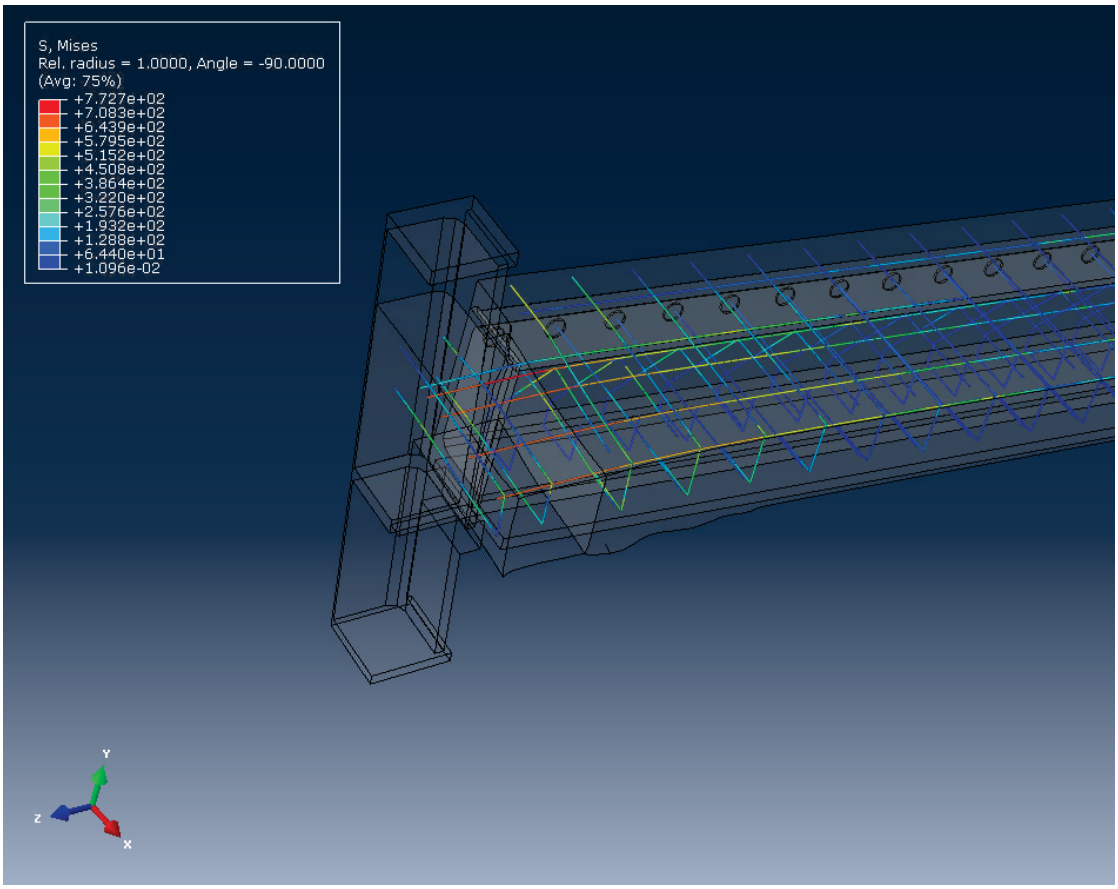

Figure D.13: Failure recognition in B31

Test B32

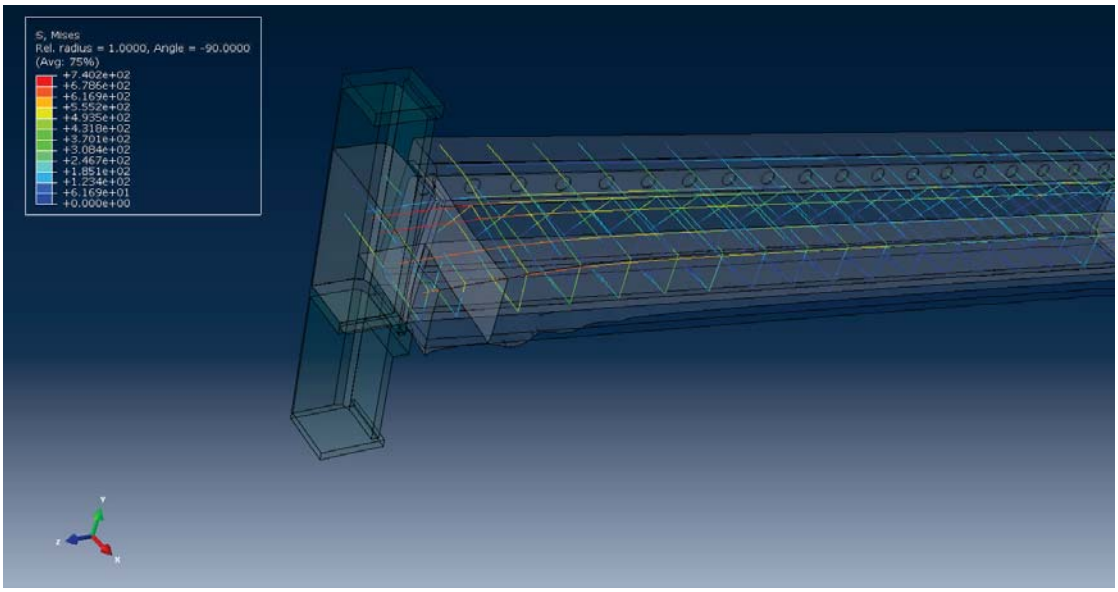

Figure D.14: Failure recognition in B32

Test E21

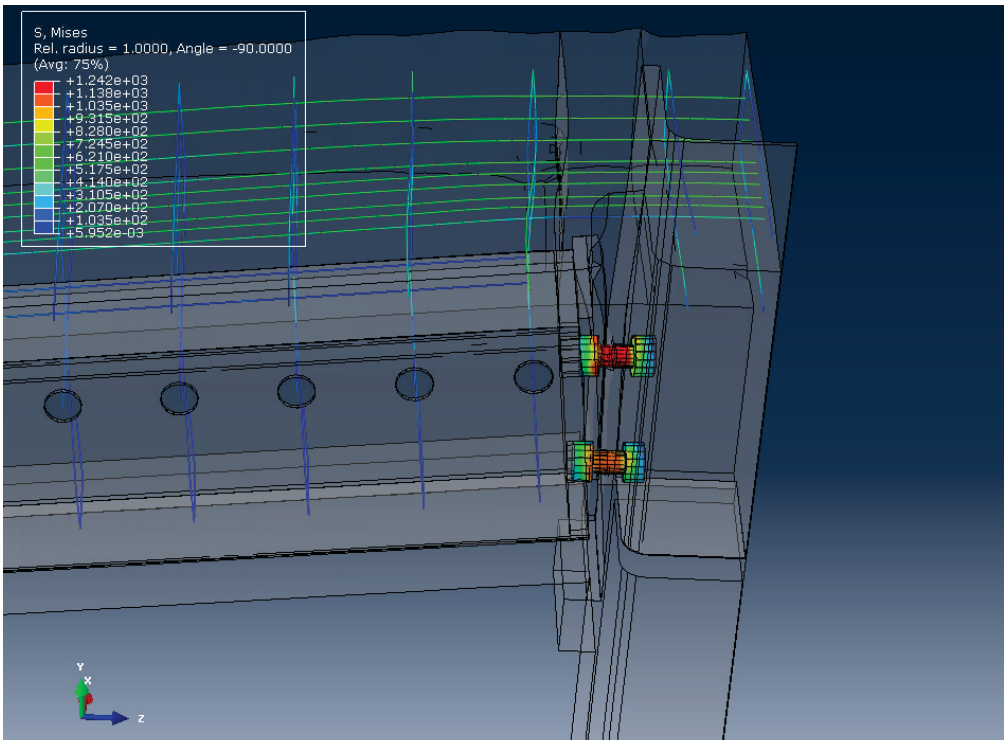

Figure D.15: Failure recognition in E21

Test E22

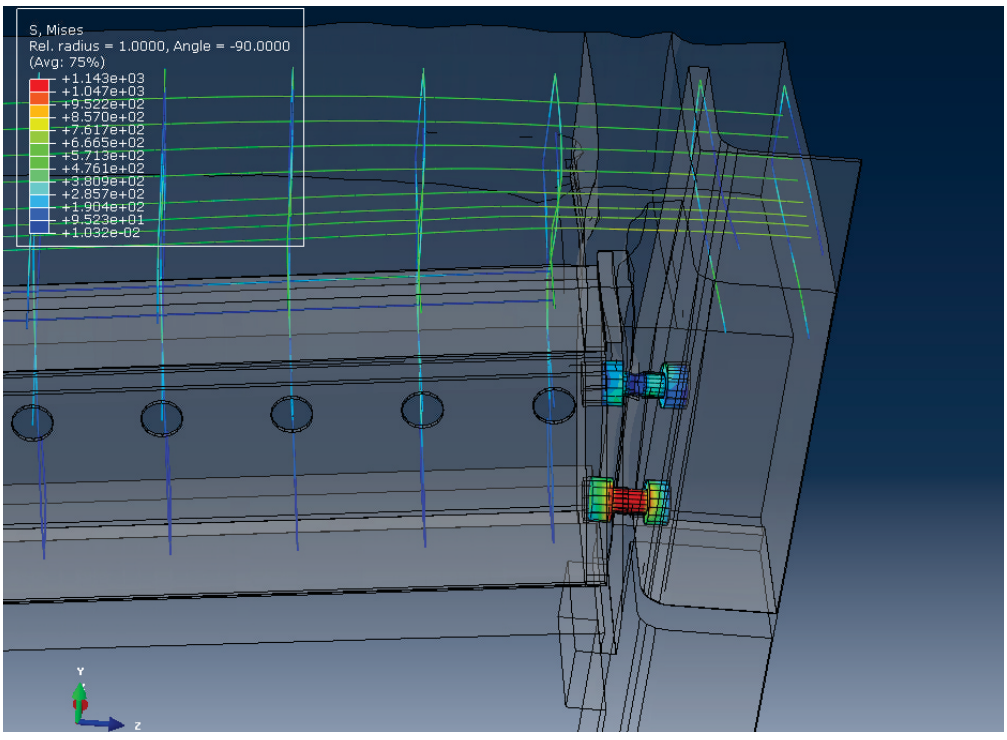

Figure D.16: Failure recognition in E22

Test E32

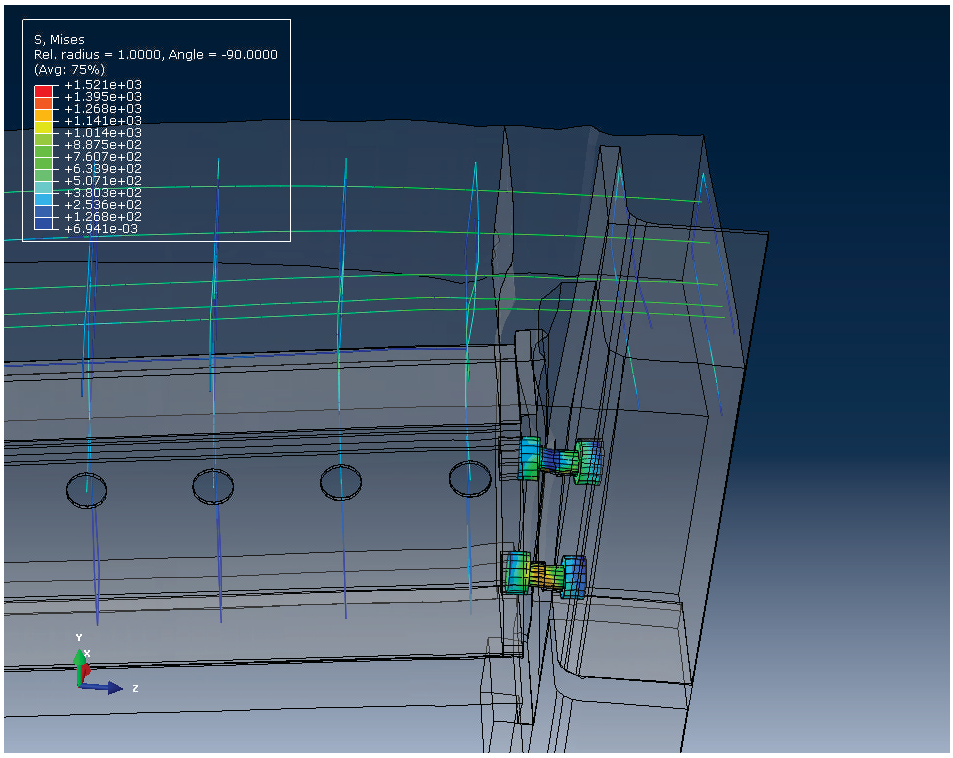

Figure D.17: Failure recognition in E32

Test C14

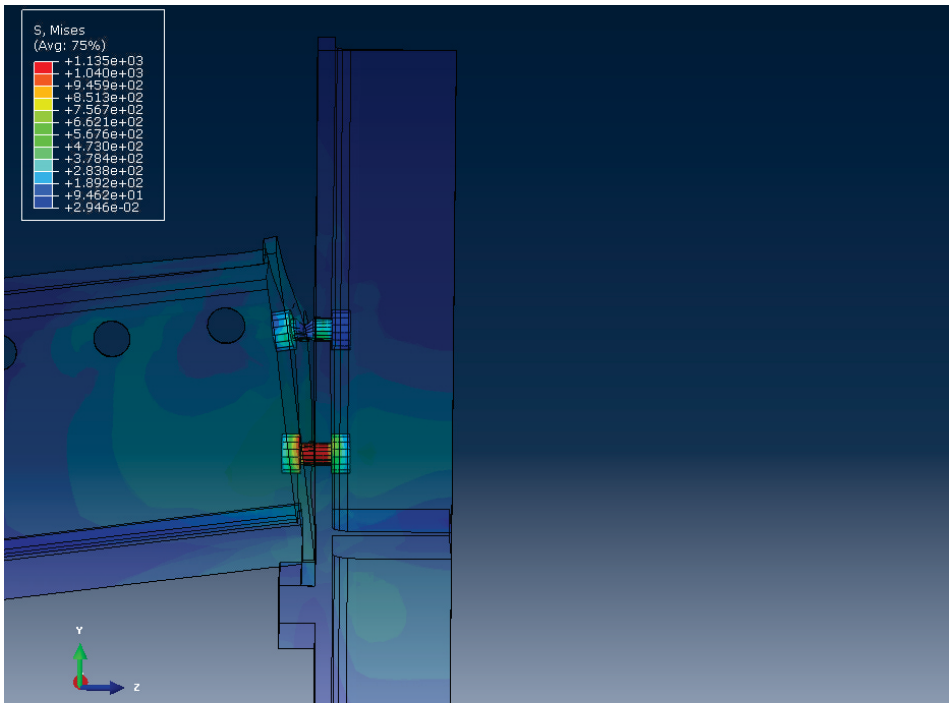

Figure D.18: Failure recognition in C14

D.3 Numerical assessment of the effective joint length

The stress distribution along the longitudinal reinforcement bars is plotted in Figure D.19. The results correspond to the stress state just prior to failure. The plots show that the reinforcement bars are not equally stressed; the inner bars close to the column section are subjected to larger stresses within a restricted rebar length, while the outer rebars are subjected to lower stresses but over a more significant length. This shows that the effective length, in which the rebars are highly subjected to tension stresses depends on the position of rebar. Thus, the notion of effective joint length must be seen as a "mean" effective length between that of inner and outer rebars.

Besides, these figures confirm the experimental findings concerning the influence of the reinforcement ratio on the effective joint length. It can be observed that a larger amount of longitudinal reinforcement induces a bigger extension of the effective joint region. The same is dedcuted from Figure D.20, where the tension damage of concrete is illustrated just before the rupture of one longitudinal rebar.

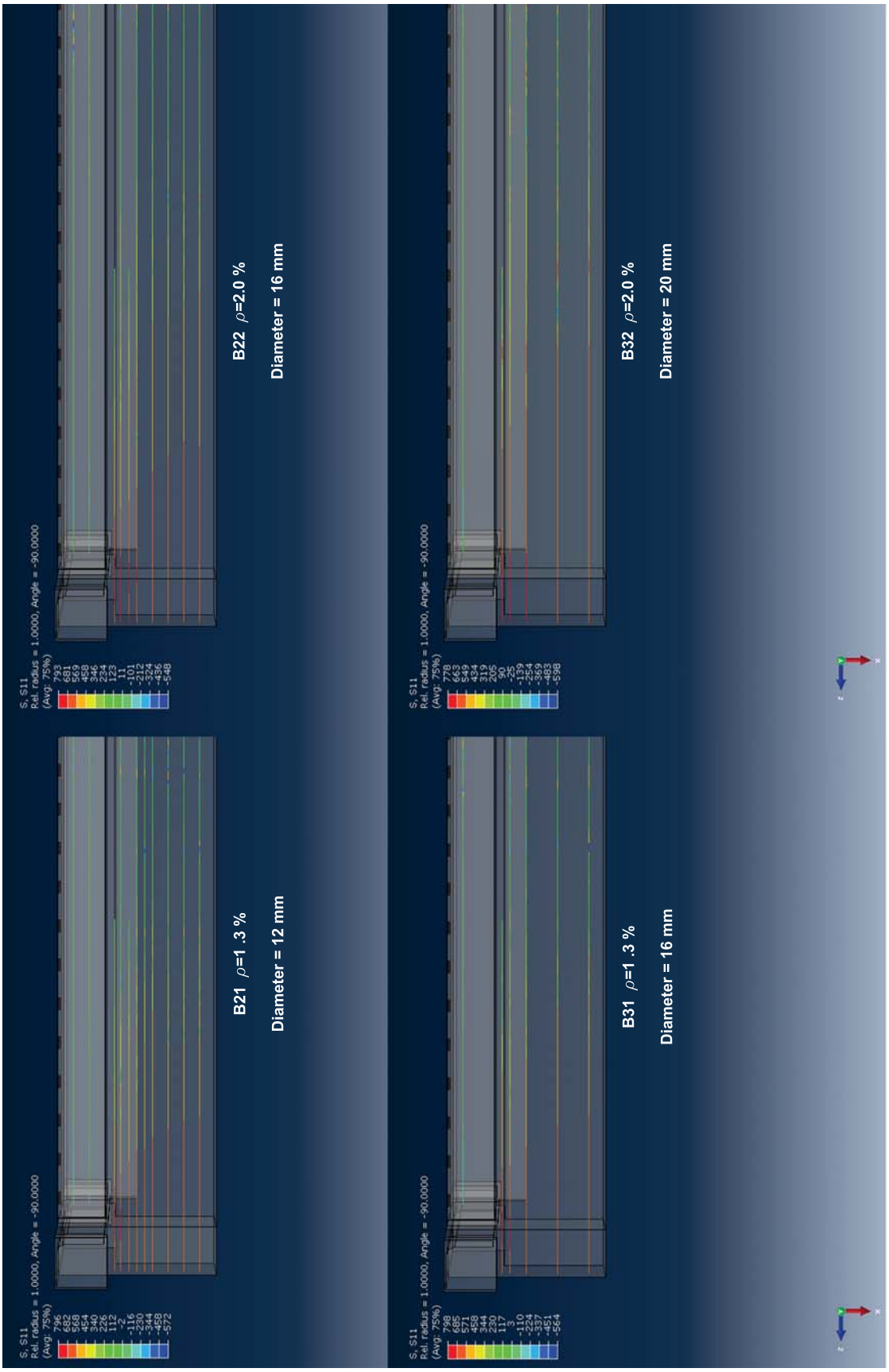

Figure D.19: Stress distribution in longitudinal reinforcement prior to failure

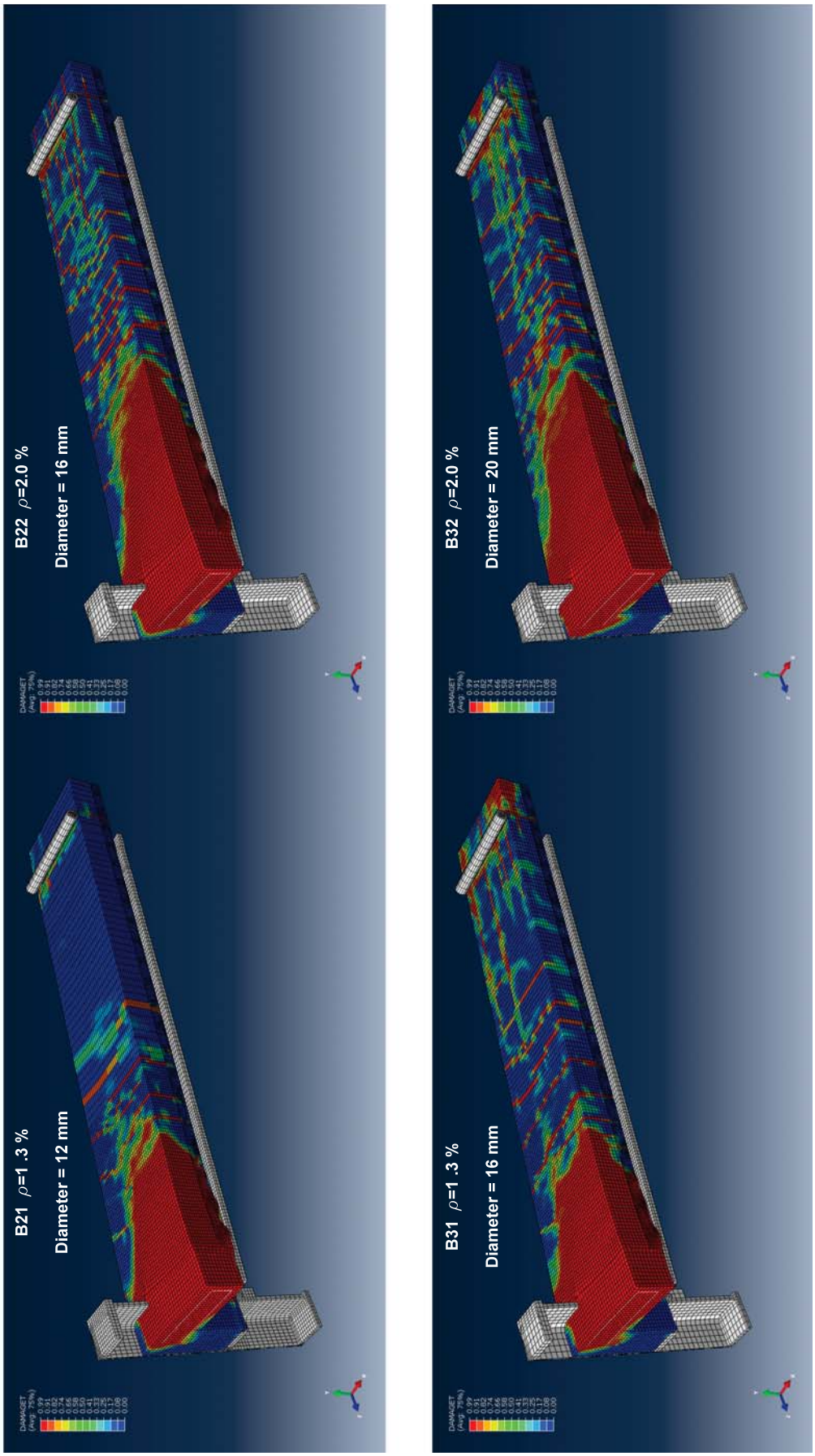

Figure D.20: Tension damage of concrete prior to failure

E Design aids for ultimate elongation of reinforced concrete member in tension

E.1 Ductility of reinforcement $\varepsilon_{su} = 5\%$

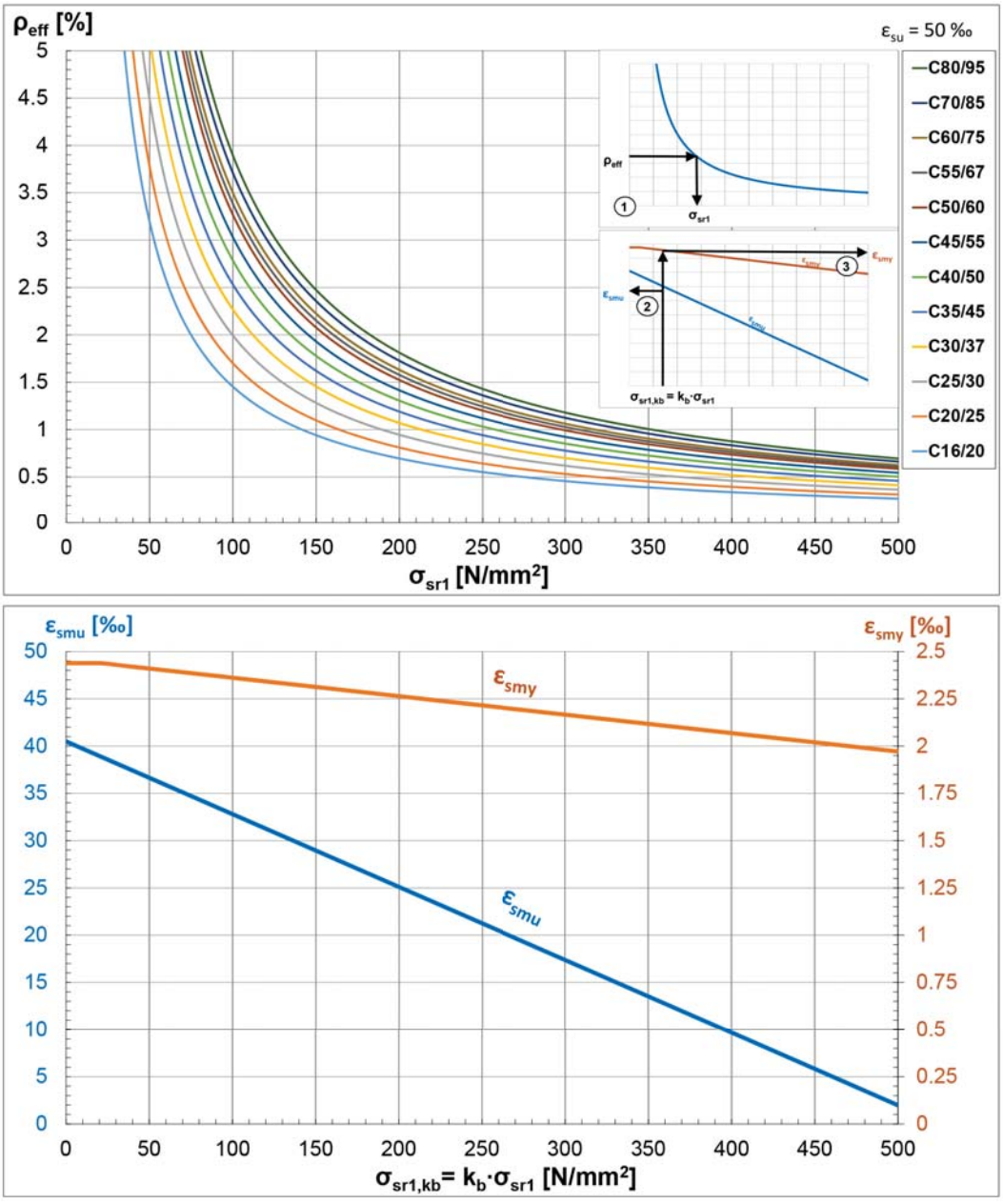

Figure E.1: Design aids for $\varepsilon_{su} = 5\%$

E.2 Ductility of reinforcement $\varepsilon_{su} = 7.5\%$

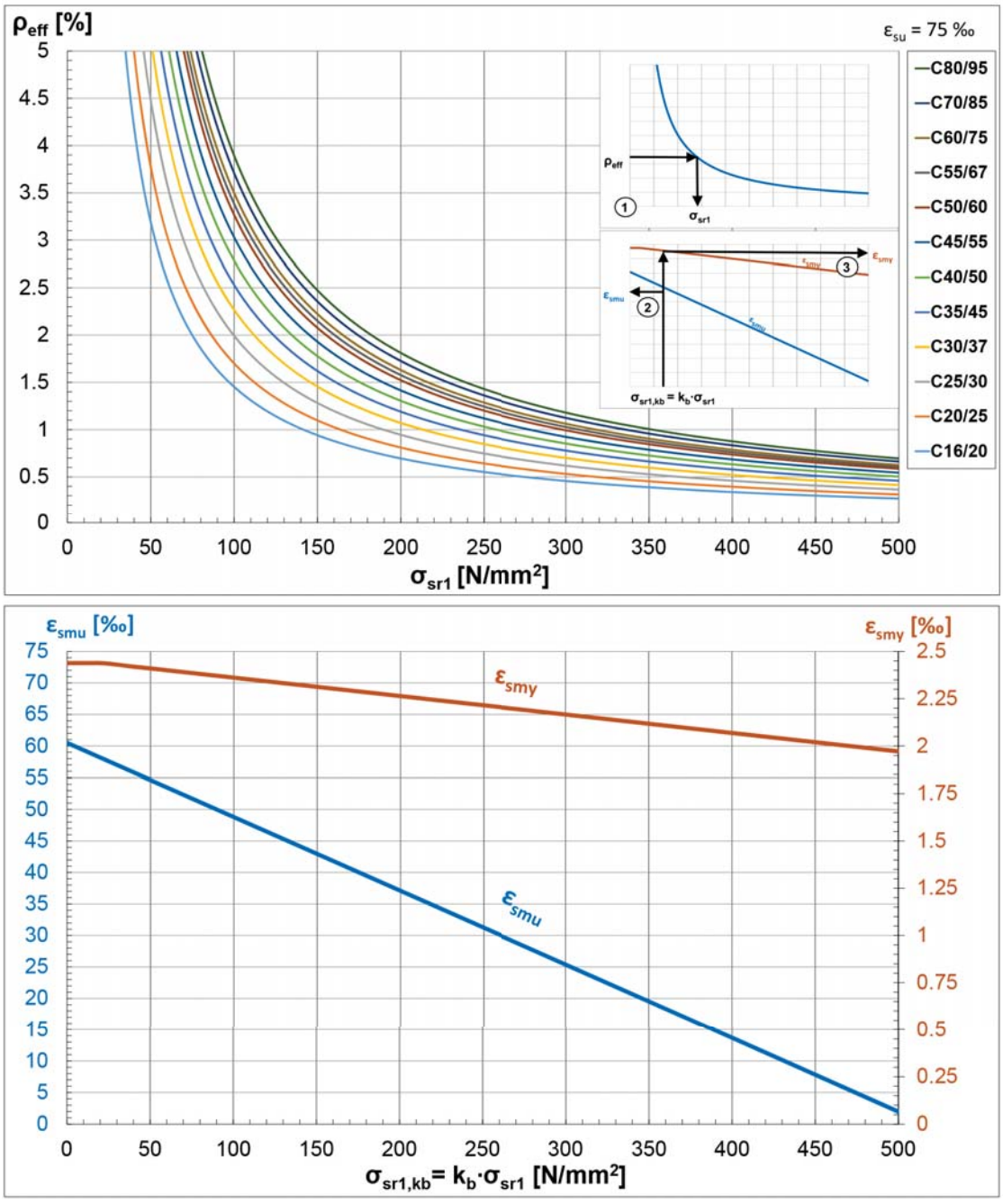

Figure E.2: Design aids for $\varepsilon_{su} = 7.5\%$

E.3 Ductility of reinforcement $\varepsilon_{su} = 8\%$

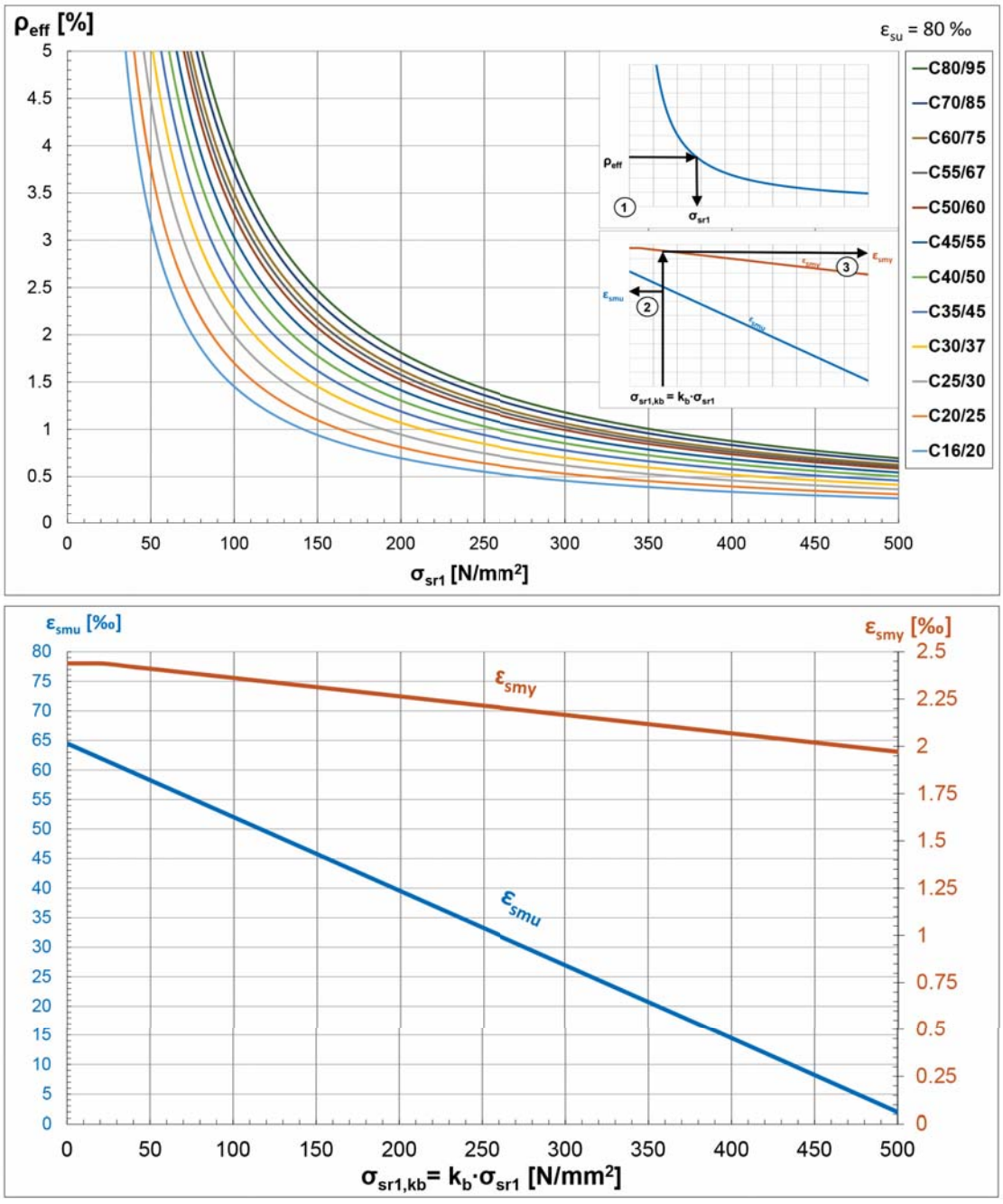

Figure E.3: Design aids for $\varepsilon_{su} = 8\%$

E.4 Ductility of reinforcement $\varepsilon_{su} = 10\%$

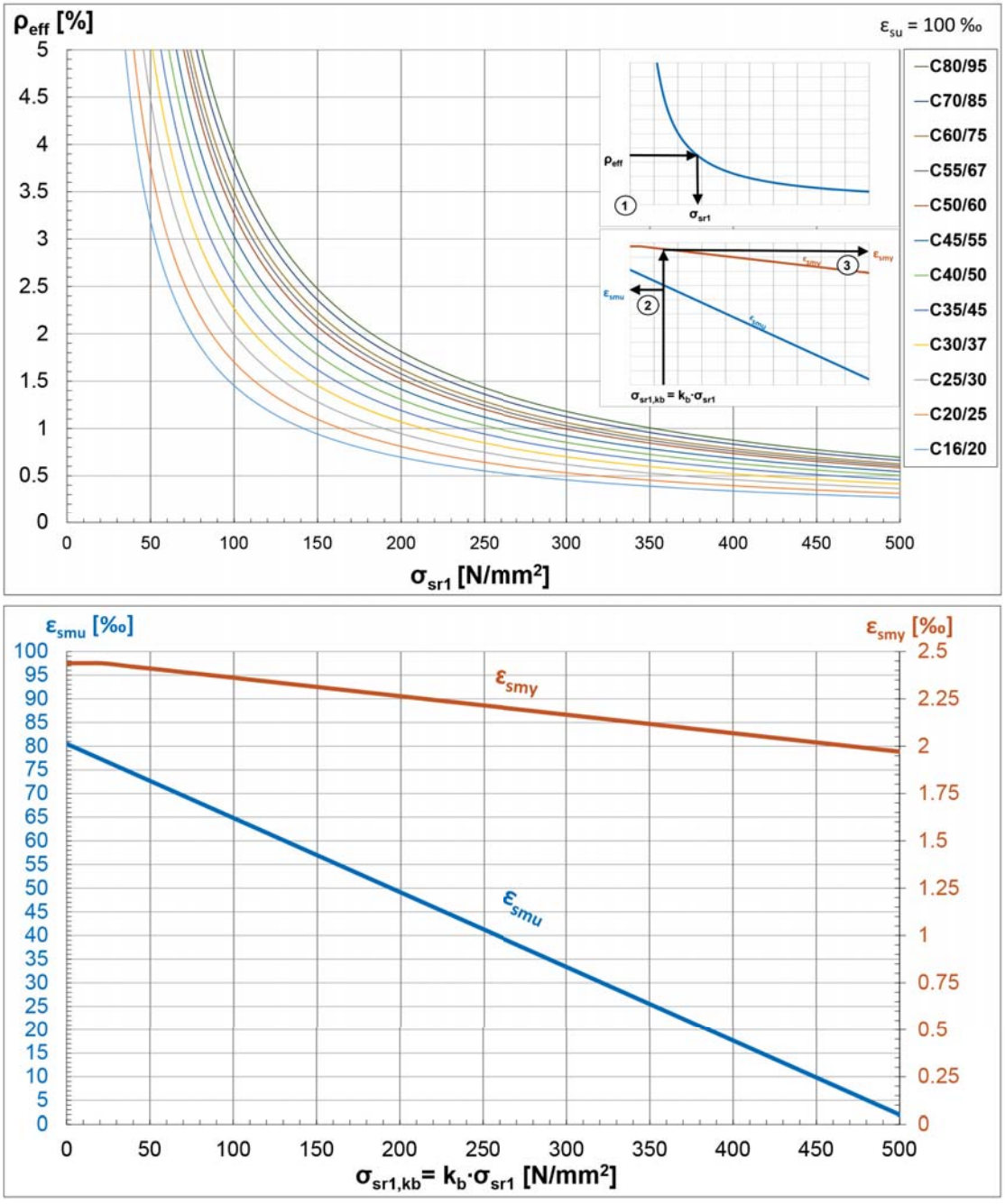

Figure E.4: Design aids for $\varepsilon_{su} = 10\%$